UNIVERSITY OF Southampton

University of Southampton Research Repository
ePrints Soton

Copyright © and Moral Rights for this thesis are retained by the author and/or other copyright owners. A copy can be downloaded for personal non-commercial research or study, without prior permission or charge. This thesis cannot be reproduced or quoted extensively from without first obtaining permission in writing from the copyright holder/s. The content must not be changed in any way or sold commercially in any format or medium without the formal permission of the copyright holders.

When referring to this work, full bibliographic details including the author, title, awarding institution and date of the thesis must be given e.g.

AUTHOR (year of submission) "Full thesis title", University of Southampton, name of the University School or Department, PhD Thesis, pagination

http://eprints.soton.ac.uk

UNIVERSITY OF SOUTHAMPTON

FACULTY OF ENGINEERING, SCIENCE AND MATHEMATICS

SCHOOL OF OCEAN AND EARTH SCIENCES

PHYSICAL CONTROLS ON THE DISTRIBUTION OF PHYTOPLANKTON AROUND THE CROZET PLATEAU, SOUTHERN OCEAN

Hugh James Venables

Thesis for the degree of Doctor of Philosophy

October 2007

UNIVERSITY OF SOUTHAMPTON

ABSTRACT

FACULTY OF ENGINEERING, SCIENCE AND MATHEMATICS
SCHOOL OF OCEAN AND EARTH SCIENCES

Doctor of Philosophy

PHYSICAL CONTROLS ON THE DISTRIBUTION OF PHYTOPLANKTON AROUND THE CROZET PLATEAU, SOUTHERN OCEAN

By Hugh James Venables

The spatial and temporal distribution of phytoplankton around the Crozet Plateau, Southern Ocean, is studied through a variety of satellite datasets and *in situ* cruise and Argo float measurements. Parts of the study area regularly contain phytoplankton concentrations significantly enhanced over the other parts, and over most of the rest of the Southern Ocean, due to natural iron fertilization from the Crozet Islands. Study is made of these contrasts in order to further understand the processes that limit phytoplankton over the mostly High Nutrient Low Chlorophyll (HNLC) Southern Ocean. The longer timescales, larger areas and regularity of naturally iron-fertilized phytoplankton blooms make them preferable to study compared to studies of the effects of iron released from a ship. Data from these experiments, and from other islands in the Southern Ocean, is investigated in the context of the results found around the Crozet Plateau.

The circulation patterns around the Crozet Plateau are studied in detail, with particular emphasis on understanding where surface water that has passed close to the Crozet Islands flows, as this is a known source of iron to the surface water. The surface mixed layer depth and incoming irradiance are also studied so that the variation in light availability with time and latitude can be understood. The distribution of phytoplankton is studied through satellite chlorophyll-a images, with values adjusted to match those observed *in situ* during the research cruises.

The initial development of the bloom is controlled by variations in light availability but the advection and lateral mixing of iron is sufficient to explain the spatial extent of the bloom and the variations in peak chlorophyll-a concentrations. The variability of the strength of the bloom is driven mostly by variations in the iron utilization by phytoplankton during the preceding winter and wind-driven variations in the circulation.

Contents

1 Introduction 1

1.1 Why we went there 1

1.2 Southern Ocean physics 3

1.2.1 Antarctic Circumpolar Current 3

1.2.2 Fronts and zones 6

1.2.3 Effects of topography 9

1.2.4 Water masses 11

1.2.5 Mixed layer processes 12

1.2.6 Long-term variability and changes in the Southern Ocean 15

1.3 Productivity 16

1.3.1 Necessities for life 16

1.3.2 Carbon export 17

1.3.3 Nutrients 18

1.4 High nutrient low chlorophyll conditions 20

1.4.1 Iron 22

1.4.2 Light 23

1.4.3 Grazing 24

1.4.4 Interactions between possible limiting factors 24

1.4.5 Exceptions to HNLC conditions 25

1.4.5.1 Fronts 26

1.4.5.2 Ice edge 28

1.4.5.3 Land effects 28

1.5 CROZEX 29

1.6 Thesis structure 30

2 Data sources 32

2.1 In situ data 32

2.2 Argo data 34

2.3 Surface drifters 37

2.4 Satellite data overview 38

2.5 Ocean colour data 40

2.5.1 Processing steps and caveats 40
2.5.2 Cross comparison and merged product 42
2.5.3 Data usage 44
2.5.4 Quality checks 46
2.5.5 Statistical distribution 46
2.5.6 Local calibration of ocean colour images 46
2.6 Photosynthetically Available Radiation 49
2.7 Sea Surface Temperature 50
2.8 Absolute Dynamic Topography 50
2.9 Wind stress 52

3 Circulation 54

3.1 Large scale circulation 54
3.1.1 Argo float trajectories 55
3.1.2 Hydrographic sections 59
3.1.3 Absolute Dynamic Topography 60
3.2 Features of circulation 63
3.2.1 Strong flow north of Crozet Plateau 63
3.2.2 Flow bifurcations west of Crozet Plateau 64
3.2.3 Effects of topography on frontal location 67
3.2.3.1 Relative strengths of the SAF branches 70
3.2.4 Lack of connection between islands and south of southern SAF branch .. 71
3.2.5 Residence time north of the plateau 73
3.2.6 Inflow into area north of the plateau 74
3.2.6.1 Cross frontal mixing 74
3.2.7 Closed circulation around the Crozet Plateau 76
3.3 Implications for phytoplankton distribution 77

4 Phytoplankton distribution 79

4.1 Introduction 79
4.2 Chl-a images 80
4.3 Seasonal composites – mean 82
4.4 Characteristics of overall chl-a distribution 84

4.5 Definition of boxes used in study 85
4.6 Seasonal progression of chl-a 87
4.6.1 North of the plateau – Spring bloom 92
4.6.2 North of the eastern islands – Persistent bloom 94
4.6.3 Over the Crozet Plateau 95
4.6.4 South of the Crozet Plateau 97
4.7 Bloom initiation 98
4.7.1 Differences between boxes for initiation of the bloom 99
4.7.2 Mean day for each pixel, across years for chl-a to reach 1 mg m^{-3} 99
4.8 Chl-a/MADT around northern edge of bloom 102
4.8.1 Local impacts of frontal mixing 108
4.9 Summary of chl-a distribution 112

5 Mixed layer depth, light and phytoplankton growth 113

5.1 Latitudinal gradients 113
5.1.1 Mixed layer depth gradients 113
5.1.2 Gradients in strength of the pycnocline 117
5.2 Source of gradients 118
5.3 Effects of gradients of light availability on phytoplankton growth rates 119
5.4 SST as a predictor of mixed layer depth 122
5.5 Stratification over the Crozet Plateau 123
5.6 Light availability in mixed layers and relationship to chl-a 129
5.6.1 Crozet area 129
5.6.2 Other Sub-Antarctic islands 135
5.7 Artificial iron enrichment experiments 142
5.8 Spatial and temporal variations in chl-a peak around Crozet Plateau 147
5.8.1 Peak of median chl-a 148
5.9 Summary of impact of light availability 154

6 Variability 155

6.1 Time and Space – introduction 155
6.2 Spatial variability 155
6.2.1 Conditions over and around the plateau 156
6.2.1.1 Atmospheric forcing 157

6.2.1.2 Ocean response to atmospheric forcing 159
6.2.2 Branches of SAF 163
6.2.3 Variations over the plateau 166
6.2.4 South of the Plateau 168
6.3 Interannual variability 171
6.3.1 Effects of winter iron utilisation 171
6.3.2 Biological response to wind stress curl 174
6.3.3 Multiple regression of bloom strength factors 176
6.3.4 Variation in initiation of bloom 176
6.3.4.1 Definition of initiation 177
6.3.4.2 Initiation dates 178
6.3.4.3 PAR and wind stress 179
6.3.5 Latitudinal progression of the bloom 2005 189
6.3.6 Winter 2000 192
6.3.7 Plateau conditions in Spring 2002 (revisited) 193
6.4 Potential for change and significance 195

7 Conclusions 196

7.1 Circulation 197
7.2 Spring Bloom 198
7.3 Persistent Bloom 199
7.4 Plateau 200
7.5 South of the plateau 201
7.6 Other areas 202
7.7 Future work 203

List of Figures

Figure 1.1 Bathymetry of the area around the Crozet Plateau (CP) from Sandwell and Smith (1997). 1
Figure 1.2 Schematic of the three-dimensional flow in the world's ocean, centred on the Southern Ocean, from Schmitz (1996)..... 5
Figure 1.3 Schematic of the biological carbon pump (left) and dissolution pump (right). 18
Figure 1.4 Climatological surface nitrate concentrations from the 2005 World Ocean Atlas. 19
Figure 1.5 Climatological surface silicate concentrations from the 2005 World Ocean Atlas. 20
Figure 1.6 Annual mean distribution of chl-a across the world's ocean..... 21
Figure 1.7 Monthly SeaWiFS images of the Southern Ocean, showing areas that have high chl-a, and the overall HNLC conditions. 26
Figure 2.1 Cruise track for cruises D285 and D286. The curved lines represent the flow pattern found on previous cruises (Pollard and Read 2001). 33
Figure 2.2 Expanded cruise track north of the eastern Islands 33
Figure 2.3 Distribution of Argo float profiles across the study area, the colour relating to day of year. DCR is the Del Cano Rise and CP is Crozet Plateau (too shallow for floats). 35
Figure 2.4 Accumulation of profile data over time in the study area. 36
Figure 2.5 Example of a transmittance profile to show strong surface effect, which is used here as a proxy for chl-a concentration..... 41
Figure 2.6 Ratio between transmittance at mixed layer depth +20m and 14m from CTD data collected on D285 and D286. 42
Figure 2.7 Comparison between MODIS and SeaWiFS chl-a estimates, with least-squares line..... 43
Figure 2.8 Merged SeaWiFS/MODIS chl-a against *in situ* chl-a values with the least squares fit lines to the data and the log transformed data (transformed back)..... 48
Figure 3.1 Plot of all Argo float trajectories from the study area, with arrows to indicate the main flows and directions. The plot includes floats from all depths..... 56

Figure 3.2 Selected Argo float trajectories, showing individual paths and direction of movement (tracks get paler with distance along track). Bathymetry contour intervals are 1000m. 56
Figure 3.3 Argo float trajectories around the Crozet Plateau split between those at 1000m and 2000m and extended south to 55°S. The 1000m contour around the Crozet Plateau is shown in blue. 57
Figure 3.4 Transport streamfunction taken from Pollard *et al.* (2007). Data used is from the Crozet cruises Discovery 285 and 286, Discovery cruises 201 and 213 and Suzil (Park *et al.* 1993). Streamlines show the transport relative to 4000 m or the bottom if shallower, measured in Sverdrups (1 Sv = $10^6 m^3 s^{-1}$). Solid lines are at 20 Sv intervals between 0 and 100 Sv, then at 40 Sv intervals to 180 Sv. A few intermediate 10 and 5 Sv contours are shown long and short dashed respectively. All station positions on which the contouring is based are shown, apart from those outside the limits of the map. 60
Figure 3.5 Absolute dynamic height (dyn cm) image from February 2005, selected to illustrate features regularly present. 61
Figure 3.6 Location of the cuts through the absolute dynamic height data used to study the variation in strength and location of the surface geostrophic flows. 62
Figure 3.7 Temperature/Salinity plots from Argo floats at 40-42°E, 46.5-51.5°E (a) and 42.5-48°E, 43.5-46°S (b), 50-52°E, 46.5-48°S (c) and 50-52°E, 48-52°S (d). The arrows schematically show the bifurcation of the flow between the cuts. The colour scale shows latitude. 66
Figure 3.8 Temperature profiles from: the flow that passes south of the Del Cano Rise (a), between Del Cano Rise and Crozet Plateau (b), the flow along the southern edge of the Crozet Plateau (c) and the flow south of 48°S (d). The colour scale shows latitude. 67
Figure 3.9 Example image of the locations of the (from north) 110, 85 and 45 dyn cm contours, over bathymetry (Sandwell and Smith 1997). Contour intervals are 1000m. 68
Figure 3.10 Latitude of dynamic heights 110 dyn cm, 85 dyn cm and 45 dyn cm, used to show the locations of the Northern SAF branch, Southern SAF branch and Polar Front respectively. 69

Figure 3.11 Time series of the strength of the two branches of the SAF, as measured by the absolute dynamic height difference across the front in dyn cm. 70
Figure 3.12 Trajectory of Argo float released south-east of the Crozet Plateau at the eastern end of an area of weak flow. 72
Figure 3.13 Argo float trajectories. The blue line is the 1000m contour of the Crozet Plateau. 73
Figure 3.14 Float trajectories showing detrainment from the northern branch of the SAF (a and b) and southern branch (c) into the area north of the Crozet Plateau. 74
Figure 3.15 Temperature and salinity from Argo float profiles at the surface (above) and 200m (below) from region 40-50°S, 47-52°E. Open symbols temperature, points salinity. 75
Figure 3.16 T/S plot for the bloom area with data from CTD profiles overlain (black)... 76
Figure 3.17 Argo float trajectories showing floats following the closed circulation around the Crozet Plateau. 76
Figure 3.18 Absolute dynamic height difference (dyn cm) between over the plateau and north of the plateau..... 77
Figure 4.1 A selection of merged SeaWiFS/MODIS chl-a images through the 2004 season. The black line is the 1000m contour of the Crozet Plateau. The full set of images from 1997-2005 is included as appendix A. 81
Figure 4.2 Seasonal composites of chl-a from SeaWiFS for each year 1997-2005. Formed by averaging across all 8-day periods with data between 4th August and 29th March. 83
Figure 4.3 Schematic of the different productivity areas around the Crozet Plateau. 84
Figure 4.4 Boxes used to study the spatial and temporal development of the bloom. Plotted over the Sandwell and Smith (1997) bathymetry. 86
Figure 4.5 Time series of box median chl-a, from SeaWiFS, north of the plateau (boxes A-C), north of the eastern islands (box D), over the plateau (box E) and south of the plateau (box F) for 1997-2005 (continued on following pages). Missing points are due to >80% cloud cover over the box. 87
Figure 4.6 Day of year that the chl-a concentration first exceeded 1 mg m^{-3}, calculated for each pixel. Day used is the start day of the 8-day period..... 100
Figure 4.7 Mean of all images included in Figure 4.6. 100

Figure 4.8 Chl-a image from the peak of the bloom in 2004 with the (from north) 100, 95 and 90 dyn cm dynamic heights shown. 102
Figure 4.9 Chl-a images from the peak of each year or close to the peak to ensure good data coverage with absolute dynamic height contours overlain at 5 dyn cm intervals. 105
Figure 4.10 Log-frequency of (absolute dynamic height, chl-a) data pairs from western edge of the bloom area (left) and north-eastern side (right)..... 106
Figure 4.11 1km resolution MODIS chl-a image (received real time on the ship and no post-processing), 30/12/2004-2/12/2004. 111
Figure 4.12 1km resolution MODIS SST image (received real time on the ship and no post-processing), 30/12/2004-2/12/2004. 111
Figure 5.1 Mixed layer depth from Argo floats (43-50°S, 40-60°E) against day of year, with sinusoidal least-squares fit. Open circles are profiles north of the plateau, dots to the south. 115
Figure 5.2 Residual mixed layer depths, after effects of time of year have been removed. 116
Figure 5.3 Density difference between base of mixed layer and 50m below the base of mixed layer. 117
Figure 5.4 NCEP/NCAR data from 2005 (used as a representative example) for a) latent heat flux (W m^{-2}) and b) precipitation rate (cm hr^{-1}) 118
Figure 5.5 PAR data for 2004 (left) and monthly average wind stress from QuikSCAT from 2004 (right). 119
Figure 5.6 Modelled variation in chl-a increase with different light availability. The 10m and 1 Einstein m^{-2} day^{-1} steps represent the effects of 1 degree of latitude in average mixed layer depth and incoming irradiance. 121
Figure 5.7 Results of model with mixed layer depth fixed (left) and PAR fixed (right).121
Figure 5.8 Mixed layer depth against surface temperature (i.e. bulk SST) for Argo float profiles around the Crozet Plateau, 43-50°S, 40-60°E..... 123
Figure 5.9 Density profiles from float 1900434, during a period when it was over the south-western part of the plateau between late June and early September 2006. ... 124
Figure 5.10 Density profiles from float 1900452 between May and July 2005 as the float went around the western edge of the plateau. 125

Figure 5.11 All SST images from August-January 2004/5 that have good coverage over the plateau. The black line is the 1000m contour..... 127
Figure 5.12 Log-frequency plots for Chl-a/SST match-ups from 45-47°S, 48-53°E. 128
Figure 5.13 Chl-a (mg m^{-3}, from merged SeaWiFS/MODIS satellite product) against light availability in mixed layer. Colour scale is day of year. a) north of the plateau, b) south of the plateau. 132
Figure 5.14 Same as Figure 5.13a but without accounting for self-shading (using a constant chl-a of 0.5 mg m^{-3} in equation 5-5). 133
Figure 5.15 Light availability (Einsteins day^{-1} m^{-2}, calculated from mixed layer depth from Argo float profiles and SeaWiFS PAR data) against day of year north and south of the plateau. 135
Figure 5.16 Chl-a values at the location of Argo float profiles against day of year for north and south of the plateau. 135
Figure 5.17 Locations of the Argo 138
Figure 5.18 Merged SeaWiFS/MODIS chl-a..... 139
Figure 5.19 Chl-a (mg m^{-3}) against light..... 140
Figure 5.20 Light (Einsteins day^{-1} m^{-2}) 141
Figure 5.21 Peak chl-a against mixed layer depth for artificial iron enrichment experiments (following de Baar *et al.* 2005)..... 143
Figure 5.22 As Figure 5.21 but taking the chl-a concentration after 10 days of the experiment rather than at the peak. 144
Figure 5.23 Growth rate for iron enrichment experiments, right hand plot is corrected for the effects of surface temperature (by dividing by $2^{SST/10}$) on growth rate (Eppley 1972; Goldman and Carpenter 1974). 144
Figure 5.24 Peak chl-a attained for each..... 150
Figure 5.25 Day of year (counting 152
Figure 5.26 Mean of all images in Figure 5.25 152
Figure 6.1 SAM index from 1997 to early 2007. The daily SAM indices were downloaded from http://www.cpc.noaa.gov/products/precip/CWlink/all_index.html. 158
Figure 6.2 Coherence squared between the SAM index and wind stress curl around the Crozet Plateau. The 95% confidence level is shown as the dashed line. 158

Figure 6.3 Coherence squared between wind stress north of the Crozet Plateau and the SAM index. The 95% confidence level is shown as the dashed line. 159
Figure 6.4 Time series of dynamic height difference west of the Crozet Plateau corresponding to the southward flow close to the plateau. 160
Figure 6.5 Time series of dynamic height difference east of the Crozet Plateau..... 161
Figure 6.6 Time series of peak absolute dynamic height above the Crozet Plateau..... 161
Figure 6.7 Coherence squared between the peak dynamic height over the plateau and local wind stress curl and SAM index. 95% Confidence level is shown by the dashed line. 162
Figure 6.8 Phase (in radians) between peak plateau height and wind stress curl around the plateau. 162
Figure 6.9 Absolute dynamic height difference across the two branches of the SAF. ... 164
Figure 6.10 Coherence squared and phase difference between the two branches of the SAF. 164
Figure 6.11 Coherence squared and phase difference between the SSAF surface geostrophic flow south of the Crozet Plateau and the northward surface geostrophic flow to the east of the Crozet Plateau..... 165
Figure 6.12 Time series of the northward surface geostrophic flow to the east of the Crozet Plateau. The vertical dashed line marks the time from when more satellite data are available so data to the left should be treated with caution. 165
Figure 6.13 Merged SeaWiFS/MODIS images, with contours of absolute dynamic height overlain, showing the anomalously high chl-a levels over the plateau in spring 2002. 167
Figure 6.14 Chl-a south of the plateau, a) 48-50°S, b) 50-52°S 168
Figure 6.15 Latitudes of three dynamic heights that pass close to 49°S. Data are not necessarily reliable before the dashed line. 169
Figure 6.16 Large area (and low colourbar limit) SeaWiFS image for peak chl-a south of the plateau in 2004 and 2005 with overlain absolute dynamic height contours. 170
Figure 6.17 Time averaged chl-a concentrations over the spring bloom plotted against the time averaged chl-a from the preceding winter period. 172
Figure 6.18 Links between the strength of the spring bloom in the ‘spring bloom area’ and the chl-a in the same area the following summer period (years are for summer rather than spring). 173

Figure 6.19 Links between the strength of the spring bloom in the 'persistent bloom area' and the chl-a in the same area the following summer period (years are for summer rather than spring). 174
Figure 6.20 3-month averages of wind stress curl around the Crozet Plateau 175
Figure 6.21 Spring chl-a in the spring bloom area against the wind stress curl the preceding winter. 175
Figure 6.22 Strength of the spring bloom against measures of the start of the bloom.... 179
Figure 6.23 Chl-a, wind stress and PAR during the initiation of the bloom in 1999..... 182
Figure 6.24 (Wind stress, PAR) data pairs from north of the plateau, 1999..... 182
Figure 6.25 Chl-a, wind stress and PAR during the initiation of the bloom in 2000..... 183
Figure 6.26 (Wind stress, PAR) data pairs from north of the plateau, 2000..... 183
Figure 6.27 Chl-a, wind stress and PAR during the initiation of the bloom in 2001..... 184
Figure 6.28 (Wind stress, PAR) data pairs from north of the plateau, 2001..... 184
Figure 6.29 Chl-a, wind stress and PAR during the initiation of the bloom in 2002..... 185
Figure 6.30 (Wind stress, PAR) data pairs from north of the plateau, 2002..... 185
Figure 6.31 Chl-a, wind stress and PAR during the initiation of the bloom in 2003..... 186
Figure 6.32 (Wind stress, PAR) data pairs from north of the plateau, 2003..... 186
Figure 6.33 Chl-a, wind stress and PAR during the initiation of the bloom in 2004..... 187
Figure 6.34 (Wind stress, PAR) data pairs from north of the plateau, 2004..... 187
Figure 6.35 Chl-a, wind stress and PAR during the initiation of the bloom in 2005..... 188
Figure 6.36 (Wind stress, PAR) data pairs from north of the plateau, 2005..... 188
Figure 6.37 Chl-a image, with overlain dynamic height contour, showing the unusual development of the bloom in early 2005..... 191
Figure 6.38 Chl-a image, with overlain dynamic height contour, showing the usual development of the bloom in early 2004..... 191
Figure 6.39 Chl-a, wind stress and PAR during the winter period in 2000. 193
Figure 6.40 Chl-a, wind stress and PAR over the plateau in 2002 and 2005..... 194
Figure 7.1 Figure 4.3 reproduced as a summary of the key circulation features and productivity areas. The Del Cano rise is the closed 2000m contour to the west, the Crozet Plateau is under the 'Plateau' area..... 196

List of Tables

Table 2.1 Remotely sensed data used in this study. 39
Table 2.2 Reference table for the start dates of NASA satellite data 8-day periods and the numbering used in this study (analysis starts at the beginning of the spring bloom). 45
Table 3.1 Standard deviations of latitude of three dynamic heights representing the three main flows in the region. 70
Table 4.1 Bounding co-ordinates for boxes used in study of temporal and spatial variation in satellite chl-a. 85
Table 4.2 8-day period after 4th August that the median chl-a value in each box north of the plateau reached 1 mg m^{-3}. Dates are relative to the mid-points of the 8-day periods. 99
Table 4.3 Areas of bloom entrainment (north) and main bloom area (south) in km^2. 108
Table 5.1 Details of artificial iron enrichment experiments. MLD and PAR values are for the time of peak chl-a where possible, otherwise they are values quoted in Boyd *et al.* (2007) or, for PAR, de Baar *et al.* (2005). EIFEX is included but not further considered due to lack of PAR data. EEP=East Equatorial Pacific, SO=Southern Ocean, NWP=North-West Pacific, NEP=North-East Pacific. 146
Table 5.2 Seasonal maximum of the 8-day median chl-a (mg m^{-3}) in each box from adjusted SeaWiFS chl-a data. 148
Table 5.3 8-day period that the seasonal maximum of the 8-day median chl-a occurs in each box from adjusted SeaWiFS chl-a data. 149
Table 6.1 Day of year for the initiation of the bloom and for the chl-a to reach 1 mg m^{-3} 178

Appendices (on CD)

Appendix A – 8-day chl-a images
Appendix B – Weekly absolute dynamic topography images

Declaration

DECLARATION OF AUTHORSHIP

I, ……,

declare that the thesis entitled

PHYSICAL CONTROLS ON THE DISTRIBUTION OF PHYTOPLANKTON AROUND THE CROZET PLATEAU, SOUTHERN OCEAN

and the work presented in the thesis are both my own, and have been generated by me as the result of my own original research. I confirm that:

this work was done while in candidature for a research degree at this University;

no part of this thesis has previously been submitted for a degree or any other qualification at this University or any other institution;

where I have consulted the published work of others, this is always clearly attributed;

I have acknowledged all main sources of help;

where the thesis is based on work done by myself jointly with others, I have made clear exactly what was done by others and what I have contributed myself;

some contents of this thesis, together with related work are being published in:

Venables, H. J., R. T. Pollard, E.E. Popova (2007). Physical conditions controlling the early development of a regular phytoplankton bloom north of the Crozet Plateau, Southern Ocean. Deep-Sea Research II.

and

Pollard, R. T., H. J. Venables, J.F. Read and J.T. Allen (2007). Large scale circulation around the Crozet Plateau controls an annual phytoplankton bloom in the Crozet Basin. Deep-Sea Research II.

Signed: ……..

Date:……

Acknowledgements

I would like to thank all the people who have helped me through my time as a PhD student: those that have helped the PhD by talking about it and those that have helped me by talking about something else. My supervisors Raymond and Katya, together with Mark, Ian, Helene and others have provided good debate about the situation around Crozet, which have helped stimulate ideas. My parents have been there for me and believed that I will get to the end, sometimes more than I did. My father, Roger Venables, proof-read the thesis but no changes of intellectual content were made as a result of this advice. I have been able to turn to my friends when I have needed sensible advice, a distraction or somewhere to sleep for a night – Catherine, Hannah, Ian, Ross, Ian, Candy, Pete, Tom, Liz and the rest, it has all been appreciated. Finally I would like to thank all the crew and fellow scientists I have sailed with, for helping create some amazing experiences, and giving me space to be myself – a very valuable thing on a ship!

1 Introduction

1.1 Why we went there

The CROZet natural iron bloom and EXport experiment (CROZEX) was a programme hosted at the National Oceanography Centre, Southampton (NOCS) as part of the BICEP (Biophysical Interactions and Controls on Export Production) Programme. The aim was to study the causes and effects of a naturally iron-fertilised bloom around the Crozet Plateau in the Southern Ocean. The main focus of the work was to quantify the enhancement of carbon export stimulated by the bloom, as previous studies have either shown no enhancement in export or only demonstrated increased export over shallow depths and therefore not out of the surface system.

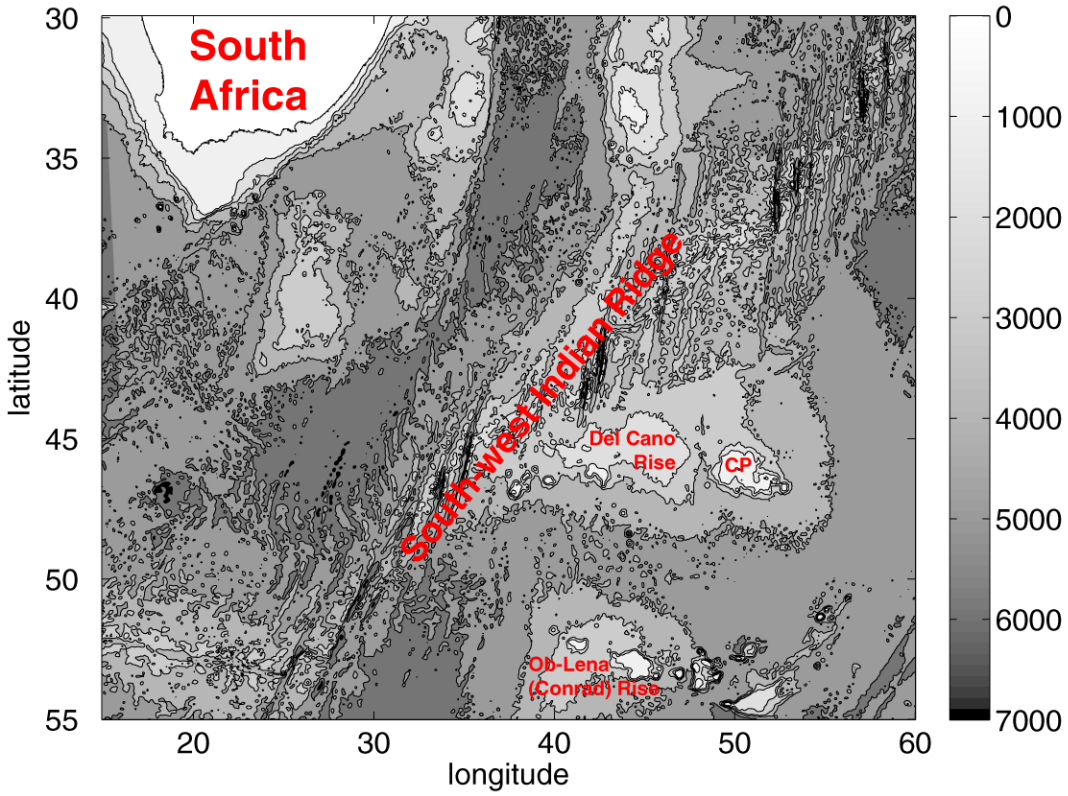

Figure 1.1 Bathymetry of the area around the Crozet Plateau (CP) from Sandwell and Smith (1997).

The area around the Crozet Plateau (46.5°S 51°E, Figure 1.1) is anomalous. The Sub-Antarctic Front (SAF) is diverted north by the Del Cano Rise, a <2000m deep seamount to the west of the Crozet Plateau, and so reaches the most northerly latitude of any part of

the Antarctic Circumpolar Current (ACC). At this point it is close to the Agulhas Return Current (ARC) and could potentially be influenced by this flow, either dynamically or through water exchange. As the SAF flows north it passes close to the Crozet Plateau and it then turns east 300km north of the Crozet Plateau. It therefore encloses an area immediately north of the plateau, which has weak circulation and long residence times. This area is downstream of flows that come in contact with the islands and plateau and therefore contains water that has been in recent contact with sediments – unlike most of the Southern Ocean. It also shows some of the highest regularly occurring chlorophyll concentrations within the ACC. It is the main hypothesis of the CROZEX program that these two facts are linked, via natural iron fertilisation of the flow as it passes the plateau and/or islands.

The flow pattern means that the area south of the plateau does not receive a significant amount of island-influenced water, and shows low chlorophyll values, typical of the Southern Ocean – generally a High Nutrient Low Chlorophyll (HNLC) area. The contrast between north and south of the plateau allows important factors limiting productivity in the Southern Ocean to be studied. Variations of factors with latitude, such as wind stress, incoming insolation and mixed layer depth, have to be studied and accounted for when making the comparisons between the areas.

In this thesis the flow patterns in the area are described to try to predict where iron from the islands and/or plateau is advected. These flows are then related to the chlorophyll distribution seen in satellite ocean colour data. The temporal structure of the bloom is also studied, using Argo float profiles and satellite irradiance data to relate chl-a to light availability. Similar methods are used to compare north and south of the plateau to study the contrast that is found, and made use of by the sampling strategy of the CROZEX cruises. These methods of comparison are then extended to other Sub-Antarctic Islands and artificial iron release experiments.

The timescale of the study is set by the availability of satellite ocean colour images so it starts with SeaWiFS in 1997. Other data sets start at various points since then so the study can be more intensive in later years. The most important addition is that from Argo floats, which starts in 2002 but with most data from 2004 onwards. Maps of absolute dynamic topography, which give information on the surface velocity structure, are also

used, mostly after early 2002 when the data were improved by the addition of more altimetric satellites. Most effort is aimed at explaining the processes at work in 2004 due to availability of cruise data for that year and to describe the conditions prior to the cruise as context for these data. Interannual variability of the data is also studied, although it is too early to study variability in Argo float data in the area.

1.2 Southern Ocean physics

1.2.1 Antarctic Circumpolar Current

As the Southern Ocean is zonally unbounded it provides a link for the transfer of heat, salt, nutrients and plankton around Antarctica and between the major ocean basins, and the controlling dynamics are different from enclosed ocean basins. It allows the vertical overturning of the oceans to be combined in one circulation and is likely to be an important source of upwelling in this circulation, due to the presence of outcropping isopycnals and the potential for mixing due to the interaction of the flow with topography (Naveiro Garabato *et al.* 2004). The ACC's transport of 134±13 Sv ($1Sv=10^6\ m^3s^{-1}$) (Rintoul *et al.* 2001) can be measured as it flows through the relatively narrow Drake Passage. It is larger than any other ocean current.

The ACC is often referred to as a wind driven current. This is correct in the sense that the energy input is predominantly from the winds, and the main flow and predominant winds are both to the east, but the actual wind driven layer moves northwards on average. Momentum input from westerly winds drives a northwards Ekman flux in the upper 50-100m. The eastward wind stress $\underline{\tau}=\rho_a C_D|\underline{u}|\underline{u}$ has a maximum meridionally (ρ_a is the density of air, C_D the drag coefficient and $\underline{u}$ the air velocity, generally taken to be the velocity at 10m above the surface with C_D chosen accordingly). The Ekman flux

$$E_F=\tau/\rho_w f \qquad \textbf{1-1}$$

(ρ_w is the density of water, f the Coriolis parameter $2\Omega\sin\phi$, at latitude ϕ) is proportional to the wind stress and so is convergent to the north of the wind stress maximum and divergent to the south (Rintoul *et al.* 2001). This causes the isopycnals to slope up towards the south, causing a meridional density gradient, which by the thermal wind

equations (1-2) will drive an eastward baroclinic transport below the Ekman layer. Buoyancy fluxes act to enhance the meridional density gradient and so increase the flow.

$$f\frac{\partial v}{\partial z} = -\frac{g}{\rho}\frac{\partial \rho}{\partial x}$$
$$f\frac{\partial u}{\partial z} = \frac{g}{\rho}\frac{\partial \rho}{\partial y} \qquad \textbf{1-2}$$

Agreeing with this view that the density stratification is important in driving the ACC, Borowski *et al.* (2002) found very small flows in their model when they ran it with wind forcing and a homogeneous ocean, as predicted from the fact that the balance had to come from non-linear and friction terms so the flow was confined near the channel boundaries. The transport was greatly increased from <10Sv to up to 90Sv when they ran wind forcing and thermohaline forcing together on a stratified ocean, while just thermohaline forcing on a stratified ocean only produced transport of about 15 Sv. This indicates that the dominant energy source is the wind stress.

The momentum input from the westerly winds has to be balanced by a drag force, otherwise the current would be permanently accelerating. The viscosity of water cannot provide the necessary drag force because a balance between wind stress and viscosity produces a transport estimate an order of magnitude too large (Phillips and Rintoul 2000). It is believed that form drag on the bottom topography, due to higher pressures on the upstream side of rises than on downstream sides, provides the required balance (Munk and Palmen 1951). This means that it behaves differently from the gyre systems in other ocean basins where the angular momentum input that drives the circulation is balanced by a zonal pressure gradient between the 2 bounding coasts. Around the latitudes of the Drake Passage (≈56°-62°S) there is no topography within 1000m of the surface, so a free zonal mode flowing in the top 1000m can be added to any solution that tries to use Sverdrup dynamics (Hughes *et al.* 1999).

There is also a significant (but smaller) barotropic component to the ACC due to lower sea levels south of the ACC than to the north, caused by the divergent (from Antarctica) Ekman flux. A constant reduction is hard to observe but low sea levels recorded by tide gauges and bottom pressure recorders around Antarctica correlate with increased circumpolar wind stress, measured by a high index of the Southern Annular Mode (SAM) (Hughes *et al.* 2003). The SAM index is an index of the zonally averaged atmospheric

pressure gradient (Thompson and Wallace 2000). The structure is such that an increased index relates to increased eastward wind stress (westerly winds) south of 45°S and increased westward wind stress north of 45°S. At or around 45°S (the latitude of the Crozet Plateau) the SAM index therefore is an index of wind stress curl rather than wind stress. The SAM is also referred to as the Antarctic Oscillation (AAO) but SAM is used in this work.

Many of the sloping isopycnals associated with the strong flow of the ACC outcrop at the surface. As isopycnal mixing is several orders of magnitude greater than diapycnal mixing, this provides a pathway for water and nutrient to reach the surface from depth. A particular feature of the ACC upwelling compared to coastal and equatorial upwelling is that isopycnals slope up from the bottom rather than the top few hundred metres (Rintoul *et al.* 2001). This may be linked to the reduced stratification or the fact that the bottom provides the drag force for the flow (Gille 1997). These pathways allow nutrients to reach the biologically active surface layer and allow wind action to work on many isopycnal layers, which might be important in closing the global thermohaline circulation (Speer *et al.* 2000; Bryden and Cunningham 2003). Figure 1.2 summarises these connections with the world's oceans and the vertical fluxes that occur in the Southern Ocean.

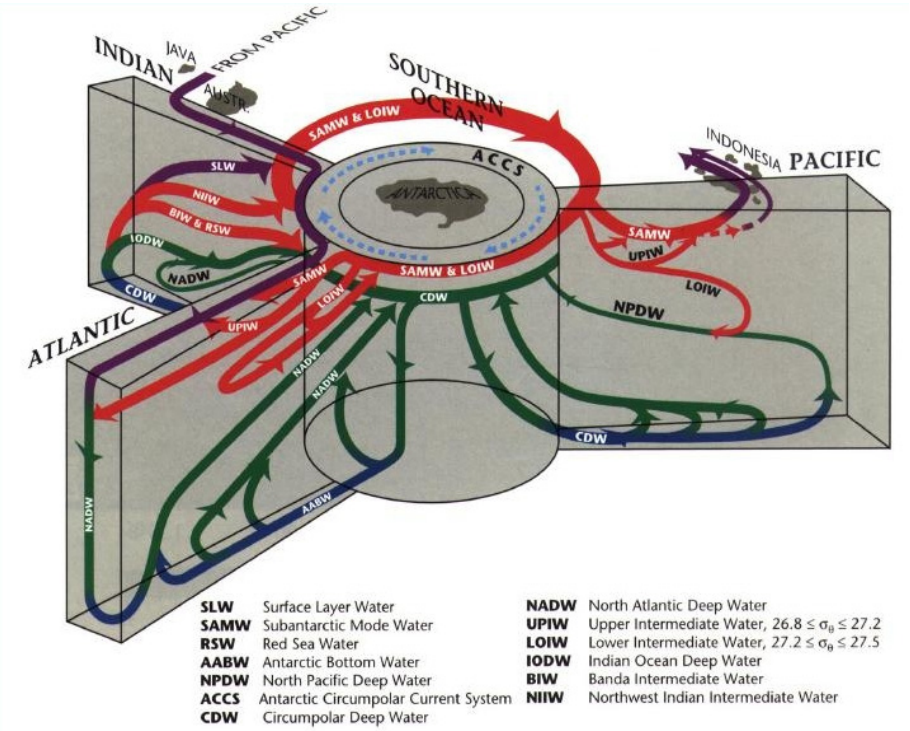

Figure 1.2 Schematic of the three-dimensional flow in the world's ocean, centred on the Southern Ocean, from Schmitz (1996)

The lack of bounding landmasses means that there can be no net geostrophic flow across the Southern Ocean. Poleward ocean heat transport across these latitudes therefore has to be by eddies and this balances the northward flux in the Ekman layer and heat lost to the atmosphere. Eddies are less effective at heat transfer than a warm southward ocean current so the high southern latitudes are colder than equivalent oceanic northern latitudes (Rintoul *et al.* 2001). The cold upwelling around the Antarctic continent due to the northward Ekman flux associated with the prevailing westerlies also helps to isolate the region from warmer waters to the north (Bryden and Cunningham 2003).

1.2.2 Fronts and zones

The transport of the ACC is not spread evenly over the latitudes of the Drake Passage, but is concentrated into narrow jets, which are seen as steps in the depth of isopycnal surfaces. These appear in most numerical models of the circumpolar flow (Gille *et al.* 2001; Tansley and Marshall 2001; Borowski *et al.* 2002)

Simplified models of circumpolar currents without initial horizontal density gradients but with forcing on the scale of the domain width, develop geostrophic flow and eddies with the flow organising into zonal jets much narrower than the domain, indicating that narrow fronts are a natural consequence of geostrophic turbulence, at least under some forcing and topography regimes. Treguier and Panetta (1994) found that stationary eddies became more important in controlling the location of the current with prominent topography but that a meridional ridge enhanced the formation of jets, as did Tansley and Marshall (2001). The separation of the jets is related to the Rhines length ($(u/\beta)^{0.5}$) in Panetta (1993) where u is the velocity of the flow and β is the planetary beta effect – the meridional gradient of the Coriolis parameter. This can be explained by the beta-effect stopping disturbances growing in the meridional direction but leaving them free to grow in the zonal direction so that they develop, in the absence of forcing (as is assumed in the consideration of geostrophic turbulence), into alternating east/west bands of flow (Naveiro Garabato *et al.* 2001). Exactly how this relates to the forced ACC over topography is not resolved but there are certainly strong qualitative similarities.

The fronts are often defined in terms of near surface criteria. These can be identified from shallow measurements and, if at the surface, satellite data. Surface criteria are useful

because surface data can be collected continuously from a ship and satellite data are the only realistic source of time series with good spatial coverage. The surface expression may not always be above the subsurface current, which is the important part of the front in transporting water and delimiting biogeochemical zones. There are many different definitions of the Southern Ocean fronts, either due to authors using different water mass characteristics or the surface expressions varying with longitude and time. These were summarised in Belkin and Gordon (1996) south to the Polar Front. The following definitions are the ones they used.

- Agulhas Return Front (ARF): south of Africa, 10°C isotherm descends from above 300m to below 800m, this range decreasing to 350m-700m north of the Crozet Plateau.
- South Subtropical Front (SSTF): subsurface S_{max} south of the front plus a sharp change in S_0 across 35.0.
- Sub-Antarctic Front (SAF): existence of intermediate S_{min} and Sub-Antarctic mode water thermostad north of the SAF.
- Polar Front (PF): northern terminus of T_{min} layer bounded by 2°C isotherm in 100-300m layer (summer); vertical 2°C isotherm (winter).
- Southern Antarctic Circumpolar Current Front (SACCF): (from Orsi *et al.* 1995) temperature >1.8°C along a temperature maximum deeper than 500m to north; salinity greater than 34.73 along a salinity maximum deeper than 800m to north; oxygen less than 4.2ml l^{-1} along an oxygen minimum deeper than 500m to north and temperature minimum <0°C shallower than 150m.

These definitions summarise the situation in many different locations at the time the measurements were taken. However fronts meander, fragment into filaments, merge, interact and exchange water, so they will clearly vary with longitude and time and the number of strong current jets will vary with longitude (Sokolov and Rintoul 2007). It is therefore quite likely that the distribution of water mass properties around a front at a given time and place will not exactly match the definition, especially if it is a scalar definition such as the location of a particular isotherm. Thorpe *et al.* (2002) found a θ_{min} of 0.5°C north of the SACCF but 0.75°C south of it, contrary to part of the definition above. The location of the front was clear in the θ-S space and in the density profiles.

They found a geopotential anomaly of 4.5 J kg^{-1} on all three of their crossings of the SACCF. They then used the geopotential anomaly to determine the location of the SACCF in historical data and found the contour to turn north at 35°W, 400km east of previous estimates, although closed contours of the chosen geopotential anomaly to the west indicate variability and considerable uncertainty in the location of the retroflection. Barth *et al.* (2001) used the geopotential anomaly at 51 m relative to 275m to identify the PF as there was too much mesoscale variability in the temperature data to apply the above definition.

Although there are advantages to measuring the flow at depth and considering the location of significant transport, the time a CTD cast takes and the length that hydrographic sections have to be means that casts are generally several 10s of kilometres apart, which can be insufficient for resolving two close but distinct fronts. Holliday and Read (1998) used continuous sampling of temperature and salinity from the ships intake to locate surface fronts south of Africa. The extra resolution (less than 1km if needed) allowed them to separate the ARF, STF and SAF which appear as the 'Crozet Front' in hydrographic sections and to give more accurate widths of the surface features, the SAF being measured as 141km wide.

It is useful to define zones in the Southern Ocean because different regimes exist in different areas. The differences include the abundance of different nutrients and plankton species, temperature and salinity levels and which is dominant in controlling density. Where the fronts are distinct, such as in the Drake Passage, the zones are defined between fronts, and generally named after the front to the south. However there are problems with this in some areas, such as around the longitude of the Crozet Islands. Here the transport associated with the PF and SAF merge over the South-west Indian Ridge but split into three pathways downstream, while north of the Crozet Islands the SAF, STF and ARF all come very close (Pollard and Read 2001). Pollard *et al.* (2002) defined zones in terms of water mass properties and the relative importance of temperature and salinity to density, arguing that these would be circumpolar features whereas current jets are not. The boundaries will often coincide with fronts where they are well defined due to the rapid change of water mass properties across most fronts. However, where there are gradual changes in water mass properties but no clear fronts the boundaries of the zones will still

be defined somewhere. These areas will show a cline of properties from one zone to another and so characteristics of both zones should be considered to have some influence. Rintoul and Sokolov (2001) found that the fronts south of Australia have multiple transport maxima and could not be considered well-defined features.

1.2.3 Effects of topography

If the ACC was purely barotropic and free from vorticity forcing, potential vorticity (PV) conservation would require it to follow contours of $(f+\zeta)/H$ where:

f=Coriolis parameter $=2\Omega\sin(\theta)$=planetary vorticity
Ω=rotation rate of earth
ζ=relative (local) vorticity $= (\nabla \wedge \underline{u})_z$
$\underline{u}$=flow vector
H=depth of ccean

ζ is smaller than f (Allen and Smeed (1996) found $\zeta=0.8f$ in a strong vortex but mostly ζ is less than 0.2f) so the PV is often approximated as f/H (Hughes and Killworth 1995; Park *et al.* 2001). In most places variation in the bottom slope is dominant over variations of f with latitude. Flow along closed contours of f/H is free in the sense that, except for frictional effects, it continues in the absence of forcing. Flow along blocked contours needs forcing in order to cross f/H contours at the blockage. A related quantity, Ertel's potential vorticity (1-3) applies in purely baroclinic cases, θ is any conservative thermodynamic property, such as potential temperature (Gill 1982).

$$\frac{\partial\theta}{\partial z}\left(\frac{f+\zeta}{\rho}\right) \qquad 1\text{-}3$$

Moore *et al*. (1999) located the PF from steep meridional gradients in satellite sea surface temperature (SST) data from Advanced Very High Resolution Radiometer (AVHRR). They found that the location of the front was variable in flat basins but well constrained in areas with steep topography, although mesoscale variability was increased near and downstream from such areas. In the study area, there are areas of steep topography around the Del Cano Rise and Crozet Plateau but also areas of much shallower slopes.

The ACC is, however, clearly not purely barotropic because the speed of the currents varies considerably with depth. Neither is it stratified strongly enough for the upper layers above the topography to be completely separated from the effects of the bottom slope. It was found in the FRAM model that the current direction did not change significantly with depth and that the flow was likened to an equivalent barotropic jet where the flow was everywhere parallel to, and a function of, the velocity at another depth (Killworth 1992). To assess the extent of topographic steering,

$$c=|\cos\theta|$$
$$=|u\cdot\nabla h|/(|u|.|\nabla h|) \qquad \textbf{1-5}$$

was calculated (after a 2° smoothing of topography) as a measure of the angle between the flow and bottom gradient and plotted against topographic slope. The average value of c was found as 0.54, which is statistically significantly smaller than the expected average of 0.637 if there was no topographic steering. Killworth (1992) showed that c is initially higher than 0.5 for shallow slopes and drops to about 0.4 for steeper bottom slopes. It could be interesting to study the output from finer scale models in smaller regions with significant bottom topography. The value of 0.4 is still reasonably high which indicates that the flow has considerable ability to cross bottom contours, which implies vertical velocities at the bottom or that the current can change direction significantly with depth. Park *et al.* (1993) found meridional flow at depth below the ACC so the flow clearly changed direction with depth. The FRAM model only extended north to 20°N so it possibly had a reduced meridional circulation, enhancing the appearance that flow was equivalent barotropic.

Craneguy and Park (1999) considered the spatially integrated PV equation applied to an inertial jet with the velocities specified at the top, bottom and a point in the middle with depth controlled by parameter c (indicates depth of maximum shear)

$$\kappa-\kappa_0+\beta V(y-y_0)/M-f_0T(h-h_0)/M=0 \qquad \textbf{1-7}$$

where κ is the jet curvature, $f=f_0+\beta y$, subscript 0 indicates the value from the initial configuration, h is the ocean depth, n the across-front direction and:

$$V = \int_{n\to-\infty}^{n\to\infty} \int_0^h v\,dn\,dz$$
$$M = \int_{n\to-\infty}^{n\to\infty} \int_0^h v^2\,dn\,dz \qquad \textbf{1-9}$$
$$T = \int_{n\to-\infty}^{n\to\infty} v(z=h)\,dn$$

They applied this to the topography of the South-west Indian Ridge to investigate the influence of topography in the splitting of the SAF from the PF. They found that, for a strongly baroclinic flow (V/T=10h) a bottom velocity of 3cm/s was needed for the SAF to turn north away from the PF. A lower bottom velocity was needed for a more barotropic case (V/T<10h). The SAF transports 50Sv (Pollard and Read 2001), is 140 km wide at the surface (Holliday and Read 1998), is about 4000m deep and so, if purely barotropic, would have a speed of about 9cm/s. An estimate for bottom velocity under jets is 2cm/s (Gille 2003) so, for these data, V/T=4.5h so 2cm/s bottom velocity is probably sufficient for significant topographic control by the SW Indian Ridge.

1.2.4 Water masses

Due to different conditions in the formation regions there are different bodies of water in the oceans with (amongst others) different temperature, salinity, oxygen and nutrient concentrations. Once out of contact with the surface the properties are changed very slowly by mixing with surrounding water masses, so a water mass can be identified far from its source region (such as North Atlantic Deep Water in the ACC), although it may not have identical properties to water of the same type closer to the source area due to the effects of mixing.

The definitions of water masses vary with different authors and locations. The following is from Rintoul *et al.* (2001) and Park *et al.* (1993). Most water masses can be identified by their position on plots of temperature against salinity for water at different depths.

Surface Waters are split into three. Antarctic surface water has T<5°C and a temperature minimum of 2°C due to the winter mixed layer not warming in the summer.
Sub-Antarctic surface waters have T<9°C, salinity S<34.0 and an O_2 maximum at 100-150m. Subtropical surface water is found north of the ACC and has T>12°C and S>35.1. It has a surface mixed layer 50-100m deep.

Mode Water is found beneath the surface waters and is formed by deep winter convection, which means that it is well mixed and thus has low potential vorticity.

$$PV = |f+\zeta|/h \qquad \textbf{1-11}$$

H is the depth of pycnostad, so large h gives small PV. It is characterised by an O_2 maximum at 300-500m but other properties vary with longitude indicating that it is produced locally. The properties mean the water mass can be traced into the subtropical gyres where it renews the lower thermocline. To form these characteristics, the upper 500m (the winter mixed layer) must be cooled by 0.5°C and freshened by 0.1 psu. For this to be achieved by air-sea fluxes this would require a loss of 10^{10}J and an input of 1.5m of fresh water. These fluxes are unrealistic (Rintoul and England 2002) so the changes must be largely due to mixing in of colder and fresher water from the south. This process would also explain why the temperature and salinity fields are mostly density compensating

Antarctic Intermediate Water has a salinity maximum at 1100-1300m and is strongly modified in the Crozet Basin (Park *et al.* 1993). It is only created in the SE Pacific and SW Atlantic and is then advected by the ACC.

Circumpolar Deep Water is often split into upper and lower parts. The upper part has an O_2 minimum at 1600-1800m north of the frontal zone and 1000m to the south, indicating the slope of properties up to the south as the isopycnals slope up in the fronts. The lower layer has a salinity maximum, indicating that it has some high salinity North Atlantic Deep Water mixed into it.

1.2.5 Mixed layer processes

The mixed layer is an area with low vertical density gradients at the ocean surface. The homogeneity is caused by turbulence, the energy for which comes from wind stress and heat loss at the surface (Donlon and Robinson 1997). The mixed layer depth is important for a range of biological (including light availability and nutrient supply) and physical (SST and air sea gas exchange) quantities. Measurement of the mixed layer depth is,

however, subjective because it depends on the definition of the base of the mixed layer (Kara *et al.* 2000). The mixed layer is variously defined as either the shallowest depth for a set change (the actual change varying with study) in temperature or density or the depth of a prescribed stratification strength. The effects of this variation are summarised in Kara *et al.* (2000) but they still conclude that definitions should vary according to the location and season. This lack of a clear definition of the mixed layer depth leads to problems in comparing between different studies of the mixed layer, between observations and models, and between geographical areas.

Mixed layers deepen if turbulence erodes the stratification at the base of the mixed layer. This turbulence can come from a range of sources – including convection due to surface cooling (Donlon and Robinson 1997), shear instabilities at the base of the mixed layer (Skyllingstad and Smyth 2000), Langmuir circulations (Li and Garrett 1997) and other wind driven turbulence (Chen *et al.* 1994). The extent to which the mixed layer deepens in such events is dependant on the strength of the turbulence and the strength and nature of the existing stratification. Where temperature dominates salinity in creating a density gradient, such as the Sub-Antarctic Zone (and more extremely but less relevantly the North Atlantic), convection can more easily create deeper mixed layers.

Factors that reduce the mixed layer depth – thermal heating and freshwater input – act at the surface. Under circumstances when these factors are dominant, the new depth of the mixed layer depends on the depth of penetration of the increased buoyancy. The penetration depth is controlled by the attenuation of the incoming irradiance and the depth of turbulent mixing. Shortwave irradiance has an e-folding length scale of about 25m (less in water with high phytoplankton or suspended particle concentration). Therefore, under calm conditions with little turbulence, a shallow mixed layer can form at a depth independent of the previous, deeper depth (Chen *et al.* 1994). Mixed layer depths can therefore decrease rapidly, with potentially significant implications to phytoplankton. A stepwise density profile can occur where previous mixed layers are still evident below recently formed shallower layers. These steps can make the diagnosed mixed layer depth very sensitive to the criteria used to define the mixed layer.

The mixed layer acts as an averaging depth for surface fluxes and light availability to phytoplankton. It can vary by approximately an order of magnitude and therefore

accurate knowledge of the mixed layer is necessary for assessing variations in sea surface temperature and salinity and the growth parameters (balance between photosynthesis and respiration) for phytoplankton.

The physics of the surface layer are further complicated by the differing attenuation of differing wavelengths in water. Incoming shortwave radiation can penetrate 10s of metres into the mixed layer whereas longwave radiation can only penetrate 10s of μm (Donlon and Robinson 1997). Sensible heat loss from the ocean is by longwave radiation and latent heat loss, which occurs at the air-sea interface. This leads to a skin temperature that is different from the bulk mixed layer temperature (by up to 1°C). It is normally cooler due to the differing penetration distances of heat gain and loss, but can be warmer (Donlon and Robinson 1997). This surface layer is measured by satellites as the SST (although different satellites use different wavelengths and therefore average over different depths) and so *in situ* measurements from 1-10m (bulk) SST and satellite values are not necessarily immediately comparable. The skin temperature also controls gas transfer velocities between ocean and atmosphere.

It is a difficult process to model the mixed layer depth because a large number of atmospheric variables can cause turbulence or affect the buoyancy flux (wind stress, incoming shortwave radiation, incoming and outgoing longwave radiation, latent and sensible heat flux, freshwater input). In addition, the physics of the mixed layer occurs mostly at length scales too small to be captured in a model leading to the need to parameterise the effects of turbulence and convection, including three dimensional processes such as Langmuir circulations. This often leads to the need to tune models to fit an existing time series in an area (Kara *et al.* 2003). The sampling interval at which data are available is also important because responses are generally non-linear. Advection of water can also significantly affect the mixed layer depth or the response to further forcing due to changes in the overall stratification. It is therefore difficult to model the mixed layer depth in areas such as the Crozet area where data are only available at sparse length scales relative to the length scales of interest and is unlikely to be sufficiently accurate due to the lack of *in situ* observations. Advection is also important, particularly close to the islands.

1.2.6 Long-term variability and changes in the Southern Ocean

Due to the remoteness of the Southern Ocean there are few areas within it where a series of measurements with high temporal resolution exists. Observations of trends in the area are therefore either from a few specific locations or from ocean scale climatologies. Any changes are likely to be important due to the way that the Southern Ocean connects the other ocean basins. Studies that have made use of repeated observations have found reductions in the salinity in a range of localities (Wong *et al.* 1999; Curry *et al.* 2003). This could be linked to increased melting of ice, releasing more freshwater into the ocean. If these studies are representative of wide areas, this increase in freshwater content and associated reduction in density could result in changes to the production of dense water that sinks to depths and therefore to the vertical circulation of the Southern Ocean.

Two studies using the climatological approach (Gille 2002; Levitus *et al.* 2005) have found widespread warming in the Southern Ocean. This could be due to an overall increase in heat content, but the dynamical response to increased wind stress would also create a similar effect due to isopycnals moving southwards. This would lead to an increase in water temperature at a fixed location.

The increase in the SAM index suggests that wind stress across the Southern Ocean has increased. The structure of the SAM is such that an increase in SAM index corresponds to an increase in the eastward wind stress (westerly winds) south of 45°S and a decrease in eastward wind stress north of 45°S (Thompson and Wallace 2000). It therefore increases wind stress over the Southern Ocean, as this is south of 45°S and already has predominantly westerly winds. Around 45°S, the approximate location of the Crozet Plateau, the dominant effect of the SAM should be a variation in the wind stress curl (increasing with higher SAM). The cause of the increasing trend of the SAM has been ascribed to both the reduction in stratospheric ozone (Thompson and Solomon 2002) and the effects of global warming (Fyfe *et al.* 1999).

The increased wind stress around Antarctica associated with the positive phase of the SAM leads to increased Ekman divergence away from the continent. This is seen in sea level height around the coast of Antarctica (Aoki 2002). Hall and Visbeck (2002) observed in model output a significant link between high SAM index and an

intensification of the ACC. The increased divergence of heat away from Antarctica associated with this change in surface forcing and circulation led to increased sea ice with increased SAM. The effect of SAM on the wind stress curl can also have dynamical consequences around Southern Ocean islands due to variations in the convergent Ekman flux. This has been demonstrated around Kerguelen Islands (Meredith and Hughes 2004).

The El Nino/Southern Oscillation (ENSO) is a source of variability in ocean and atmosphere at a planetary scale. Links have been demonstrated between ENSO indices and SST in the Southern Ocean over timescales of 17-18 years (Kwok and Comiso 2002; Trathan and Murphy 2003). Due to the infrequency of ENSO cycles there is insufficient data to investigate them in this study, although there is the possibility of effects (possibly lagged by several years) from the 1997/8 El Nino event.

1.3 Productivity

1.3.1 Necessities for life

Phytoplankton need light, CO_2, O_2 and nutrients to grow and reproduce. The nutrients they need are a source of nitrogen – nitrate, nitrite, ammonium or (for nitrogen fixers) dissolved nitrogen; phosphate; orthosilicic acid, hereinafter silicate, (for some classes, including diatoms) and micronutrients, such as iron, zinc and manganese. Any of the above could be a limiting factor, although generally it is not magnesium, calcium, potassium, sodium, sulphate, chloride, CO_2 or O_2 in the open ocean (Lalli and Parsons 1997).

Light is clearly a limiting factor in winter at high latitudes and can be limiting at other times if the mixed layer is deeper than the critical depth. This is defined as the depth over which depth averaged losses (respiration and grazing) are balanced by depth averaged growth through photosynthesis. There needs to be sufficient forcing for the mixed layer to frequently overturn for this approach to be valid (Huisman *et al.* 1999). In some cases, often before restratification in spring, the mixed layer is quiescent enough for there to be little transfer of phytoplankton between the euphotic zone (zone with enough photosynthetically available radiation for net growth of phytoplankton at a fixed depth) and the part of the water column between the euphotic zone and the base of the mixed

layer. This can lead to phytoplankton growth occurring before density stratification. In areas where the mixed layer is very variable there will also be losses through dilution as the mixed layer deepens and some phytoplankton will then remain below the temporary pycnocline once restratification occurs.

1.3.2 Carbon export

The uptake of carbon by phytoplankton and the subsequent sinking of the carbon to deep waters and the sediment (possibly via zooplankton grazing) removes CO_2 from the surface waters of the ocean. Surface waters equilibrate with the atmosphere and so this is a sink of atmospheric CO_2 (Figure 1.3). This has been termed the biological pump (Eppley 1972). The timescale of overturning of the world's oceans is 1500 years on average so this can represent a long-term removal of carbon from the atmosphere, relative to the time scales of anthropogenic influence on CO_2 concentrations. The small percentage of carbon that enters the sediments is removed for a much greater period, probably $>10^7$ years. Under constant conditions, the removal of carbon to deep waters is balanced by outgassing of CO_2 from upwelled waters, but an increase in the biological pump does represent a long-term removal of carbon so long as the increase is away from a strong upwelling region.

Artificially increasing the biological pump has been proposed as a method for sequestering anthropogenic CO_2 and studying the efficiency of such a method is one context of the CROZEX project. Measuring the effects of iron enrichment from ships on deep carbon export has proved difficult, possibly due to the relatively small scales of the blooms created and the timescales of observations.

It has also been hypothesised that the biological pump was stronger in the Southern Ocean during glacial periods (Martin 1990) due to increased dust input (that being due to reduced terrestrial vegetation) although the balance between this and the reduced effective area of the Southern Ocean (due to increased sea ice extent) means that it is likely that this process can contribute at most 30 ppm of the 80-100ppm change in atmospheric CO_2 concentrations observed (Bopp *et al.* 2003).

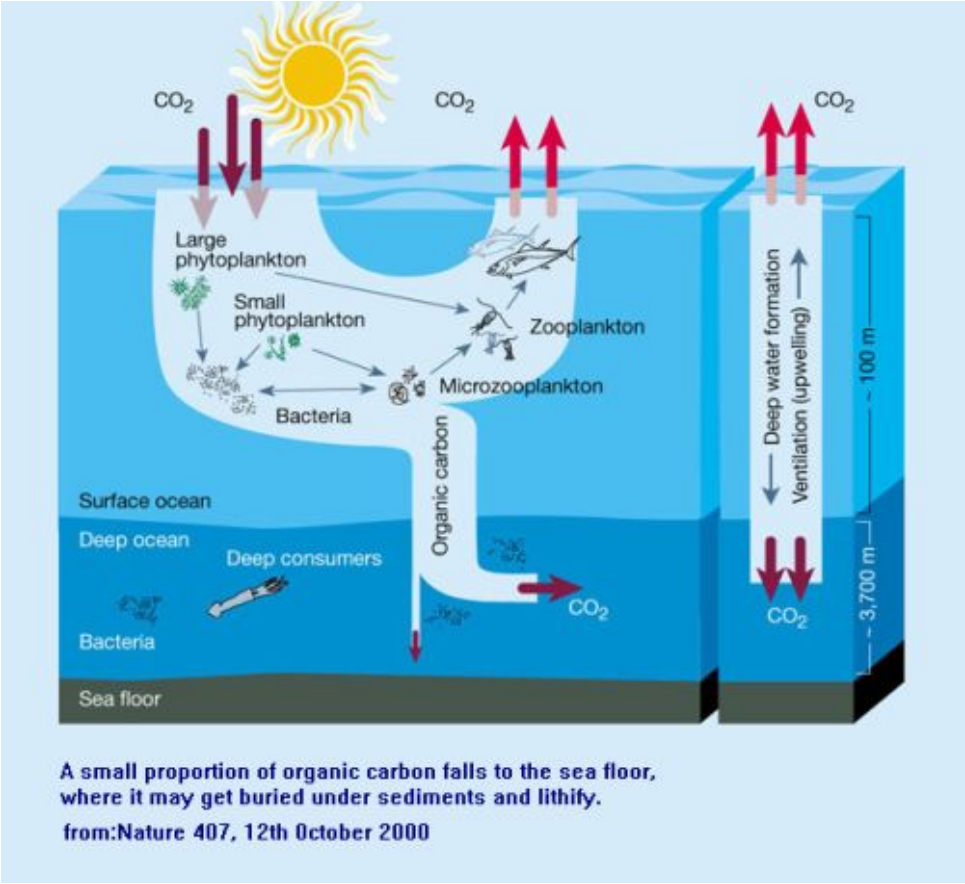

Figure 1.3 Schematic of the biological carbon pump (left) and dissolution pump (right).

CO_2 is also removed to deep water through the physical dissolution pump (right hand panel of Figure 1.3). This effect is due to the increased CO_2 concentrations of the sinking water, which has been in contact with present day atmospheric concentrations, relative to the CO_2 concentrations in upwelling water, which was mostly exposed to pre-industrial CO_2 concentrations when it formed (Sabine *et al.* 2004).

1.3.3 Nutrients

The three dimensional flow described in section 1.2.1 brings water from close to the bottom of the Southern Ocean to the surface, leading to a very strong vertical supply of nutrients to the surface layers. Estimating the upwelling from Ekman divergence, Pollard *et al.* (2006) estimated the vertical supply of nitrate and silicate to be 13.7 and 50.8 Tmol $year^{-1}$ respectively. Martin (1990), using an upwelling of 60Sv for the Southern Ocean and an estimate for nitrate concentration and the Redfield ratio, calculated a potential new production of 40 mmol C m^{-2} day^{-1} for the summer months. The discrepancy

between this and the observed production of 1.6 mmol C m^{-2} day^{-1} is used as support for his hypothesis that iron is limiting in the Southern Ocean.

Figure 1.4 shows that the resulting surface concentrations of nitrate are higher than in any other part of the world's ocean. The distribution of phosphate, to first order, is the same as for nitrate but at $1/16^{th}$ of the concentration (the Redfield ratio) so is not shown. Most of the world's ocean is limited by the availability of macronutrients (nitrate and phosphate) so this large supply of macronutrients to the Southern Ocean makes it possible that there could be extremely high productivity in the Southern Ocean. There is also a similar pattern to the distribution of silicate in the surface waters (Figure 1.5) although the peak concentrations are further south, linked to the deeper remineralisation of silicate exported from the surface ocean. Silicate is not a prerequisite for phytoplankton but where it is present siliceous organisms, especially diatoms, often dominate, especially when productivity is high (Hoffman *et al.* 2006).

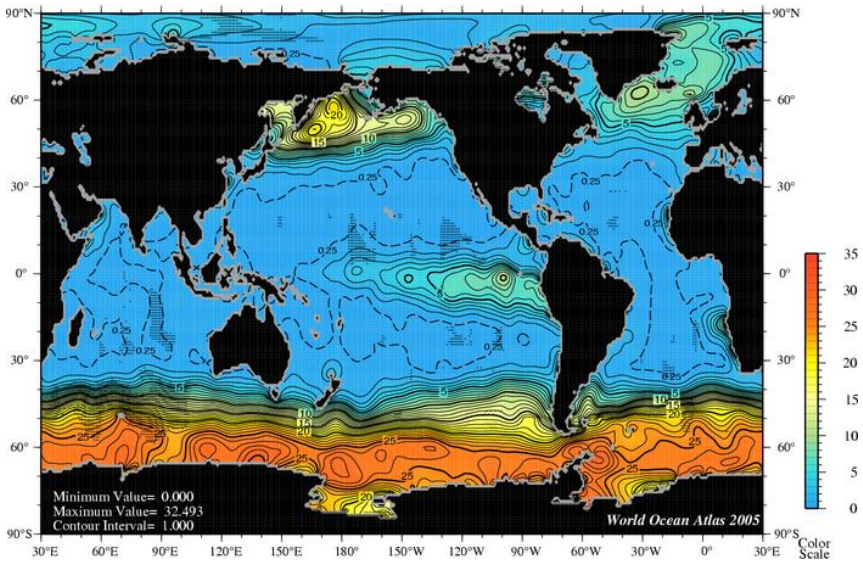

Figure 1.4 Climatological surface nitrate concentrations (µmol/l) from the 2005 World Ocean Atlas.

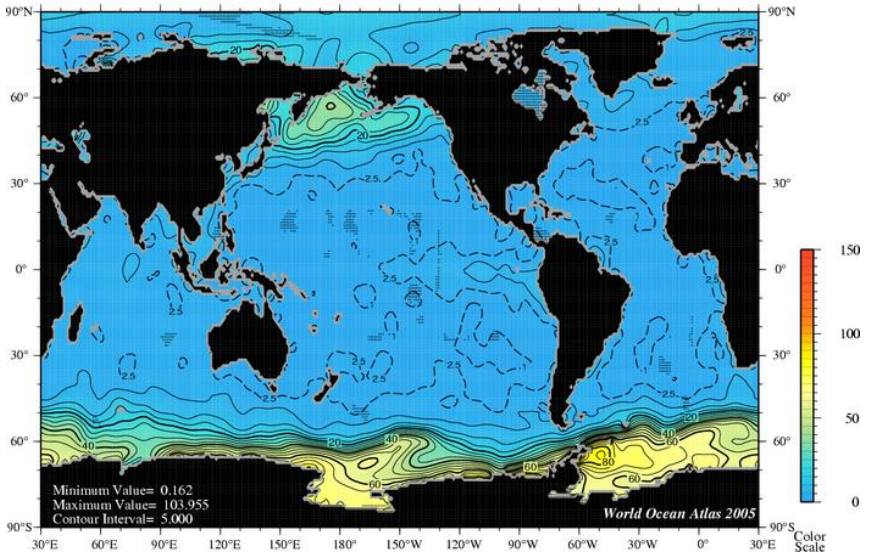

Figure 1.5 Climatological surface silicate concentrations (µmol/l) from the 2005 World Ocean Atlas.

The distribution and biological utilisation of silicate is such that, unlike nitrate and phosphate, it reduces to limiting values over parts of the study area during the growing season. For this reason changes in silicate are sometimes considered in this work but changes in nitrate and phosphate are not. Although silicate is not itself necessary for phytoplankton in general, a reduction of silicate to limiting concentrations when the phytoplankton community structure has developed in the presence of silicate can have significant consequences. It will force a faunal shift towards non-siliceous species that have until that point been out-competed by the diatoms.

1.4 High nutrient low chlorophyll conditions

Most of the oceans are oligotrophic, that is one of the macronutrients limits phytoplankton growth, but this is not the case in the Southern Ocean where high levels of macronutrients are still found at the end of the growth season. The area is therefore referred to as a High Nutrient, Low Chlorophyll (HNLC) region. There are other HNLC areas (North Pacific and Equatorial Pacific) where macronutrients are significantly above limiting levels but primary productivity is not high enough to deplete them through the seasonal cycle (Martin *et al.* 1990; Coale *et al.* 1996; Johnson *et al.* 1997; Boyd *et al.* 1999; Boyd *et al.* 2001; de Baar *et al.* 2005).

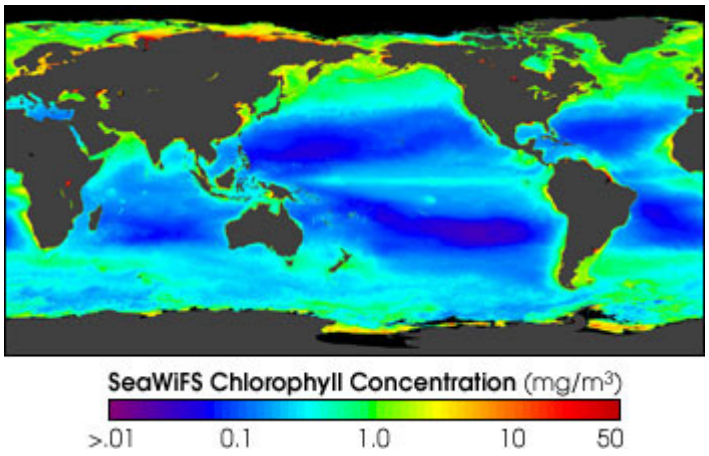

Figure 1.6 Annual mean distribution of chl-a across the world's ocean.

The description 'low chlorophyll' is relative to the concentrations (>5mg m^{-3}) that would be expected if there were no other significant limits on phytoplankton growth – under which circumstances growth continues until self-shading effects cause light limitation – rather than relative to other locations in the ocean. Many of these HNLC areas have higher chl-a concentrations than certain oligotrophic regions (Figure 1.6). Also, in areas considered exceptions to the HNLC conditions (high chl-a concentrations within a wider area considered HNLC) such as the sites of major blooms around islands, the macronutrients (with exception of silicate in some cases) are not fully utilised by the end of the bloom, which in most cases is before light is limiting again. The alleviation from HNLC conditions is therefore not complete.

HNLC areas are of particular interest for climate studies, both on glacial-interglacial and global warming timescales. This is due to the potential for significant changes in the strength of the biological pump in these areas if there is greater usage of the standing stock of nutrients. Any such change in usage of the nutrients could also have impacts elsewhere in the global ocean as they will affect nutrient availability downstream in the global overturning circulation (Sarmiento *et al.* 2004).

There have been numerous theories proposed to explain the lack of utilisation of the macronutrients. These all relate to the other conditions experienced by phytoplankton. Temperature (Reay *et al.* 2001) is a factor determining rates of growth and nutrient uptake, but phytoplankton blooms are associated with ice melt (Arrigo and van Dijken 2004) in waters <0°C, showing that low temperatures cannot be the proximate limiting

factor. Micronutrient (especially iron) availability, light availability, and grazing are discussed in detail below, followed by consideration of interactions between these factors.

1.4.1 Iron

Iron has been proposed as a limiting micronutrient in HNLC areas. Iron addition experiments onboard ships (Takeda 1998; Franck *et al.* 2000; Sedwick *et al.* 2002) and in the ocean (Coale *et al.* 1996; Boyd *et al.* 2000; Gervais and Riebesell 2002; Tsuda *et al.* 2003; Boyd *et al.* 2004; Coale *et al.* 2004; Hoffman *et al.* 2006) result in increased phytoplankton growth rate, establishing that iron is the proximal limiting factor in the Southern Ocean.

Iron is limiting in the Southern Ocean due to the low dust supply to the region (Duce and Tindale 1991; Jickells *et al.* 2005), this being due to the recirculating westerly winds only interacting a small amount with the neighbouring land masses of South America, southern Africa and Australia. The Fe:N ratio in water upwelled in the Southern Ocean is insufficient for full biological utilisation of the nitrate. This is due to the low solubility and short residence time of iron in oxygenated seawater, which leads to greater removal of iron from deep waters and thus a reduction in the Fe:N ratio relative to the sinking particles that transport nutrients to the deep ocean (Jickells *et al.* 2005).

Other sources of iron are more localised than dust deposition. Hydrothermal fluxes are not well constrained but generally will not immediately affect the euphotic zone concentration and iron is likely to precipitate out locally to the source (Jickells *et al.* 2005) In shallow waters iron supply from the sediments is found to be dominant in the Californian upwelling (Johnson *et al.* 1999) system and around and downstream of the Kerguelen Plateau (Blain *et al.* 2001; Bucciarelli *et al.* 2001; Blain *et al.* 2007). Sedwick *et al.* (2002) suggested that the slightly increased levels of iron measured in the Crozet basin were from an iron source around the Crozet Plateau.

Iron is a necessary element for phytoplankton due to its presence in components of the photosynthesis electron transfer system (Strzepek and Harrison 2004). Iron is also needed

to synthesise the enzymes that reduce nitrate and nitrite to ammonium (Lalli and Parsons 1997). Low iron levels therefore reduce a cell's ability to take up inorganic nitrogen. The Si:N uptake ratio in diatoms is significantly higher in iron limited environments, due to lowered N uptake and a reduction in average cell size through phenotypic shifts within a species or a change in the species composition (Timmermans *et al.* 2004). Smaller average cell size increases the surface area to volume ratio, significant because silica requirement is related to surface area as it is used to create a frustule around the cell whereas N requirement is related to the volume inside the frustule (Takeda 1998). As both Si and N are present in non-limiting concentrations, uptake will vary with the requirements.

1.4.2 Light

Light limitation has been proposed as factor causing the HNLC conditions of the Southern Ocean due to the stormy weather and deep mixed layers (Mitchell *et al.* 1991) although it now seems unlikely that light is the dominant limiting factor (Aumont and Bopp 2006; Boyd *et al.* 2007). Light limitation is however clearly evident in winter months in the Southern Ocean due to deep mixed layers and low incoming irradiance (Aumont and Bopp 2006). This is important in areas where there is a supply of bio-available iron to the surface waters (such as Crozet) because it provides time for accumulation and advection of iron without significant biological utilisation. The increase in iron during this period will lead to a spring bloom stronger than that which can be sustained by the continuous supply of iron during the period of light availability, leading to temporal structures of phytoplankton abundance and species composition within the period of light availability. Spatial structures can also be created during the alleviation of light limitation at the beginning of spring, either through latitudinal gradients in mixed layer depth and irradiance (this work) or mesoscale physical influences on pycnocline depth (Pollard and Regier 1992; Allen and Smeed 1996; Strass *et al.* 2002).

Light can also be important in influencing the dynamics of a strong phytoplankton bloom, both through the impact on the growth rate (Huisman *et al.* 1999) and through self-shading effects limiting the maximum possible phytoplankton concentration in a given mixed layer depth with a given incoming irradiance (Sverdrup 1953; Platt *et al.*

2003). In a synthesis of artificial iron enrichment experiments de Baar *et al.* (2005) showed a significant link between light availability and phytoplankton response over the different experiments, though it is not stated whether growth rate or self shading is the dominant source of the connection. During SOIREE self-shading led to a reduction in the euphotic depth, from 84m to 45m, due to the bloom induced by the artificial release of iron (Boyd *et al.* 2000). This gives some indication that self shading might be important in slowing phytoplankton growth rates near the peak of the bloom, but other experiments such as SOFEX-N (Coale *et al.* 2004) show a short timescale peak in chl-a, which is not consistent with just self-shading effects, which would produce a prolonged period of enhanced but relatively constant chl-a concentrations.

1.4.3 Grazing

Grazing pressure has also been suggested as a control on phytoplankton concentrations. Losses to grazing clearly reduce the phytoplankton concentrations but the timescale of growth for zooplankton is much greater than that of phytoplankton. Therefore, when conditions suddenly become conducive to phytoplankton growth (spring stratification or iron addition) phytoplankton concentrations can reach bloom concentrations before zooplankton populations respond.

1.4.4 Interactions between possible limiting factors

Although iron has been shown to be the proximal limiting factor for Southern Ocean productivity, all three factors are inter-related. The ecumenical iron hypothesis (Morel *et al.* 1991) proposes that low iron concentrations force a shift towards smaller phytoplankton cells because this increases the surface area:volume ratio (Fennel *et al.* 2003). This reduces the level of iron stress, as iron requirement scales with volume while the uptake rate is proportional to the surface area. Small phytoplankton are more easily grazed and the rapid growth rate of microzooplankton allows grazing control to be dominant. If the small phytoplankton are still iron stressed, their growth rates will be reduced, further allowing time for zooplankton populations to respond. This hypothesis is borne out in observations (Timmermans *et al.* 2001). Apparently counter to this hypothesis, large heavily silicified diatoms are also present in HNLC areas. These take

the alternative approach of low growth rate but reduce mortality sufficiently to allow net growth (Smetacek *et al.* 2004; Moore *et al.* 2007).

Due to the requirements for iron in the photosynthesis system, iron demand is a function of light availability (Raven 1990; Sunda and Huntsman 1997; Maldonato *et al.* 1999). Iron demand increases at low light levels due to the increased chl:Carbon ratio needed to capture sufficient photons. Under iron limitation this full adjustment may not be possible. During iron enrichment experiments chl:C ratios are observed to increase rapidly, before an increase in biomass, indicating that before enrichment the chl:C ratio was sub-optimal for the light intensity, due to iron limitation (de Baar *et al.* 2005). This has implications for using chlorophyll concentrations as a measure of phytoplankton biomass.

One factor alone does not therefore necessarily completely cause the HNLC conditions, because phytoplankton communities stressed by one factor may be less able to cope with stress from another limiting factor. HNLC conditions can nevertheless be relieved by the removal of one limiting factor, as has been seen in response to iron released from natural sources (Blain *et al.* 2007; this study and others within CROZEX, see section 1.5) and from research ships (de Baar *et al.* 2005; Boyd *et al.* 2007).

1.4.5 Exceptions to HNLC conditions

Within the broad geographical regions defined as HNLC there are areas of high chl-a, as shown in Figure 1.7. Study of the particular reasons for these exceptions helps to understand the dominant processes, both in these biologically important areas but also in the surrounding HNLC ocean. The main reasons for the exceptions are considered below.

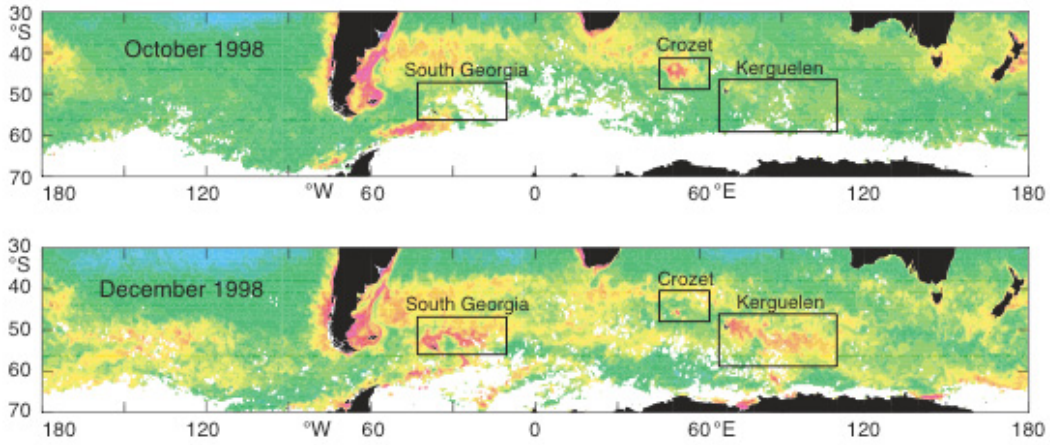

Figure 1.7 Monthly SeaWiFS images of the Southern Ocean, showing areas that have high chl-a, and the overall HNLC conditions.

1.4.5.1 Fronts

Enhanced chlorophyll is often observed along fronts. This could be due to advection of iron along the front from a source upstream (de Baar, *et al.* (1995). Moore *et al.* (1999) however found enhanced chl-a along fronts away from shallow topography. Fronts are associated with sloping isopycnals, via the thermal wind equations, and some of these reach the euphotic zone. Isopycnal mixing is much greater than diapycnal mixing so sloping isopycnals provide a pathway for nutrients to be mixed up to the surface. In summer, this may be prevented by the formation of seasonal stratification.

Potential Vorticity (PV) conservation creates vertical circulations along and across meandering fronts. $|f+\zeta|/h$ is a material invariant so h (the depth between 2 isopycnals) must increase if ζ increases (f will be approximately constant because the fluid particles are moving predominantly zonally and $|f|>|\zeta|$ is always the case). ζ is positive to the north of a westward current core and negative to the south. If the front bends to the left ζ will increase in magnitude to the north and decrease to the south (through zero if meandering is strong enough). Along the ACC (eastward, f<0 because southern hemisphere) this must lead to h decreasing to the north and increasing to the south (and then decreasing again if ζ goes through zero but still less than the change to the north). The surface of the ocean does not move so increasing h causes downwelling and decreasing h causes upwelling. An ageostrophic meridional horizontal flow must occur due to different velocities on each side of the jet core and mass conservation constraints.

This leads to a helical circulation because the ageostrophic motion is advected by the much greater geostrophic current associated with the front (Pollard and Regier 1992; Naveiro Garabato *et al.* 2001).

Cross frontal exchange will occur through this helical motion and through larger scale water mass movements driven by baroclinic instabilities of the flow. Cross-front exchange of nutrients where different nutrients are limiting on each side of the front can cause enhanced productivity along a front (Read *et al.* 2000).
The vertical motions can raise nutrients (iron being relevant in the Southern Ocean, nitrate in non HNLC areas) into the euphotic zone and hence increase biological activity. They also raise the pycnocline and so increase the mixed layer light availability. If the upwelled water is mixed away by the actions of an eddy, phytoplankton have time to fully utilise the extra nutrients. However if the waters are downwelled again then the phytoplankton may still be growing, leading to the counter-intuitive situation of phytoplankton maxima at downwelling locations (Strass *et al.* 2002). Barth *et al.* (2001) found that the phytoplankton distribution was fixed relative to meanders of the PF and not water packets, indicating a rapid response to upwelled nutrients and subduction of phytoplankton.

Hense *et al.* (2003) found mixed layers in their model of 35m in summer and 120m in winter in the PF compared to 60m and 155m away from the front. This means that more phytoplankton can survive the winter and spring in the frontal systems than in the deeply mixed layers away from the fronts. This produces a greater stock for the population to grow from in the summer, but the increased chlorophyll at the PF was only found if they included iron in the model, supporting the idea that there is sufficient light in the summer at high latitudes and that the seeding effect of the overwintering population is not dominant.

Moore *et al.* (1999), using SeaWiFS data, found that chl-a was enhanced along the fronts, especially in the vicinity of prominent topography. This included the Pacific-Antarctic ridge, which is deeper than 2000m, so this cannot be due to a direct supply of iron. Instead they considered that enhanced mesoscale variability caused localised upwelling of iron to the surface waters.

1.4.5.2 Ice edge

It is a common, although not universal, feature for chlorophyll to be enhanced in regions of ice melt (Arrigo and van Dijken 2004; Reddy and Arrigo 2006). This is due to the melt water providing stable stratification and a source of iron. It is not necessarily simnple to distinguish which is the dominant effect: even if the effect of increased iron was dominant, with changes in light not significant, a link would still be expected between shallow mixed layer depths and high chlorophyll concentrations. This is because the iron will be diluted down through the mixed layer, so deeper mixed layers will lead to lower iron concentrations. The point away from the ice where stratification broke down could also be where dilution by offshore water with low iron became significant, or mark a complete switch to such water across a water mass boundary. It is therefore hard to use such areas to study the effects of iron and light independently.

1.4.5.3 Land effects

Very high levels of iron (>10 nM) have been found in surface waters and >20nM in near bottom waters downstream from the Kerguelen Islands, compared to 0.25nM upstream of the islands in the SAF, showing strong surface and sediment inputs. At the time of measurements however there was only a modest biological response to the enhancement, with light limitation and grazing also required to explain the distribution of chlorophyll concentrations (Blain *et al.* 2001; Bucciarelli *et al.* 2001). It is clear from satellite chlorophyll images that much higher chlorophyll concentrations occur later in the season in areas with high initial iron concentrations.

Very high concentrations of phytoplankton are also found around South Georgia (Atkinson *et al.* 2001; Korb *et al.* 2004), and more widely in the Drake Passage. Although it has yet to be proven that iron from the islands or sediments causes these blooms (though work is in progress on the subject) the pattern of high productivity downstream of South Georgia contrasting with low productivity upstream (Korb and Whitehouse 2004) and the relative physiological states of the phytoplankton assemblages (Holeton *et al.* 2005) strongly imply that this is the case.

As well as having a significant impact on the local chlorophyll concentrations, the topography around Kerguelen (Park and Gamberoni 1995; Craneguy and Park 1999), South Georgia (Thorpe *et al.* 2002; Meredith *et al.* 2003; Meredith *et al.* 2005) and the Crozet Islands (Pollard and Read 2001) also significantly influences the circulation. High chlorophyll concentrations are observed in areas of both weak and strong flow. Other islands in the Southern Ocean, such as Macquarie Island, Prince Edward Islands and Bouvet, have a much less significant effect on both the local flow patterns and chlorophyll values. Some effect is seen around Prince Edward Islands (Ansorge *et al.* 1999) but it is on a smaller scale than Kerguelen, Crozet or South Georgia. It is possible the scale of the fertilisation effect is linked to effects on the circulation but geological, and possibly hydrological, differences are likely to be most important.

1.5 CROZEX

CROZEX (CROZet circulation, iron fertilisation and EXport production experiment) is a multidisciplinary project studying the causes and consequences of an annual phytoplankton bloom north of the Crozet Plateau. The study area comprises the area north and south of the plateau. The former is the location of the bloom and an area hypothesised to receive water that has been in contact with the sediments and/or islands of the Crozet Plateau while the latter is a control area where water has not been in recent contact with shallow sediments or island run-off. The focus of the science was measuring the iron flux to the bloom area and quantifying the carbon exported out of the surface ocean due to the enhanced productivity.

The majority of the sampling was carried out during a pair of cruises aboard RRS Discovery – D285 (3/11/2004-10/12/2004) and D286 (13/12/2004-21/1/2005). Full details of sampling can be found in the cruise report (Pollard and Sanders 2006) and results in a special CROZEX edition of Deep Sea Research II (Pollard *et al.* 2007). Further *in situ* underway measurements were taken during the Benthic Crozet cruise D300 (1/12/2005-14/1/2006), full details of which can be found in Wollf (2006). The aim of the Benthic Crozet project was to study the effect of the contrasting productivity regimes either side of the plateau on the benthic fauna.

Much of the cruise was planned around a series of Major Stations every two or three days. At each Major Station (M1-M10) a series of CTD casts was made. A full depth CTD with the stainless steel rosette (sCTD) to sample physical parameters, currents (LADCP) and nutrients through the whole water column and phytoplankton down to 500m; a cast with the titanium rosette (not always to full depth) for iron and phytoplankton productivity sampling; a second sCTD cast for ^{234}Th sampling and a Stand Alone Pumping System (SAPS) deployment. Other work at Major Stations included zooplankton nets, radium samples and Pelagra deployments. In between Major Stations there were some additional sCTD casts, to fill in hydrographic details, and SeaSoar tows. Underway parameters measured were temperature, salinity, transmission, fluorescence, current to 300-500m (depending on sea conditions), surface nutrients, iron from a TMS (trace metal) fish, CO_2, microbial abundance by flow cytometry, aerosols and rain.

1.6 Thesis structure

This work studies the effects of circulation and light availability on the spatial and temporal distribution of phytoplankton around the Crozet Plateau. This requires data from several sources: satellite measured ocean colour, sea surface temperature, sea surface height, irradiance and wind stress; Argo float trajectories and profiles; surface drifters; and *in situ* data from three research cruises. The sources and processing of these data are covered in chapter 2. The circulation in the study area is then investigated in chapter 3 because this controls the wide scale biogeochemical conditions as well as the local advection of iron from shallow topography. Variability in the flow pattern also needs to be considered when making comparisons between different years.

The distribution of phytoplankton is studied in chapter 4. The spatial patterns are related to the knowledge of the circulation because these are driven by the relative availability of iron. The initial temporal development of the bloom however is light controlled so analysis of this requires study of the surface mixed layer and incoming insolation. These data are presented at the beginning of chapter 5. Once the relationship between light availability and phytoplankton response is known in the initially iron-replete bloom area, this information can be used to study other areas: the bloom area after the bloom, the areas outside the bloom area, other Sub-Antarctic Islands and mesoscale iron enrichment experiments.

The relatively long time history of satellite data now allows some assessment of the magnitude and causes of interannual variability in the circulation and phytoplankton distribution. This is investigated in Chapter 6. Chapter 7 concludes this study. Appendices A and B – the full history of satellite chl-a and absolute dynamic height – are included on a CD.

2 Data sources

2.1 In situ *data*

Two consecutive research cruises, D285 and D286, were conducted to the area around the Crozet Plateau (51°E, 46°S) from November 2004 to January 2005 on RRS Discovery as part of the CROZEX project (Pollard and Sanders 2006). The work programme included CTD sections/SeaSoar tows, biological stations and underway sampling. Further underway data were collected during the Benthic Crozet cruise D300 (Wollf 2006), again on RRS Discovery, in December 2005 to January 2006. The causes of the contrast of high productivity to the north of the plateau and low to the south, together with its effects on phytoplankton community structure, carbon export and benthic fauna were the focus of the CROZEX and Benthic Crozet projects.

Figure 2.1 shows the cruise track from the cruises D285 and D286, with the area around the islands expanded as Figure 2.2. Stations were occupied north and south of the plateau to study the contrast seen in satellite images, between high chl-a to the north of the islands and low values to the south. The area close to the eastern islands – Ile de la Possession and Ile de l'Est – was the hypothesised source of iron so was studied in detail. Some station positions, especially M8E and M8W were chosen after study of near-real time satellite chl-a images from RSDAS at PML. The locations of M5 and M6 were driven by the needs of the Benthic Crozet project that required sites at the same depth with suitable topography for benthic studies where one was in a bloom influenced area and one was away from the bloom influence. The cruise track for D300 was much simpler, and ran, approximately, from M9 to M5 to M6 to M3 to M9. Due to the lack of reliable charts for the area the ship did not enter any of the shallow areas on the plateau.

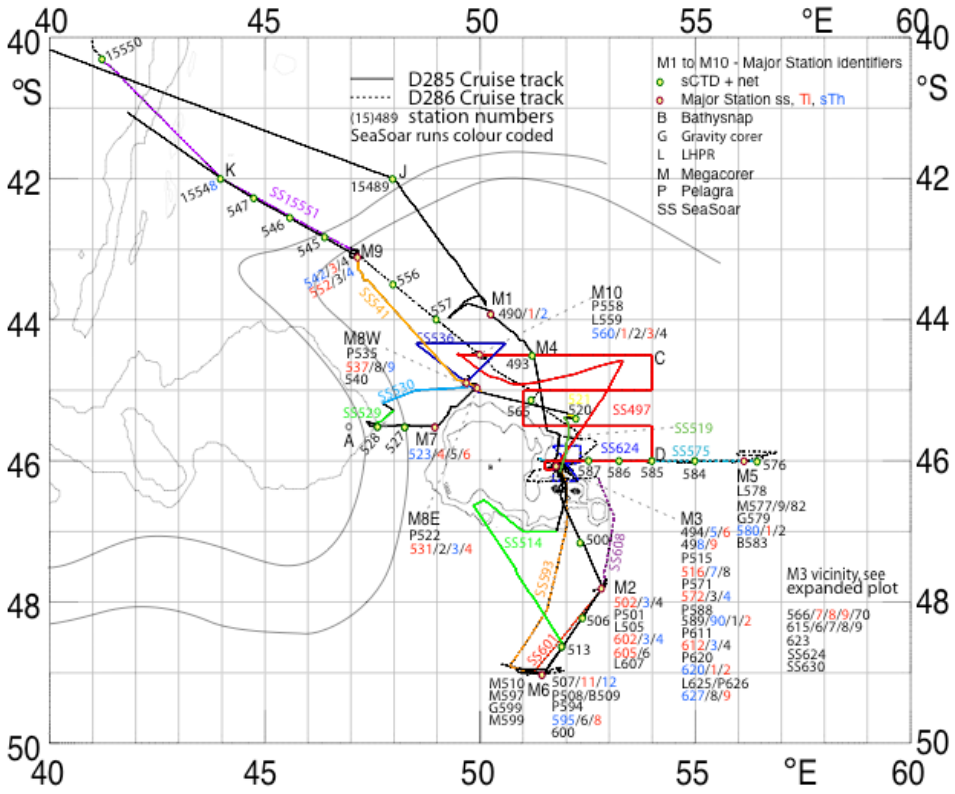

Figure 2.1 Cruise track for cruises D285 and D286. The curved lines represent the flow pattern found on previous cruises (Pollard and Read 2001).

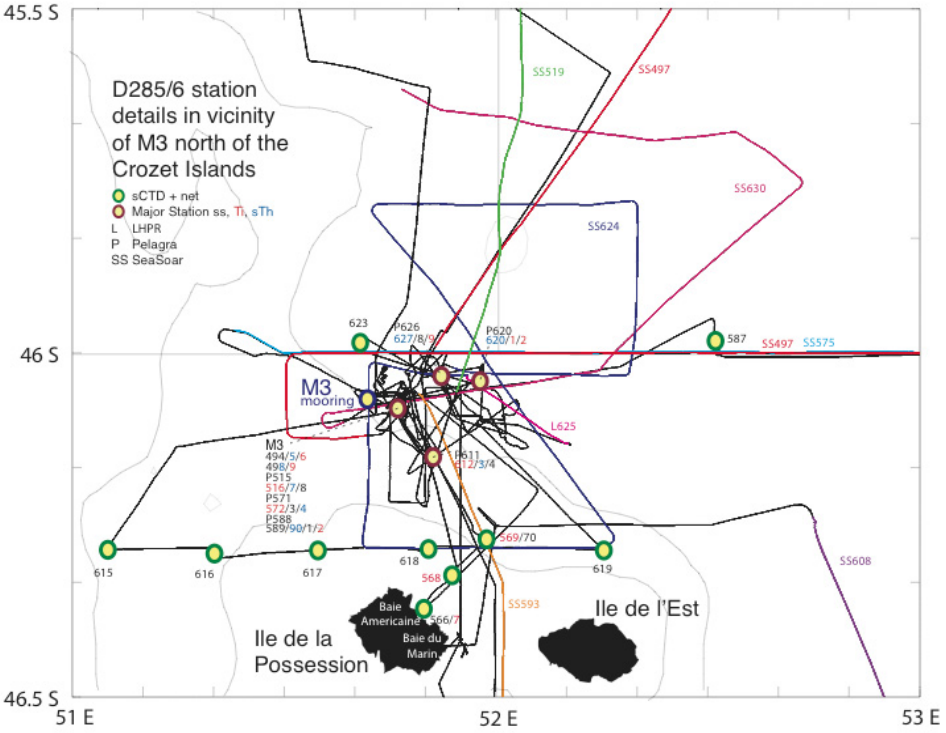

Figure 2.2 Expanded cruise track north of the eastern Islands

As the focus of the project was quantifying the export from the bloom, the ship arrived in the area after the peak of the bloom. This means that the conditions that caused the phytoplankton population to start declining have to be inferred from conditions sampled several weeks after the event. It also means that satellite data are valuable in studying the seasonal progression of the bloom to put the export figures in context. The extra spatial coverage provided by satellite images is also valuable. Due to constraints of time on the multi-disciplinary cruises and poor weather the hydrographic sections are not long enough or at sufficient resolution to fully describe and quantify the flow during the cruise, but measurements taken during the cruise have been combined with historical data in Pollard *et al.* (2007b) to produce estimates of the flow in the area.

In situ chl-a measurements taken during the three cruises have been used to locally calibrate satellite ocean colour data. Chl-a concentrations were determined from water samples collected from the non-toxic ship supply (≈5m depth) that were taken approximately hourly while the ship was in transit. Figure 2.1 shows that the cruise samples were taken from a wide area and both north and south of the plateau. Chl-a concentrations found from the 5m bottle samples from CTD casts have also been included. 200ml of seawater was filtered onto a GF/F filter. The filters were placed in 20ml glass scintillation vials and 10mls 90% HPLC grade Acetone was added for pigment extraction over 24 hours in a fridge. Chl-a-a concentration was measured using a Turner fluorometer following the Welschmeyer (1994) protocol. The fluorometer was calibrated with a chl-a standard (Sigma) read on a Spectrophotometer. It will be shown that the satellite values are lower than *in situ* values by a factor of two.

2.2 Argo data

Argo floats drift for ten days at either 1000m or 2000m (consistent for each float) and surface every 10 days, taking temperature and salinity profiles. Floats set to 1000m sometimes first sink to 2000m and then start the profile from there. Position and profile data are then relayed by satellite. They are the only source of sub-surface data other than ship-based observations and provide greater temporal and spatial coverage.

Argo trajectory, profile and meta data were downloaded from http://www.usgodae.org/cgi-bin/argo_select.pl for the area 40° to 55°S, 40° to 60°E at all times of year. All profiles southwards of 30°S, from 1st August through to 30th April of each year from 2002 and for all longitudes were also downloaded from the same location and subsets of this dataset have also been used. Figure 2.3 shows the distribution of data across the area, which is reasonably uniform in time of year and space. Exceptions are the areas of the Del Cano Rise and Crozet Plateau, which are too shallow for floats to enter, and a patch south of the Crozet Plateau, which may be due to low flow with some closed flow contours in this area, reducing the chances of a float entering the area. Figure 2.4 shows the history of data acquisition from the area. The first profiles are from 2002 but the rate of data acquisition increases significantly in late 2004 due to deployments from the D285 cruise. Although this rate has subsequently reduced slightly it is still higher than before the cruise due to the increased overall density of Argo floats in the Southern Ocean.

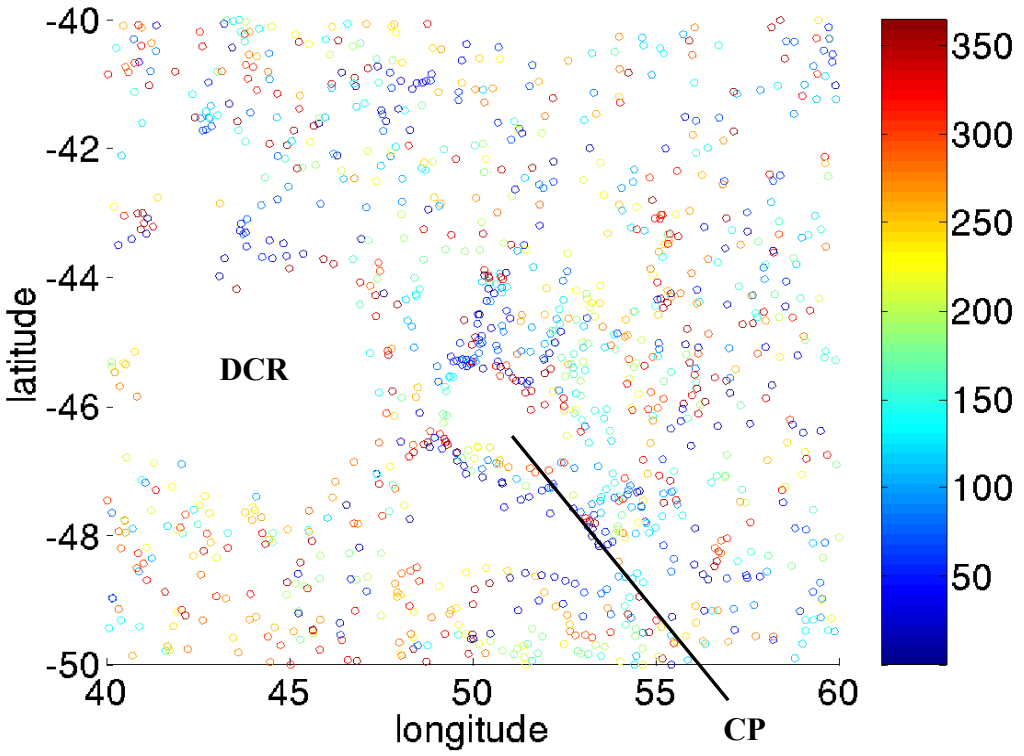

Figure 2.3 Distribution of Argo float profiles across the study area, the colour relating to day of year. DCR is the Del Cano Rise and CP is Crozet Plateau (too shallow for floats).

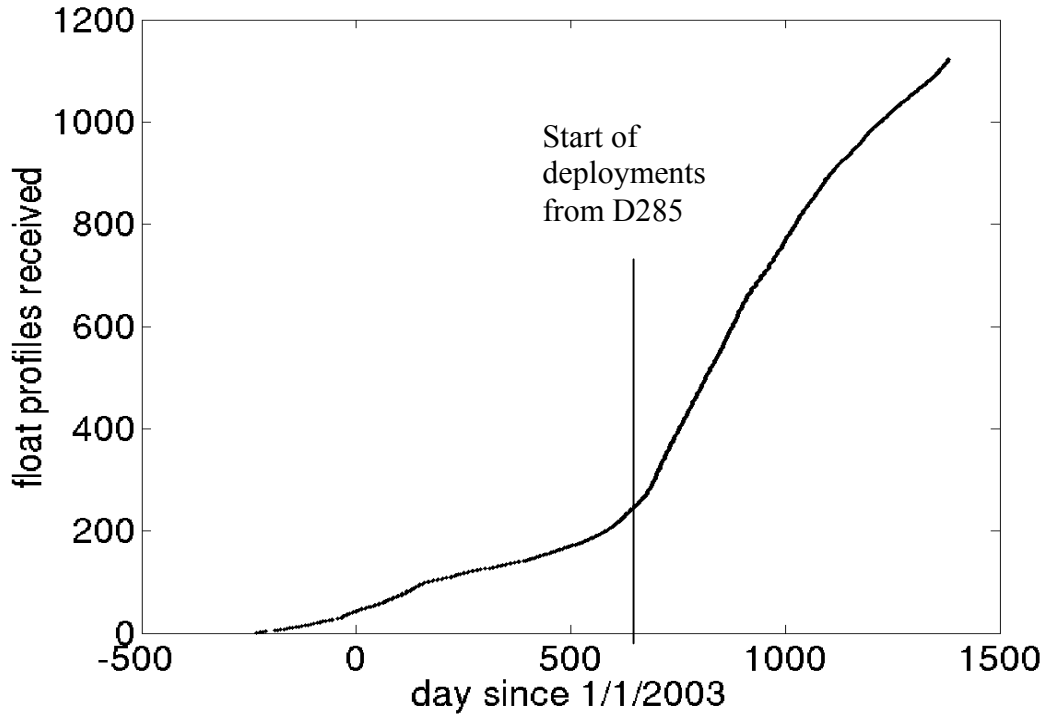

Figure 2.4 Accumulation of profile data over time in the study area.

One of the principles of Argo data is to make data available after minimal delay, approximately a day, in real-time mode. This means that the newer data have only undergone automatic checks to ensure they are within reasonable bounds. As a result of these tests each datapoint down the profile is flagged as: 0 no QC tests have been performed, 1 observation good, 2 observation probably good (implies some uncertainty), 3 observation thought to be bad but may be recoverable, 4 observation thought to be bad and irrecoverable. If all data flags are '1' then the overall quality control flag is set to 'A', otherwise it is set to 'B', 'C' or 'F'. If flags are missing then it is set to 'E'. The data are later checked more rigorously and re-released as delayed mode data with some data corrected but bad data still included, again flagged as above. Overall data quality flags were read and data were only used if all the flags were good or absent. Argo temperature and salinity sensors are rated to an accuracy of 0.005°C and 0.01 respectively.

As unchecked data and real-time data that have not been thoroughly checked have been used, further checking was done during the processing. This involved discarding profiles where the density decreased with increasing depth by > 0.01kg m^{-3} between two datapoints. Three floats had regular problems with this check and inspection of the

density profiles revealed that all profiles should be discarded. Some profiles also had spikes in density at the surface. The profiles otherwise looked good so these spikes were removed by checking the surface density value of profiles and, if too low, replacing it with the next datapoint down the profile. The profiles where this was implemented were checked to confirm that the procedure did not alter the mixed layer depth. Nearby profiles were then plotted together on one graph to check for any significant outliers. It is possible for the sensors on the floats to drift and although this is corrected for in some floats, after comparison with climatological data, real-time data are not checked for sensor drift. No outliers were found. This was a crude way of checking but a drift in a sensor is unlikely to significantly affect the mixed layer depth so further checking was not deemed necessary. This does mean that using float data for other purposes, such as characterising the temperature/salinity (T/S) relationship, should be done with caution. In total 1123 out of 1303 profiles passed the quality checks. Of these, 838 were south of 43°S – analysis of mixed layer depths excludes the area between 40-43°S to exclude the area north of the SAF, where mixed layers deepen significantly due to the increased importance of temperature in setting the density and so increased convection in winter.

The trajectories of the floats provide a useful measure of the circulation at 1000m and 2000m, but should be interpreted with some caution. Errors occur because floats can move significant horizontal distances while coming to the surface and at the surface before reporting their position. The most obvious example is from two floats that drifted into water shallower than 1000m while at or near the surface. Their trajectories are therefore significantly affected by spending time on the seabed. They did however return valuable profiles from the shallow areas.

2.3 Surface drifters

All available drogue-on data were downloaded from the NOAA website http://www.aoml.noaa.gov/envids/gld/dirkrig/parttrk_spatial_temporal.php for the area 40-50°S, 40-60°E. Drifter tracks provide a set of realisations of the surface flow across the study region. The drogue, approximately 5 metres long and centred at 15m depth, very significantly reduces the direct wind forcing on the drifter float, but this forcing will bias the tracks slightly to being downwind (and so generally eastward). While some

tracks closely follow current features seen in other sources (including surface geostrophic velocities) other drifter tracks are predominantly eastward and do not follow circulation features. It is possible that such drifters have lost their drogues, despite being flagged as 'drogue-on'. A total of 226 floats have entered, or been released within, the study area. Drifters report their position every 6 hours. They are used in this study to give examples of surface water trajectories and to estimate residence and transit times within and around the bloom area.

2.4 Satellite data overview

Remotely sensed data are invaluable in this study. Indeed the entire project was conceived after the match was seen between *in situ* hydrographic data and SeaWiFS chl-a images. There are many benefits to using satellite data. The extra coverage in space allows the cruise observations to be put into context and near real time data sent to the ship were used when deciding the sampling strategy. The extra coverage in time allows the observations made from the ship to be put into a seasonal perspective and also across years to look at the consistency and variability of the observed features. The datasets used in this study are summarised in Table 2.1.

There are also problems with satellite data and these have to be considered when interpreting the data. Firstly what is measured is largely controlled by what it is feasible to measure, rather than what it would be ideal to measure. In addition, atmospheric effects between the signal at the ocean surface and the satellite can be significant. The particular issues for each dataset are dealt with in the appropriate sections.

Table 2.1 summarises the data used and the time period they are available in – there is not a full suite of satellite data for the full period 1997-2006 of SeaWiFS data.

Sensor	Parameter	Data type and URL	Years
SeaWiFS	Chl-a, PAR	Daily and 8 day, 9km Level 3 Mapped http://oceancolor.gsfc.nasa.gov	1997-2006
MODIS	Chl-a,	Daily, 4km Level 3 Mapped http://oceancolor.gsfc.nasa.gov	2004-2006
SeaWiFS/MODIS merged product	Chl-a	Daily and 8 day, 9km Level 3 Mapped http://oceancolor.gsfc.nasa.gov	2004-2006
Merged – altimeters and GRACE	Mapped Absolute Dynamic Topography	http://www.aviso.oceanobs.com/html/donnees/produits/hauteurs/global/madt_uk.html#upd	2001-2006
QuikSCAT	Wind stress	Daily, 0.25° http://poet.jpl.nasa.gov	1999-2006

Table 2.1 Remotely sensed data used in this study.

2.5 Ocean colour data

Two sources of ocean colour data were used: the Sea-viewing Wide Field-of-view Sensor (SeaWiFS) and Moderate Resolution Imaging Spectroradiometer (MODIS). These are both NASA sensors and data are downloaded in the same way. Ocean colour data were downloaded by ftp from a file system accessed through http://oceancolor.gsfc.nasa.gov/ as level 3 mapped data. MODIS derived chl-a concentrations (O'Reilly *et al.* 1998; Feldman and McClain 2006) were processed using the standard OC3v1.1 algorithm and are available at '4km' (1/24 of a degree) resolution. SeaWiFS derived chl-a concentrations (O'Reilly *et al*. 1998, Feldman and McClain, 2006b) were processed using the standard OC4v5.1 algorithm and are available at '9km' (1/12 of a degree) resolution. Images are composites of individual swaths over either 1 or 8 days.

The 8-day images were used to study the progression of the bloom due to the extra spatial coverage they offered meaning that the data for each area were much less noisy – the main source of variation is sampling different areas as cloud cover varies. The 8-day images were used to reduce this problem while maintaining reasonable temporal resolution. For match-ups with *in situ* values, daily images were used due to the problems of advection and temporal change that could have occurred with 8-day images.

2.5.1 Processing steps and caveats

There are many processing steps that are carried out between the satellite collecting the spectral shape of the water-leaving irradiance and the production from this shape of an estimate for chl-a concentrations in the surface waters. First, the atmospheric effects have to be removed, as best they can, so that the colour of the ocean can be estimated. From the spectral shape of water-leaving irradiance an empirical function is used to estimate surface chl-a concentrations from the spectral densities at different wavelengths. This can be compromised by suspended sediment and coloured dissolved organic matter that also affect the irradiance. Differences in optical characteristics of different phytoplankton communities, or other spatial variations in atmospheric or water properties not captured in the processing, also mean that the single algorithm that is used for the entire world ocean is less accurate in certain areas, especially the Southern ocean (see section 2.5.6).

Satellite chl-a images may not give a representative impression of the contrast in biomass. One reason is that chl-a per cell is higher in areas with high iron concentration, as was seen in several iron addition experiments (de Baar *et al.* 2005). The greatest increase in chl-a:carbon observed was over four-fold at the surface (Landry *et al.* 2000). This effect is due to iron being needed for photosynthetic units, which contain chl-a (Sunda and Huntsman 1997). The deeper mixed layers found to the south will also lead to greater mixed layer integrated biomass per surface chl-a, if other factors are equal. Deep chl-a maxima also cause significant problems for interpreting satellite data from the surface in some areas but there is no evidence from CTD casts of these. Figure 2.6 shows the ratio between transmittance at mixed layer depth+20m and 14m and no other depth relative to the mixed layer showed any different pattern. Transmittance increased below the mixed layer in all cases, except two casts where deep fluorescence and turbidity was presumably a sinking mass of phytoplankton. Transmittance is to first order a function of biomass in the water, as proven by the vertical structure shown with a reduction in the mixed layer (Figure 2.5). It is used here in preference to fluorescence because the data are less noisy and to avoid problems of sunlight quenching of fluorescence causing low values close to the surface. 14 m was chosen as a surface value to avoid problems of a further surface reduction, presumably linked to moving the instrument through the skin layer and bubbles.

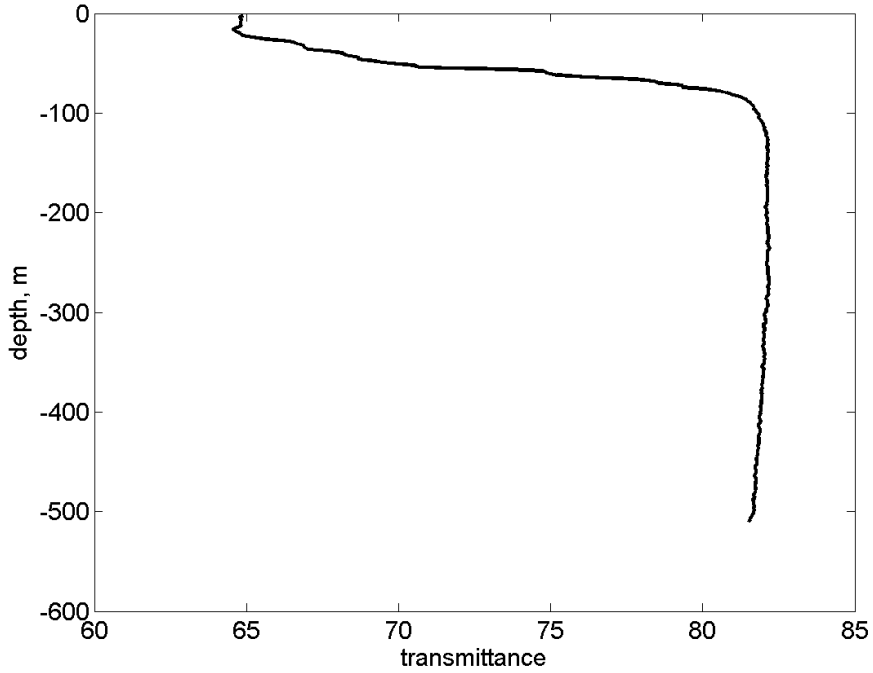

Figure 2.5 Example of a transmittance profile to show strong surface effect, which is used here as a proxy for chl-a concentration.

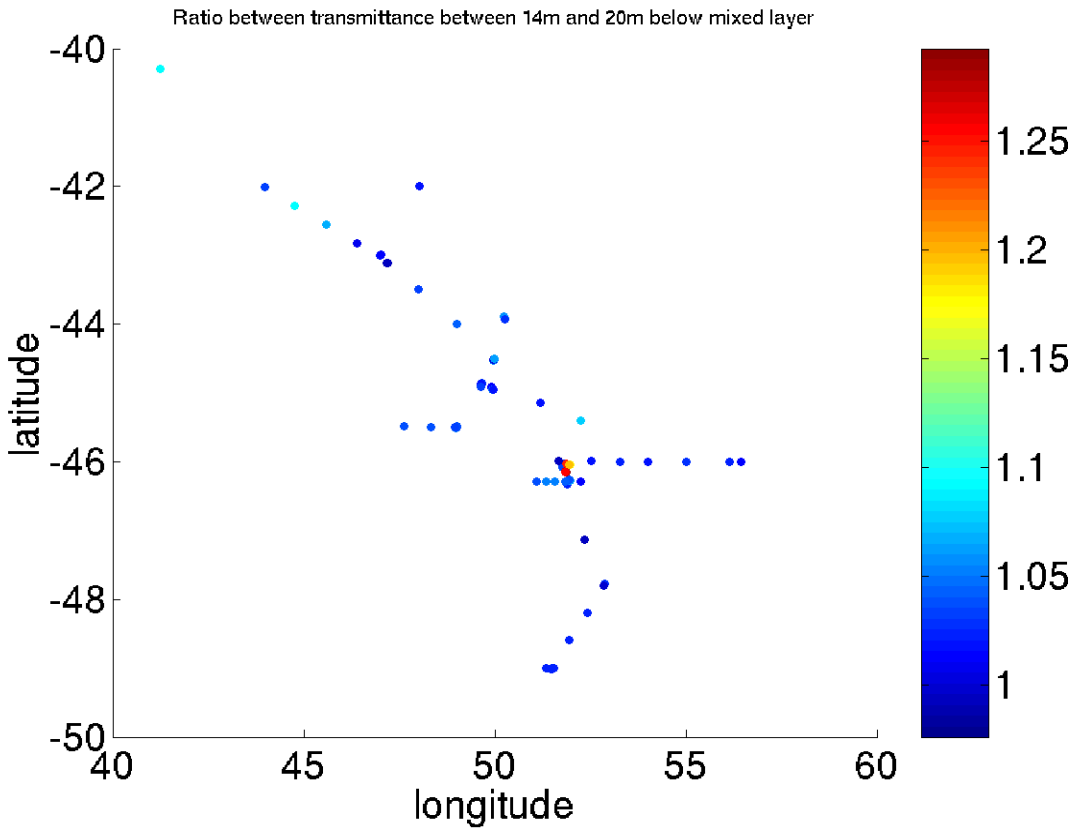

Figure 2.6 Ratio between transmittance at mixed layer depth +20m and 14m from CTD data collected on D285 and D286.

Despite the problems with chl-a to biomass ratios, satellite calibration in the Southern Ocean and cloud cover (luckily not a significant problem in this study although there are some problems with data from 2001) satellite chl-a images are still hugely valuable in observing the chl-a distributions over large time and space scales. Without such images the original idea for studying the region would not have been formed. The images allow the progression of the bloom to be characterised, both over the 9 years for which data are available and also for 2004 in particular to put findings from the cruise in the context of the preceding bloom.

2.5.2 Cross comparison and merged product

The merged product is created by merging the SeaWiFS and MODIS chl-a estimates. These two individual products are not further processed to ensure that they match so there are potential problems with inconsistencies between MODIS and SeaWiFS data. To test whether these issues were significant, MODIS and SeaWiFS data were cross-calibrated

by cross-comparing a sample of daily images. For each SeaWiFS pixel with data the corresponding value from MODIS was found. It was done this way around to avoid double counting the same SeaWiFS pixel, because MODIS pixels are a quarter the size of SeaWiFS pixels (1/24 degree 'square' compared to 1/12 degree 'square'). There is a close match between SeaWiFS and MODIS chl-a estimates:

$$CHL_{seawifs} = -0.003 \pm 0.006 + (1.01 \pm 0.02) \times CHL_{modis},\ r^2 = 0.73 \quad \textbf{2-1}$$

(data from 10474 matching pixels), see Figure 2.7. Despite the fact that the merged product is used as 8-day composites the comparison was done with daily images because there could be several (up to 7) days between when the SeaWiFS satellite captured data for a pixel relative to when data were obtained by MODIS, due to shifting cloud patterns and the different satellites' orbits. Using 8-day datasets leads to a much greater spread in the data pairs, but not a systematic shift in the relationship.

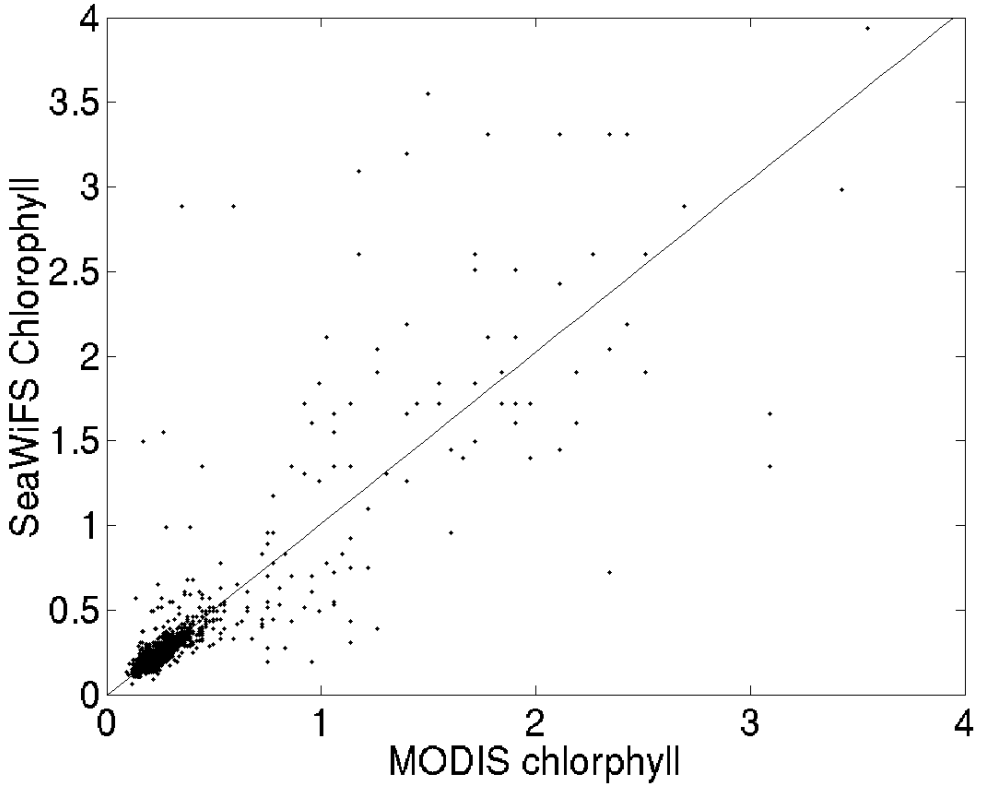

Figure 2.7 Comparison between MODIS and SeaWiFS chl-a estimates, with least-squares line.

This one-to-one relationship between the source datasets gives good confidence in using the merged product in this area. Any variability added by using the two sources is more than compensated for by the increased coverage in space, which significantly reduces the noise introduced by sampling different areas within sampling boxes that are defined to analyse the data. The merged product will also have more data from throughout the 8-day period, meaning that even where there is already data for a given pixel in the individual products the data for the merged product will be, on average, more representative of the whole 8-day period. This will reduce noise in the time series introduced by problems of data potentially being predominantly from one end of the time period.

2.5.3 Data usage

SeaWiFS data were used for comparisons between years, from 1997-2005 so that the same dataset is used each time. The merged product is used for all the images from 2002. MODIS images were used for comparisons between chl-a and Sea Surface Temperature (SST) as both products are from the same sensor and thus with almost identical coverage. In some parts of this work, the 8-day periods are numbered, or Julian days are used. Table 2.2 provides a reference table between these measures of time and actual dates.

jday	Non-leap year	Leap year	8-day period number
1	1-Jan	1-Jan	20
9	9-Jan	9-Jan	21
17	17-Jan	17-Jan	22
25	25-Jan	25-Jan	23
33	2-Feb	2-Feb	24
41	10-Feb	10-Feb	25
49	18-Feb	18-Feb	26
57	26-Feb	26-Feb	27
65	6-Mar	5-Mar	28
73	14-Mar	13-Mar	29
81	22-Mar	21-Mar	30
89	30-Mar	29-Mar	31
97	7-Apr	6-Apr	32
105	15-Apr	14-Apr	33
113	23-Apr	22-Apr	34
121	1-May	30-Apr	35
129	9-May	8-May	36
137	17-May	16-May	37
145	25-May	24-May	38
153	2-Jun	1-Jun	39
161	10-Jun	9-Jun	40
169	18-Jun	17-Jun	41
177	26-Jun	25-Jun	42
185	4-Jul	3-Jul	43
193	12-Jul	11-Jul	44
201	20-Jul	19-Jul	45
209	28-Jul	27-Jul	46
217	5-Aug	4-Aug	1
225	13-Aug	12-Aug	2
233	21-Aug	20-Aug	3
241	29-Aug	28-Aug	4
249	6-Sep	5-Sep	5
257	14-Sep	13-Sep	6
265	22-Sep	21-Sep	7
273	30-Sep	29-Sep	8
281	8-Oct	7-Oct	9
289	16-Oct	15-Oct	10
297	24-Oct	23-Oct	11
305	1-Nov	31-Oct	12
313	9-Nov	8-Nov	13
321	17-Nov	16-Nov	14
329	25-Nov	24-Nov	15
337	3-Dec	2-Dec	16
345	11-Dec	10-Dec	17
353	19-Dec	18-Dec	18
361	27-Dec	26-Dec	19

Table 2.2 Reference table for the start dates of NASA satellite data 8-day periods and the numbering used in this study (analysis starts at the beginning of the spring bloom).

2.5.4 Quality checks

In general the ocean colour data are quite smooth but there are some unrealistically high datapoints (reaching 40 mg m^{-3}). These were searched for and removed; 15mg m^{-3} was taken as the upper limit of 'acceptable' data. This value is chosen to be significantly higher than the vast majority of datapoints so that real data are very unlikely to have been removed. Some spikes are still visible in plots as single pixels significantly higher than all surrounding pixels but no way was found to remove these that did not risk removing more good data than bad. Any bad values that were still present should not significantly affect the mean over a wide area due to the large number of datapoints being averaged and the fact that there can be no very high data spikes due to the filtering. In the case of studying the bloom progression the median is used, which will be affected negligibly by data spikes if at all.

2.5.5 Statistical distribution

Chlorophyll values approximately follow a log-normal distribution (Campbell 1995). In this study the median is used when looking at bloom progression because it best describes the bulk of the data. The mean is used in other parts of the CROZEX program for the time series of chl-a values when they are used to estimate total productivity (Seeyave *et al.* 2007) or in comparison with spatial differences in export estimates (Salter *et al.* 2007) where the small number of high values are significant. Being less than 15 mg m^{-3}, the few remaining bad values will have little impact on the mean over a large number of pixels and will have negligible impact on the median.

2.5.6 Local calibration of ocean colour images

For each of the 810 *in situ* chl-a measurements the value from the corresponding individual pixel of the ocean colour image of the day of collection was recorded, if the pixel was cloud free.

224 pairs of *in situ* and satellite data for the merged SeaWiFS/MODIS product were found. Four outliers were removed, either because of small-scale patchiness in the chl-a that will not be well represented by a 9km x 9km pixel (such areas were targeted on D285

and D286) or because of a series of bad *in situ* values. The remaining data are shown in Figure 2.8 and have least squares regression fits, with 95% confidence intervals:

$$CHL_{merged} = 0.12 \pm 0.04 + (0.38 \pm 0.03) \times CHL_{in\ situ},\ r^2 = 0.78 \qquad \textbf{2-2}$$
$$CHL_{in\ situ} = -0.08 \pm 0.08 + (2.05 \pm 0.15) \times CHL_{merged}$$

The same process with just SeaWiFS data produced 113 *in situ* and satellite data pairs as described above. After the same removal of outliers, the relationships

$$CHL_{seawifs} = 0.13 \pm 0.05 + (0.39 \pm 0.03) \times CHL_{in\ situ},\ r^2 = 0.85 \qquad \textbf{2-3}$$
$$CHL_{in\ situ} = -0.15 \pm 0.12 + (2.21 \pm 0.18) \times CHL_{seawifs}$$

were found. In both cases, removing the outliers did not significantly affect the gradient or intercept of the relationships but did increase the correlation co-efficient from approximately 0.6 and narrowed the confidence intervals.

Although 118 such data pairs were found for MODIS they did not span a wide range of *in situ* values and so satellite data from +/- 1 day were also included, if a match was not found for the same day. This produced 240 data pairs and widened the range of *in situ* values slightly but it was still narrower than for the above two relationships. The relationships are found:

$$CHL_{modis} = 0.17 \pm 0.04 + (0.32 \pm 0.04) \times CHL_{in\ situ},\ r^2 = 0.52 \qquad \textbf{2-4}$$
$$CHL_{in\ situ} = 0.06 \pm 0.09 + (1.64 \pm 0.20) \times CHL_{modis}$$

The linear fits are significantly influenced by the few high values found in the SeaWiFS match-ups. To check the relationship for the merged product the data were log transformed and a least squares fit found to those datapoints. The result, transformed back to a linear scale, shows good agreement with the original linear fit at low chl-a values but deviates away from the datapoints and linear regression line at high values (Figure 2.8). Therefore the linear fit

$$CHL_{in\ situ} = -0.08 + 2.05 \times CHL_{merged} \qquad \textbf{2-5}$$

has been used in the rest of this work, applied to SeaWiFS, MODIS and the merged product.

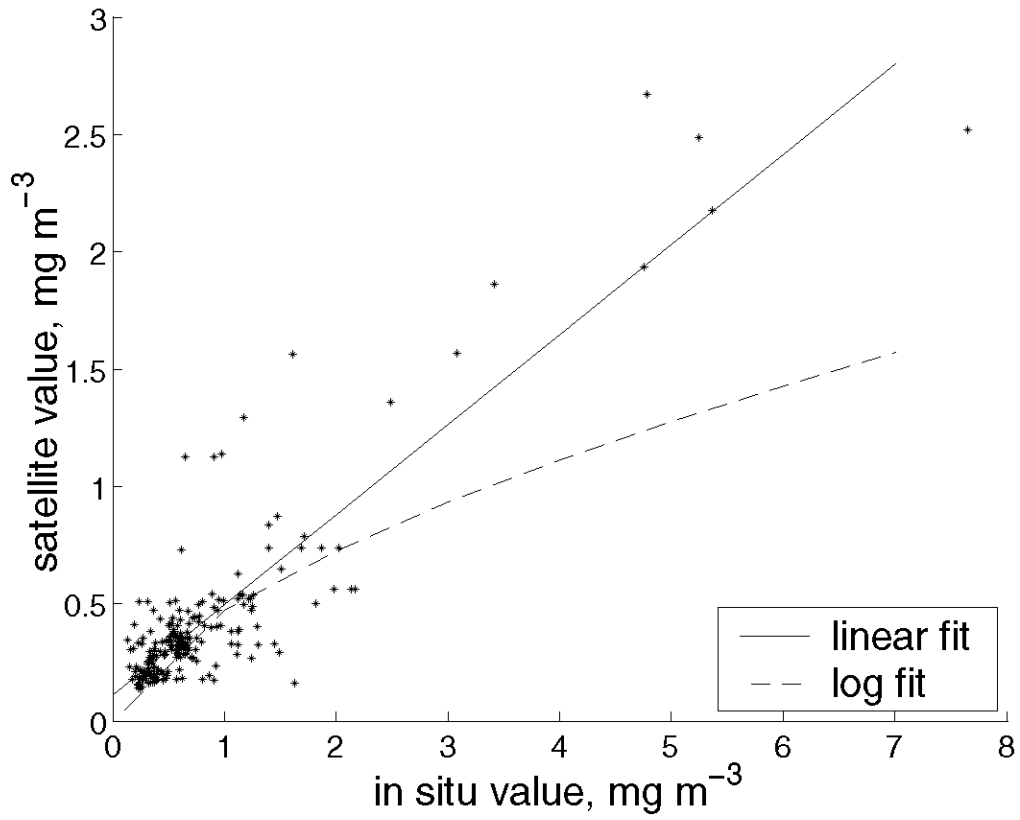

Figure 2.8 Merged SeaWiFS/MODIS chl-a against *in situ* chl-a values with the least squares fit lines to the data and the log transformed data (transformed back)

The Southern Ocean is recognised as an area where ocean colour derived chl-a estimates differ significantly from *in situ* measurements (O'Reilly *et al.* 1998; Moore *et al.* 1999; Gregg and Casey 2004; Holm-Hansen *et al.* 2004; Korb *et al.* 2004). The relationship found is similar to that found by Korb *et al*. (2004) and Dierssen and Smith (2000). A linear relationship was found to be better for our data set, in large part because of the sensitivity of a log/log fit when there is considerable scatter in the data. The differences between the relationship found in this study,

$$CHL_{seawifs} = 0.13 \pm 0.05 + (0.39 \pm 0.03) \times CHL_{in\ situ},\ r^2 = 0.85 \qquad \textbf{2-6}$$

compared to that found from around South Georgia,

$$CHL_{seawifs} = 0.30 + 0.28 \times CHL_{in\ situ},\ r^2 = 0.61 \text{ (Korb } et\ al. \text{ 2004)} \qquad \textbf{2-7}$$

will be largely due to the higher *in situ* values in the latter dataset. The SeaWiFS values for these are generally lower than the regression line that would fit the rest of the data (see figure 3 in Korb *et al* 2004) and so cause the gradient of the regression line to be lower and the intercept higher. This is either due to SeaWiFS underestimating high values most significantly, for which there is some evidence in Gregg and Casey (2004) and Moore *et al* (1999) or the use of 8-day images in the South Georgia study, which are less likely to capture the high values due to advection and temporal change in chl-a.

2.6 Photosynthetically Available Radiation

Photosynthetically Available Radiation (PAR) data were downloaded from the same location as ocean colour data, also as 8-day mapped images (Feldman and McClain 2006b). The algorithm used to produce the data estimates daily PAR reaching the ocean surface from atmospheric conditions and cloud cover. PAR is defined as the quantum energy flux from the Sun in the spectral range 400-700 nm and is expressed in Einstein m^{-2} day^{-1} (Frouin *et al.* 2001). 1 Einstein m^{-2} day^{-1} = 1 photon m^{-2} day^{-1}.

$$PAR(z) \equiv \int_{400nm}^{700nm} \frac{\lambda}{hc} E_0(z,\lambda) d\lambda \qquad \textbf{2-8}$$

Where λ is the wavelength, h=6.6255x10^{-34} J s is the Planck constant and c=3.0x10^{17}nm s^{-1} is the speed of light. This relationship accounts for the fact that it is the number of photons available within the wavelength band that is relevant to the rate of photosynthesis, rather than the energy within each photon, the latter being a function of the wavelength.

Data flagged as missing and zero values were searched for and removed. The data are output from a model that takes into account effects of clouds so the coverage is complete for each 8-day image but errors could be introduced by the model or the model assumptions.

2.7 Sea Surface Temperature

The 8-day mapped Sea Surface Temperature (SST) data from MODIS were downloaded at 4km resolution for the same time periods as MODIS chl-a from the same source (Feldman and McClain 2006a). This allows co-located chl-a and SST images to be studied.

The SST data were noisy, the main problem was with cloud edge effects. Clouds can have similar thermal properties to the sea surface and it is therefore hard to automatically remove them from the data. However it is often clear visually that there is a ring of warm or cold water around an area with no data. This was found in a related study (Popova *et al.* 2007) to produce spurious mesoscale features when SST was assimilated into a numerical model of the area. Due to this, it is necessary for data values outside the expected range (which varies with time of year) to be searched for and removed, possibly removing good data as well. Even after this process it is likely that bad data will still be present and this has to be considered when interpreting the analysis. A further problem, common to all satellite SST measurements, is that the sensor actually measures the skin temperatures, which can be significantly different, by up to 1°K, from the more physically relevant bulk temperature of the mixed layer. The skin temperature can exceed the bulk temperature in calm sunny conditions or the skin temperature can be cooled by wind speeds of up to10 ms^{-1}. At wind speeds greater than this, frequent around Crozet, turbulence means that the bulk and skin temperature become the same (Donlon and Robinson 1997).

2.8 Absolute Dynamic Topography

These data provide an estimate of the geostrophic flow from satellite altimetry data. This is done by removing, as much as is possible, the effects of the geoid on the sea surface height (SSH). The geoid affects the SSH through gravitational anomalies.

The data and information regarding its processing were downloaded from http://www.aviso.oceanobs.com/html/donnees/produits/hauteurs/global/madt_uk.html#upd The altimeter products were produced by Ssalto/Duacs and distributed by Aviso, with support from Cnes (Rio and Hernandez 2004). They combine altimetry data from

Topex/Poseidon, Jason-1, Envisat, GFO and ERS1/2, a reference geoid from the GRACE mission and *in situ* observations to create the absolute dynamic topography product.

The altimeter data were combined to create the mean shape of the sea surface during the period covered by the altimetry data. It is corrected for seasonal variations and corresponds to the sum of geoid and mean ocean circulation contributions to SSH. The relief of this surface is contributed to by density and relief variations in the Earth and ocean currents and water masses of varying densities in the ocean, leading to sea level variations of several metres and on short wavelengths.

There are now direct measurements of the geoid to allow these effects to be removed from the sea surface height signal and thus allow ocean currents to be recovered from the data. However, wavelengths shorter than 400km are filtered out of the EIGEN-GRACE03S geoid due to the accuracy of the sensor. Such wavelengths are also removed from the altimeter product. The two surfaces are then subtracted, to provide a large-scale mean dynamic topography (MDT), but this contains no information at wavelengths shorter than 400km.

The direct method MDT is then merged with Levitus climatology data. The Levitus climatology provides realistic ocean circulation patterns where data are available (mostly at low and mid-latitudes), but at high latitudes the quality is reduced. The MDT is computed using Levitus climatology dynamic heights to 1500 dbar (extended toward the coast).

The merging is performed by weighting these two surfaces: Levitus climatology is used at low and mid-latitude with an increasing contribution of the direct method MDT toward the poles. Once the two filtered surfaces are merged, the high wavelength contribution of the Levitus climatology MDT is added back. Levitus climatology is therefore the dominant contribution at low and mid-latitudes but the circulation of the subpolar gyre and Antarctic Circumpolar Current are enhanced by gravimetric information.

Local estimates of the MDT are created by subtracting the satellite altimetry derived sea level anomaly (SLA, from the 1993-2002 mean) from the dynamic height calculated from hydrographic profiles (using space-time objective analysis to match the data sets). In a

similar way, geostrophic velocities deduced from surface drifters can be used together with geostrophic velocity anomalies computed from gradients in altimeter derived sea surface heights to calculate the dynamic contribution to the sea surface height signal. The height and velocity estimates are combined in a multivariate objective analysis to improve, locally, the output of the direct method.

The sea level anomaly (SLA) is then added to the mean dynamic topography to produce the mapped absolute dynamic topography (MADT). The time and length scales present in the MADT product used are therefore set by the length scales present in the SLA data. Small-scale features could be significantly influenced by errors in the geoid, which are largest at small scales, and by the relatively coarse sampling by altimetry satellites. However comparison between the flow patterns inferred from the MADT images (geostrophic flow is along contour lines) and gradients in SST and chl-a (the latter being totally independently acquired data, but influenced strongly by the flow patterns) show that the meanders in the Sub-Antarctic Front, at scales of approximately 100km, appear to be well represented in the MADT data. Data since 2002 represent well the flow between the Del Cano Rise and Crozet Plateau due to an increase in the number of altimetry satellites. Some data from before this point is presented, but highlighted as being unreliable. No further data quality checks were needed on the data before use.

2.9 Wind stress

Wind stress is measured with a microwave scatterometer but the moving atmosphere does not create a significant signal in the received radiation. Instead the effect of the wind on the ocean surface is measured from the shape of the sea surface, as wind stress over the ocean generates ripples and waves, which roughen the sea surface. These waves modify the radar cross-section (sigma-0) of the ocean surface and hence the magnitude of backscattered power. Using a relationship known as the geophysical model function the wind velocity is recovered from sigma-0. The geophysical product retrieved from QuikSCAT (Perry 2001) observations is the equivalent of neutral winds at 10-m height, from which the surface wind stress (or momentum flux) can be derived independent of the atmospheric density stratification. The specification of the system is to measure winds between 3 and 30 m/s with an accuracy better than (the greater of) 2 m/s or 10% in speed

and 20° in direction. The Liu and Tang algorithm (Tang and Liu 1996) for derived wind stress was used. Clouds do not block microwaves so each swathe is complete.

The wind stress data from the QuikSCAT sensor were received from http://poet.jpl.nasa.gov for each year 1999 to 2006 (data starts at the beginning of August 1999) for the area 40º-50ºS, 40º-60ºE at a resolution of 0.25º. Both morning and afternoon passes were used because the absence of any large areas of land means that there is no reason why these would be significantly different in the area. The two datasets from each day were used individually because the rapid temporal changes in wind mean that averaging the data is likely to lead to a different statistical distribution of the data within the areas where the morning and afternoon data overlap relative to where they do not. This would then bias spatial comparisons made between areas of single data and areas of averaged data. Data are gridded for each day but the width of the swathes means that data coverage is full every 3 days. Daily data have been used averaged over the same boxes used for studying chl-a, because temporal variations over 3 days will be much greater than spatial variations over the scale of the boxes and it is important to capture the extreme wind events in understanding the effects on stratification.

3 Circulation

The main hypothesis of the CROZEX program is that the bloom observed close to the Crozet Plateau is due to natural iron enrichment of the water close to the islands and/or plateau alleviating the iron limitation typical of Southern Ocean conditions (Martin *et al.* 1990; de Baar *et al.* 1995; Boyd *et al.* 2000; Gervais and Riebesell 2002; de Baar *et al.* 2005; Blain *et al.* 2007). Under this scenario the location and shape of the bloom will be largely controlled by where the iron is advected to. It is therefore crucial to understand the circulation patterns in the area. The suspected iron sources are close to, or at, the surface of the ocean, so the surface flows are of particular interest. This chapter presents data from Argo float trajectories, hydrographic data and satellite altimetry derived maps of absolute dynamic topography. Reference is also made to analysis in Pollard *et al.* (2007), which includes study of surface drifter trajectories.

Satellite chl-a images show a very strong contrast in chl-a concentration between north and south of the Crozet Plateau. This contrast has been used in the sampling strategy to compare bloom conditions with a nearby area (49°S, 51.5°E) more typical of the Southern Ocean. The main issues of this chapter are therefore concerned with the characteristics of these areas: the main currents, the biogeochemical zonation, and the interaction of the flows with shallow topography.

3.1 Large scale circulation

There are several sources of information on the flow around the Crozet Islands. A certain amount of data from hydrographic sections and current meter moorings are available from prior to the CROZEX cruises. These are from the SWINDEX cruises in 1993 and 1995 (Holliday and Read 1998; Pollard and Read 2001) and Suzil (Park *et al.* 1993). The findings of the CROZEX project were added to the above work and given in Pollard *et al.* (2007). The following draws on work in Pollard *et al.* (2007) and extends it in space and time by use of Argo float data (float trajectories and water mass characteristics) and satellite derived absolute dynamic height.

The trajectories of Argo floats give an indication of the large scale flow in an area at the drifting depths of the floats (mostly 1000m or 2000m). Due to displacements during ascent, at the surface and descent they are not exact streamlines. It is possible that there are systematic differences between a series of trajectories and the mean streamlines at the drifting depth if the effects of the displacements when not at the drifting depth are not representative of possible flows at the drifting depth, but overall they are likely to give a good indication of the flow patterns.

Satellite altimetry combined with independent estimates of the geoid gives excellent spatial (1/3 degree) and temporal (7 day, through year) coverage of surface geostrophic currents. Knowledge of the depth structure of the circulation from hydrographic data and Argo float trajectories is needed to estimate what these imply at depth.

The data from the above sources is presented in section 3.1.1-3.1.3 to describe the flow in the area. From these, particular features are identified and discussed in more detail in section 3.2. The implications of these features on the potential distribution of iron are discussed in section 3.3.

3.1.1 Argo float trajectories

Figure 3.1 shows all the trajectories from Argo floats from the study area. As shown in Figure 2.4 most of these are from after 11/04 (data downloaded up until mid October 2006). Figure 3.3 extends Figure 3.1 south to 55°S and splits the trajectories into those at 1000m and 2000m.

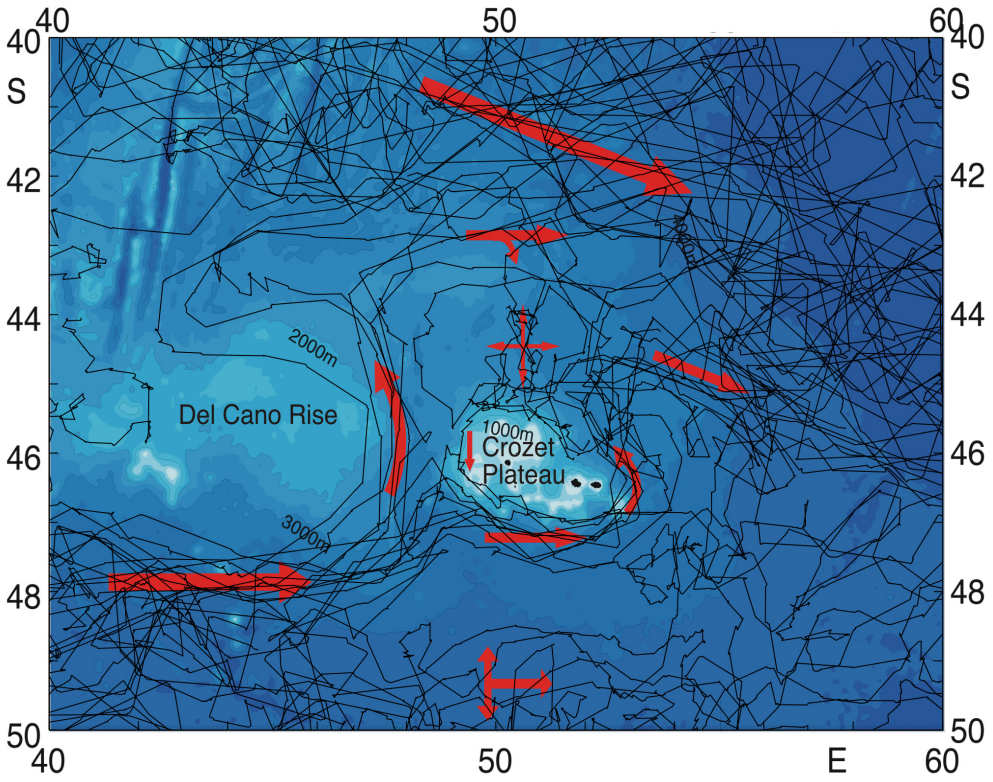

Figure 3.1 Plot of all Argo float trajectories from the study area, with arrows to indicate the main flows and directions. The plot includes floats from all depths.

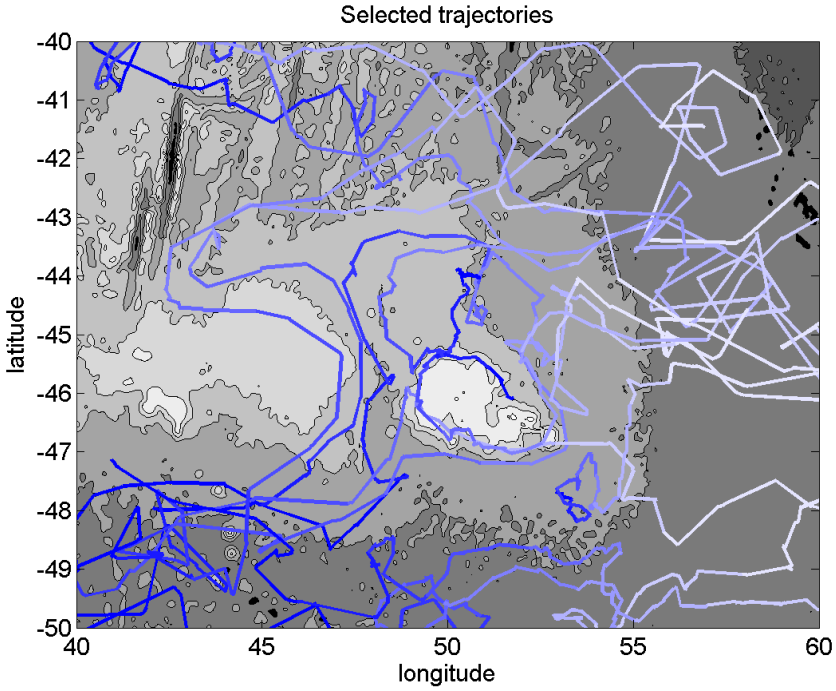

Figure 3.2 Selected Argo float trajectories, showing individual paths and direction of movement (tracks get paler with distance along track). Bathymetry contour intervals are 1000m.

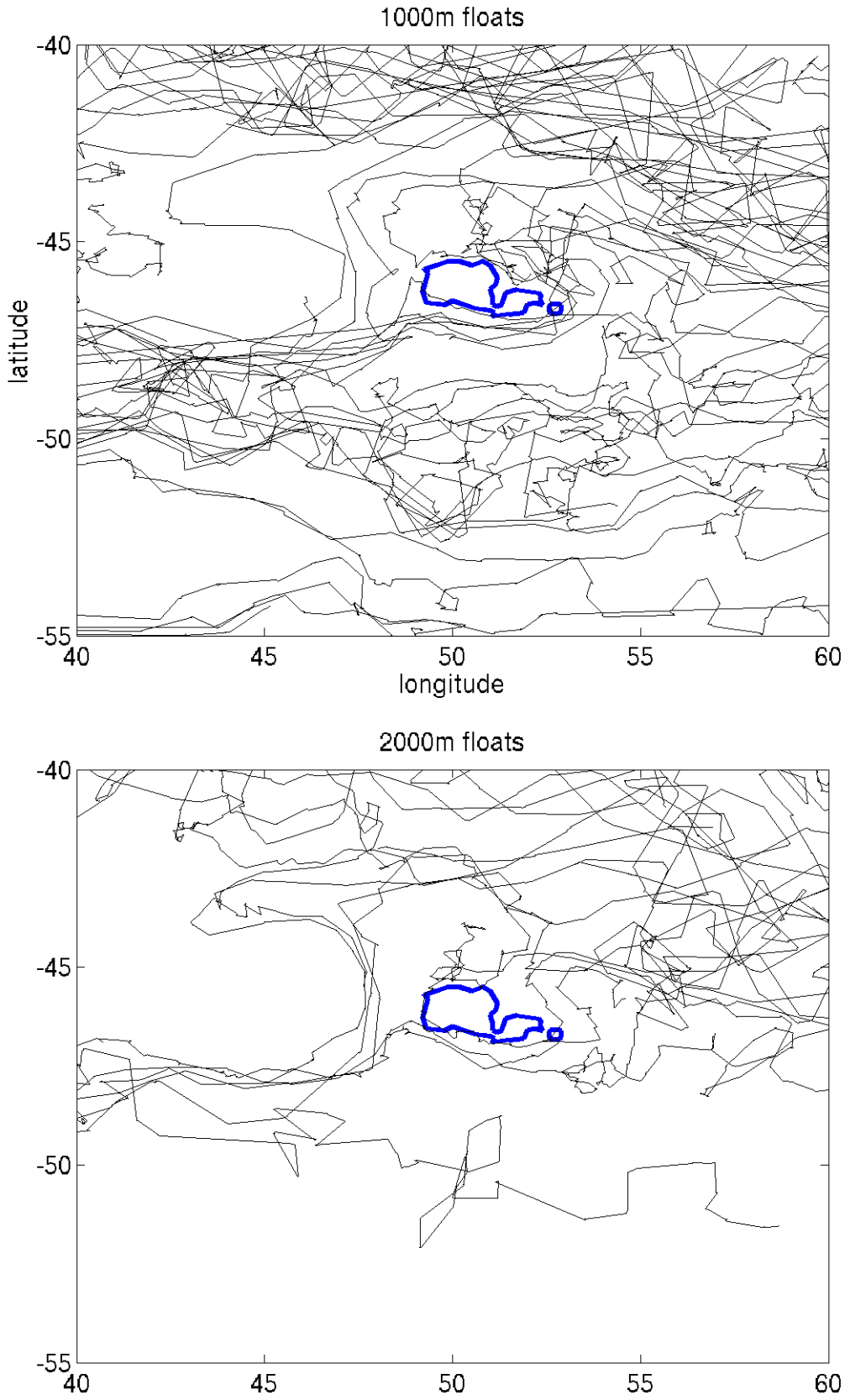

Figure 3.3 Argo float trajectories around the Crozet Plateau split between those at 1000m and 2000m and extended south to 55°S. The 1000m contour around the Crozet Plateau is shown in blue.

There are now sufficient Argo float trajectories to pick out major features of the flow. These are introduced in this section. Similarities and differences seen in satellite derived absolute dynamic topography (section 3.1.2) and hydrographic data (section 3.1.3) are discussed in the respective sections. Each feature is then analysed in detail in section 3.2.

There is a strong east-south-east flow across the north of the area. This comprises the Agulhas Return Current (ARC) and the Sub-Tropical Front (STF) (Read and Pollard 1993; Lutjeharms and Ansorge 2001; Boebel *et al.* 2003). East of approximately 48°E the flow that passes anticyclonically around the Del Cano Rise joins these fronts. Due to the strong meandering of the fronts in the area the Argo float trajectories from the different fronts overlap, because the time dimension is suppressed when they are all plotted together. This is described in more detail in section 3.2.1.

The other main inflow into the region is a strong eastward flow at 40ºE south of 46.5ºS. At approximately 45ºE this flow splits, one branch turning slightly southwards, the other continuing to follow the topography of the Del Cano Rise. The northerly branch follows the topography of the Del Cano Rise. It then splits again at approximately 48ºE. One branch continues to follow the Del Cano Rise while the other follows the south side of the Crozet Plateau, most of it following the topography around the eastern end of the Crozet Plateau before retroflecting eastwards. The northern branch also retroflects eastward, variably between 43° and 48ºE. The splitting of the flow is described in more detail in section 3.2.2. The topographic control of the flow is covered in section 3.2.3.

There is a gap in the float trajectories centred on 48ºS, 51ºE, strongly suggesting an area with closed circulation and a very long residence time. The expected rate for floats to enter such a region is very low, making it reasonably likely that none have yet entered, given that the timescales of such flows can be comparable with the period of time Argo floats have been in the world's ocean. If any did, then they would be expected to then stay for a considerable time. This area of very weak and recirculating flow prevents any float that has passed close to the Crozet Plateau from then moving southwards to the non-bloom sampling station at 50ºE 49ºS. This feature is described in more detail in section 3.2.4.

There is a long residence time in the area north of the main area of the Crozet Plateau (43.75-45.75°S, 49.2-51.2°E). The floats here travel short distances in each 10-day period between profiles and have no preferred direction. The inflow into this area is from detrainment from both branches of the SAF. This is described in more detail in section 3.2.5.

The float trajectories pick out an anticyclonic closed circulation around the Crozet Plateau. One float, deployed north of the plateau, flows westward along the northern edge of the plateau, southwards through the gap between the Del Cano Rise and Crozet Plateau (against the strong northwards flow slightly to the west) and then eastwards along the southern edge and around the eastern edge of the plateau, close to the two eastern islands. Other floats closely follow the edge of the plateau for shorter distances. This is described in more detail in section 3.2.7.

3.1.2 Hydrographic sections

Figure 3.4 shows a similar pattern of large scale circulation to Figure 3.1 although the Polar Front is not well resolved, possibly due to it mostly lying outside the area of study for Figure 3.4. The splitting of the SAF is clear, with the southern branch found to be considerably weaker than the northern branch in terms of volume flux. The area of long residence time also shows as a large area with no streamlines, although Figure 3.4 suggests that this area extends further east than the float trajectories show it. Smaller scale features, such as the closed circulation around the plateau and detrainment into the area of long residence time are not captured, due to the large time and space scales between CTD casts and the lack of casts close to the edge of the plateau, although steep topography causes considerable problems in the interpretation of hydrographic data in such areas.

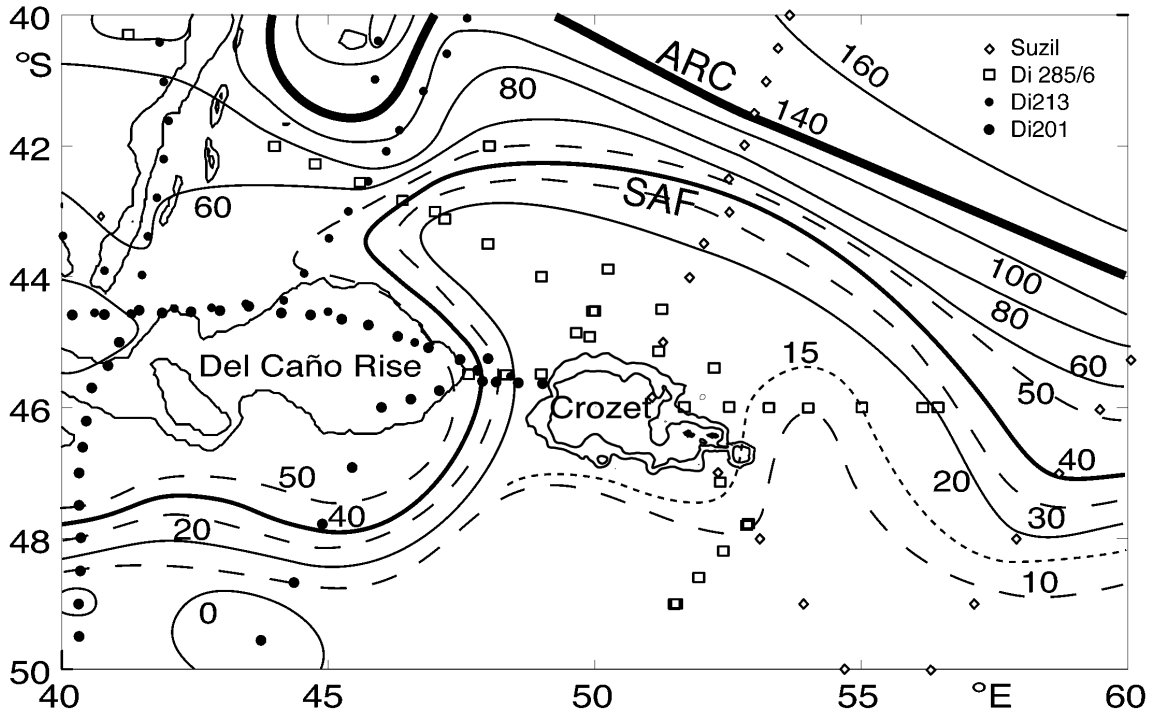

Figure 3.4 Transport streamfunction taken from Pollard *et al.* (2007). Data used is from the Crozet cruises Discovery 285 and 286, Discovery cruises 201 and 213 and Suzil (Park *et al.* 1993). Streamlines show the transport relative to 4000 m or the bottom if shallower, measured in Sverdrups (1 Sv = $10^6 m^3 s^{-1}$). Solid lines are at 20 Sv intervals between 0 and 100 Sv, then at 40 Sv intervals to 180 Sv. A few intermediate 10 and 5 Sv contours are shown long and short dashed respectively. All station positions on which the contouring is based are shown, apart from those outside the limits of the map.

3.1.3 Absolute Dynamic Topography

Figure 3.5 shows a sample image of absolute dynamic height contours (Rio and Hernandez 2004) from February 2005. The contours, through the geostrophic relationship, are streamlines of the surface geostrophic flow. The image has been deliberately chosen to illustrate all of the features present in the area – whereas each feature is seen frequently in other images, it is rare to have them all present in one image. A full set of weekly images from the 2004/5 season is included as Appendix B.

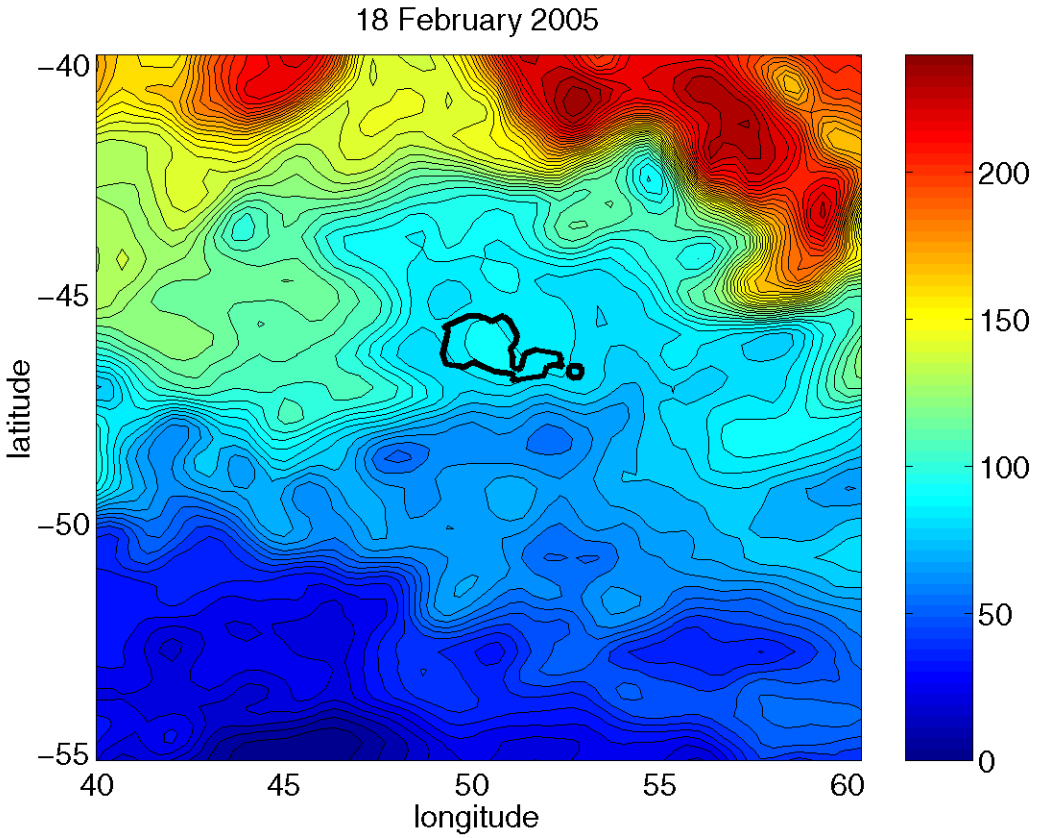

Figure 3.5 Absolute dynamic height (dyn cm) image from February 2005, selected to illustrate features regularly present.

There is an overall similarity between Figure 3.5, the Argo float trajectories (Figure 3.1) and the map derived from hydrographic sections (Figure 3.4). The comparison confirms that the surface flows shown in the surface height gradients extend to depth, giving confidence in using the surface geostrophic currents to study the overall circulation. Conversely it also gives confidence in using the deep flows shown by float trajectories to interpret the surface currents and so the advection of iron.

The repeated features, relative to those introduced in section 3.1.1 from study of Argo float trajectories, and discussed in section 3.2, include: the strong east-south-east flow to the north of the study area; bifurcation of the SAF south-west of the Crozet Plateau; an indication of detrainment from the northern branch (other images show detrainment from the southern branch north of the islands); closed circulation over the plateau; and the weak flow and closed circulations north of the western part of the plateau.

There is also a closed circulation south of the southern branch of the SAF. This is a regular feature in dynamic height images (see Appendix B). It agrees with the fact that no Argo float has yet entered the area, suggesting that this feature extends to at least 2000m. This area, together with the southern branch of the SAF, separates the area to the south from flow that has passed close to the plateau and/or islands.

A feature seen in Figure 3.5 that is also seen in several ocean colour images is the cyclonic eddy that is shed occasionally to the west (43.5°S, 44°E) as the northern branch of the SAF retroflects eastwards again north of the Del Cano Rise.

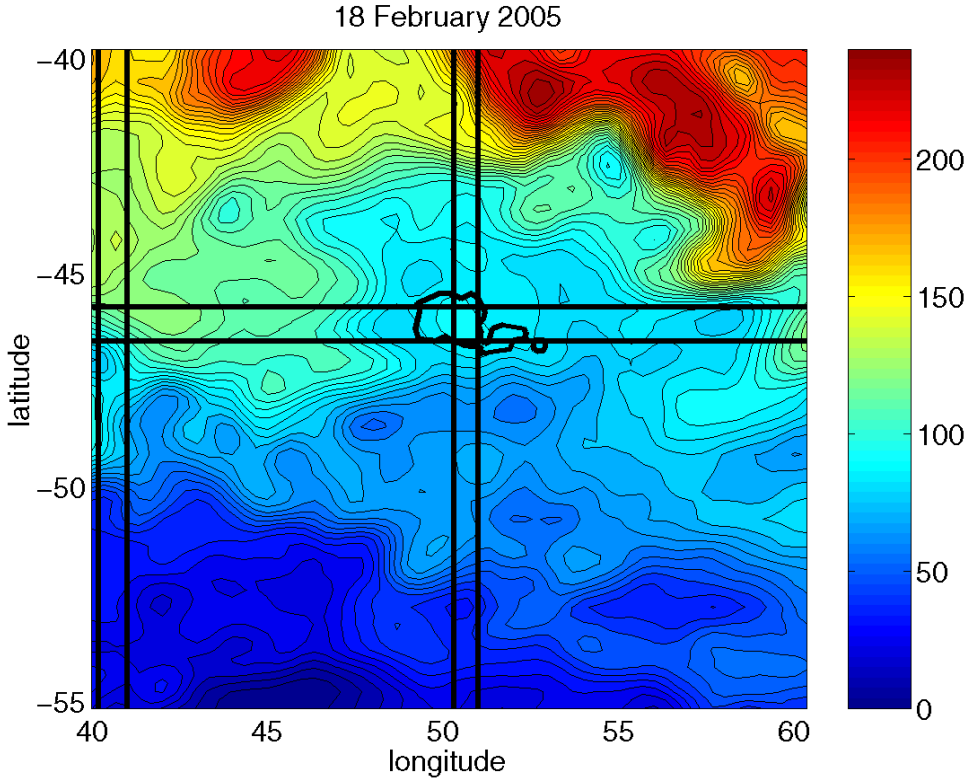

Figure 3.6 Location of the cuts through the absolute dynamic height data used to study the variation in strength and location of the surface geostrophic flows.

To investigate some of the flows identified, cuts were made through weekly absolute dynamic height data: an east/west cut 45.8-46.6°S, 40-60°E and two north/south cuts 40-60°S, 50.3-51°E and 40-60°S, 40.3-41°E (Figure 3.6). Along the first two of these cuts regions were specified and consecutive minima and maxima found within these regions. The gradient between these gives a measure of the surface geostrophic velocities and so

the difference across a flow is a comparative measure of the volume flux close to the surface, on the assumption that there is a consistent depth structure across the time or area of the comparison. These surface geostrophic flows are a significant contribution to the surface flows that advect iron and plankton. In addition, by the overall agreement found above between surface and deep flows, these surface data give an indication of the relative strengths, persistence and location of the deep extending fronts.

To study the variability of the paths of the fronts, the latitudes of specified dynamic heights in the cuts were found. If the dynamic height occurred at more than one latitude the one closest to the mean (specified for first image, then calculated from preceding images) was chosen.

The time series for these latitudes and differences in dynamic height runs from October 1992 until March 2007 (754 weeks). However, data from before April 2002 are either omitted or used with caution due to there being fewer altimetric satellites meaning that there is reduced spatial and temporal information used to create the mapped absolute dynamic topography data.

3.2 Features of circulation

3.2.1 Strong flow north of Crozet Plateau

As has been well documented (Read and Pollard 1993; Holliday and Read 1998; Lutjeharms and Ansorge 2001), there is a very strong flow north of 43°S at 50°E. This comprises the Agulhas Return Current (ARC), Sub-Tropical Front (STF) and the Sub-Antarctic Front (SAF). It is not easy to distinguish these three flows in hydrographic sections (hence it sometimes being referred to as the Crozet Triple Front (Belkin and Gordon 1996) but they can be distinguished from surface data (Holliday and Read 1998).

This strong front corresponds to a strong gradient in many variables: temperature, salinity and, probably, iron increasing significantly while macronutrients decrease. It is therefore possible that mixing across this front can produce significant changes in the properties of the bloom area south of 43°S. This possibility is investigated in section 3.2.6.1. The stratification is dominated by temperature to the north of the SAF (Pollard *et al.* 2002) so

the winter mixed layer depths initially increase to the north of 43°S because deeper winter convection is possible.

3.2.2 Flow bifurcations west of Crozet Plateau

The flow passing between the Del Cano Rise and Ob-Lena (Conrad) Rise at 40°E has been identified as the Sub-Antarctic Front (SAF) and Polar Front (PF) merged together (Read and Pollard 1993). It can be seen from Figure 3.3 and Figure 3.5 that this flow then splits into three flows. Firstly, a flow separates to the south between 42-46°E. The southerly branch from this split passes to the south of the area with long residence time. To the east of 46°E, the northern branch splits again. The southerly branch passes close to the southern edge of the Crozet Plateau while the northern branch continues to follow the steep topography around the edge of the Del Cano Rise.

As these two splits produce three flows from the original flow that passed between the Del Cano Rise and Ob Lena (Conrad) Rise – the PF and SAF merged together – it is necessary to study the characteristics of these three flows to see which features of these two fronts they possess. To do this, the T/S characteristics (Figure 3.7) and temperature profiles (Figure 3.8) have been found using Argo float data in 4 areas: one across the western area where the fronts are merged and one for each of the three identified flows to the east.

The flow that passes between the Del Cano Rise and the Crozet Plateau (Figure 3.7b and Figure 3.8b) has no temperature minimum and also marks the southern edge of the Sub-Antarctic Zone (Pollard *et al.* 2007). Figure 3.8 shows that both temperature and salinity are important in controlling the stratification, illustrated by the different areas of T/S space where one is relatively constant while the other varies. To the north of this flow there are salinity minima present in profiles, indicating a dominance of temperature in the stratification. The northern flow is clearly therefore the Sub-Antarctic Front (Pollard *et al.* 2002). The southern flow (Figure 3.7d and Figure 3.8d) has a 2°C temperature minimum at 200m so is the Polar Front according to several definitions (Orsi *et al.* 1995; Belkin and Gordon 1996; Pollard *et al.* 2002). The middle flow (Figure 3.7c and Figure 3.8c), along the southern edge of the Crozet Plateau is intermediate between these flows.

Some profiles show a temperature minimum at 200m but between 2-3°C while others show no temperature minimum. It therefore fulfils some but not all criteria for the Polar Front and some but not all criteria for the Sub-Antarctic Front (it certainly does not fulfil any criteria regarding the conditions to the north). In this work it is referred to as the southern branch of the SAF (SSAF), mostly because it bifurcates from the northern branch after both have bifurcated from the Polar Front and because it is convenient to give it a name – it could equally be called the northern branch of the Polar Front. Consequently, the flow passing northwards between the Del Cano Rise and Crozet Plateau is referred to as the northern branch of the SAF (NSAF). That the traditional schematic of two current cores is not always valid was discussed in Pollard *et al.* (2002). Recent work (Sokolov and Rintoul 2007) using high resolution satellite images has also shown that although flow is concentrated by geostrophic turbulence into jets (Rhines 1975), the number of jets varies in space and that these jets can be persistent in time.

This analysis shows that the area north of the Crozet Plateau, where the phytoplankton bloom occurs, is in the Polar Frontal Zone, as is the area south of the plateau (though this may also be expected to show some characteristics of the Antarctic Zone. Both these zones are part of the HNLC Southern Ocean so are replete in macronutrients (nitrate, phosphate, silicate) at the end of winter, due to mixing up from depth where concentrations are persistently high (Pollard *et al.* 2002; Pollard *et al.* 2006).

We reached the study area after the peak of the bloom, so after significant biological utilisation of nutrients in the mixed layer. Despite this, all surface and CTD bottle samples showed levels of nitrate and phosphate considerably above limiting levels (18.3 and 1.3 μmol l^{-1} respectively at 8m on CTD cast 15490, the first in the bloom area, being typical). Silicate was however depleted in the surface (<0.25 μmol l^{-1} on the same cast down to 65m). Below the mixed layer though it rapidly increased to 11.3 μmol l^{-1} at 100m and 18.6 μmol l^{-1} at 200m. These concentrations, either side of the normal level of the winter mixed layer (and both probably shallower than the deepest mixed layer that occurs during the winter) are strongly indicative of surface concentrations before significant biological uptake. There were also other casts within the bloom area (e.g. 15494 at M3 and 15532 at M8E) where surface silicate values were not limiting (>7.5 and 2.8 μmol l^{-1} respectively at 8m).

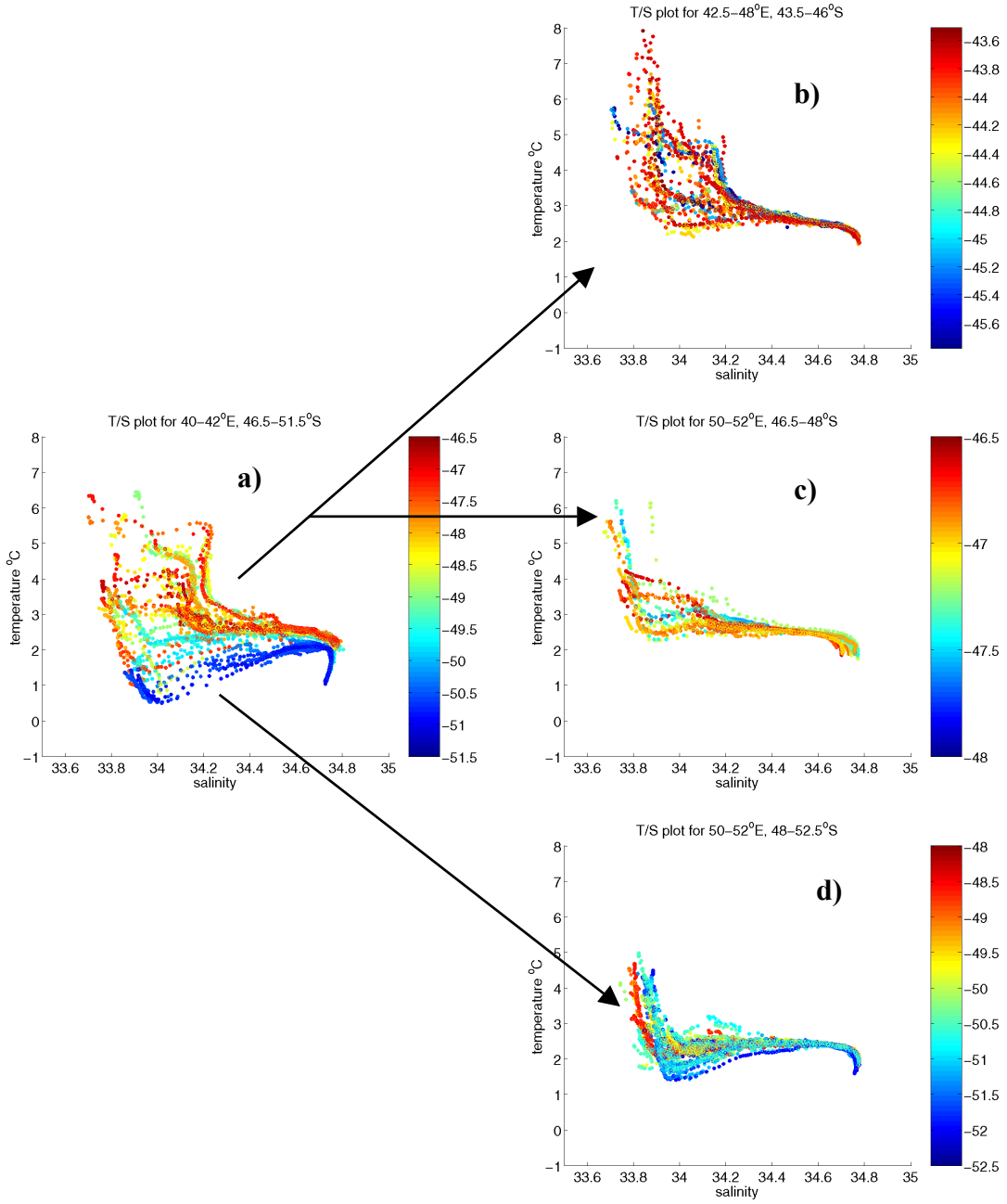

Figure 3.7 Temperature/Salinity plots from Argo floats at 40-42°E, 46.5-51.5°E (a) and 42.5-48°E, 43.5-46°S (b), 50-52°E, 46.5-48°S (c) and 50-52°E, 48-52°S (d). The arrows schematically show the bifurcation of the flow between the cuts. The colour scale shows latitude.

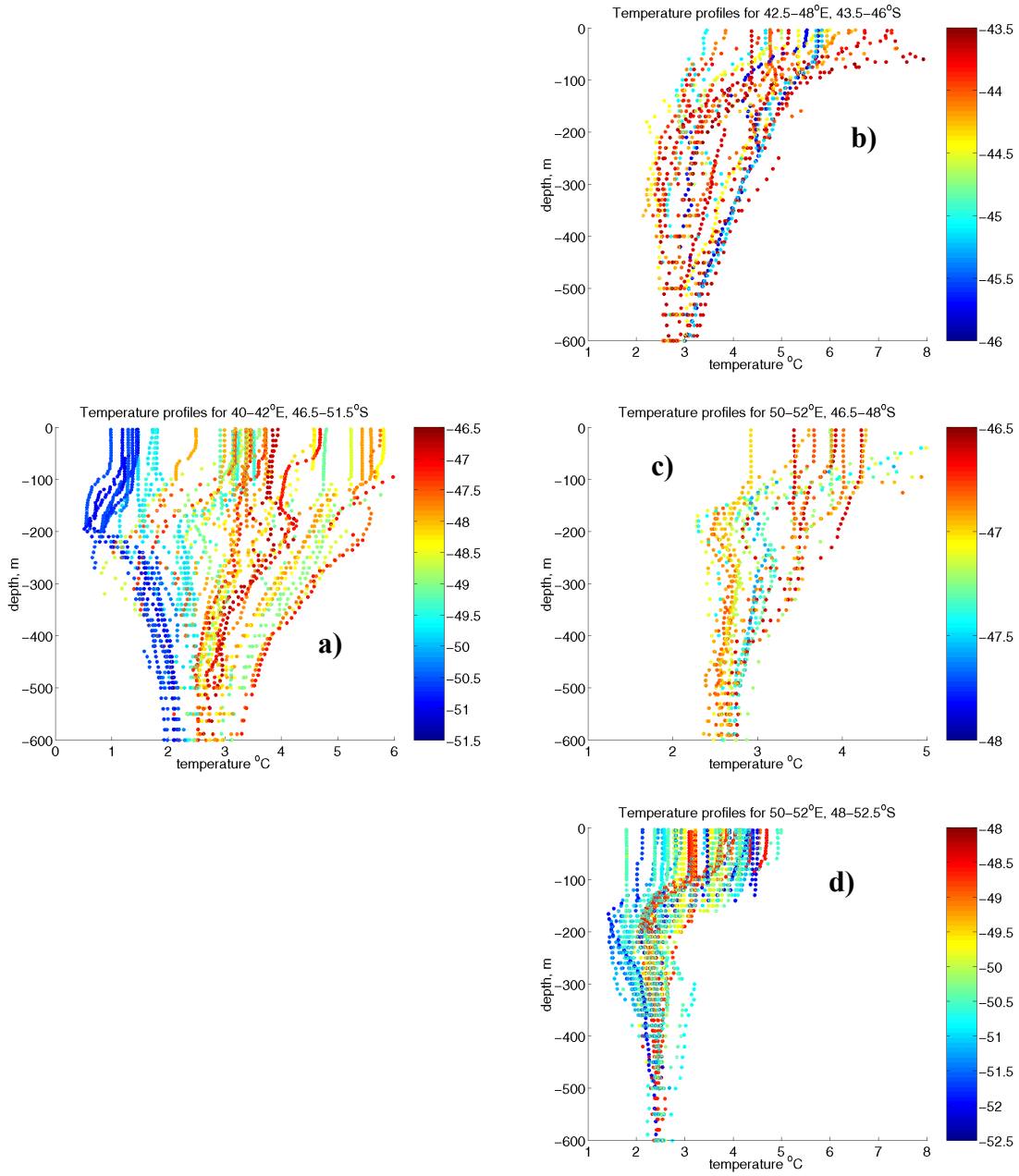

Figure 3.8 Temperature profiles from: the flow that passes south of the Del Cano Rise (a), between Del Cano Rise and Crozet Plateau (b), the flow along the southern edge of the Crozet Plateau (c) and the flow south of 48°S (d). The colour scale shows latitude.

3.2.3 Effects of topography on frontal location

The topography affects both the time-mean location of the fronts and the variability around this. The influence on the time-mean can be seen in Figure 3.9 as the surface geostrophic streamlines follow paths of approximately constant depth for long periods.

Figure 3.1 and Figure 3.4 also show this pattern, and Figure 3.10 shows that the variation of latitude of the fronts with time is small compared to the effects of topography on the latitude of the fronts. The physical reasons (potential vorticity) for this effect on flows on a rotating sphere have been investigated in section 1.2.3.

The dynamic heights 110dyn cm, 85dyn cm and 45dyn cm were chosen to represent the Northern SAF branch (NSAF), Southern SAF branch (SSAF) and Polar Front respectively. The criteria for selecting these heights were as follows: NSAF, a height that always passed south of the Del Cano Rise and then turned northward to the west of the Crozet Plateau; SSAF, a height that always passed close to the south of the Crozet Plateau; PF, a height that always passed between the Del Cano Rise and Ob-Lena (Conrad) Rise close to the Ob-Lena (Conrad) Rise. Figure 3.9 shows how the flows approximately follow lines of constant depth, as expected. The divergence of bathymetry contours south of the Crozet Plateau east of 45°E causes the 45 and 85 dyn cm contours to diverge as they follow the two sides. This will cause an area of weak flow, as is observed.

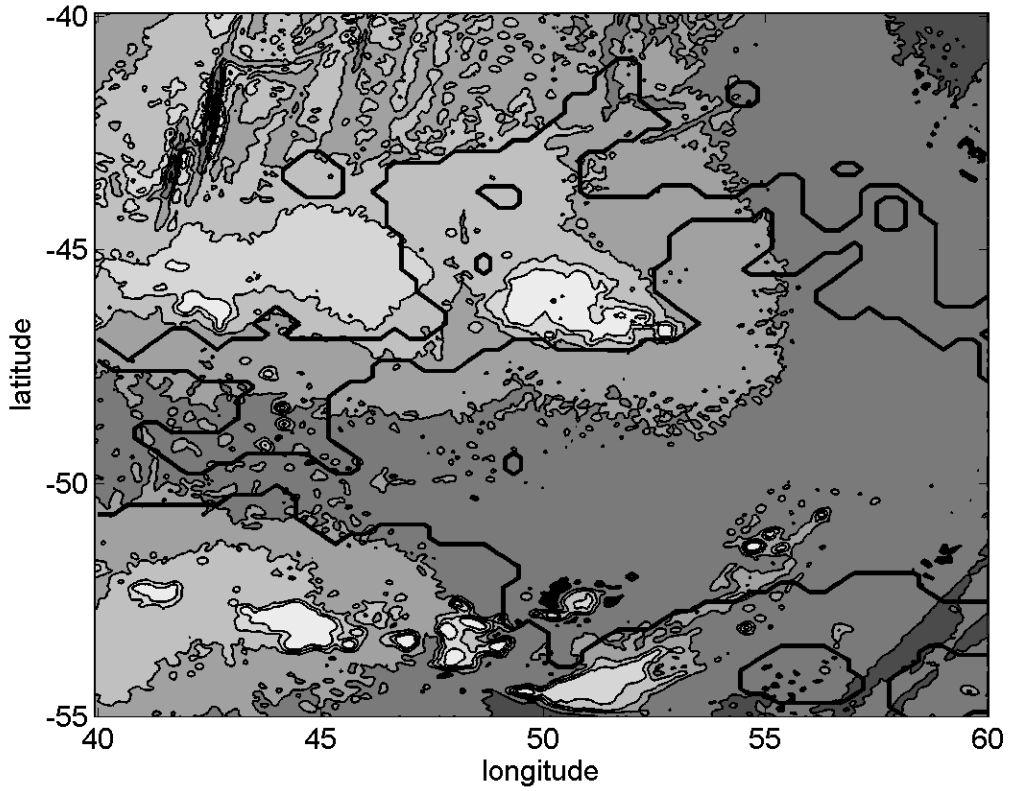

Figure 3.9 Example image of the locations of the (from north) 110, 85 and 45 dyn cm contours, over bathymetry (Sandwell and Smith 1997). Contour intervals are 1000m.

The latitudes of these dynamic heights were found at 40°E and 50°E and the time series of these latitudes are shown in Figure 3.10.

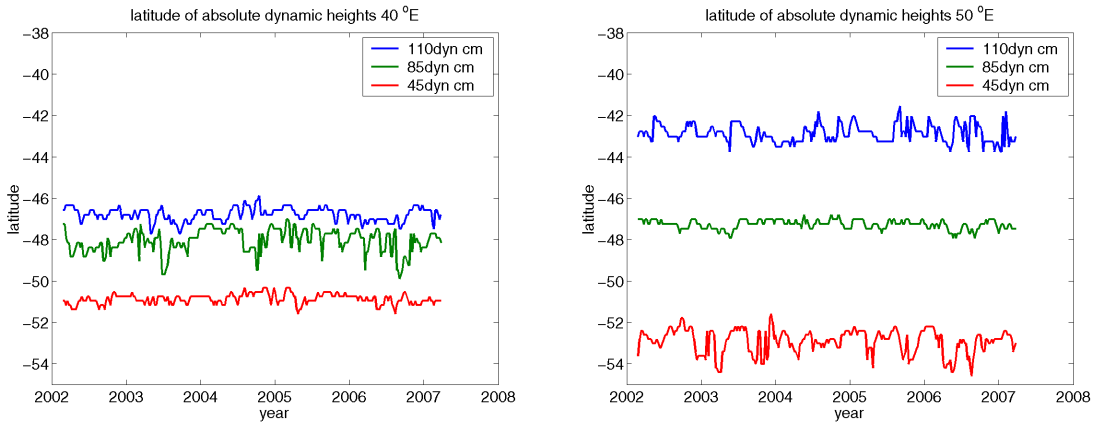

Figure 3.10 Latitude of dynamic heights 110 dyn cm, 85 dyn cm and 45 dyn cm, used to show the locations of the Northern SAF branch, Southern SAF branch and Polar Front respectively.

The standard deviation of the latitude for each height is shown in Table 3.1. The paths of the SSAF at 50°E and PF at 40°E are tightly controlled by the topography of the Crozet Plateau and the Ob-Lena (Conrad) Rise respectively. The NSAF at 40°E (or at least the dynamic height that picks it out at 50°E, there being no overall need to distinguish the SSAF and NSAF at this longitude) is also influenced, to a lesser extent, by the Del Cano Rise. The SSAF at 40°E and NSAF and PF at 50°E are not strongly controlled by bathymetry and this is reflected in the greater variation seen in their location. Argo float trajectories, Figure 3.3, also show greater variability in location away from topographic control, this being especially evident south of the Crozet Plateau where there is consistency in the location and direction of the trajectories close to the plateau but greater variability further south.

The fact that the locations of some of the flows in the area are controlled by topography decreases the interannual variability in the location of different biogeochemical zones. This consistency allows comparisons between the same geographical area between years with reduced problems of observed differences being driven by changes in the overall biogeochemical zone being sampled.

	Height\Longitude	40°E	50°E
NSAF	110 dyn cm	0.33	0.44
SSAF	85 dyn cm	0.58	0.23
PF	45 dyn cm	0.25	0.59

Table 3.1 Standard deviations of latitude of three dynamic heights representing the three main flows in the region.

3.2.3.1 Relative strengths of the SAF branches

Time series of the absolute dynamic height differences across the SSAF and NSAF are shown in Figure 3.11. The SSAF here is defined as the difference between a maximum in 45.6-46.8°S and a minimum in 47.4-49.3°S at 50°E. The NSAF is defined as the difference between a maximum in 44.7-48.0°E and a minimum in 47.0-50.7°E.

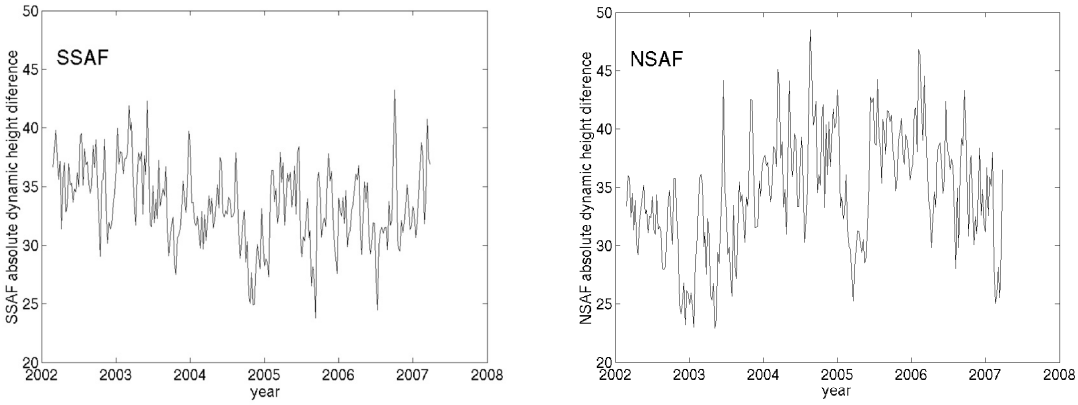

Figure 3.11 Time series of the strength of the two branches of the SAF, as measured by the absolute dynamic height difference across the front in dyn cm.

The mean dynamic height difference across the SSAF is 33.8 dyn cm. This is very similar to the difference across the NSAF of 34.4 dyn cm. There are however issues with a direct comparison. Firstly the 'SSAF' in this location and quantified in this way includes the closed circulation around the plateau because both currents flow in the same direction south of the plateau whereas the closed circulation flows against the NSAF and is therefore excluded. There is an average height difference of 7.5 dyn cm across the closed circulation (section 3.2.6) so it would be expected that a similar contribution from the closed circulation has been included in the SSAF. Accounting for the closed circulation,

the relative strengths are 34 and 26 dyn cm for the NSAF and SSAF respectively, approximately a 4:3 ratio.

This ratio contrasts with evidence from hydrography (Figure 3.4) that shows transport estimates of 30 and 5 Sv for the NSAF and SSAF. Floats drifting at 2000m also seem to be more likely to follow the path of the NSAF (4/6 follow NSAF) compared to shallower floats that are more likely to follow the path of the SSAF (3/9 follow NSAF). Due to the depth of the Del Cano Rise (approximately 1500m) it is to be expected that deep flows will be influenced by it more than surface flows. The SSAF therefore can be seen to be an important surface flow, with implications for the advection of iron, but much less significant when considering full depth volume transport.

3.2.4 Lack of connection between islands and south of southern SAF branch

All the available data sources show that the meridional flow past the plateau is predominantly northwards, the exception being the southwards branch of the recirculation along the western edge of the plateau (which feeds into the northern edge of the SSAF and continues eastward along the south edge of the plateau). The extent of any possible flow southwards from the Crozet Plateau is important due to the sampling strategy of the CROZEX program that took the area to the south, in particular a station at 49°S, 51.5°E, as an HNLC 'control' location to compare with 'island-influenced' conditions north of the plateau.

Immediately south of the Crozet Plateau is the SSAF, an eastward flowing front that would advect surface water off to the east and possibly around the eastern end of the plateau to the north of the plateau. South of this flow is an area of long residence time. This is inferred from the fact that no floats have entered the area, the closed contours in absolute dynamic height (Figure 3.5) and the lack of streamlines in the area found in hydrographic sections (Figure 3.4). Evidence for a long residence time comes from a float that was released at 47.7°S, 52.9°E, at the eastern end of the area. This float spent 270 days close to the point of release before leaving the area to the north-east (Figure 3.12).

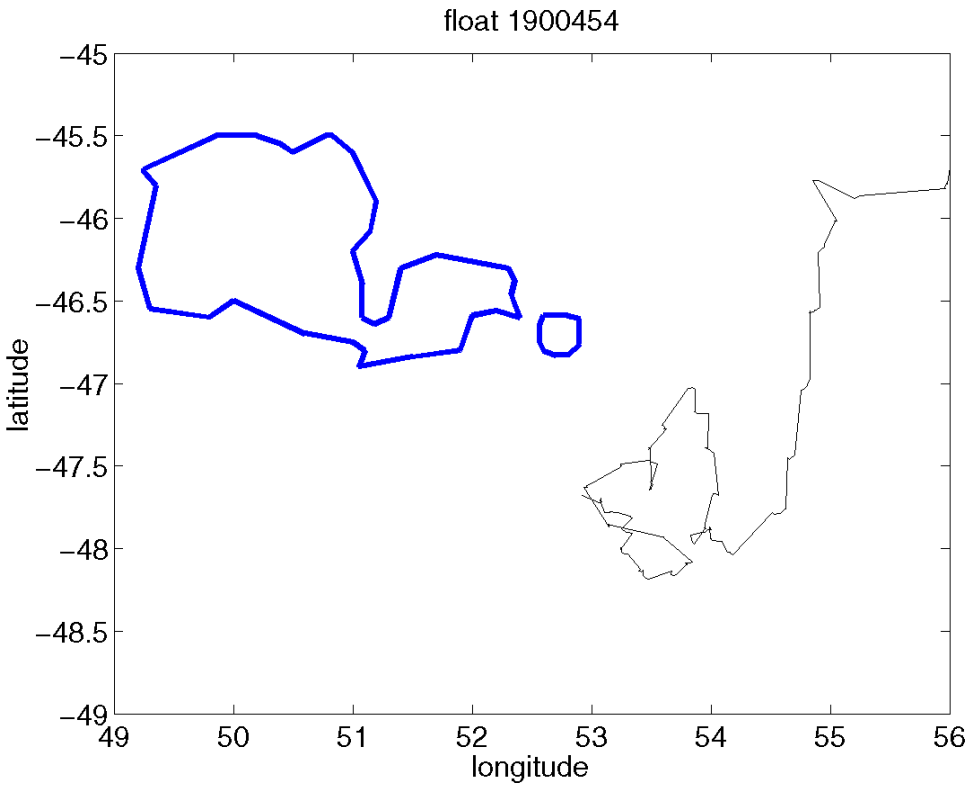

Figure 3.12 Trajectory of Argo float released south-east of the Crozet Plateau at the eastern end of an area of weak flow.

There is no indication from the float or drifter trajectories that island influenced water can reach significantly south of the plateau as far south-west as 49°S, 51.5°E where the southerly HNLC control station was located. Some absolute dynamic topography images, such as Figure 3.5, do however suggest that it may be possible for water from the southern edge of the SSAF to recirculate southwards, then westwards, towards the sampling location because they show closed contours around the area of weak circulation just described. This means that it is possible for island influenced water to reach the station, carrying enhanced iron concentrations, although such a path would require surface waters to cross the SSAF without being advected off to the east and without lateral mixing removing the majority of the iron concentration signal. Analysis in chapters 4 and 5 of satellite chl-a images and light availability show that phytoplankton in this area respond very differently compared to north of the plateau given the same levels of light and macronutrients, supporting the interpretation here that this area does not receive a significant iron flux, as is suggested by most of the available circulation data.

3.2.5 Residence time north of the plateau

It was observed in section 3.2.2 and 3.2.3 that part of the SSAF follows the topography around the eastern end of the Crozet Plateau. Following the CROZEX hypothesis, this is therefore an important flow because it is likely to become naturally enriched with iron as it passes close to the two eastern islands. Where this water goes after passing the islands is likely to be key to determining the location of the iron fertilised bloom. The residence time is also very important because it sets how long water can build up during the winter period (when there is insufficient light for biological utilisation of the iron). These issues are addressed by the study of Argo float trajectories, following the assumption that these are representative of surface flow characteristics (similarities between absolute dynamic height contours and Argo float trajectories already noted support this assumption).

Argo float trajectories around the Crozet Plateau are shown in Figure 3.13. They show that the average residence time for floats (between 1000m and 2000m) in the area 49.2-51.2°E, 43.8-45.8°S (red box) is 132 days. This compares to 57 days for the area 51.2-53.2°E, 44.5-46.5°S (green box) that is the same size but centred on the region of net flow. This net flow is the part of the SSAF that is deflected northwards around the eastern end of the Crozet Plateau.

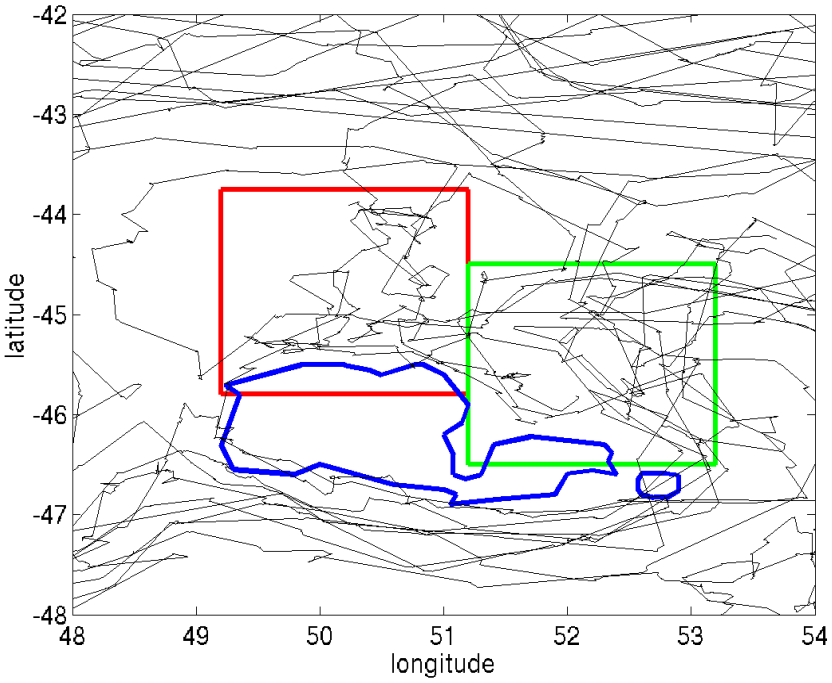

Figure 3.13 Argo float trajectories. The blue line is the 1000m contour of the Crozet Plateau.

3.2.6 Inflow into area north of the plateau

The trajectories in Figure 3.13 also show that both of these boxes receive water that has passed close to the plateau and islands at the eastern end (Ile de la Possession and Ile de l'Est). Within the eastern box this is net flow – the part of the SSAF that turns northwards around the eastern end of the plateau. Within the red box the inflow from the south is water that has detrained from the SSAF and this water is mixed with water that has detrained from the NSAF. This pattern of mixing between water that is likely to have enhanced iron concentrations after passing the islands and water from the NSAF that is likely low in iron, having not passed shallow topography, is likely to cause a gradient in iron concentrations, reducing to the north and west. Three examples of float trajectories that demonstrate these flow patterns are shown in Figure 3.14.

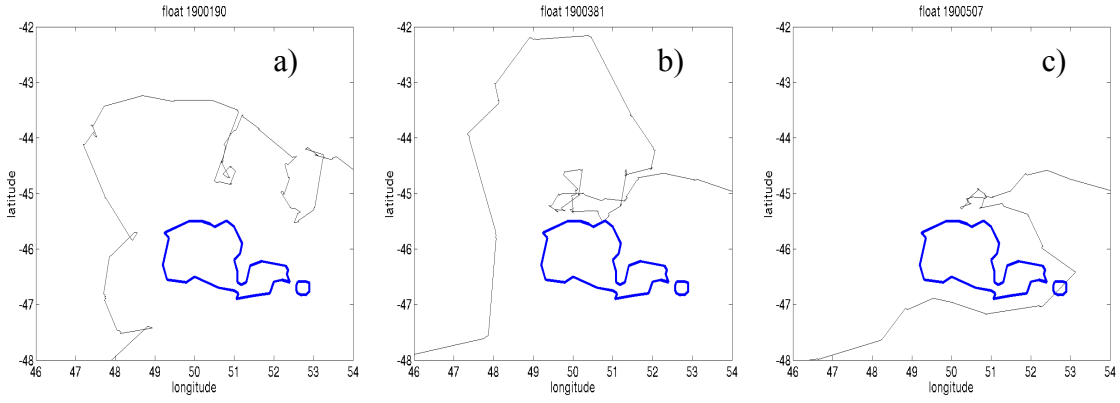

Figure 3.14 Float trajectories showing detrainment from the northern branch of the SAF (a and b) and southern branch (c) into the area north of the Crozet Plateau.

3.2.6.1 Cross frontal mixing

Another possible source of water to the area north of the plateau is mixing across the NSAF (as opposed to detrainment from it). Figure 3.15 shows the temperature and salinity from Argo float profiles at 200m and 10m (surface value for Argo floats) between 47 and 52ºE. The strong gradients north of 43ºS correspond to the SAF, STF and ARC. It is clear that if this water crossed the SAF and entered the bloom region (43-46ºS) there would be a signal in both temperature and salinity. It is also likely that the signal would extend down to at least 200m. The increases in surface temperatures in the region 43-46°S are associated with low salinities and the increase is not seen at 200m. This analysis shows that cross frontal mixing is not a significant source of water to the bloom

area. This means that the area north of the NSAF does not have to be considered as a possible source of iron or other oceanographic properties. The lower panel shows a constant temperature and salinity at 200m, again indicating a lack of mixing. It also indicates that the higher surface temperatures will be associated with greater density stratification.

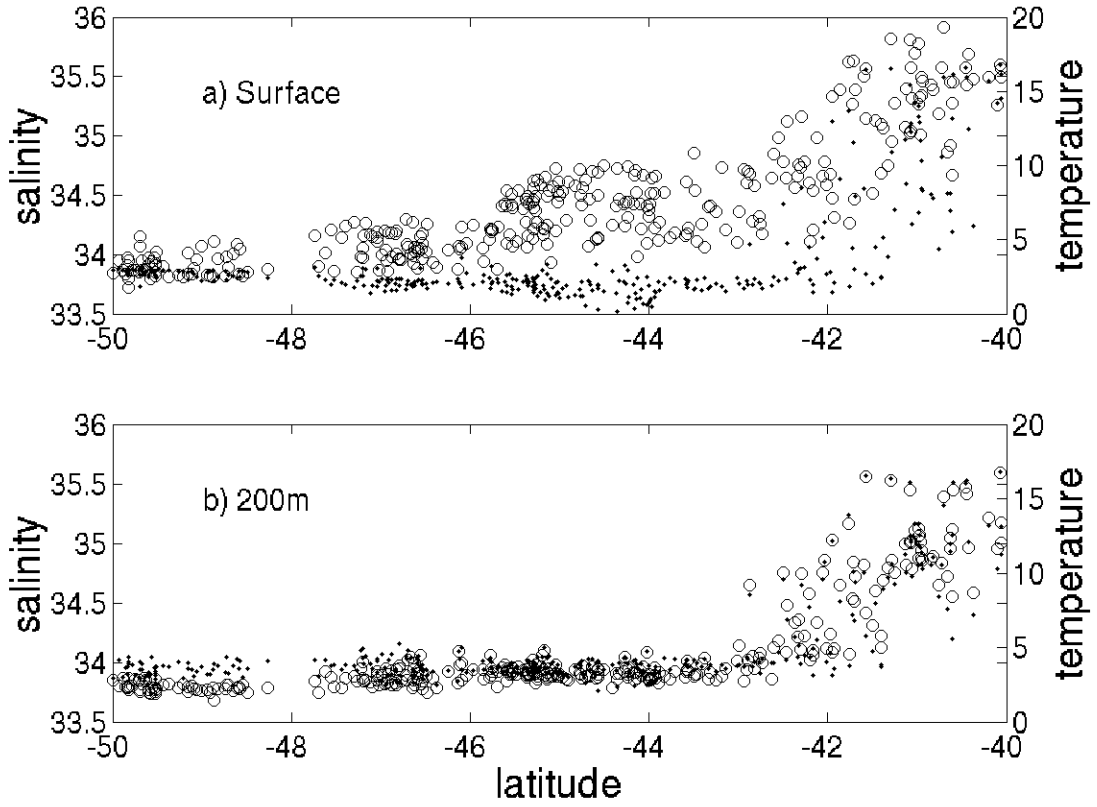

Figure 3.15 Temperature and salinity from Argo float profiles at the surface (above) and 200m (below) from region 40-50°S, 47-52°E. Open symbols temperature, points salinity.

It is noticeable in Figure 3.15 that there are very low surface salinities in the bloom region, between 44 and 45°S. It is however likely that these are due to Argo floats with a salinity offset as Figure 3.16 shows that at depth these floats have an offset of up to 0.2 relative to the CTD salinities at the equivalent point of the T/S plot. The salinities there are consistent between all CTD casts, including a cast from late 2005, so it is likely that natural variability is small. No attempt has been made to correct the Argo float salinities because a constant small offset will make little difference to the shape of the density profile and hence the mixed layer depth, which is the main use made of the Argo float salinity data in this work.

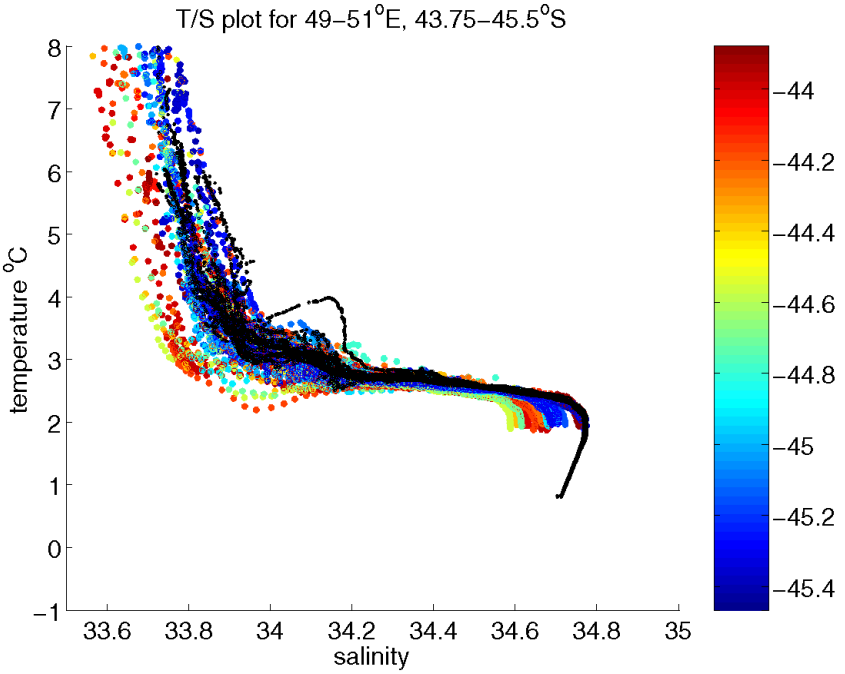

Figure 3.16 T/S plot for the bloom area with data from CTD profiles overlain (black).

3.2.7 Closed circulation around the Crozet Plateau

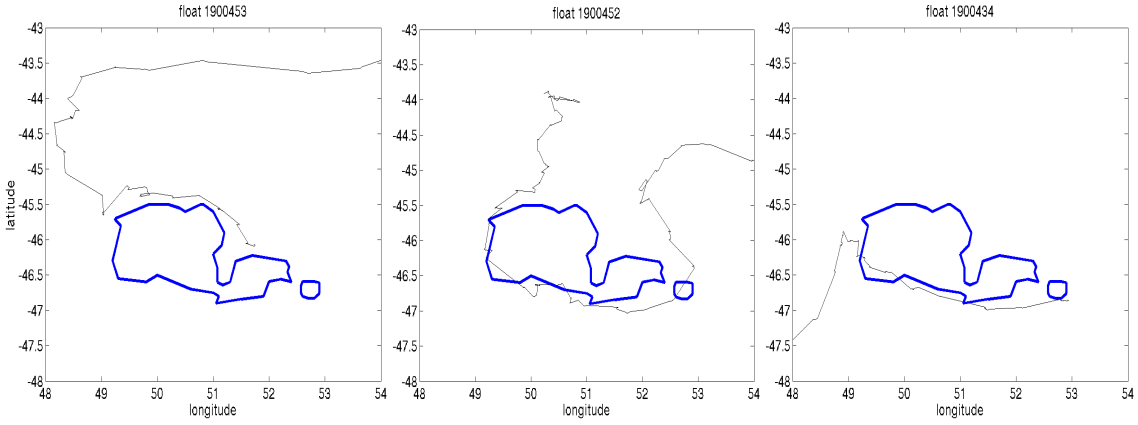

Figure 3.17 Argo float trajectories showing floats following the closed circulation around the Crozet Plateau.

Using the north-south cut through the absolute dynamic topography data at 50°E, the difference between the minimum in the range 44.5-45.5°S and maximum in 45.5-47°S is used to quantify the strength and persistence of the closed circulation. The time series for this flow is given in Figure 3.18. The mean difference is -7.5 dyn cm with a standard deviation of 2.7 dyn cm.

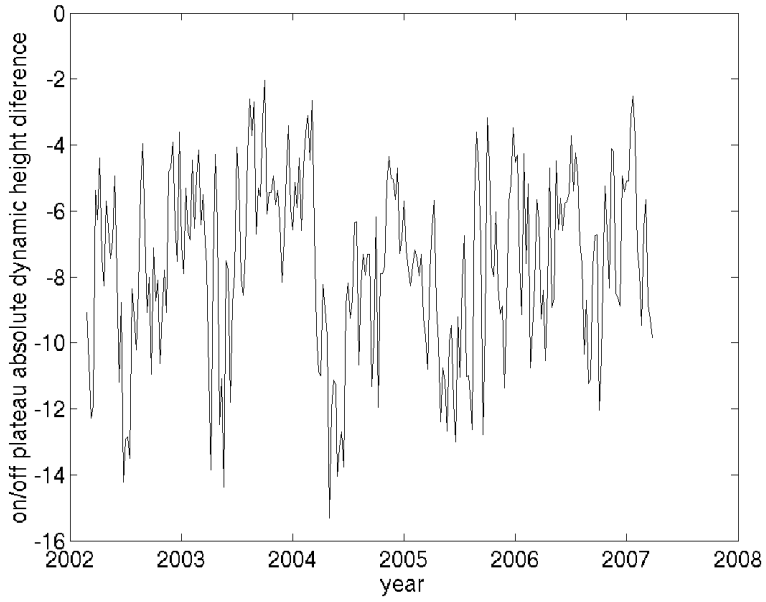

Figure 3.18 Absolute dynamic height difference (dyn cm) between over the plateau and north of the plateau.

There is also a persistent southward flow to the west of the Crozet Plateau, which has a mean difference of -11.1 dyn cm with a standard deviation of 3.3 dyn cm. This flow is enhanced by including part of the southern branch of the SAF returning south-east to the southern side of the Crozet Plateau after splitting from the northern branch, but does show that the westward flow to the north of the plateau continues around the plateau. It is not possible to isolate the recirculation from the net flow to the south and east of the plateau because it is in the same direction there as the SSAF. As shown in section 6.2.1.2 the closed circulation is caused by wind stress curl around the plateau.

3.3 Implications for phytoplankton distribution

The main hypothesis of the CROZEX study is that iron from the Crozet Plateau or Islands causes enhancement of phytoplankton growth over prevailing HNLC conditions. It is therefore worth summarising the findings of the circulation in the context of this hypothesis. This involves assessing the areas that water close to the plateau/islands is advected to.

The net flow around eastern end of the Crozet Plateau (part of the SSAF), together with the closed circulation around the plateau, leads to a northerly flow past the islands. This

then splits into a flow that continues north before turning eastward close to the NSAF and a weaker flow that continues westward along the northern flank of the plateau. Ekman flux off the plateau will also be predominantly northward due to the prevailing westerly winds. Combined, this leads to an advection of iron from the islands and plateau to the area north of the plateau. This area has been identified as having a long residence time, leading to this iron fertilised water building up there during the winter period, but also reducing the resupply iron to the area after this iron has been biologically utilised. There is a second identified source of water into this region – detrainment from the NSAF. This flows along the eastern flank of the relative deep (≈1500m) Del Cano Rise. This flow is kept away from the shallow Crozet Plateau by the southward flowing closed circulation so it is not expected that this flow is iron fertilised over background concentrations. This therefore may create a gradient in the iron concentrations due a source of high concentrations from the south (plateau) and/or south-east (islands) and low concentrations from the west and north (detrainment from the NSAF).

Some of this iron may be advected south by the closed circulation at the western end of the plateau. This will then be carried close to the southern edge of the plateau by the combined SSAF/closed circulation or returned over the plateau by Ekman drift. For water that has been close to the plateau to be advected south it would have to cross the SSAF and then follow around the eastern end of the area of closed circulation. The possibility of water following this route cannot be discounted but it is likely that there will be a small volume flux that becomes very heavily diluted.

4 Phytoplankton distribution

4.1 Introduction

Satellite ocean colour data show that there is a regular phytoplankton bloom to the north of the Crozet Plateau each austral spring in contrast to the prevailing high nutrient low chlorophyll (HNLC) conditions of the Southern Ocean. Observation of the bloom in SeaWiFS images and the links between the distribution of enhanced chl-a concentrations and the known circulation in the area (Pollard and Read 2001) led to the CROZEX project. The hypothesis was that natural iron fertilisation from the islands and/or plateau alleviates the iron limitation generally present in the Southern Ocean (Martin *et al.* 1990; de Baar *et al.* 2005; Boyd *et al.* 2007). It was seen in chapter 3, and also Pollard *et al.* (2007) that the flow pattern around the Crozet Plateau is such that the great majority of water that passes close to the islands and plateau flows to the northern side of plateau. This chapter uses 9 years of SeaWiFS data, together with knowledge of the circulation from the previous chapter and Pollard *et al.* (2007), to define four productivity regimes that occur around the Crozet Plateau due to the interactions between topography and both the circulation and the biogeochemistry. The distribution of enhanced chl-a concentrations is also used as a tracer to further investigate the circulation. Some data are presented about the initiation of the bloom but analysis and explanation is given in chapter 5, after the distribution of light availability is investigated.

The Crozet region is one of three areas of the Southern Ocean where there are enhanced chl-a levels associated with Sub-Antarctic islands and shallow topography (Pollard *et al.* 2007). The others are South Georgia (Atkinson *et al.* 2001; Korb and Whitehouse 2004; Holeton *et al.* 2005) and Kerguelen (Blain *et al.* 2001; Bucciarelli *et al.* 2001; Blain *et al.* 2007). There are also Sub-Antarctic islands that do not have a large impact on the chl-a concentrations. These include the Prince Edward and Marion Islands (Ansorge *et al*. 1999) and Macquarie Island (Moore and Abbott 2000).

4.2 Chl-a images

The 8-day images for each year are shown in appendix A, starting from early August of each year (the start of the spring bloom and also close to when data were first collected in 1997) and running through to early August of the following year. The images are produced after applying the adjustment

$$CHL_{in\ situ} = -0.08 + 2.05 \times CHL_{satellite}$$

to satellite values to best estimate *in situ* chl-a values (equation 2.5, section 2.5.6). From 2002 onwards these images are derived from the merged SeaWiFS/MODIS product whereas before that SeaWiFS is the only data source. This leads to increased coverage and to a slight systematic shift, especially at low chl-a values, but the change is minor – see section 2.5.2. It is quite possible that the adjustment is not valid north of the SAF so the chl-a values here may not be representative, but this area is not considered further in this work. To illustrate the overall characteristics of the bloom, a selection of chl-a images from the 2004/5 season are repeated here as Figure 4.1.

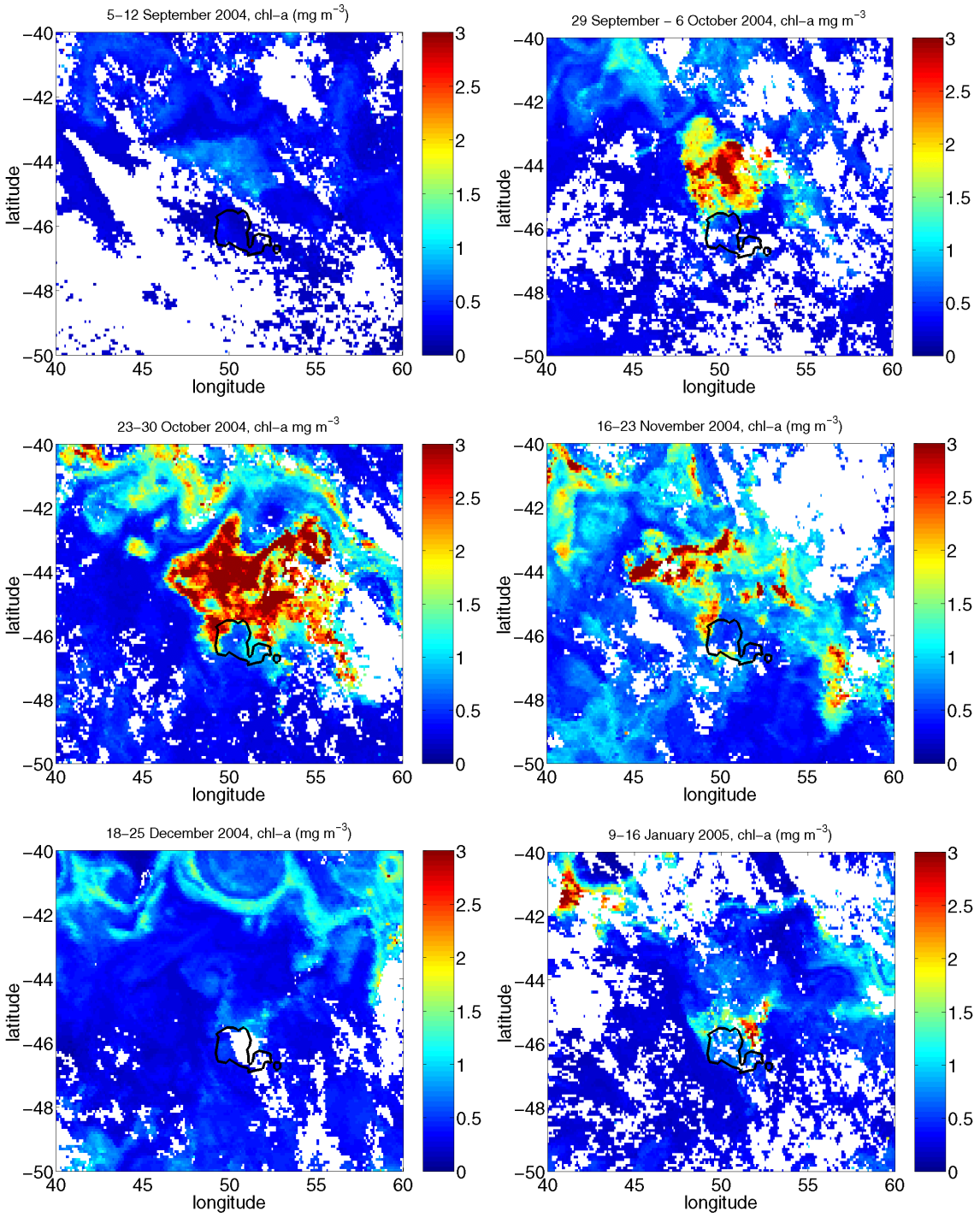

Figure 4.1 A selection of merged SeaWiFS/MODIS chl-a images through the 2004 season. The black line is the 1000m contour of the Crozet Plateau. The full set of images from 1997-2005 is included as appendix A.

4.3 Seasonal composites – mean

Another way to visualise the data is to average in time throughout the period of light availability. Seasonal composites of SeaWiFS chl-a data, presented in Figure 4.2, show the mean chl-a in each pixel (averaged across those with data) from 4th August (of the year given) to 29th March (the following year). The seasonal mean gives an indication of the spatial variation in productivity in different areas around the plateau. Caveats about using satellite chl-a as a proxy for productivity are detailed in section 2.5.1 and there is the added problem here that no allowance has been made for data missing due to cloud cover. This latter effect could cause a positive or negative bias to each pixel (and bias for neighbouring pixels will clearly not be independent) depending on the distribution of missing data through the year. The similar patterns each year however suggest that the overall spatial contrasts are robust to missing data.

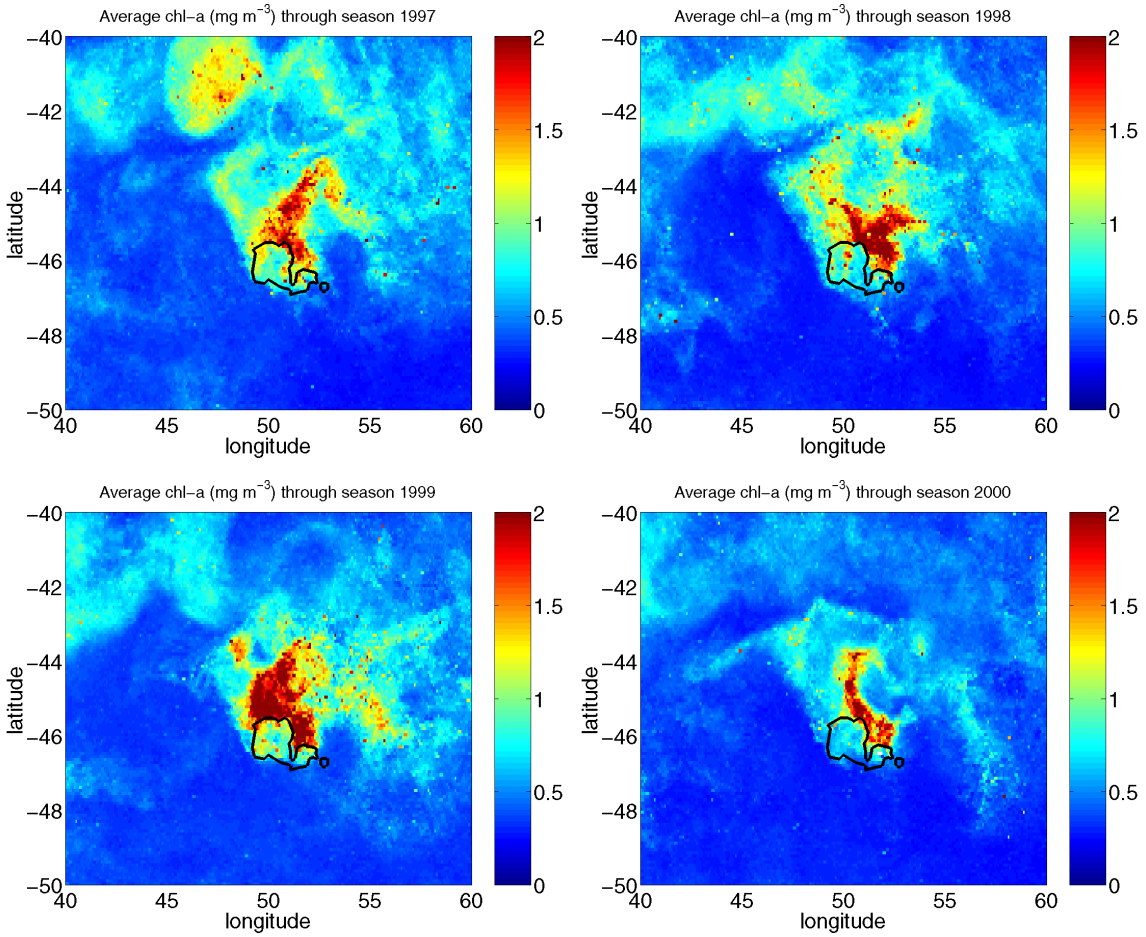

Continued on next page

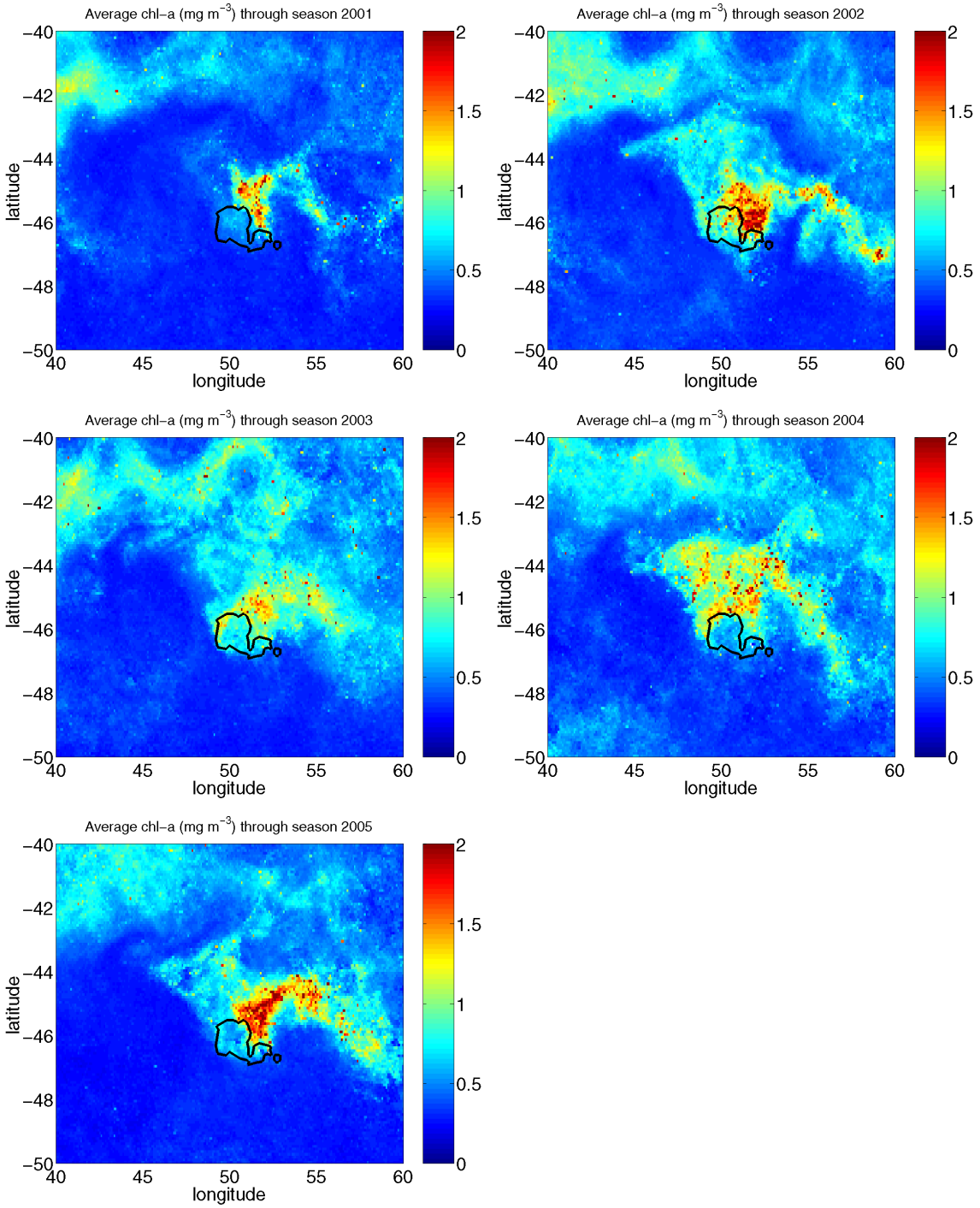

Figure 4.2 Seasonal composites of chl-a from SeaWiFS for each year 1997-2005. Formed by averaging across all 8-day periods with data between 4th August and 29th March.

4.4 Characteristics of overall chl-a distribution

Figure 4.1, Figure 4.2 and appendix A show that there are four distinct productivity zones in the area. These are marked schematically in Figure 4.3. These are the bloom area to the north of the Crozet Plateau, split into 'spring bloom' and 'persistent bloom'; the area over the plateau; and the area to the south of the plateau. After presenting area-averaged data from each year the spatial and temporal characteristics of each of the four areas are discussed in detail in section 4.6

The bloom is bounded to the west and north by very low chl-a concentrations in the NSAF, separating it from increased levels further north associated with the Sub-Tropical Front and Agulhas Return Current. These contrasts show the strong meandering of these fronts. Water exchange between the NSAF and the bloom area increases the chl-a concentration in the NSAF downstream to the east as iron-enriched water is entrained into the front from the bloom area, this is examined further in section 4.8.

The area identified north of the SAF is largely comprised of the Agulhas Return Current. Figure 1.1 and the associated discussion show that there is no significant input of water from this area into the area where the bloom occurs. It therefore does not need to be considered in understanding these areas and it is omitted from this study.

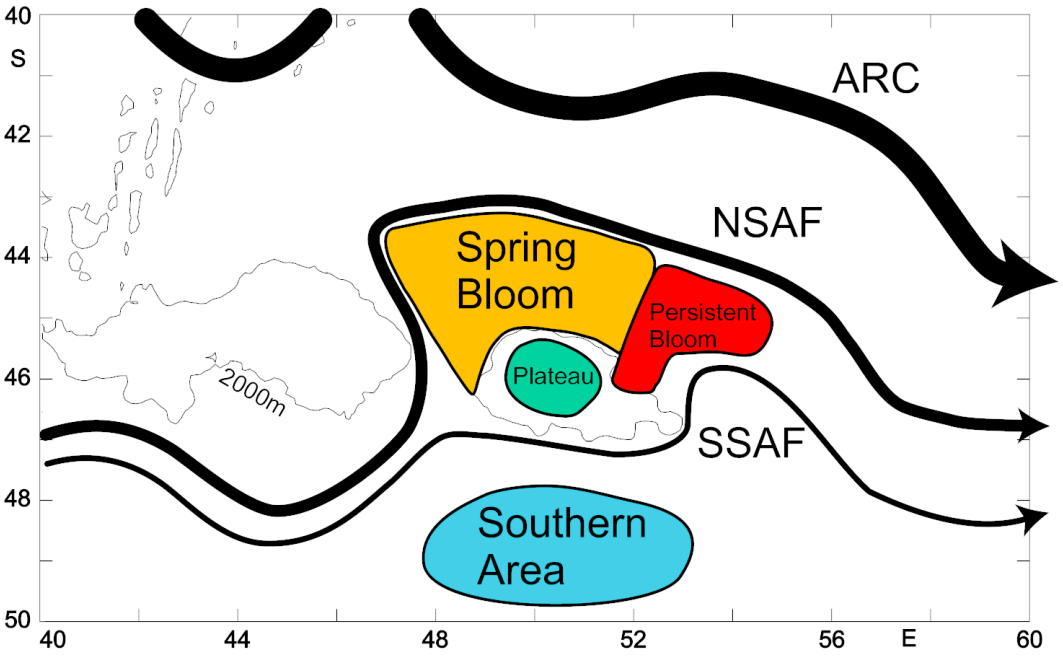

Figure 4.3 Schematic of the different productivity areas around the Crozet Plateau.

4.5 Definition of boxes used in study

In order to quantify the temporal and spatial progression of the bloom and investigate the four main areas of productivity, across the 9 years of SeaWiFS data, 6 boxes were defined (Figure 4.4). The median chl-a values are calculated for each box (and for boxes A-C combined) for each 8-day merged SeaWiFS/MODIS image. The four boxes north of the plateau were chosen to investigate the effect of the increasing distance north away from the plateau and to be away from the edge of the bloom area because the location of the boundary changes with the meandering of the SAF. Box C was set narrower than boxes A and B to study more closely the effects of the edge of the plateau and box D was set off to the south-east to study the effects of the two main islands and the flow around the eastern end of the plateau. Further boxes over the plateau (box E) and to the south (box F) are used to study the other two productivity regimes. Boxes A, B and C together have been used to characterise the regime north of the islands for comparison with these other areas.

Box	Longitude W	Longitude E	Latitude N	Latitude S
A	49.0°E	52.0°E	43.0°S	44.0°S
B	49.0°E	52.0°E	44.0°S	45.0°S
C	49.0°E	52.0°E	45.0°S	45.5°S
D	51.3°E	52.4°E	45.5°S	46.3°S
E	49.6°E	51.0°E	45.7°S	46.3°S
F	49.0°E	52.0°E	48.0°S	50.0°S

Table 4.1 Bounding co-ordinates for boxes used in study of temporal and spatial variation in satellite chl-a.

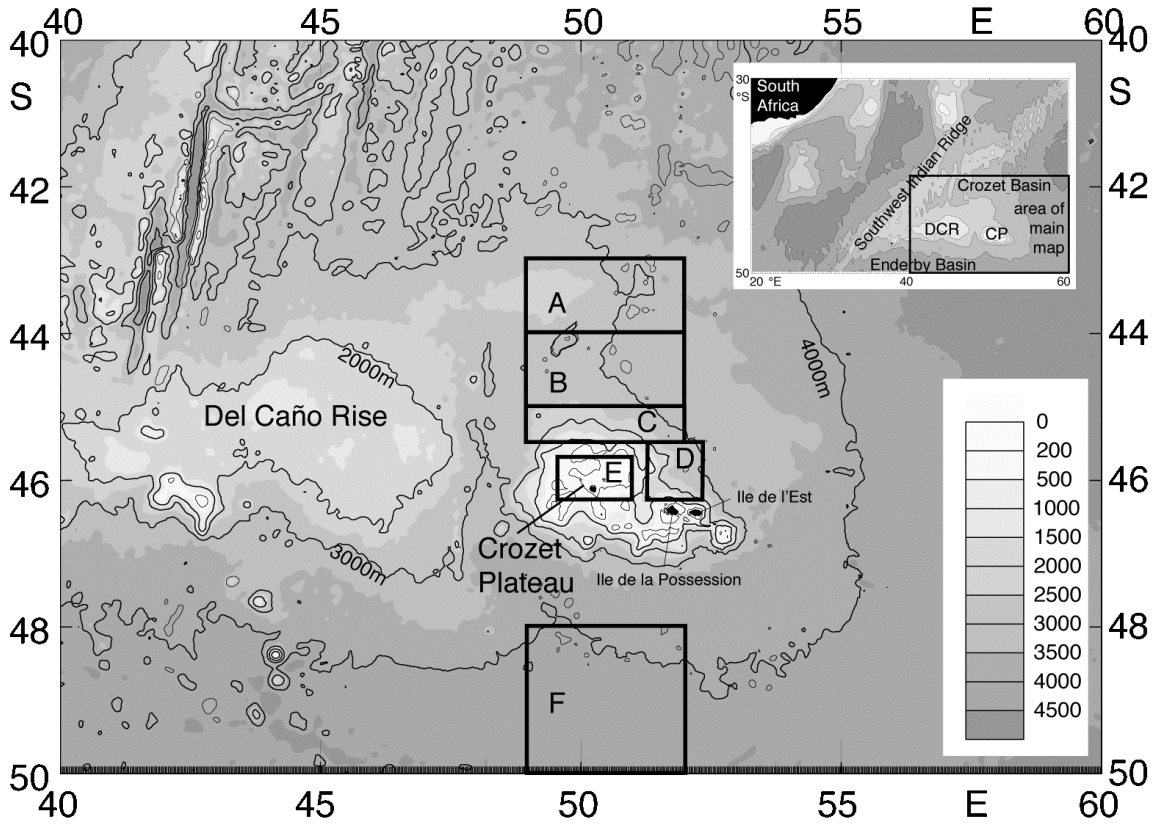

Figure 4.4 Boxes used to study the spatial and temporal development of the bloom. Plotted over the Sandwell and Smith (1997) bathymetry.

4.6 Seasonal progression of chl-a

Figure 4.5 shows the progression of chl-a concentrations through each year from 1997-2005. The progression in each area is discussed separately in the following sections.

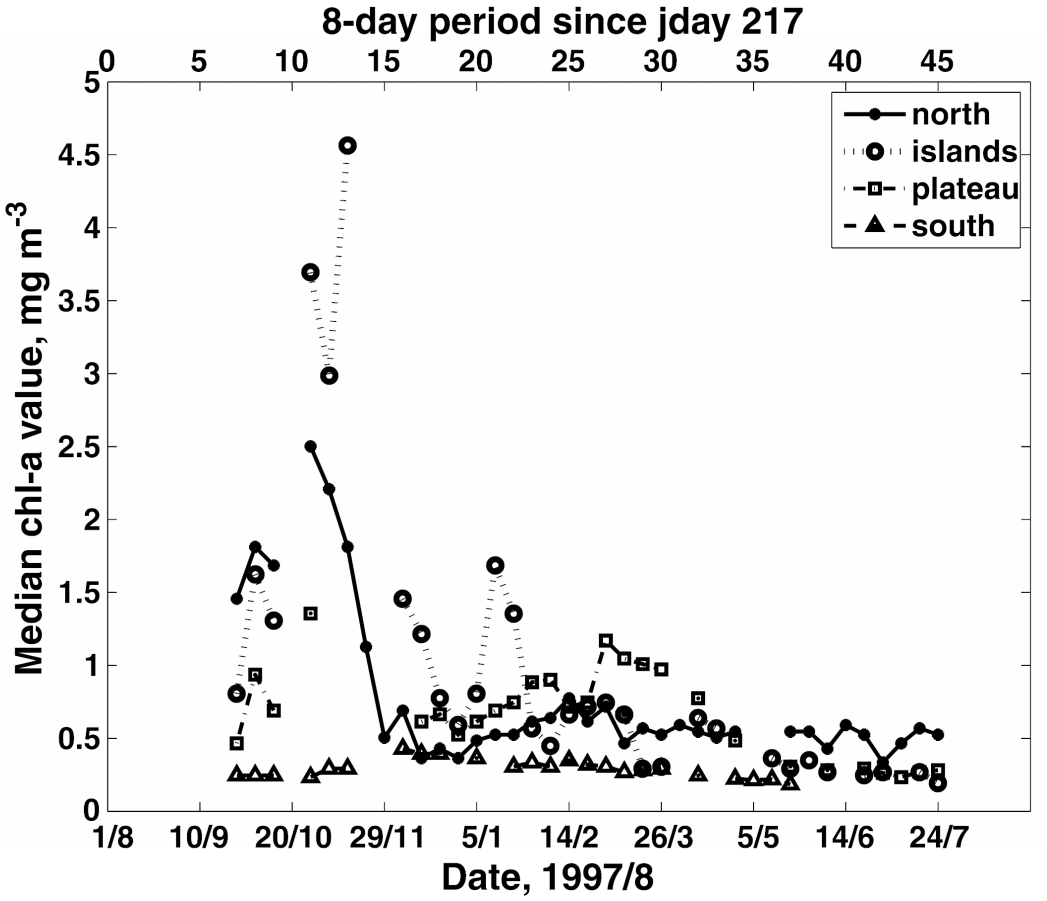

Figure 4.5 Time series of box median chl-a, from SeaWiFS, north of the plateau (boxes A-C), north of the eastern islands (box D), over the plateau (box E) and south of the plateau (box F) for 1997-2005 (continued on following pages). Missing points are due to >80% cloud cover over the box.

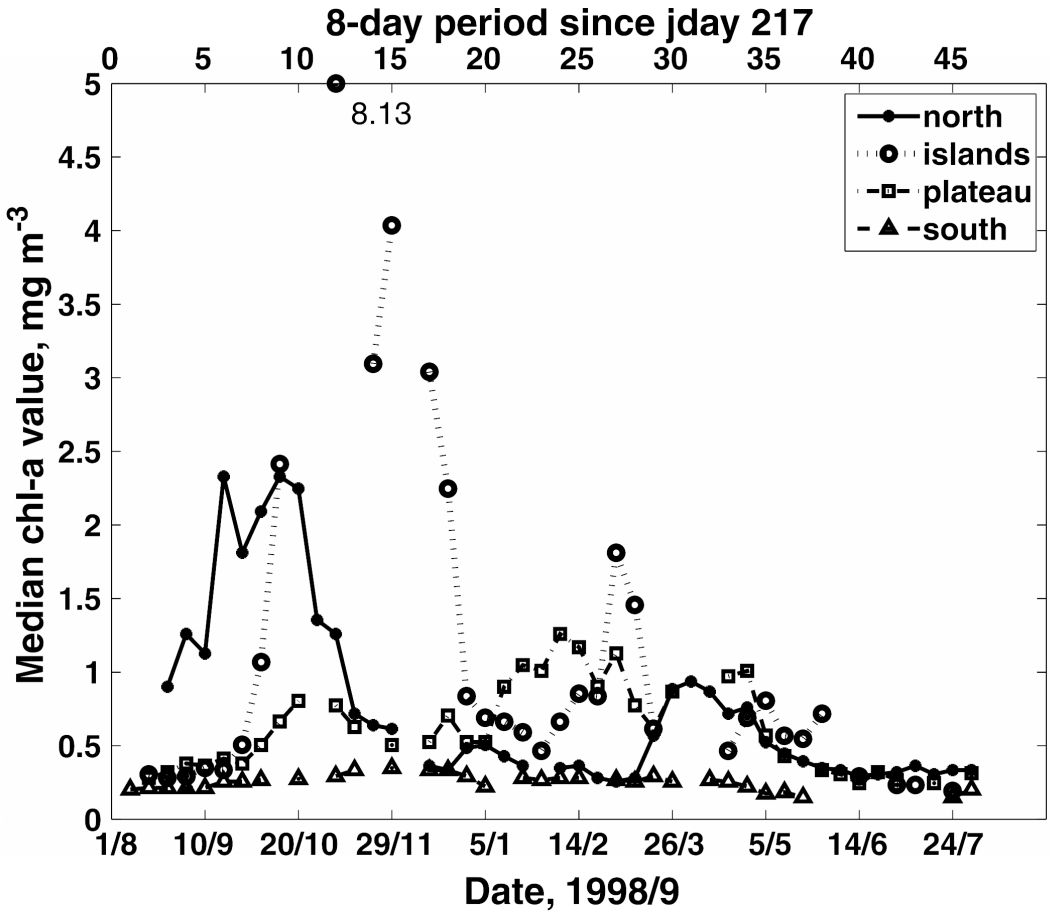
8-day period since jday 217
0 5 10 15 20 25 30 35 40 45
8.13
north
islands
plateau
south
Median chl-a value, mg m-3
0 0.5 1 1.5 2 2.5 3 3.5 4 4.5 5
1/8 10/9 20/10 29/11 5/1 14/2 26/3 5/5 14/6 24/7
Date, 1998/9

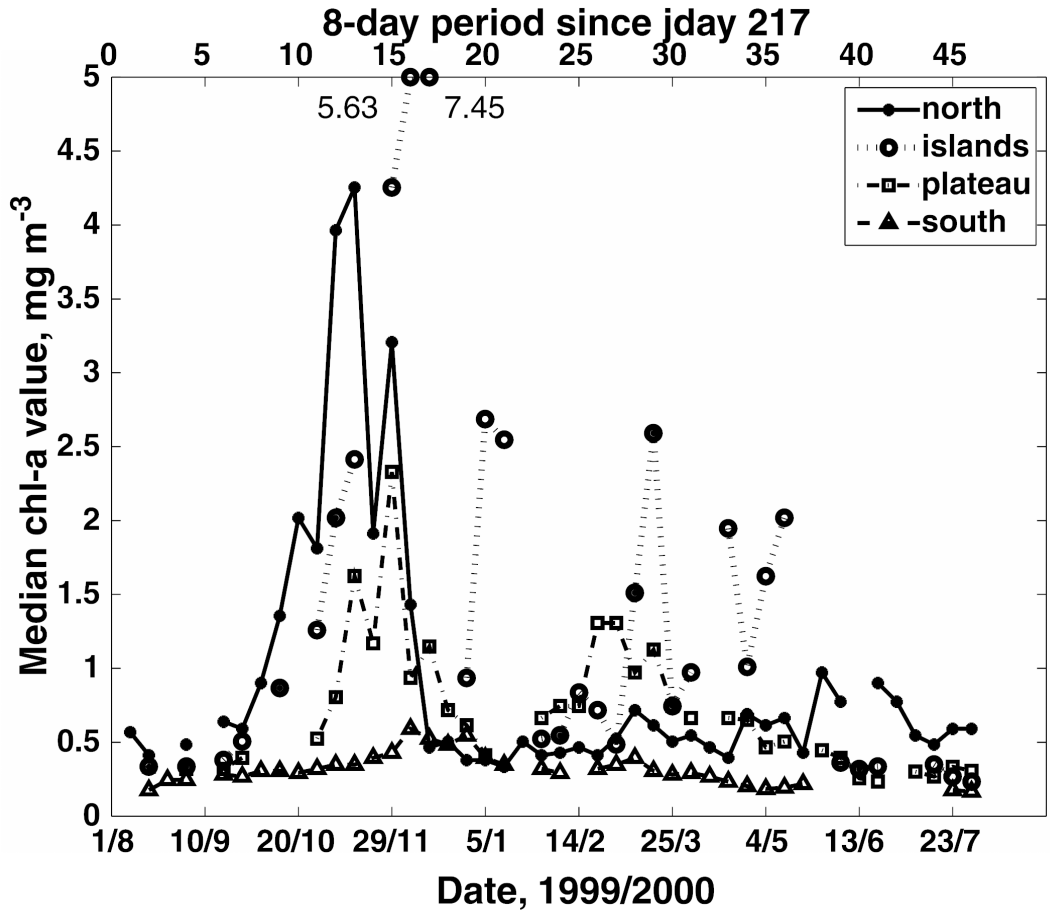
8-day period since jday 217
0 5 10 15 20 25 30 35 40 45
5.63
7.45
north
islands
plateau
south
Median chl-a value, mg m-3
0 0.5 1 1.5 2 2.5 3 3.5 4 4.5 5
1/8 10/9 20/10 29/11 5/1 14/2 25/3 4/5 13/6 23/7
Date, 1999/2000

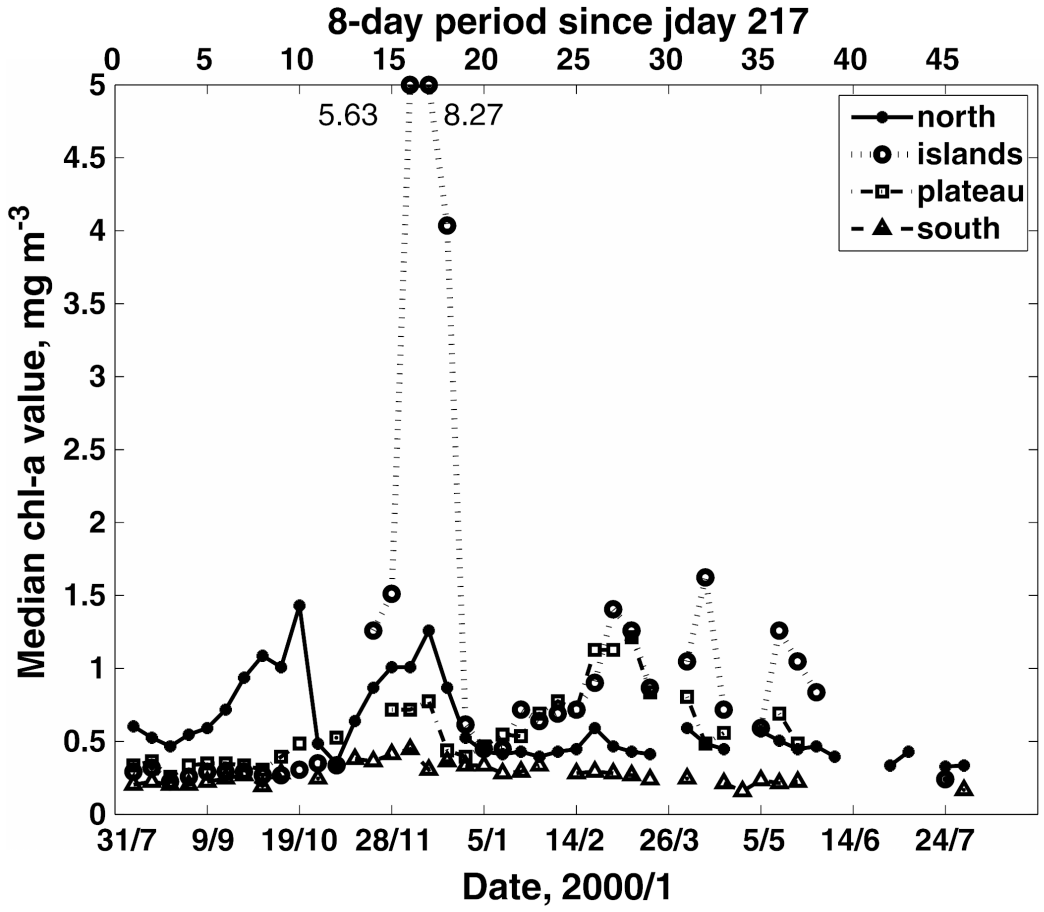
8-day period since jday 217
0 5 10 15 20 25 30 35 40 45
5.63
8.27
north
islands
plateau
south
Median chl-a value, mg m-3
0 0.5 1 1.5 2 2.5 3 3.5 4 4.5 5
31/7 9/9 19/10 28/11 5/1 14/2 26/3 5/5 14/6 24/7
Date, 2000/1

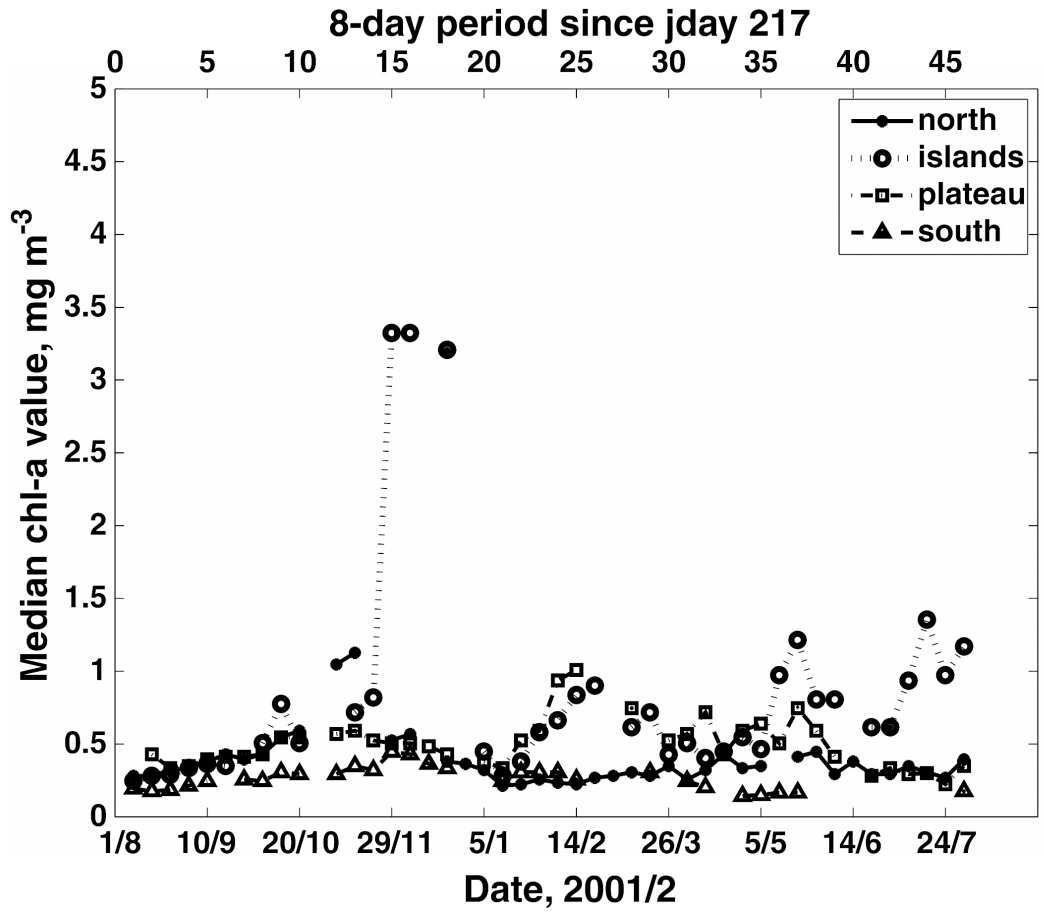
8-day period since jday 217
0 5 10 15 20 25 30 35 40 45
north
islands
plateau
south
Median chl-a value, mg m-3
0 0.5 1 1.5 2 2.5 3 3.5 4 4.5 5
1/8 10/9 20/10 29/11 5/1 14/2 26/3 5/5 14/6 24/7
Date, 2001/2

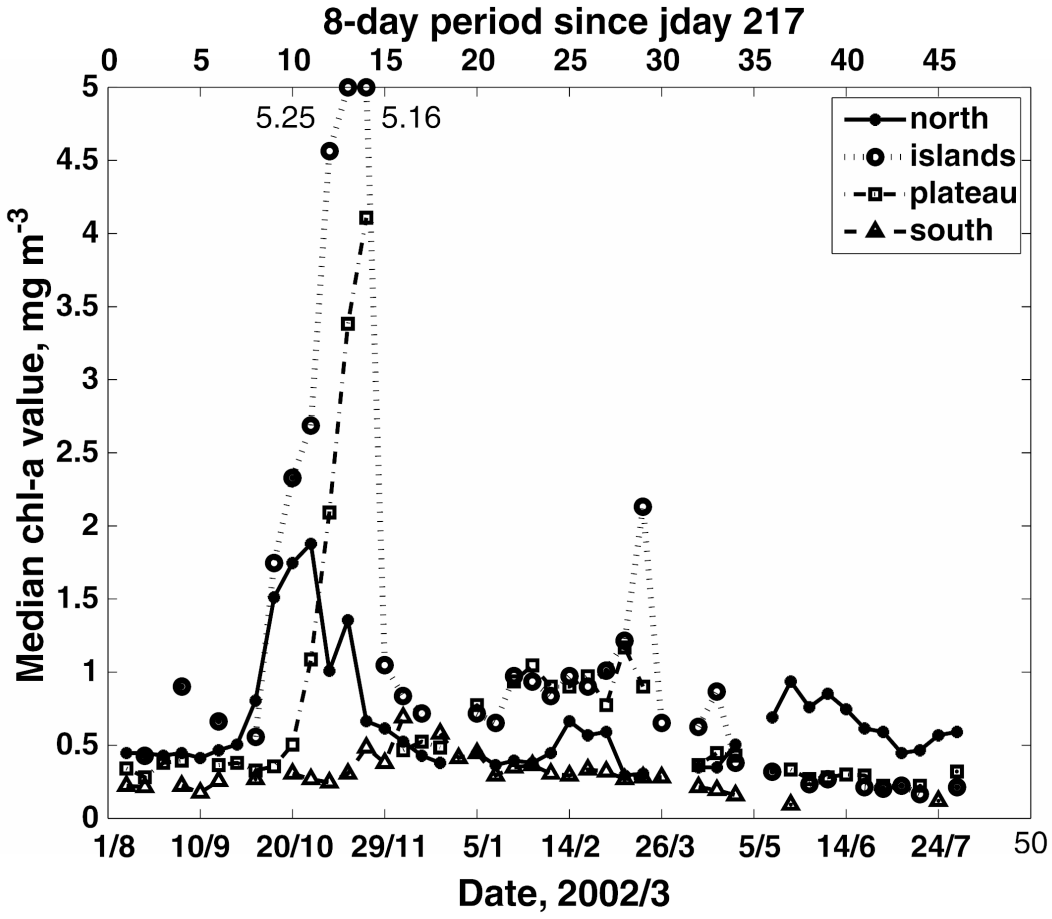
8-day period since jday 217
0 5 10 15 20 25 30 35 40 45
5.25
5.16
north
islands
plateau
south
Median chl-a value, mg m-3
0 0.5 1 1.5 2 2.5 3 3.5 4 4.5 5
1/8 10/9 20/10 29/11 5/1 14/2 26/3 5/5 14/6 24/7 50
Date, 2002/3

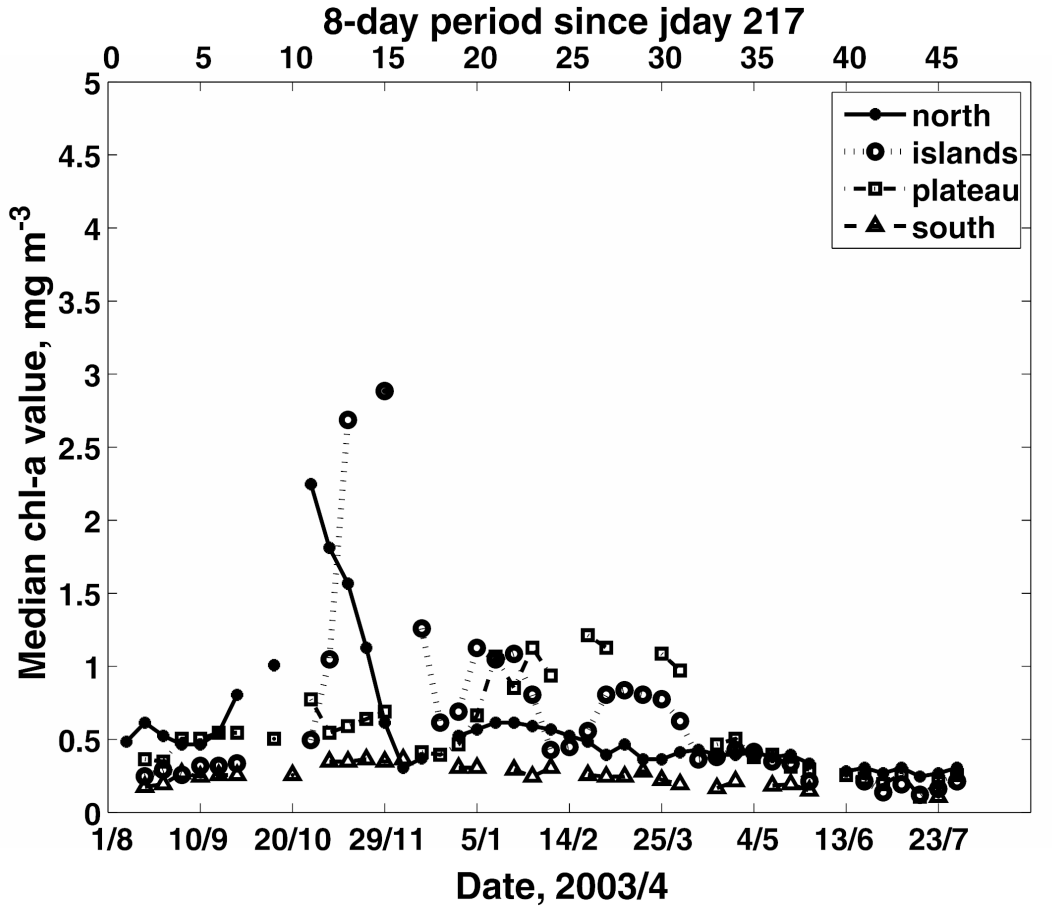
8-day period since jday 217
0 5 10 15 20 25 30 35 40 45
north
islands
plateau
south
Median chl-a value, mg m-3
0 0.5 1 1.5 2 2.5 3 3.5 4 4.5 5
1/8 10/9 20/10 29/11 5/1 14/2 25/3 4/5 13/6 23/7
Date, 2003/4

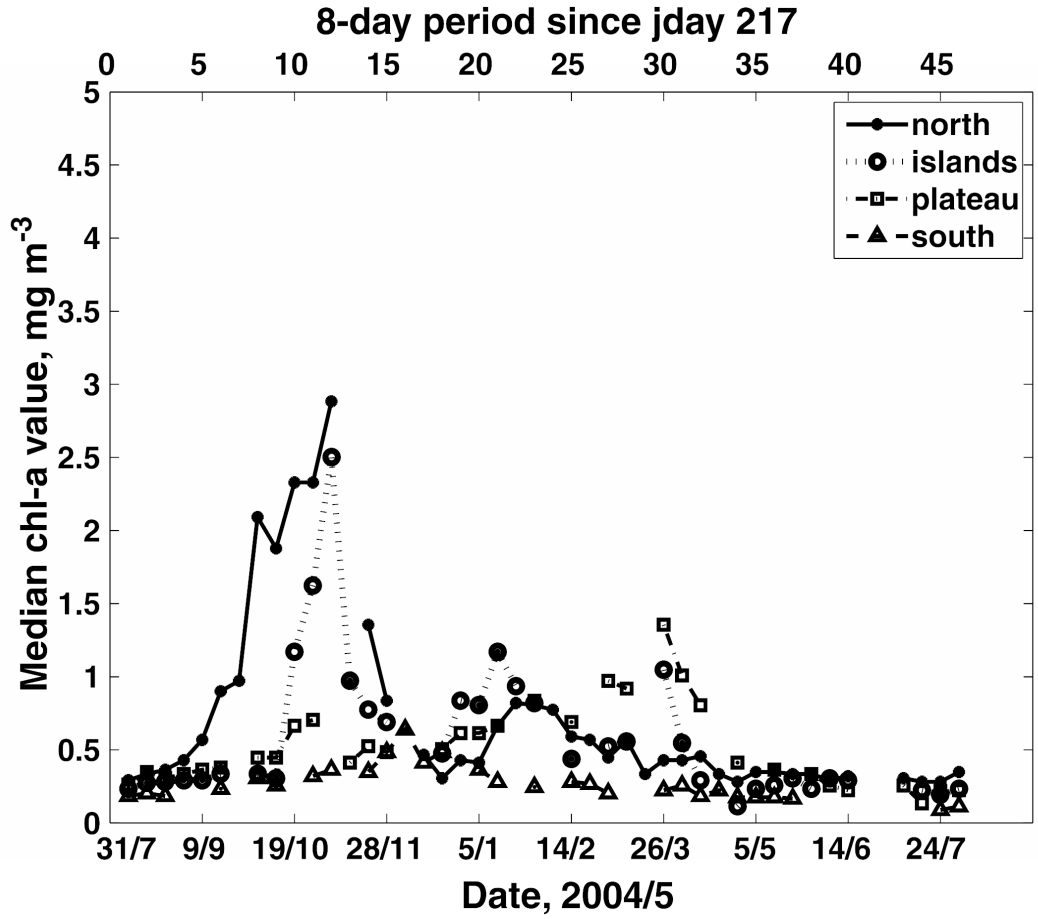
8-day period since jday 217
0 5 10 15 20 25 30 35 40 45
Median chl-a value, mg m-3
0 0.5 1 1.5 2 2.5 3 3.5 4 4.5 5
north
islands
plateau
south
31/7 9/9 19/10 28/11 5/1 14/2 26/3 5/5 14/6 24/7
Date, 2004/5

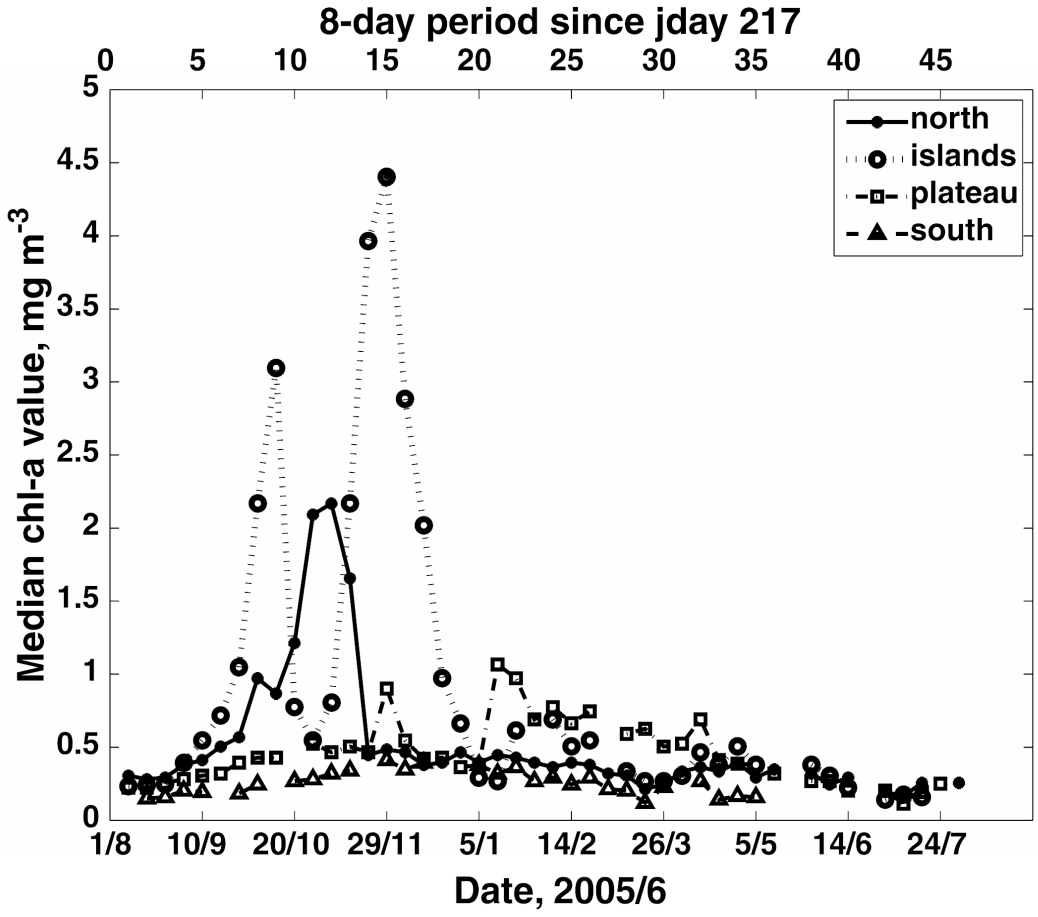
8-day period since jday 217
0 5 10 15 20 25 30 35 40 45
Median chl-a value, mg m-3
0 0.5 1 1.5 2 2.5 3 3.5 4 4.5 5
north
islands
plateau
south
1/8 10/9 20/10 29/11 5/1 14/2 26/3 5/5 14/6 24/7
Date, 2005/6

4.6.1 North of the plateau – Spring bloom

High chl-a concentrations occur to the north of the plateau (spring bloom). The bloom starts in early-mid September with enhanced chl-a levels initially separated from the plateau by a strip of low chl-a waters, approximately 100km wide (Figure 4.1a). The bloom then spreads south across this strip (Figure 4.1b). There are two main inflows into the spring bloom region. Water with presumed low iron concentrations is detrained from the NSAF and enters the bloom area from the west and north. This causes the patches of low chl-a in the western side of the bloom (Figure 4.1c). Water also detrains from the flow around the eastern end of the plateau, this has passed close to the eastern islands so it is enhanced in dissolved iron (Planquette *et al.* 2007). The anticyclonic flow around the plateau described in section 3.2.7 advects chl-a southwards around the western side of the plateau (Figure 4.1b-d), but this does not appear to reach the southern edge of the plateau.

To the north of the plateau the increase in chl-a is approximately exponential through August-October from pre-bloom concentrations of ≈0.3 mg m^{-3}. The exponential increase is consistent with light limitation being suddenly lifted from an area already replete in iron because under these conditions the phytoplankton are effectively free from growth controls except for the light intensity. The population growth rate will then be proportional to the population size and the growth will therefore be exponential. The constant of proportionality in this relationship is a function of light availability so there will be a break from an approximately exponential increase when the phytoplankton population significantly reduce the light availability, through self-shading. If self - shading did occur then the growth rate would decrease. This would lead to the chl-a concentrations levelling off at high concentrations. The chl-a concentrations do stay relatively constant in 1998 but not in other years, though it is not clear whether self-shading was the dominant effect controlling the bloom in 1998 because the northern box also included an area of low chl-a water that had entered the bloom area and which would have affected the box median. Overall there is little evidence for self-shading significantly affecting the overall progression in chl-a concentrations.

The dates for the start of the increase are bounded by 15th August and 23rd September with chl-a levels reaching 1 mg m^{-3} between 2nd September and 12th November. The peak in chl-a is between 1 and 4.5 mg m^{-3}, with the peak falling between 18th September and

13th November although this range narrows to 12th October to 5th November if the end of the high chl-a period in 1998 is used and 2001 is excluded (there was significant cloud cover during the spring bloom period so satellite images are hard to interpret).

Following the approximately exponential increase there is a sharp collapse of the bloom from the peak values. The chl-a concentrations drop to approximately pre-bloom levels of 0.3 mg m^{-3} over a period of 2-4 weeks. The time of this collapse is in the period 28th October-21st November. Due to the timings of the research cruises there is no *in situ* data from the area at the peak of the bloom in 2004 (or any other year). It is therefore not possible to be certain what the causes are, but the evidence available strongly suggests that the peak was caused by depletion of iron concentrations, probably strongly affected by exhaustion of silicate in the bloom area (Pollard *et al.* 2007). The timing is significantly before even the peak in light availability (around late December, see next chapter for full details) and so certainly before light is limiting again. Although light availability will vary rapidly it cannot explain the regular bloom collapse in all years. Another influence on phytoplankton growth is grazing by zooplankton, but it is highly unlikely that this process can significantly reduce a phytoplankton bloom so rapidly once it is established. Grazing pressure was not high when we did arrive in the area (Fielding *et al.* 2007), even relative to the then lower chl-a concentrations.

There is also other evidence in support of the hypothesis. On our arrival in the area, just after the bloom collapse, both silicate and iron had low concentrations in the surface waters (Planquette *et al.* 2007; Pollard *et al.* 2007). There had also been a community shift from diatoms, which were seen in deep sediment traps (Salter *et al.* 2007) and were also the cause of the silicate depletion, to non-siliceous species, especially Phaeocystis (Poulton *et al.* 2007). During incubation experiments, phytoplankton increased with the addition of iron (Moore *et al.* 2007). This suggests that the phytoplankton community structure had responded to a reduction in silicate concentration but overall was iron limited. The exact relationship between the timing of the depletion of silicate and iron is not clear. Iron stressed diatoms continue to take up silicate (Takeda 1998) so during the bloom collapse silicate will still be being used by the high concentration of diatoms. If silicate reached limiting concentrations before the depletion of available iron then it would drive a community shift to non-siliceous species. These new species may have a different (possibly higher) iron requirement than the diatoms they replace and also there

may be a strong export event associated with the collapse of the diatom population, which may remove a significant amount of iron.

Following the collapse, chl-a levels increase again to greater than pre-bloom levels at various points through the rest of the year, including in winter (e.g. May/June 2003). Chl-a concentrations, however, rarely reach 1mg m^{-3}. This suggests that there is little resupply of iron to the surface waters away from the plateau, within the bloom area during the period of light availability. This is consistent with the hypothesis of winter supply to the area because the biological utilisation of the iron in summer will be rapid, and largely closer to the eastern islands, as described in the next section.

4.6.2 North of the eastern islands – Persistent bloom

The temporal progression of chl-a concentrations in box D, north of the eastern islands Ile de la Possession and Ile de l'Est follows a broadly similar pattern to that north of the plateau. It starts at similar low levels (≈0.3 mg m^{-3}) before increasing approximately exponentially to a peak of between 3 and 8 mg m^{-3}. In all years except 2005 this increase occurs later than the increase north of the plateau, the bloom normally starting in October (Figure 4.1b). It is worth noting, with relevance to other work as part of the CROZEX project, that in most years the concentrations observed in this area are higher than in 2004. There is also a sharp collapse to pre-bloom levels, very likely also due to nutrient limitation. Full utilisation of iron is likely even close to the iron source of the eastern islands (Planquette *et al.* 2007) because the initial peak in chl-a is associated with iron that has been supplied to the surface waters through the light limited period. This therefore will lead to a phytoplankton response that exceeds that which could be supported by just the continuous iron supply. This mechanism causes the first chl-a peak to be higher than any subsequent maxima during the period of light availability. At the peak of this bloom iron utilisation will exceed iron supply and the bloom will collapse at some point because the remaining iron and the new iron being supplied will be fully utilised.

In contrast to the area north of the plateau, however, there is a large variability in the chl-a concentrations after the initial bloom, with chl-a concentrations exceeding 2 mg m^{-3} frequently. These high summer concentrations indicate that the iron supply from the

islands is strong throughout the year but not continuous – being affected either by variations over the islands, such as rainfall, or by oceanographic conditions surrounding the islands.

Figure 4.2 shows that, due to the higher peak values and greater temporal extent of the persistent bloom close to the islands, this area has higher integrated chl-a than the larger spatial scale spring bloom that extends northwards to the NSAF (as seen in Figure 4.1c). Figure 4.2 also provides very strong support for the main iron source being from the eastern islands, in agreement with the findings of Planquette *et al.* (2007) who found enhanced iron concentrations around Ile de la Possession, the western of the two islands to the east and calculated that the flux from these islands would support the enhanced chl-a concentrations observed. The main reasoning behind interpreting these images as support for this view of the iron supply comes from considering the flow pattern in the area. This involves a northward flow past the islands and eastern end of the Crozet Plateau (section 3.3) that either continues northwards or turns westward along the northern edge of the Crozet Plateau. These routes are picked out as areas of enhanced chl-a, which can be used as a marker for iron supply (Boyd *et al.* 2007; Moore *et al.* 2007). The flow patterns do not support the possibility that the enhanced chl-a close to the islands could be due to iron advected there from further away than the islands. There is evidence in some years of enhanced production along the entire northern edge of the plateau, which could be due to advection along the westward flow there or *in situ* supply of iron to the surface through vertical mixing. This could be due to mixing of iron up from the sediments (water depth approx 250m) or it could be lateral advection from the islands. There are also islands on the plateau that could provide an iron source.

4.6.3 Over the Crozet Plateau

Low to medium (0.2-1 mg m^{-3}) chl-a levels occur over the plateau itself, despite this area presumably having the highest nutrient concentrations. Over the plateau nutrients, including iron, are likely to be enhanced over background Southern Ocean concentrations due to supply from the shallow plateau (much of it shallower than 250m) and several small islands. There is, however, a difference between the geology of the eastern Crozet Islands and the main plateau (Gunn *et al.* 1972; Giret *et al.* 2002), which might cause a difference between the iron supply. The western islands are also considerably smaller

than the eastern islands. Unfortunately, due to poor charts there is no *in situ* data for this area. An iron source has been identified from Ile de la Possession (Planquette *et al.* 2007). Although the closed circulation around the plateau (section 3.2.7) advects this iron around the plateau, it may act as a barrier to it actually flowing over the plateau. Ekman flux in the area is also predominantly northerly due to the prevailing westerly winds, which again will act against this flow crossing southwards onto the plateau.

The chl-a concentrations over the plateau increase to a low peak most years: <1 mg m^{-3} in 6 years, just over 1 mg m^{-3} in 1997 and 3-4 mg m^{-3} in 1999 and 2002. Chl-a levels then oscillate mostly in the range 0.5-2 mg m^{-3} (reaching 3 mg m^{-3} in 1999 and 4 mg m^{-3} in 2002). If the low early peak is due to nutrients becoming exhausted, this implies a very weak supply of iron to the surface waters from the plateau and western islands. However the relatively high concentrations reached in the subsequent oscillations imply that there is a reasonably strong supply of iron. It is therefore surprising that there is not a stronger spring bloom because this supply could be expected to build up through the light limited winter period. Factors other than iron supply may therefore be important in the area. Unfortunately, due to the lack of charts we do not have cruise data from the area over the plateau. The following is therefore necessarily speculative and further work, if possible, would help greatly in the understanding of this apparent anomaly.

A possible cause of the lack of spring bloom is increased light limitation over the plateau. If this was the case it would delay phytoplankton growth, reducing the peak bloom due to spreading the time for nutrients to be used and allowing more time for zooplankton to increase. Another possibility is that a higher overwintering zooplankton population over the plateau and around the western islands exerts strong grazing control on the phytoplankton from the beginning of the season.

Tidal and mean flows over the topography may lead to enhanced mixing at the base of the water column, which could merge with the surface mixed layer. This would lead to very deep mixed layers that would exert light limitation on the phytoplankton community. The water could also then be more turbid, further reducing the light availability. High iron concentrations would be likely if the water column was mixed down to the seabed and so a strong bloom would be expected when stratification did occur. Deeper stratification would also cause the SST to be lower over the plateau, but

this is not observed in satellite SST images (see section 5.5). Two Argo floats have entered the shallow area due to drift at the surface. These show mixed layer depths typical of the latitude (100-150m in August) with significant stratification beneath them.

The possibility of the water being turbid also makes the satellite chl-a values less reliable, but it is more likely that they would be biased high by suspended particles in the surface waters (International Ocean-Colour Coordinating Group 2000) so it is unlikely to be the cause of the significant difference between this area and north of the plateau.

Grazing control could occur over the plateau due to a greater standing stock of zooplankton overwintering in the shallow shelf waters. Studies at nearby Kerguelen Islands found counts of a neritic species *Drepanopus pectinatus* – a species found around the Crozet Plateau (Fielding *et al.* 2007) – in a coastal bay were two orders of magnitude higher than counts of copepods at an offshore site (KERFIX) in winter (Razouls *et al.* 1996; Razouls *et al.* 1998). *D. pectinatus* has also been shown to respond rapidly to chl-a changes, with a peak growth rate of 0.10 day^{-1} (Alonzo *et al*. 2003). Grazing control by a species able to rapidly respond to changes in phytoplankton concentrations would also be consistent with the oscillating pattern (period ≈30 days) seen later in the season (Ryabchenko *et al.* 1997). It therefore seems most likely that, if there is a strong iron supply that is not being fully utilised, grazing control rather than light limitation is the proximate control on the phytoplankton population.

4.6.4 South of the Crozet Plateau

Low chl-a concentrations (0.2-0.7 mg m^{-3}) occur to the south of the plateau (Figure 4.1b-d). These values show no increase over concentrations upstream to the west, indicating little or no effect from the islands. The high values to the south-east in Figure 4.1d are downstream of the bloom. The contrast between north and south of the plateau is visible in SeaWiFS images at this time of year (September-December) back to 1997 (the beginning of the SeaWiFS mission).

The flow patterns discussed in chapter 3 and Pollard *et al.* (2007) mean that the area south of the plateau does not receive a significant amount of water that has been close to the plateau and islands. This means it will not receive a significant amount of iron from

the islands or plateau (Planquette *et al.* 2007). There is also a less favourable light climate as the mixed layer deepens to the south by 11m degree^{-1} on average, described in section 5.1.1, which will reduce phytoplankton growth rates and increase iron demand (Sunda and Huntsman 1997). The productivity regime is therefore similar to the open ocean areas of the Polar Frontal Zone between the Polar Front and Sub-Antarctic Front (Banse 1996; Moore *et al.* 1999). There is still a well defined, but low, peak in chl-a values at the beginning of December. The consistent feature of chl-a beginning to decline while light availability is still increasing indicates that light limitation does not control phytoplankton growth south of the plateau for a significant period of the year. This is shown in more detail in section 5.6.1. After the low peak, chl-a values are consistently low south of the plateau, either indicating tight grazing control or a limiting nutrient. The very high silicate/nitrate removal ratio (Pollard *et al.* 2007) indicates that iron limitation is strong but grazing pressure was also found to be high in the area, reaching 90% of daily primary production (Fielding *et al.* 2007). The increase in grazing to the south may be due to the longer timescale for the increase in phytoplankton, allowing the zooplankton populations time to respond. Low iron concentrations also favour small phytoplankton species which are better able to absorb iron due to a greater surface area:volume ratio but these are more easily grazed. The consistency of the low chl-a values indicates that there is not significant re-supply of iron during the summer. If this is the case, and if rates are similar through the year, the area will not become significantly iron fertilised over the winter.

4.7 Bloom initiation

It has been observed in section 4.6.1 that there is an overall progression of the bloom southwards during its initial development. That is, the first areas to show enhanced chl-a north of the plateau are separated from the plateau by an area where chl-a concentrations are still low. To quantify the southward progression, 4 boxes were defined north of the plateau (see section 4.5).

4.7.1 Differences between boxes for initiation of the bloom

The median chl-a was found in each box for each 8-day period. The first period that the median chl-a exceeded 1mg m^{-3} was chosen as the point at which the bloom was formed. Table 4.2 shows these periods for each year and box A-D (the first period starts on 4th August). Except for 2005 the bloom formation is later to the south (towards box D).

Year\Box	A	B	C	D
1997	7	7	7	12
1998	5	6	6	8
1999	8	9	11	11
2000	7	8	10	14
2001	12	13	14	15
2002	8	9	9	9
2003	9	11	11	12
2004	7	7	8	10
2005	11	8	8	7
Mean:	**8.22**	**8.67**	**9.33**	**10.89**
Date of mean:	**6/10**	**10/10**	**14/10**	**27/10**

Table 4.2 8-day period after 4th August that the median chl-a value in each box north of the plateau reached 1 mg m^{-3}. Dates are relative to the mid-points of the 8-day periods.

Means from this table give rates of 5.9 days $degree^{-1}$ latitude for the southwards spread of the bloom north of the plateau, between boxes A and C (3.5 days $degree^{-1}$ between boxes A and B, 10.8 days $degree^{-1}$ between boxes B and C). The delay between boxes C and D – between the spring bloom and the persistent bloom is 19.1 days $degree^{-1}$.

4.7.2 Mean day for each pixel, across years for chl-a to reach 1 mg m^{-3}

Rather than considering the box median, another approach is to apply the same criteria (selecting the first 8-day period where the chl-a value exceeds 1mg m^{-3}) to each pixel individually. Figure 4.6 shows the Julian day that corresponds to the start of the 8 day dataset selected by this criteria. White areas are where the chl-a never exceeded 1 mg m^{-3}.

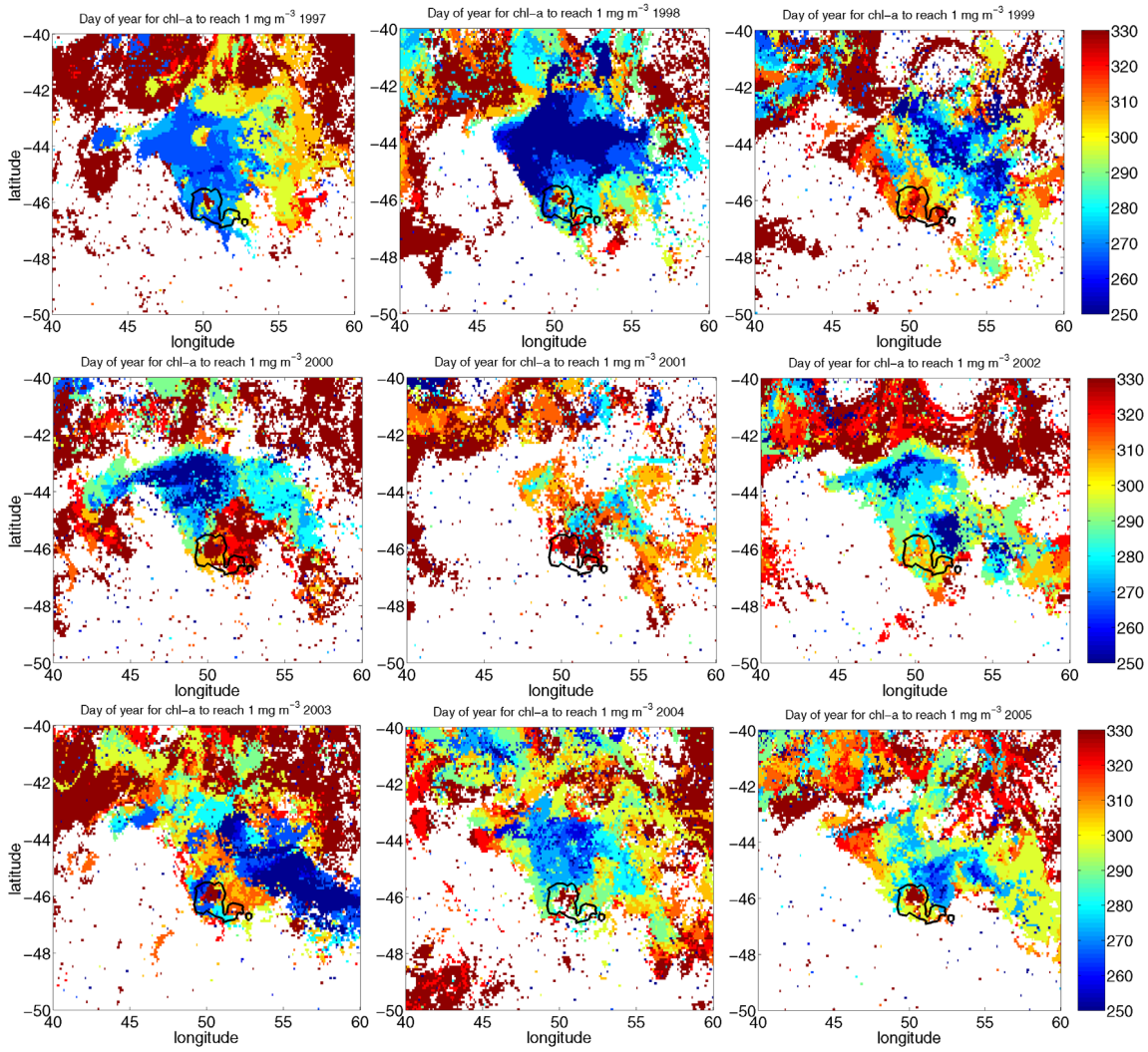

Figure 4.6 Day of year that the chl-a concentration first exceeded 1 mg m^{-3}, calculated for each pixel. Day used is the start day of the 8-day period.

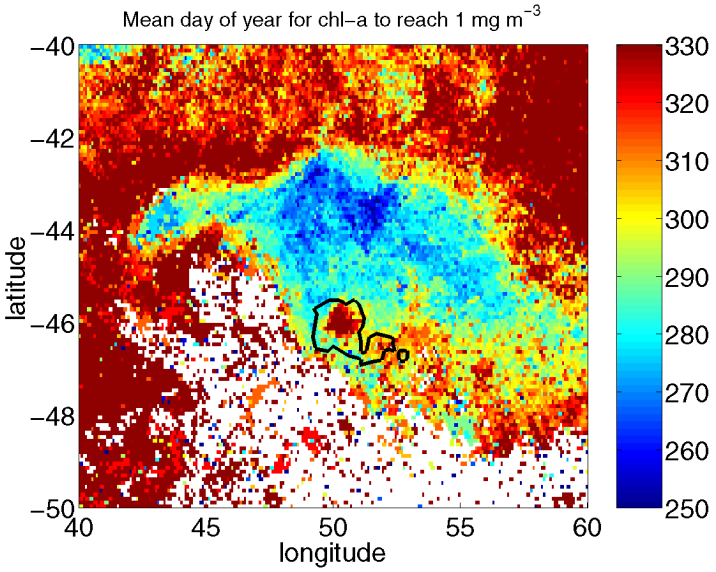

Figure 4.7 Mean of all images included in Figure 4.6.

Figure 4.7 shows the mean of each of these images (pixel by pixel). Figure 4.7 supports the analysis of section 4.7.1 that, on average, the bloom is established to the north first, before spreading southwards towards the plateau. The mean dates shown in Figure 4.7, averaged over boxes A-D gives Julian days of 272.2, 279.8, 284.8 and 294.6 for boxes A-D respectively (taking the midpoint date of the 8-day periods). This gives rates of 7.6, 10.0 and 15.1 days degree^{-1} latitude for the southwards spread of the bloom, considering differences between boxes A and B, B and C, and C and D respectively.

These differences are in good agreement with the data in Table 4.2 where the 8-day periods convert to Julian days of 278.3, 281.8, 287.2 and 299.6 for boxes A- D respectively (again taking the mid-point date of the 8-day periods). The fact that the dates from the pixel-by-pixel approach are slightly earlier than those found above using box averages is in agreement with the lognormal distribution of chl-a because the positive skewness of this distribution will lead to small patches of early high chl-a. These will cause the corresponding pixels to record the early date but will not affect the box median.

It is not possible to reconcile this southward spread being caused purely by the circulation or iron supply. 7 days degree^{-1} corresponds to 0.18 m s^{-1} so advection is not possible – flow in the spring bloom area is weak and variable in direction while that in the persistent bloom area is mostly northwards (the wrong way). It is also expected, and supported by the satellite composite images, that iron supply will be weakest to the north, so this factor should not cause an earlier, or more rapid, start to the bloom to the north. As is shown in the next chapter, gradients in light availability do explain the southward spreading of the bloom.

Chl-a concentrations north of the plateau reach 1mg m^{-3} significantly earlier within the bloom area (the blue area in Figure 4.7) than the same latitudes to the east of west. These areas are likely to have a similar temporal pattern to light availability. The delay is therefore likely to be due to different population dynamics outside the bloom area, possibly driven by lower iron concentrations.

4.8 Chl-a/MADT around northern edge of bloom

It has been noted in section 4.4 that the bloom is bounded to the west and north by the NSAF and that this is picked out in ocean colour images by the low chl-a concentrations in the front. This idea can be investigated by trying to find an absolute dynamic height that bounds the bloom, because contours in absolute dynamic height correspond to geostrophic streamlines. Figure 4.8 shows an attempt to do this with 3 dynamic heights: 100, 95 and 90 dyn cm. It is clear that there is an overall connection between the shape of the bloom and the dynamic height contours, supporting the view that the bloom is bounded by the NSAF. However it is not possible to select a dynamic height contour that bounds the bloom all around the western and northern edge: contours that are on the edge on the western side are within the bloom to the north-east.

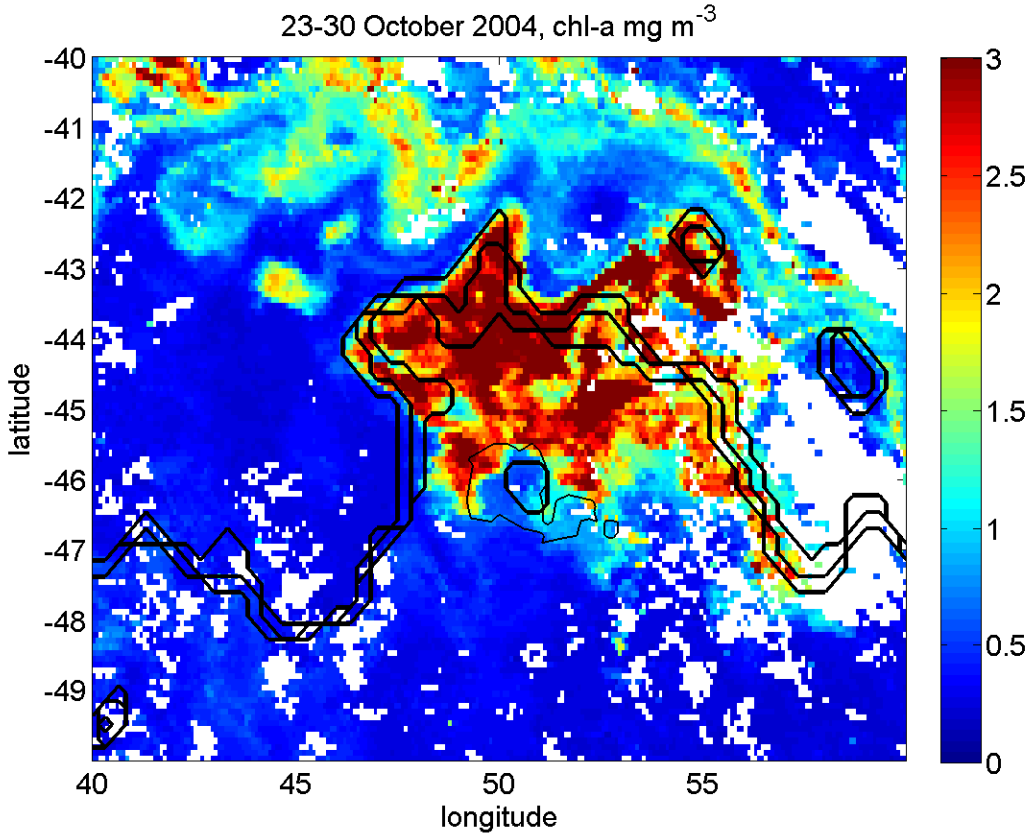

Figure 4.8 Chl-a image from the peak of the bloom in 2004 with the (from north) 100, 95 and 90 dyn cm dynamic heights shown.

The spread of the bloom across dynamic height contours shows that there is an exchange of water between the bloom area and the NSAF. From Figure 4.8 it appears that this is mostly a local process because the line of low chl-a beyond the bloom that picks out the

NSAF becomes thinner across the northern edge but remains coherent. There is also evidence of larger-scale events transferring water across the NSAF. An eddy can be seen at 43.5°S, 45°E moving from the bloom area across the NSAF, picked out by high chl-a. A second feature, at 45°S, 49°E shows low chl-a water entering the bloom area. This feature is described in Read *et al.* (2007). Overall though, section 3.2.6.1 shows that there is not a significant input of waters with other than Sub-Antarctic origin. This spread occurs all around the bloom, including in a south-westward direction to the west of the bloom area so it is unlikely to be due to Ekman flux, which will be predominantly north due to the prevailing westerly winds.

The spread of the bloom across the dynamic height contours can be used to estimate the rate of inflow into the bloom area from detrainment from the NSAF if it is assumed that the volume flux of the NSAF does not change significantly so the volume of water entrained into the front equals the volume of water detrained from the front, and that this detrained water then mixes with the water in the bloom area.

To estimate the detrainment rate, images with good spatial coverage from close to the bloom peak are selected from each year from 2002 (once there were enough altimetric satellites such that the absolute dynamic height can be trusted to sufficient accuracy). These, with absolute dynamic height contours overlain, are shown in Figure 4.9.

Two boxes have then been selected: a western box (44-46°S, 45-50°E) and an eastern, further downstream, box (43-45.5°S, 51-56°E). Within these boxes, the absolute dynamic height (ADH) was found for each ocean colour pixel (chl-a) and the frequency of the (ADH, chl-a) data pairs was found, with intervals of 5cm for ADH and 0.25 mg m^{-3} for chl-a. The results are shown in Figure 4.10, with the log frequency used for ease of plotting. The left hand column shows the result for the western box while the right hand column is from the eastern box.

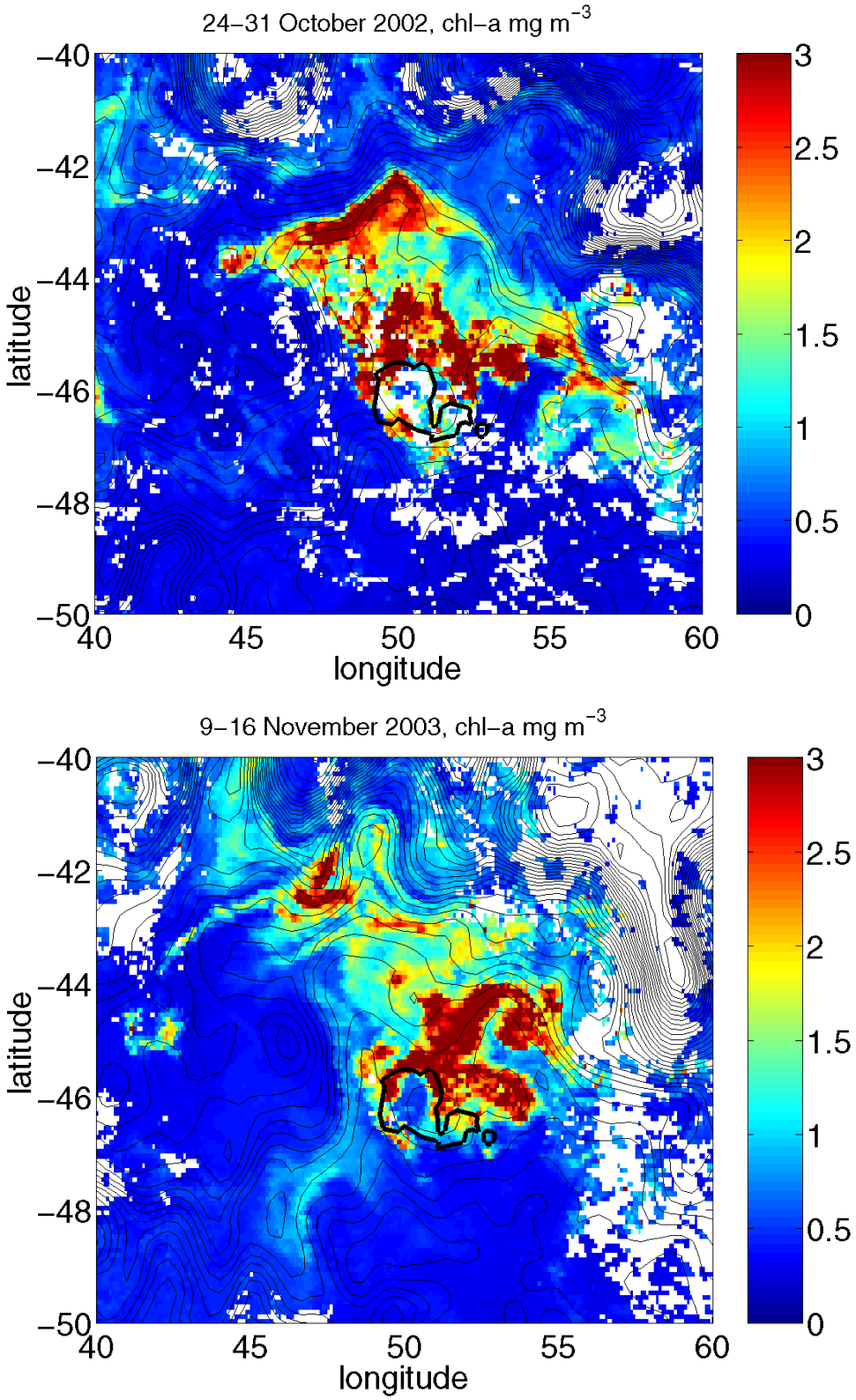

Continued on next page

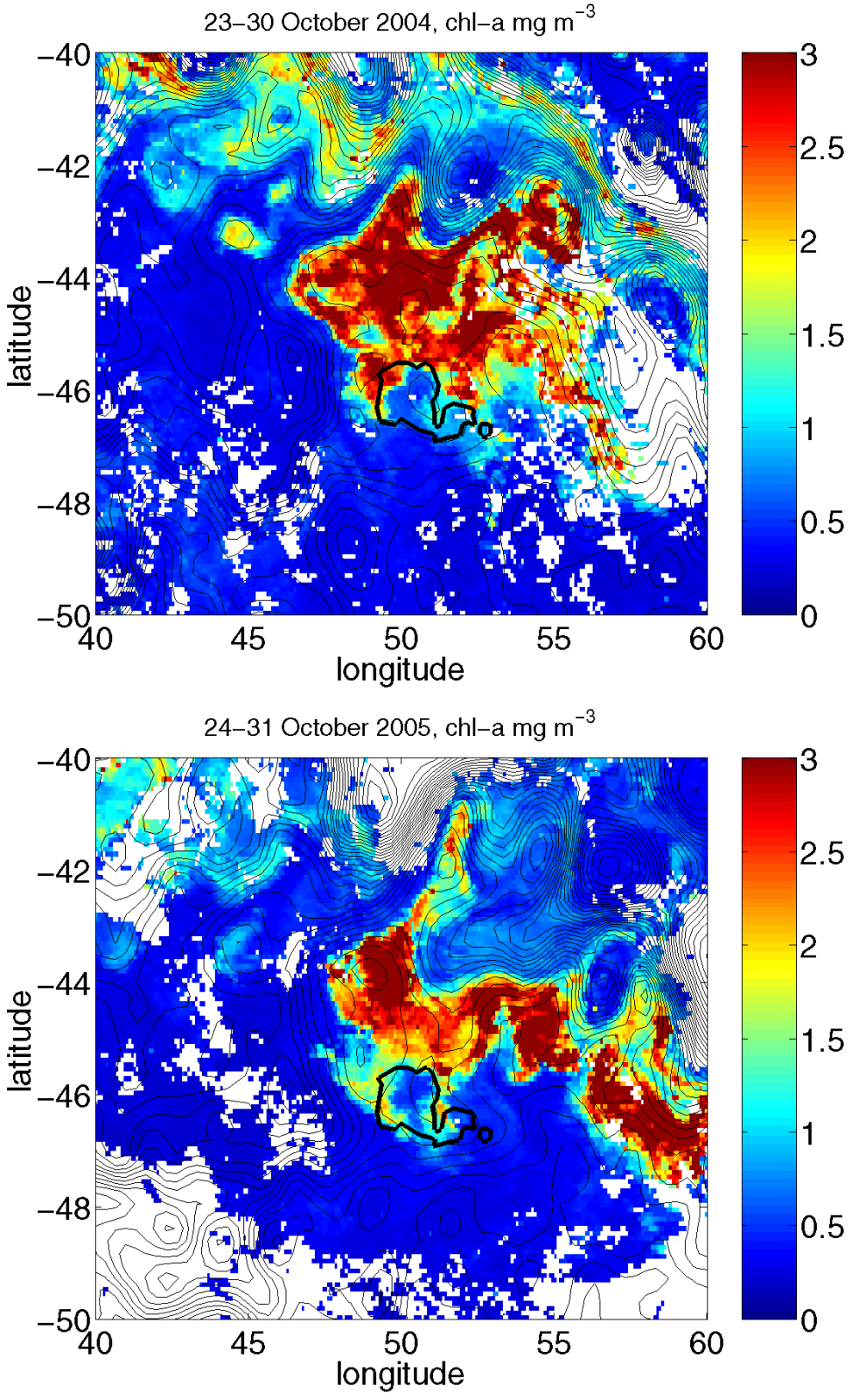

Figure 4.9 Chl-a images from the peak of each year or close to the peak to ensure good data coverage with absolute dynamic height contours overlain at 5 dyn cm intervals.

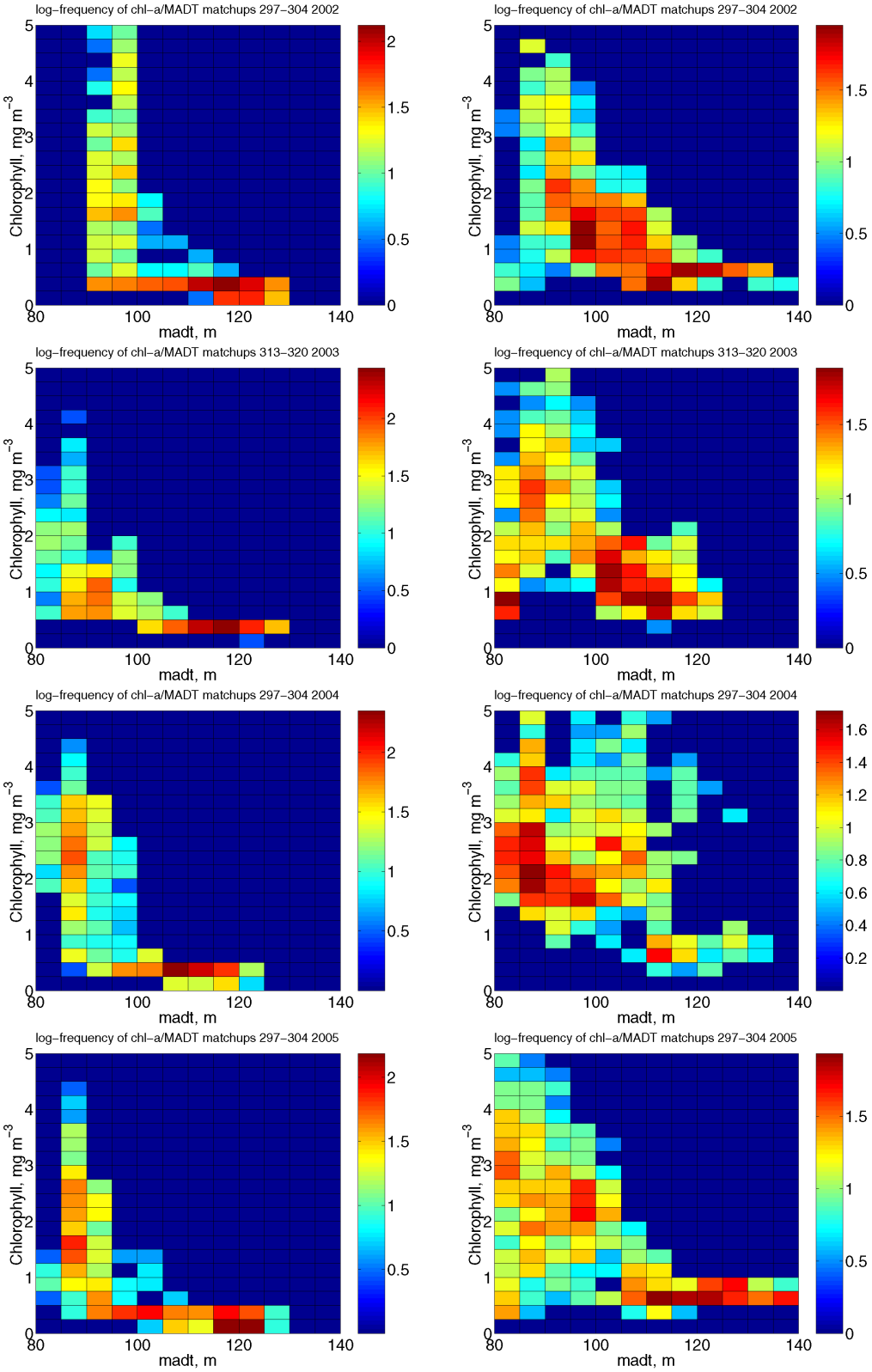

Figure 4.10 Log-frequency of (absolute dynamic height, chl-a) data pairs from western edge of the bloom area (left) and north-eastern side (right).

It is possible to calculate an approximate rate of entrainment into the NSAF from the spreading of the chl-a, effectively using it as a marker of enhanced iron concentrations, which in turn are used as a tracer for bloom-area water. The process followed is to find the area of pixels within the ranges (100<madt<120, 0.5<chl) and (80<madt<100, 0.5<chl). The first of these is the area of enhanced chl-a in the NSAF while the latter is an adjoining area to the south that is considered the main bloom area. If the 100 dyn cm contour is taken as the original boundary between the bloom area and NSAF the area of enhanced chl-a on the NSAF side (higher madt, generally to north) of this contour is a measure of the extent of mixing. Due to the sharp boundary to the enhanced chl-a within the NSAF it is has been assumed that there the area south of this is well mixed (50% NSAF, 50% bloom area water) but mixing does not extend beyond this boundary.

If the transit time of the water is D days, the areas of enhanced chl-a north and south of the 100 dyn cm contour are N and S respectively, the above assumption of 50% mixing within the area of enhanced chl-a north of the 100 dyn cm contour is used and the residence time within the bloom is R days, then the proportion of water entering the bloom area from the NSAF is the volume flux entering (and, by assumption, leaving) the NSAF divided by the total volume flux in to the main bloom area:

$$(N/2\times D^{-1})/(S\times R^{-1})=(R\times N)/(2\times S\times D) \qquad \textbf{4-1}$$

The transit time can be estimated from drifter tracks. 20 drifters pass through 44-46°S, 45.5-49°E and 42-44.5°S, 52-55°E and the mean transit time between these boxes (measured between the midpoints of entering and leaving each box) was 50 days. This corresponds to a flow speed of approximately $0.1 ms^{-1}$, which is reasonable for the NSAF.

The residence time can also be estimated from drifter tracks. The mean time between drifters' first entry and final departure into the area (44-46°S, 49-53.5°E, down to 46.5°S 51.2-53.5°E) was 38 days, after the removal of drifter tracks that either start within the area and rapidly leave or those that cut the corner of the defined area (both of which bias the residence time low). The residence time goes down to 25 days if the short staying drifters are not removed. This process is however very imprecise, the maximum residence time was 172 days so the 20 drifters used to calculate the mean are unlikely to fully

represent the variability. Some suspiciously westerly drifter tracks have been included – they are flagged as drogue-on but they do not follow known current features unlike other drifters – and this probably biases the estimate low.

The two areas N (north) and S (south) can be calculated for years with reliable satellite altimetry by counting the number of pixels that satisfy the conditions (100<madt<120, 0.5<chl) for the northern area and (85<madt<110, 0.5<chl) for the southern area and then multiplying by the size of a satellite pixel (60km^2). These areas are given in Table 4.3.

Year	Area North	Area South
2002	80000	162000
2003	114000	141000
2004	68000	161000
2005	38000	150000
Mean	75000	153000

Table 4.3 Areas of bloom entrainment (north) and main bloom area (south) in km^2.

$$(R\times N/2)/(S\times D)=(38\times 75000)/(2\times 153000\times 50) \qquad \textbf{4-2}$$
$$=0.2$$

Therefore approximately 20% of the water in the bloom area is from detrainment from the NSAF, 80% from plateau/SSAF detrainment. This means that close to the NSAF supply from detrainment from the NSAF will be a considerable proportion of the total inflow.

4.8.1 Local impacts of frontal mixing

It is also interesting to note that some images in Figure 4.2 (especially 1997 and 2000) show high mean chl-a values in a thin strip along the northern edge of the bloom, separated from the high values to the south by the typical lower values of the spring bloom. These areas also sometimes show higher peak chl-a, as is shown in Figure 4.11. It seems likely that the proximity to the NSAF causes this effect due to its location but the exact mechanisms are not clear. It is very likely that the NSAF is not enriched with iron

because the chl-a concentrations within it are very low (see Figure 4.9) and it has not been in close contact with shallow topography. The mixing gradient caused by the inflow of NSAF water is likely to produce a gradient in the iron concentration across the whole bloom area. This is consistent with the gradients in integrated chl-a seen in Figure 4.2 and discussed in relation to the bloom peak and light availability in section 5.8. A direct supply of iron is therefore unlikely to be the cause of the enhanced chl-a concentrations.

The low chl-a levels in the NSAF will mean that water in the NSAF likely remains high in silicate, because biological utilisation will be low. Silicate levels are initially well above limiting values in the bloom area (section 3.2.2) but reduce to low concentrations (Pollard *et al.* 2007). This shows that there is heavy biological utilisation of silicate, consistent with a large diatom bloom (Moore *et al.* 2007; Poulton *et al.* 2007; Salter *et al.* 2007). Silicate reaching limiting levels is very likely to be the cause for the shift in the community structure observed during the CROZEX cruises (Poulton *et al.* 2007; Seeyave *et al.* 2007) from diatoms to non-siliceous Phaeocystis. This shift in community structure is likely to impact the iron requirements of the phytoplankton community, through a large diatom export event and/or a change in the cellular iron demand from the succeeding species. A continued supply of silicate may therefore help to prolong the bloom, even if the high silicate waters entering the system are low in iron. This is similar to the chemostat effects observed during SOIREE, an artificial iron-enrichment experiment (Abraham *et al.* 2000; Boyd *et al.* 2000).

Vertical velocities associated with mesoscale dynamics may act to supply iron and silicate from below the depleted mixed layer (Allen *et al.* 2005), offsetting the low iron supply. Indeed, this may be the dominant process in prolonging the bloom. Mesoscale dynamics could also act to create temporary high light environments by shoaling the mixed layer (Strass *et al.* 2002) but because this effect occurs at the end of the spring bloom this area will not be light limited at this time. The peak of the bloom was not sampled and the frontal dynamics of the NSAF not studied so interpretation remains speculative.

These issues are best illustrated by using two real-time images received from the remote sensing group at Plymouth Marine Laboratory during the CROZEX cruises. They are shown as Figure 4.11 (chl-a) and Figure 4.12 (SST). These have undergone minimal

processing and the chl-a concentrations have not been calibrated against *in situ* concentrations so they are used purely for the structures that they show. However, being 1km resolution they show these structures far better than any other images used in this work. The separation of the enhanced chl-a from the plateau suggests that the effect is local, rather than being due to advection of iron from close to the plateau, as close to the islands this leads to enhanced chlorophyll much closer to the iron source.

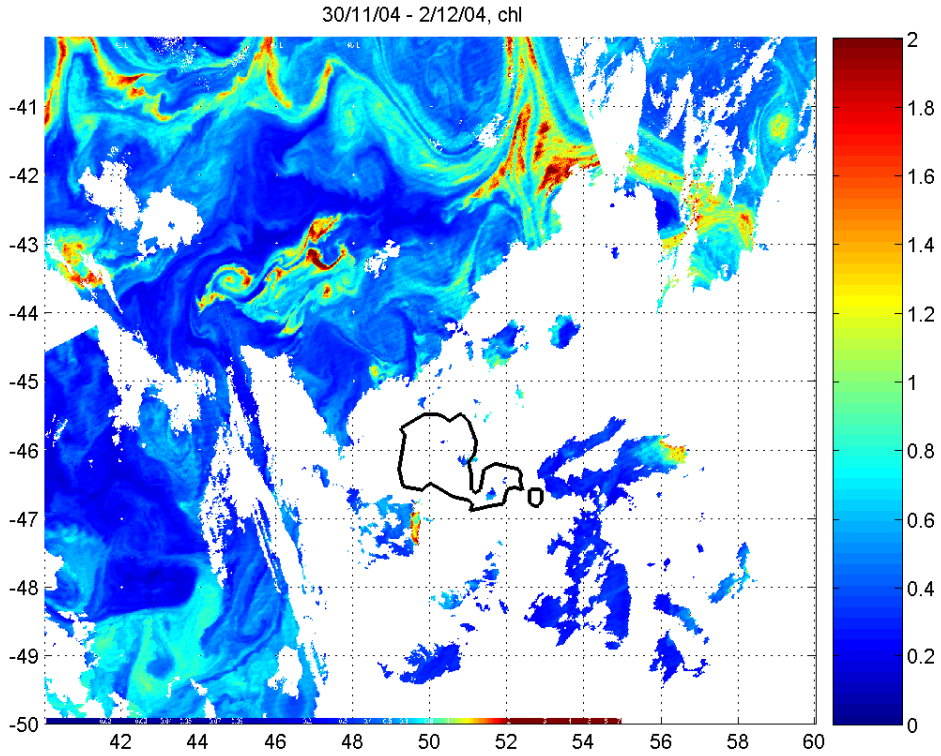

Figure 4.11 1km resolution MODIS chl-a image (received real time on the ship and no post-processing), 30/12/2004-2/12/2004.

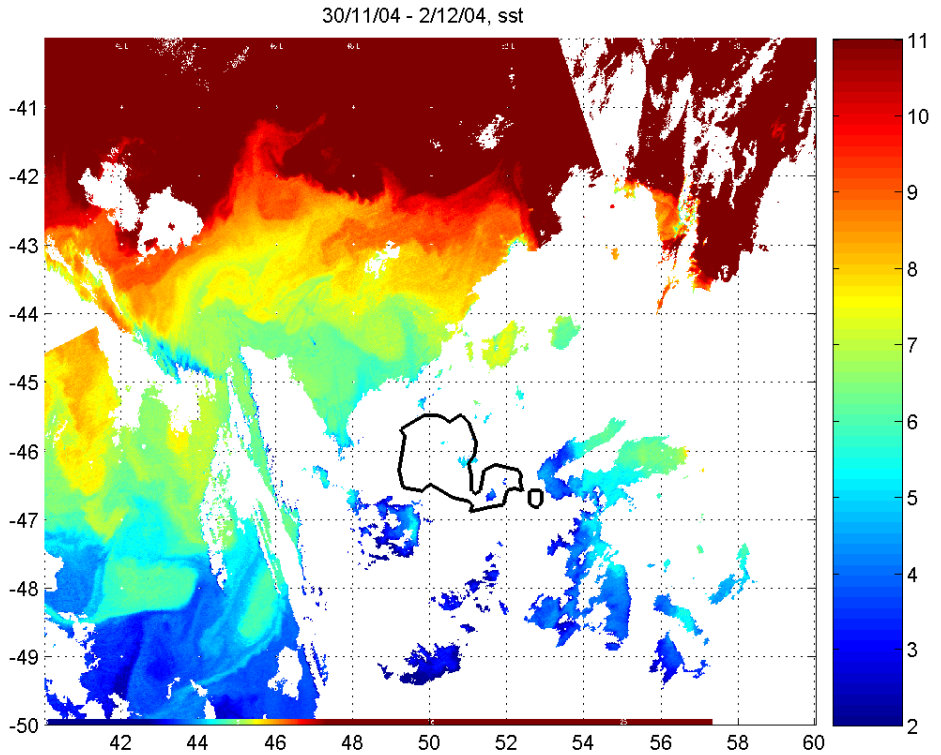

Figure 4.12 1km resolution MODIS SST image (received real time on the ship and no post-processing), 30/12/2004-2/12/2004.

4.9 Summary of chl-a distribution

Most of the features of the bloom identified in this chapter can be explained by reference to the circulation pattern, indicating that advection of iron is dominant in setting most of the bloom characteristics. The main findings are that the area can be split into four productivity regimes: south of the plateau upstream of the topography; the area over the plateau, mostly isolated from other areas by the closed circulation around the plateau; the spring bloom area, fertilised in winter by iron from the islands but not strongly resupplied through the summer; and the persistent bloom area close to the eastern islands that starts as the flow passes the islands and persists through the period of light availability, providing very strong support that the eastern islands are the primary source of iron to the Crozet area. Both the bloom areas have an unsustainable spring bloom that is triggered by alleviation of light limitation and which utilises supply built up through the winter and the continual supply. This collapses when the winter supply is depleted and the subsequent chl-a levels are indicative of the continual supply (vertical advection, iron recycling and new iron). The study of the spread of chl-a into the NSAF provides further information about the circulation through using chl-a as a marker of iron, which itself is being used as a tracer.

Data are also presented on the temporal development at the initiation of the bloom, which cannot be explained by the circulation or iron distribution: the bloom starts away from the islands and spreads south towards it, faster than advection could move it and against the iron gradient. This feature is investigated in the next chapter, where it is shown that light availability dominates this process. Knowledge of the light availability and the chl-a response to it within the bloom then allows further investigation of the bloom characteristics, including in relation to other Sub-Antarctic islands and mesoscale iron release experiments. The interannual variability in bloom features is investigated in chapter 6. Findings about the variability of the bloom provide further support for the analysis presented in this chapter.

5 Mixed layer depth, light and phytoplankton growth

It was shown in the previous chapter that there was a regularity in the temporal development of the bloom. In 8 of the 9 years it starts first in the northern part of the bloom area and spreads southwards towards the islands. This progression is investigated here through studying the spatial and temporal distribution of light availability, using mixed layer depths from Argo floats and Photosynthetically Available Radiation (PAR) from the SeaWiFS satellite. Light is studied as, according to the hypothesis of natural iron enrichment (confirmed by Planquette *et al.* (2007) and strongly supported at a wider scale by the analysis of the previous chapter) and the macronutrient distribution described in Chapter 3, the area where the bloom occurs should be replete in both micro- and macro-nutrients at the end of the winter period. The bloom is therefore triggered, and initially controlled by the alleviation of light limitation from an iron-fertilised area.

The study of light in this area and the strong response of phytoplankton allows a critical light level for phytoplankton growth to be estimated empirically. This is used to study the level of light limitation south of the Crozet Plateau. The concept is widened to investigate conditions around other Sub-Antarctic Islands and also during artificial iron release experiments.

5.1 Latitudinal gradients

5.1.1 Mixed layer depth gradients

The surface mixed layer depth has a strong control on the amount of light received by phytoplankton. This is because phytoplankton are advected vertically around in the mixed layer and therefore experience the light intensity averaged over the mixed layer depth. The light intensity reduces exponentially with depth such that the 1% light level is normally at 60-80m (deeper in very clear water, shallow if the water is turbid due to phytoplankton and/or suspended sediment). The depth at which growth exceeds loss – the Sverdrup depth (Sverdrup 1953) – can vary depending on the incoming irradiance, the ability of the phytoplankton species present to utilise light and other factors controlling the loss terms, such as grazing. Within the study region the overall seasonality of the chl-a distributions shows that, similarly to many places, the deepest mixed layer depth cause

light limitation, but the shallowest do not. This chapter investigates in detail the responses of phytoplankton to light availability and the relative importance of this to iron availability in different locations and at different times.

In order to obtain a year-round mixed layer depth dataset, the mixed layer depth was diagnosed from the 838 Argo float profiles within 40-60°E, 43-50°S that passed the quality checks. Density was calculated from the temperature, salinity and pressure at each datapoint. The mixed layer was calculated following (Kara *et al.* 2000) but using a density difference of 0.05 kg m^{-3}. This involved taking the shallowest density value as a reference value and working down the profile one density value at a time. If the value being checked was within 0.005 kg m^{-3} of the reference value, the reference value was redefined to be that value. If it was >0.05 kg m^{-3} greater than the reference value, then the depth corresponding to a density difference equal to 0.05 kg m^{-3} was estimated using linear interpolation between the depths with data. Density is used rather than temperature as both temperature and salinity contribute to density stratification in the area. The density difference used is less than the 0.125 kg m^{-3} that is used in some other studies (Spall 1991; Huang and Russell 1994; Bhaskar *et al.* 2006) but from study of the density profiles it was considered that a density difference of 0.05 kg m^{-3} best characterised the mixed layer. This is due to the reduced strength of the pycnocline compared to areas with higher surface temperatures, meaning that the density gradient at the base of the mixed layer was weaker than in other study areas. As the pycnocline is weaker to the south of the study area (see section 5.1.2), a larger density difference leads to an increased latitudinal gradient.

To remove the seasonal effect on the mixed layer depth, a sinusoidal plot, as a function of day of year, was fitted to the data (Figure 5.1) and residuals were calculated from this. Although mixed layer depths in any given place do not follow a sinusoidal curve it was found to be a good fit to the data, which has come from a large spatial area and over 5 years. Winter mixing depths are in the range 100-250m south of the plateau but north of the plateau they are mostly in the range 75-150m. In the summer, mixed layer depths are 40-100m south of the plateau while those north of the plateau mostly under 60m. It should be noted that these are actual measured mixed layer depths and it is therefore likely that any extreme and short-lived events will not be sampled. Estimates of the

deepest mixed layer from oxygen concentrations in CTD casts are likely to be greater than those shown here.

Mixed layer depths change rapidly and significantly over short time and space scales due to changes in meteorological forcing and between adjacent water masses. It is therefore to be expected that there is considerable scatter in the plots. The confidence intervals for the gradient of residual mixed layer depth against latitude are, however, away from zero so there is a significant signal.

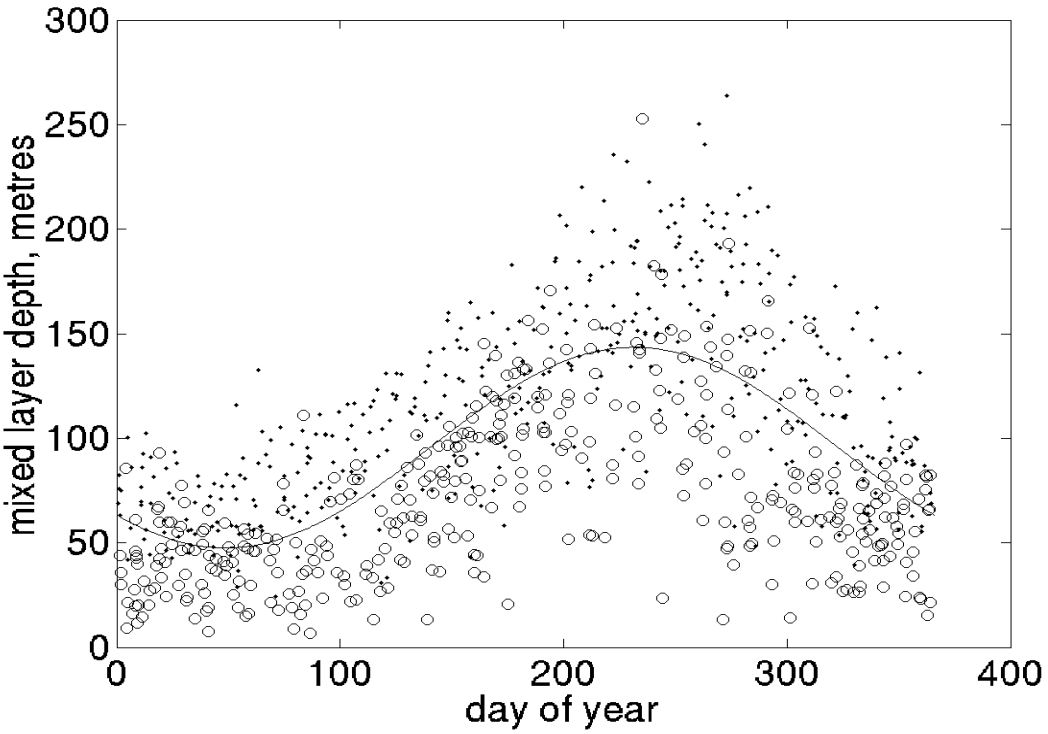

Figure 5.1 Mixed layer depth from Argo floats (43-50°S, 40-60°E) against day of year, with sinusoidal least-squares fit. Open circles are profiles north of the plateau, dots to the south.

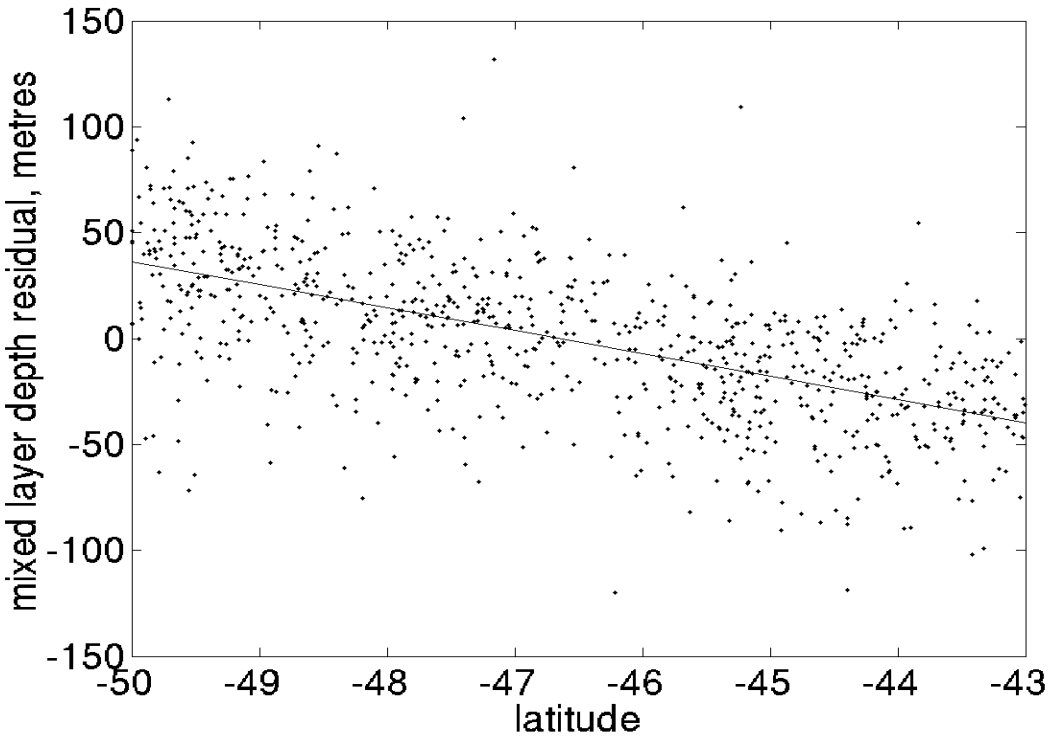

Figure 5.2 Residual mixed layer depths, after effects of time of year have been removed.

There is a northwards reduction in the residual mixed layer depth of 10.8 ± 1.0 metres degree^{-1} latitude (Figure 5.2, n=838). There is no significant difference between the gradient in winter (9.7±1.6 metres degree^{-1} latitude, n=328) and summer (11.7±1.2 metres degree^{-1} latitude, n=510). When only the data from north of the islands, during the time period of the bloom (September-February) are used, the gradient is similar: 8.8 ± 3 metres degree^{-1} latitude (n=388). This relates to a deepening, on average, of 30m across the bloom and 50m between north and south of the plateau.

The mixed layer depth, in a given location, may decrease rapidly from deep winter levels to shallow summer values. The timing of this jump will depend on the atmospheric forcing, which is likely to vary over large spatial scales, and the existing density profiles, which will vary little within water masses but change rapidly over small spatial scales between water masses. Argo float profiles indicate that this re-stratification occurs earlier to the north but do not provide sufficient information to extract a reliable timescale.

5.1.2 Gradients in strength of the pycnocline

The density difference between the mixed layer and 50m below the bottom of the mixed layer also increases to the north, as shown by Figure 5.3. The equivalent differences in temperatures and salinity (not shown) show that surface heating is the dominant source of the density difference. The stronger pycnocline to the north of the plateau will lead to less variable mixed layer depths as it increases the work needed to mix against the density gradient and reduces the depth that convection will penetrate to. This will allow phytoplankton within the mixed layer to develop in a more consistent light environment to the north and with reduced losses from the population caused by mixing and re-stratification events. This will further enhance the ability of phytoplankton to develop earlier in the north of the bloom area. The vertical re-supply of nutrients to the surface through mixing will however be reduced. This is consistent with the fact that enhanced chl-a concentrations persist close to the plateau but not further north, although this will largely be due to the proximity of the plateau as a source of nutrients.

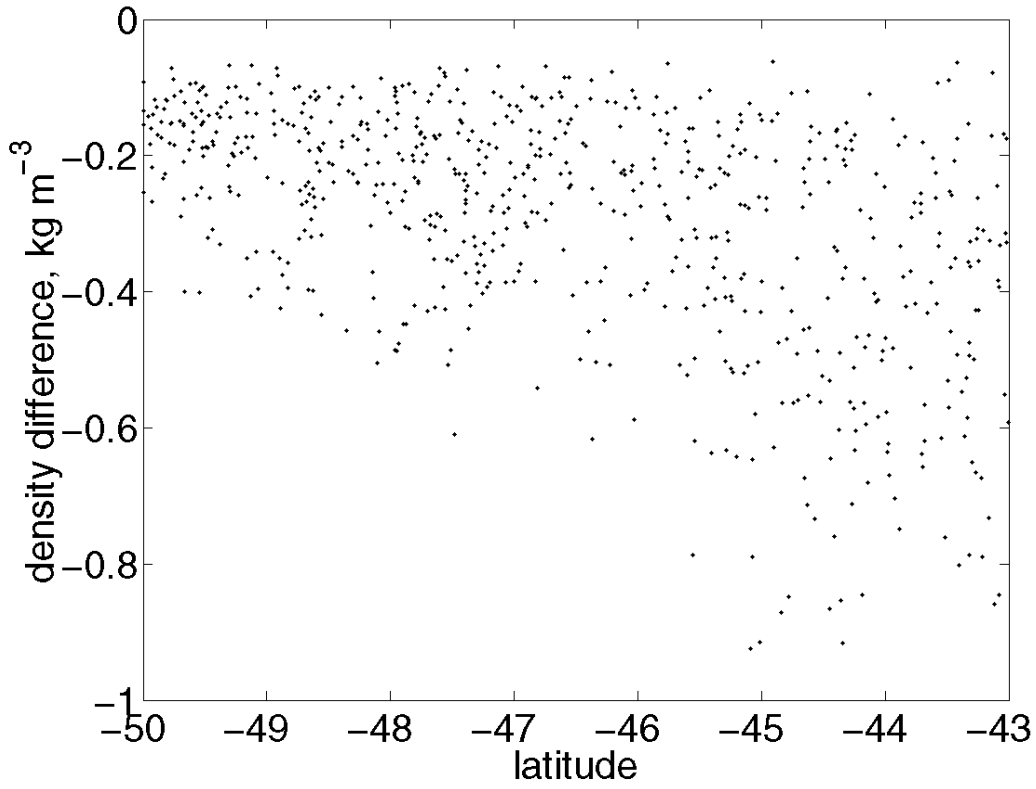

Figure 5.3 Density difference between base of mixed layer and 50m below the base of mixed layer.

5.2 Source of gradients

The two main inputs into the bloom area that control the nature of the vertical density profiles near the surface are the source of inflowing water and surface buoyancy fluxes. It is clear that there is inflow of water into the area of Sub-Antarctic origin (Pollard *et al.* 2007). Due to the very sharp temperature and salinity gradients in the area, a relatively low volume flux from cross-frontal mixing may have a significant effect on the temperature and salinity in the bloom area. However, Figure 3.15 shows that there is not a significant source of water from north of the northern branch of the SAF.

The gradients in mixed layer depth must therefore be due to *in situ* forcing through buoyancy fluxes and wind stress. It is not possible to create a complete buoyancy budget for the region at the required resolution. NCEP data (from their website: http://www.cdc.noaa.gov/) is available at 2.5° resolution and due to the lack of *in situ* observations in areas such as the study area re-analysis products have to be used with caution. The data shows that there is no trend in precipitation or evaporation between August and November (Figure 5.4) so freshwater fluxes are not driving the temporal changes in stratification. There is also no significant difference between 42.9°S and 44.8°S in either variable (Figure 5.4) although evaporation may be slightly higher to the north, which would reduce the gradient in surface buoyancy as it would produce cooler, more saline water to the north.

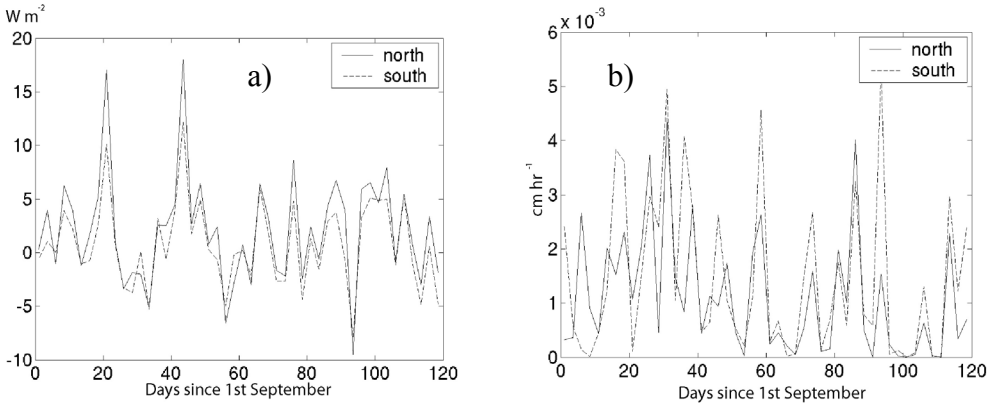

Figure 5.4 NCEP/NCAR data from 2005 (used as a representative example) for a) latent heat flux (W m^{-2}) and b) precipitation rate (cm hr^{-1})

PAR data from SeaWiFS (which will be strongly correlated to total incoming irradiance) do show significant spatial and temporal gradients (Figure 5.5) of approximately 1

Einstein m^{-2} day^{-1} $degree^{-1}$ and 1/3 Einstein m^{-2} day^{-2} respectively. Most of the density difference is due to heating so this agrees with the strong gradients occurring in heat flux rather than freshwater flux. Gradients in PAR will also affect the phytoplankton directly through varying light levels in the mixed layer. Wind stress also shows latitudinal gradients across the area (Figure 5.5), increasing to the south, and this will contribute to the gradient in mixed layer depth observed. The decrease in wind stress between August and September will also act to allow re-stratification of the surface water column.

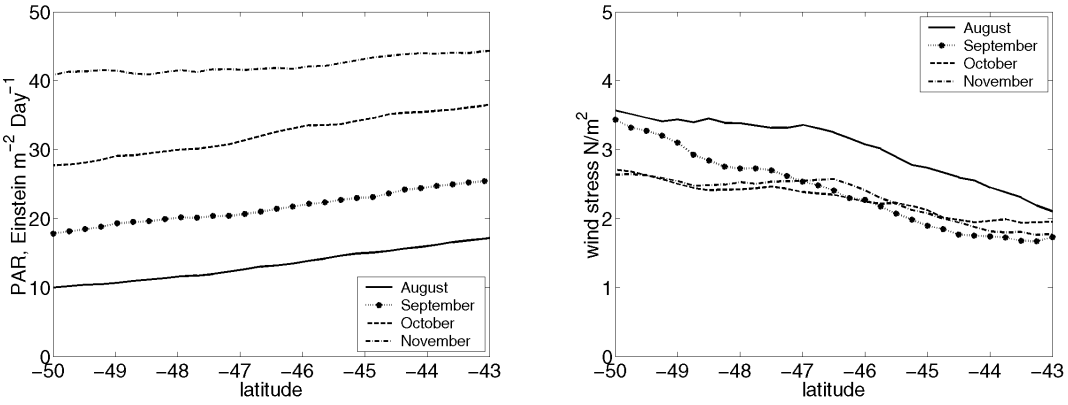

Figure 5.5 PAR data for 2004 (left) and monthly average wind stress from QuikSCAT from 2004 (right).

5.3 Effects of gradients of light availability on phytoplankton growth rates

The latitudinal gradient in the mixed layer depth will produce increasingly good conditions for phytoplankton growth with distance north, assuming nutrient availability to be non-limiting at the initiation of the bloom. This effect is enhanced by increasing PAR to the north. This will lead to chl-a concentrations increasing more rapidly to the north. To test the magnitude of this effect a simple model of phytoplankton growth was used with differing inputs to represent the effects of one degree of latitude:

$$\frac{dC}{dt} = f(h,I)C \qquad \textbf{5-1}$$

where C is the chl-a concentration, h is the mixed layer depth and I is the PAR at the surface and t is time. It is assumed that there was a rapid reduction in the mixed layer depth so that it reduced suddenly, at the same time across the bloom area and that subsequently h was constant in time. The conditions were considered to be purely light

limited so the growth rate *f* was defined as the maximum phytoplankton growth parameter κ multiplied by the average light over the mixed layer depth. Using an exponential decay in light intensity with a diffuse downwelling attenuation coefficient, K_d, calculated using an empirical self-shading relationship found from light and chl-a profiles on the CROZEX research cruises D285 and D286 (Mark Moore *pers. comm.*):

$$K_d = 0.04 + 0.063C^{0.38} \qquad \textbf{5-2}$$

where C is the value of chl-a in mg m^{-3}. This leads to equation 5-3. The temporal change in the PAR data was included by setting *b* as 0.3 Einstein m^{-2} day^{-2} in equation 5-4.

$$f(h,I) = \frac{\kappa I}{h}\left(\frac{1-e^{-K_d h}}{K_d}\right) \qquad \textbf{5-3} \qquad I = I_0 + bt \qquad \textbf{5-4}$$

Equation 5-1 then has to be solved numerically. An initial value C_0 of 0.33 was used to match the satellite data. κ was set at 0.0085 m^3 $Einstein^{-1}$ so that it took approximately 32 days for *C* to increase from C_0 to 1 mg m^{-3} for a mixed layer of 50m, to fit the timescale found in satellite images.

The model was used to test the effect of 1 degree of latitude on time for chl-a to increase to 1 mg m^{-3}. To do this *h* and I_0 were set at 40m and 11 Einstein m^{-2} day^{-1}, 50m and 10 Einstein m^{-2} day^{-1} and 60m and 9 Einstein m^{-2} day^{-1} to account for the observed changes in mixed layer depth and insolation with latitude. Each step represents the effects of 1 degree of latitude on each variable. The results are shown in Figure 5.6.

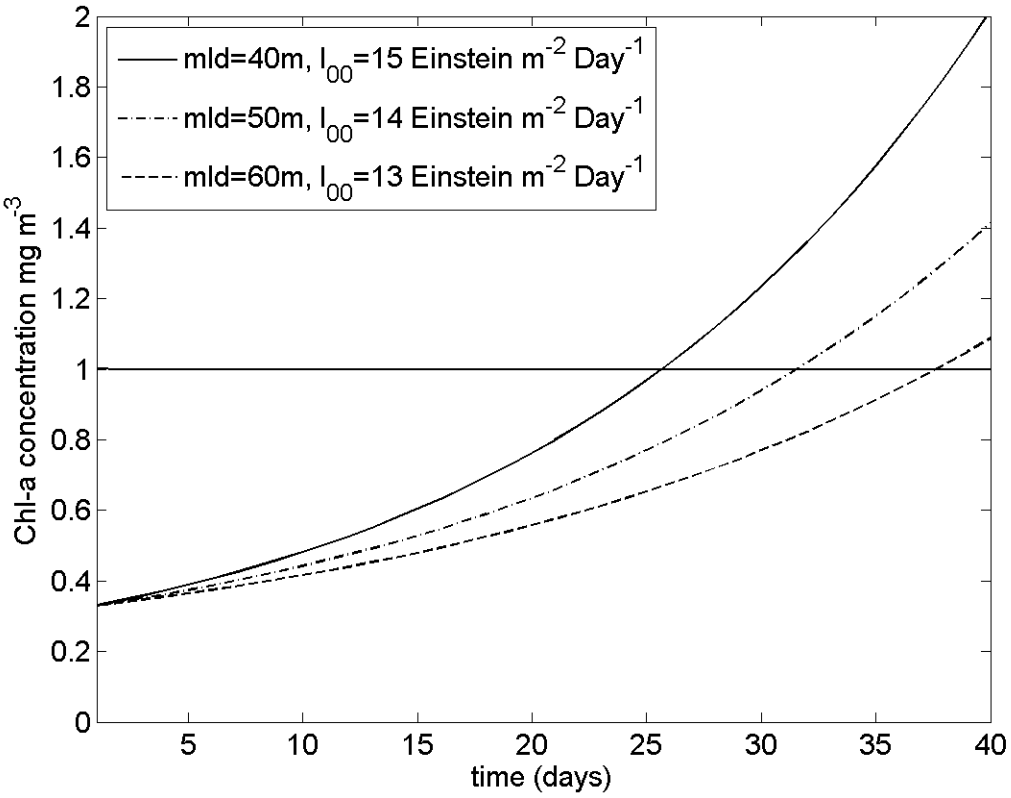

Figure 5.6 Modelled variation in chl-a increase with different light availability. The 10m and 1 Einstein m^{-2} day^{-1} steps represent the effects of 1 degree of latitude in average mixed layer depth and incoming irradiance.

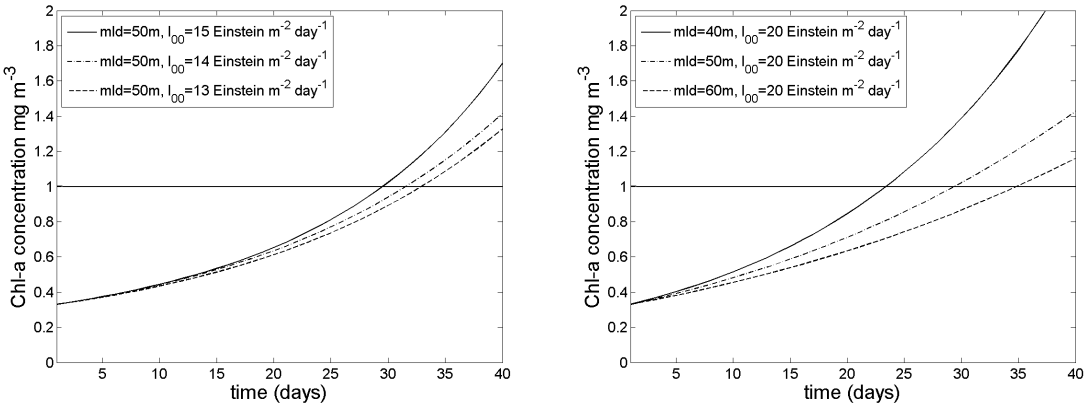

Figure 5.7 Results of model with mixed layer depth fixed (left) and PAR fixed (right).

The time taken for chl-a to reach 1 mg m^{-3} increased by approximately 6 days $degree^{-1}$ (Figure 5.6), which agrees with the average progression of 5.9 days $degree^{-1}$ found in satellite data between boxes A and C (see section 4.7.1). This estimate from the model is not particularly sensitive to the choice of the tuned parameter κ. The change is

approximately proportional to the change in the timescale for the mld=50m estimate of chl-a to reach 1mg m^{-3} and this is reasonably well constrained by the satellite data.

It is possible that rather than being best modelled as a step function, the mixed layer depth could gradually decrease. If it did, and phytoplankton increased linearly with light – that is, they were always close to the self-shading limit – the resulting delay from a similar model is 7 days $degree^{-1}$.

This agreement between the modelled and observed delay shows that, initially, light availability controls the southwards progression of the bloom. The variation in the mixed layer depth had a greater influence than the variation in insolation though the latter was not negligible (Figure 5.7). The difference between boxes C and D is 19 days $degree^{-1}$. The extra delay, over that predicted from the large scale mixed layer depth gradients, is consistent with the northerly flow into that area bringing water with stratification typical of further south. Evidence of this flow can often be seen as a tongue of cold water in SST images. A bloom does form and persist in box D eventually in most years, indicating that water there is iron fertilised.

This section confirms that the Crozet bloom is initiated by increased light in an area already enriched with iron (Planquette *et al.* 2007). This is in contrast with the artificial iron enrichment experiments where iron was added to areas with a favourable light climate. The similarities and differences observed between the Crozet bloom and artificial iron enrichment experiments can therefore be used to help assess the use of the latter in studying the effects of increased iron supply to currently iron limited areas.

5.4 SST as a predictor of mixed layer depth

Figure 5.8 shows that increased temperatures are associated with shallower mixed layer depths, but with the inevitable noise associated with mixed layer depth. This link within the study area suggests that satellite SST images can be interpreted as containing some information about the mixed layer depth. This can be used as an indication of the behaviour of the mixed layer depth over the plateau, where there are very few subsurface data.

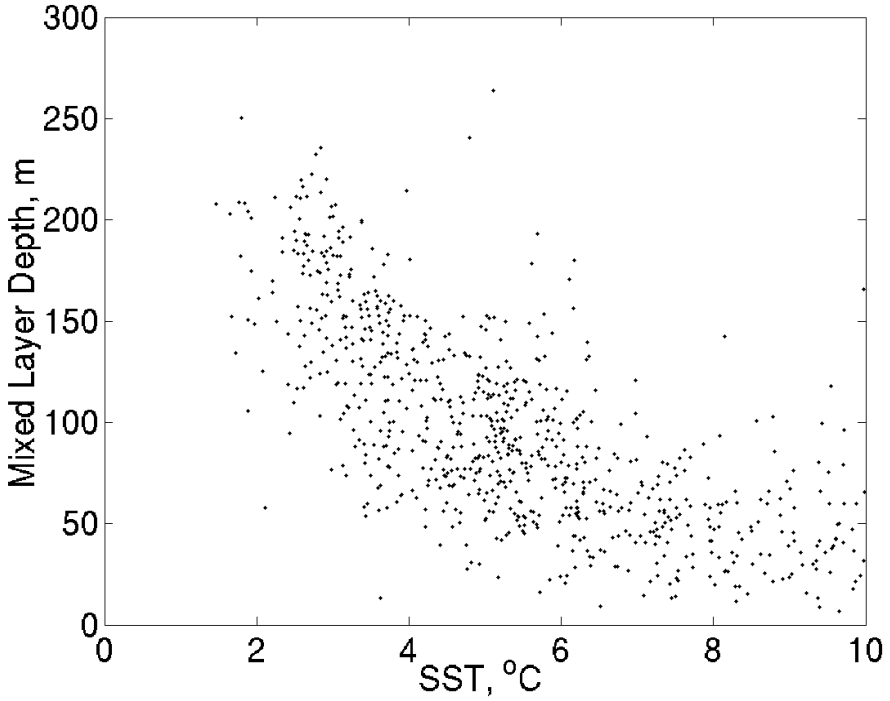

Figure 5.8 Mixed layer depth against surface temperature (i.e. bulk SST) for Argo float profiles around the Crozet Plateau, 43-50°S, 40-60°E.

5.5 Stratification over the Crozet Plateau

A deep mixed layer over the plateau would occur if the wind-driven mixed layer at the surface merged with a bottom mixed layer, driven by mean and tidal currents. It is important to know about the level of stratification over the plateau for two main reasons. A completely mixed water column would allow for strong transfer of iron coming out of the sediment to the surface waters and it would explain the low chl-a concentrations over the plateau despite presumably high iron levels (Planquette *et al*, 2007). However, due to poor charts meaning the ship could not enter into the area, there are no *in situ* cruise data from over the plateau.

Although Argo floats are meant to drift at either 1000m or 2000m, two floats have drifted over the Crozet Plateau. Movements during their ascents, descents and while at the surface carried them across depth contours so that the descent left them grounded. In each case this happened during the austral winter around the western and south-western edges of the plateau. This provides an opportunity to get data from the area. The density profiles are shown in Figure 5.9 and Figure 5.10.

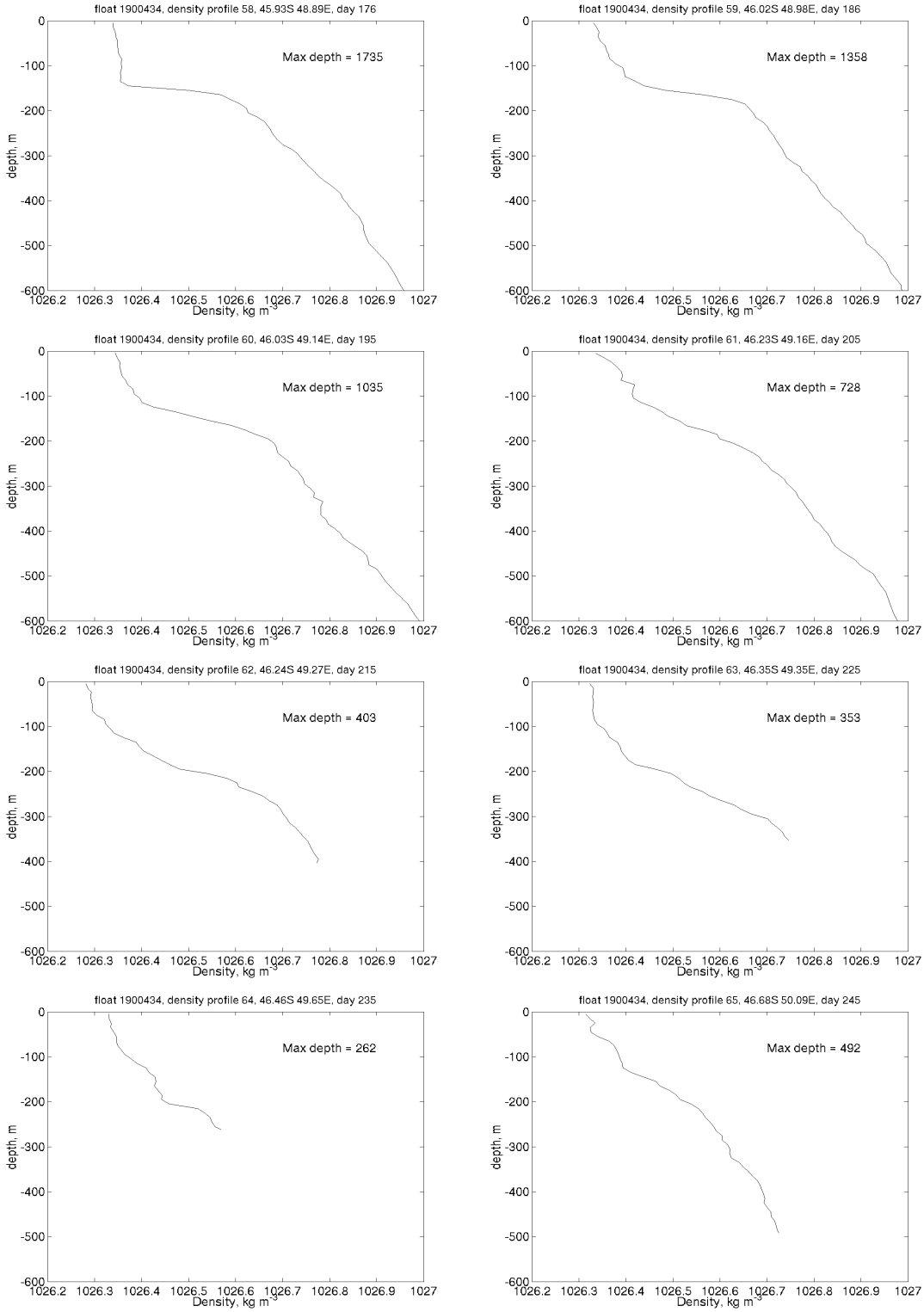

Figure 5.9 Density profiles from float 1900434, during a period when it was over the south-western part of the plateau between late June and early September 2006.

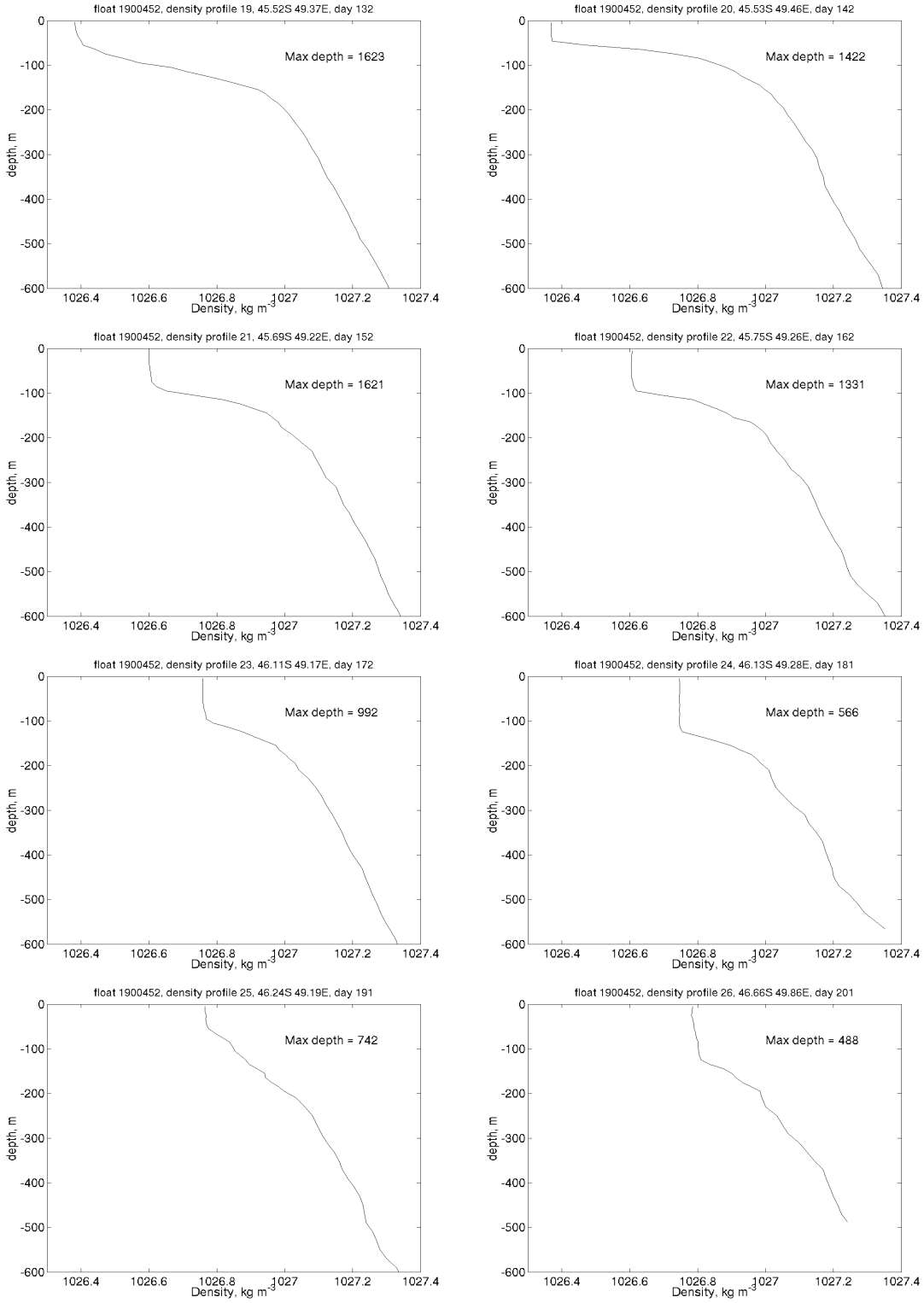

Figure 5.10 Density profiles from float 1900452 between May and July 2005 as the float went around the western edge of the plateau.

How close to the bottom these profiles start is not known, although there is no reason to suppose, from the programming of an Argo float, that it was significantly away from the sea bed. The movement on the ascent and steep topography in the area means the location given is not sufficient to calculate the depth the float was grounded at. The shallowest profile was 260m and neither this profile, nor any others, show signs of a significant change in the stratification over other float profiles in deeper water and there is no indication of a bottom mixed layer.

A feature that is likely to be evident if the water above the plateau is unstratified is a horizontal gradient in SST where stratification starts. This is because the unstratified water column would be a greater volume of water for the incoming irradiance to heat. Figure 5.8 shows a relationship between higher bulk SST (shallowest value from Argo profile) and shallower mixed layer depths, which supports this view (the overall trend is considered so the comparison between bulk SST and satellite derived SST is very likely to be valid). The recirculation of water over the plateau could however allow it acquire a different SST than water advected to close to the plateau, either from the north or south. There is also net flow along the southern edge and around the eastern end, and this leads to lower SST away from the plateau across the front.

Figure 5.11 shows a selection of SST images from 2004. It includes all 8-day periods from August-January with significant coverage of the plateau and surrounding area. None of the images show any SST features that appear to pick out a distinction between on- and off- plateau water. There is also no increase in chl-a with SST over and around the plateau (Figure 5.12) as might be expected if the suppression of chl-a was due to deep mixed layers.

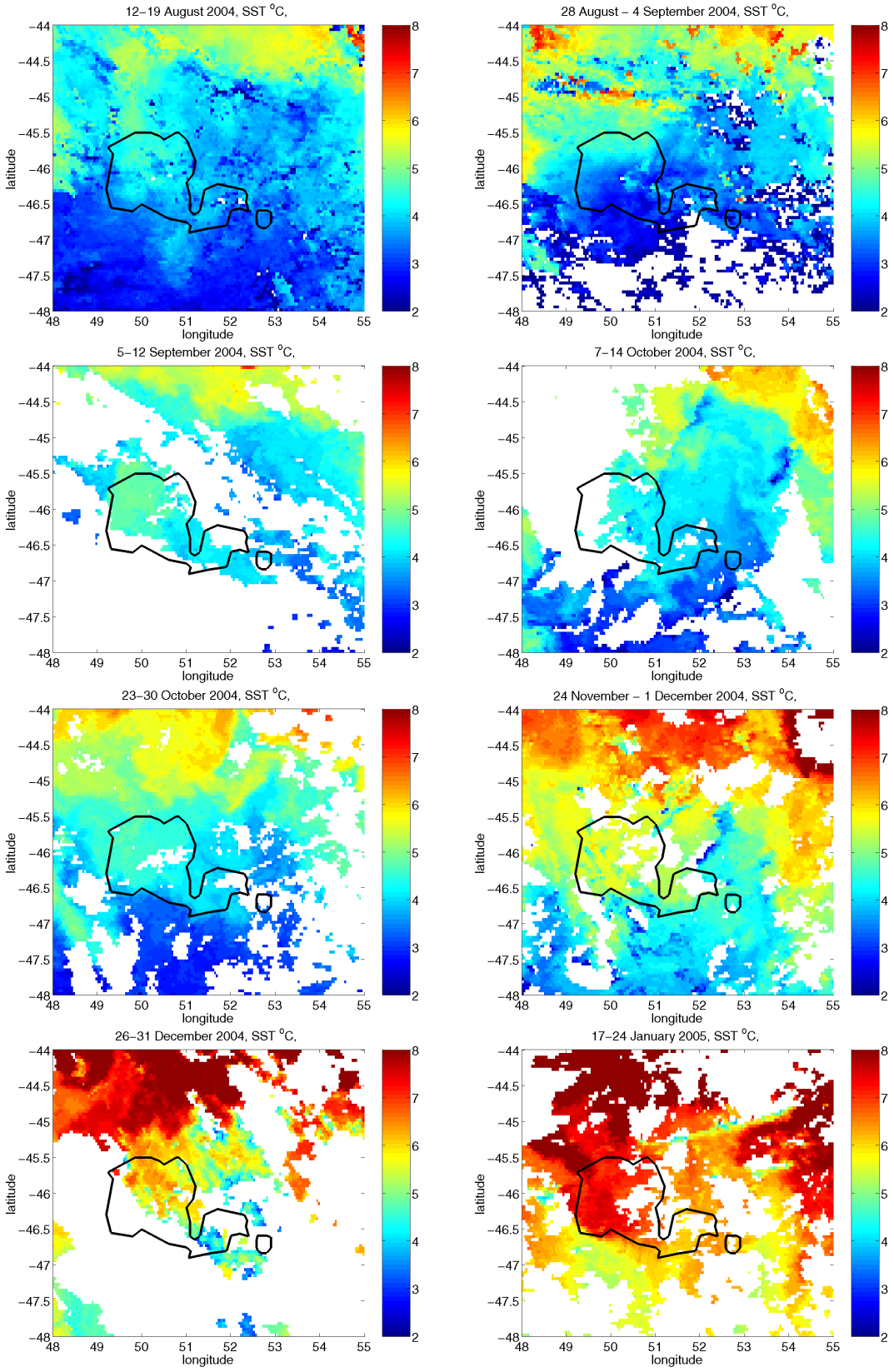

Figure 5.11 All SST images from August-January 2004/5 that have good coverage over the plateau. The black line is the 1000m contour.

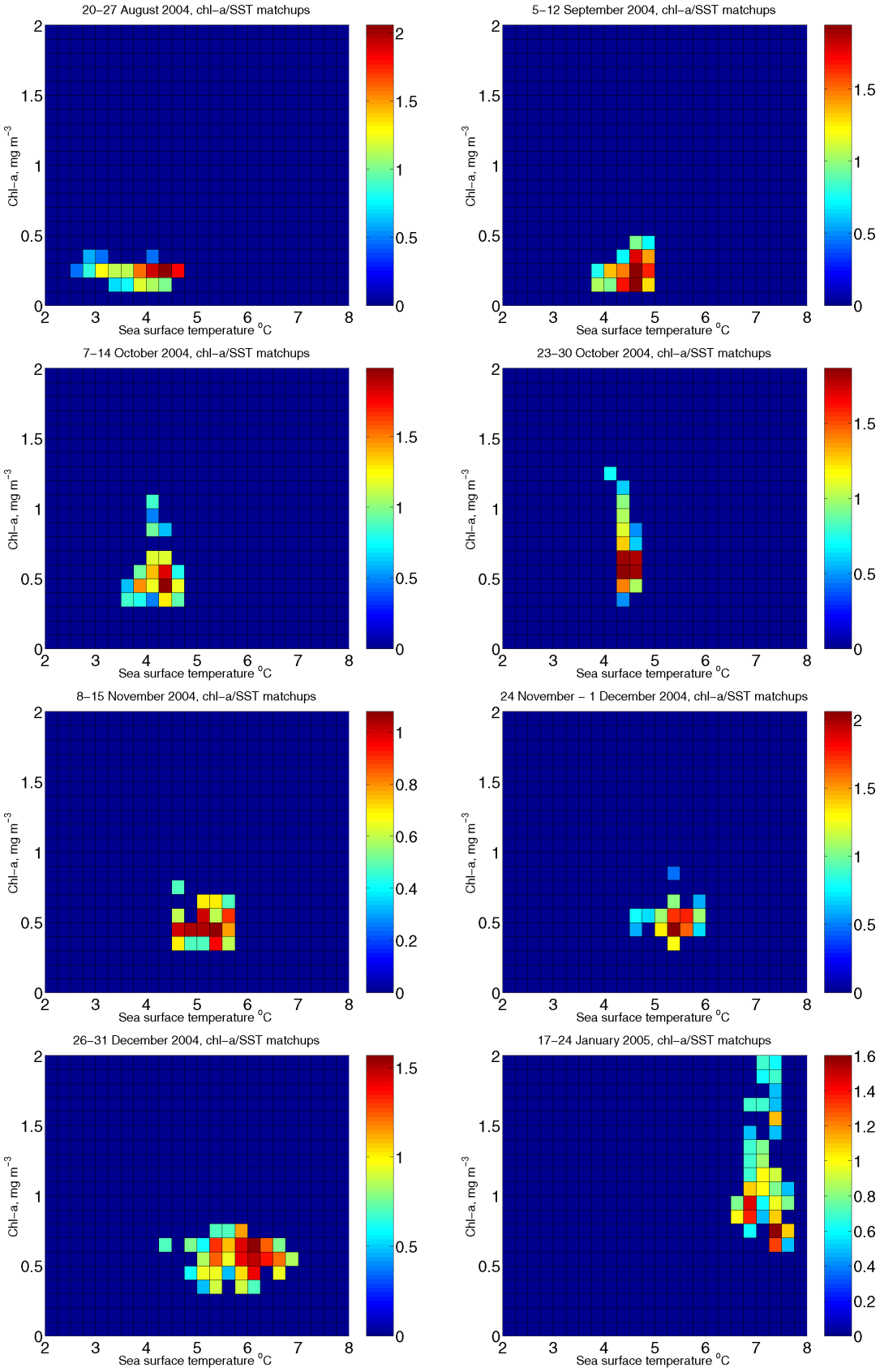

Figure 5.12 Log-frequency plots for Chl-a/SST match-ups from 45-47°S, 48-53°E.

The area (45.7-46.3°S, 49.6-51.0°E) was chosen to include water over the plateau and immediately around it. Data used are MODIS chl-a and SST images (from the same sensor so very similar coverage) and creating data pairs from the matching pixels. The plots show the frequency of such data pairs (SST, chl) in each 0.5°Cx0.2 mg m^{-3} area. The same 8-day periods have been selected as above, to include images with good coverage in the area. The two images from August have been excluded as chl-a is very low everywhere.

The inference from this lack of correlation between SST and chl-a is that the limiting factor for chl-a over the plateau is independent of light. To follow on from the arguments of section 4.6.3 iron is unlikely to be limiting as the chl-a is regularly higher over the plateau than to the south through the season (or the north on occasions late in the season). If iron was limiting, a similar pattern to north of the plateau and islands would be expected with a strong spring bloom followed by consistently low concentrations, but this is not found. This suggests a continuous availability of iron, due to a continuous supply and/or the winter concentrations never being fully utilised. Since neither iron nor light appears to be limiting chl-a over the plateau the conclusion is therefore that grazing is the likely cause of the limitation.

5.6 Light availability in mixed layers and relationship to chl-a

5.6.1 Crozet area

To further study the links between light and phytoplankton, satellite derived chl-a and Photosynthetically Available Radiation (PAR) were retrieved from the location of each Argo float profile. The datasets used were 8-day merged MODIS Aqua/SeaWiFS chl-a and 8-day PAR from SeaWiFS. If a chl-a value was not present in the location of the profile the surrounding pixels were checked ('radius' of search increasing from 1 to 3 pixels) and also chl-a images from the previous and following 8-day period. If a wider search area found data, the median was used. If both adjacent images in time had data the mean of the two values was used, otherwise the closest data were used (with priority given to checking a wider area around the profile). Although it would in some ways be preferable to use daily images, this would significantly reduce the number of times a satellite chl-a value was available from the location of the float. It would also bias the

dataset to times of low cloud cover and so high PAR. The long time period of 8 or 24 days means that this bias is significantly reduced.

There are several potential sources of noise in the data. The satellite data have inherent errors (though the chl-a values used are adjusted to account for systematic difference between *in situ* and satellite values, see section 2.5.6) and the use of a small number of pixels means that some small spikes may affect some profiles. It is also possible that the value found from the satellite data is not representative of the exact location of the profile, even when only one pixel is used. The diagnosis of a mixed layer depth is inherently arbitrary and certain profiles yield significantly different mixed layer depths from very similar criteria. The potential separation between mixed layer depth and chl-a also introduces noise into the data due to changes in light availability over short time and space scales, which phytoplankton concentrations do not respond to immediately. Light availability can reduce due to deepening of the mixed layer or through a reduction in PAR due to a change in the weather. Mixed layer deepening would reduce chl-a through dilution to a similar degree to the reduction in light but mixed layer shallowing would not lead to an immediate chl-a increase. The data therefore has to be interpreted with caution, with weight placed more on the overall pattern than individual datapoints.

The average light availability through the mixed layer was calculated from the Argo derived mixed layer depth and satellite PAR and chl-a. This was done by using an exponential attenuation of light, integrating the light over the mixed layer depth and then dividing by the mixed layer depth. This leaves the units as Einsteins day^{-1} m^{-2} as they are for the PAR data. The diffuse downwelling attenuation coefficient, K_d, is calculated using an empirical self-shading relationship found from light and chl-a profiles on the CROZEX research cruises D285 and D286 (equation 5-2). From this, together with satellite PAR, I, and mixed layer depth, h, the average light availability in the mixed layer can be found:

$$I_{av} = \frac{1}{h}\int_0^h Ie^{-K_d z}dz \qquad \textbf{5-5}$$

$$I_{av} = \frac{I}{K_d h}\left(1 - e^{-K_d h}\right) \qquad \textbf{(5-6)}$$

Figure 5.13 and Figure 5.14 show these data, split between north and south of the plateau (43-46.5°S and 47-50°S, 48-60°E). Despite the relatively sparse sampling from the Argo float profiles the difference between high and low chl-a values to the north and south respectively is clear. Sampled chl-a concentrations north of the plateau reach 2 mg m^{-3}, with a considerable number of datapoints exceeding 0.6 mg m^{-3}. In contrast to the south no datapoint exceeds 0.5 mg m^{-3}, despite the light levels often exceeding those found north of the plateau associated with high chl-a concentrations. If this analysis is repeated with a constant light attenuation (K_d=0.088, corresponding to a chl-a concentration of 0.5 mg m^{-3} in equation 5-5) rather than one that is a function of chl-a the results are qualitatively the same (Figure 5.14), showing that this effects is not just due to self-shading.

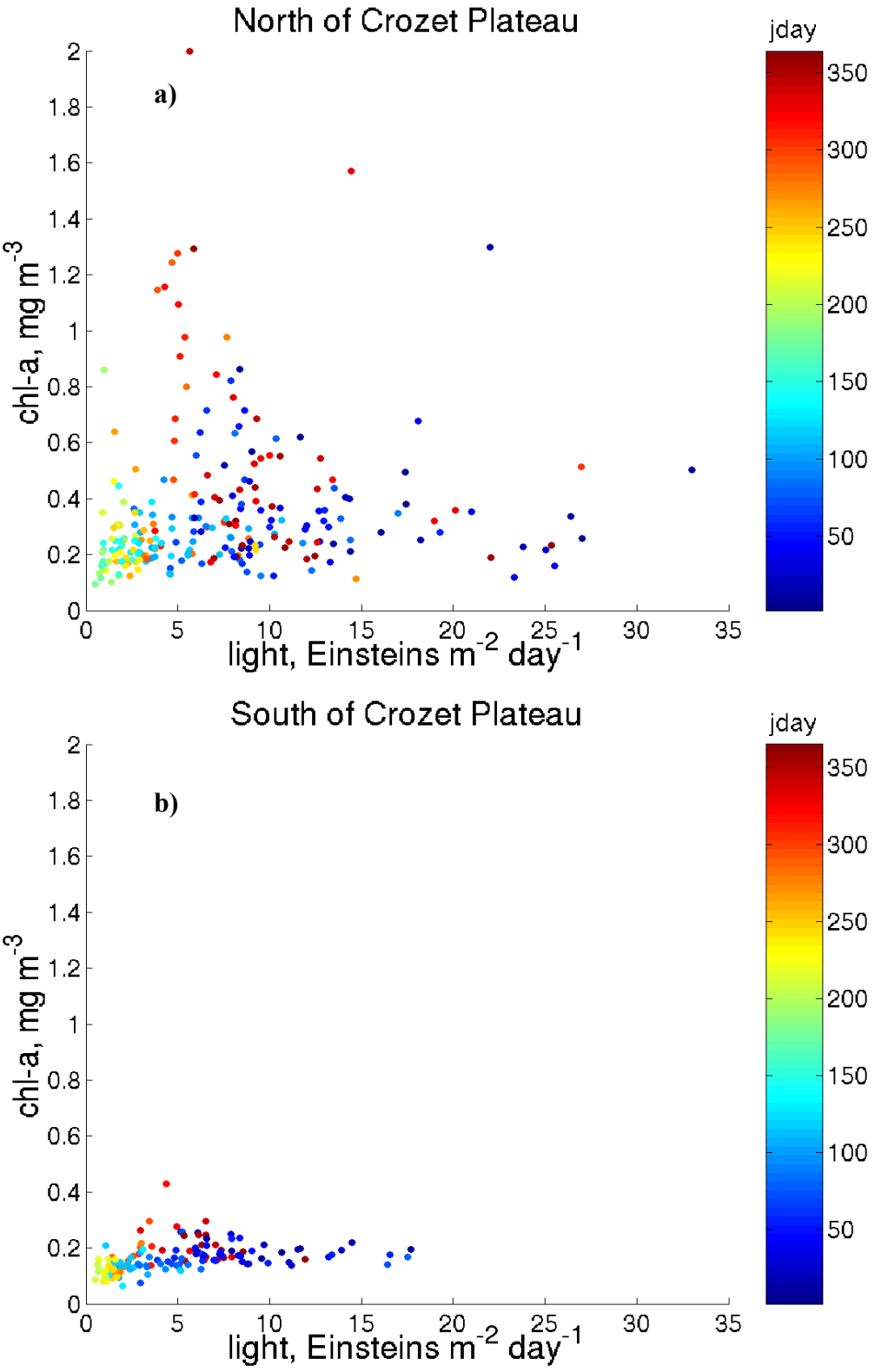

Figure 5.13 Chl-a (mg m^{-3}, from merged SeaWiFS/MODIS satellite product) against light availability in mixed layer. Colour scale is day of year. a) north of the plateau, b) south of the plateau.

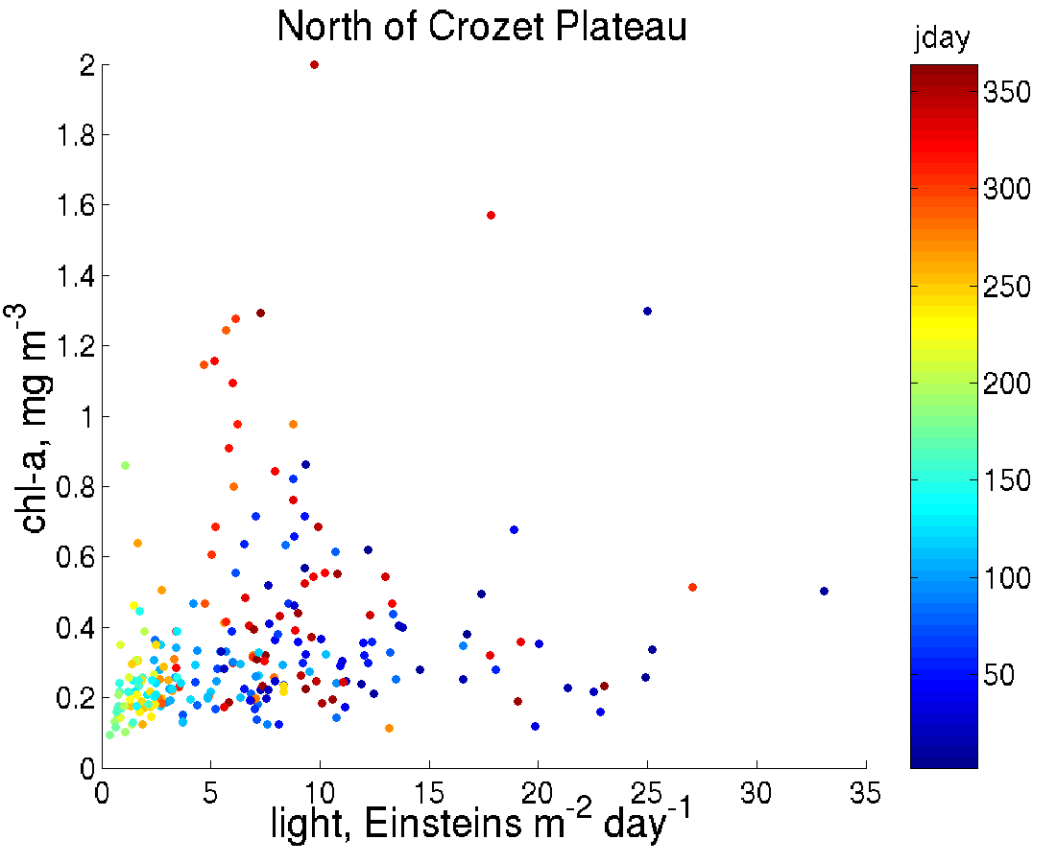

Figure 5.14 Same as Figure 5.13a but without accounting for self-shading (using a constant chl-a of 0.5 mg m^{-3} in equation 5-5).

Figure 5.13 shows a similar overall pattern north and south of the plateau. In the winter months (jday 130-260, approx. May-August,) both light is low (<3 Einsteins day^{-1} m^{-2}) and chl-a is low <0.3 mg m^{-3}). At this time both areas are light limited. Through September and October (jday 250-300) the light level increases and this is reflected in an increase in the chl-a, both north and south of the plateau. Chl-a concentrations increase after a relatively small increase in light to about 4 Einsteins day^{-1} m^{-2}.

Without accounting for self-shading the light availability for the high chl-a values to the north of the plateau is 6 Einsteins day^{-1} m^{-2} (Figure 5.15). According to section 4.6 (satellite time series) this increase in chl-a to 1 mg m^{-3} would have taken approximately 30 days, during which time average light availability would have increased by approximately 2 Einsteins day^{-1} m^{-2} (Figure 5.15). Therefore, again, 4 Einsteins day^{-1} m^{-2} is likely to be the threshold that triggers phytoplankton growth. This applies both north and south of the plateau.

The magnitude of the response however is significantly different: to the north chl-a values reach 2 mg m^{-3} whereas to the south the peak is 0.6 mg m^{-3}. The fact that these different responses occur at similar light levels proves that the area to the south of the plateau was not light limited. In addition, the fact that the areas are replete in macronutrients, including silicate at the beginning of spring, strongly implies that the differences are the effect of differences in the iron distribution. Grazing may be different between the areas as the light levels increase more slowly to the south, thus giving zooplankton more time to grow. This may increase the contrast due to the shift to smaller, more easily grazed phytoplankton under low iron concentrations (Morel *et al.* 1991; Moore *et al.* 2007) but this change in grazing alone is unlikely to cause such a significant difference if everything else is equal.

Taking 4 Einsteins day^{-1} m^{-2} as the light level that triggers a significant response in chl-a, Figure 5.15 shows that both north and south of the islands are not light limited for a significant period, and in this period light does not drop below the threshold value at any point sampled. Figure 5.15 predicts that the light level reaches 4 Einsteins day^{-1} m^{-2} (and so a significant increase in chl-a should be seen) at around jday 260 (17^{th} September) to the north and 310 (6^{th} November) to the south. These dates agree with the progression of chl-a seen in the ocean colour data (Figure 4.5). Though this is, in part, a circular argument (the critical light level being estimated empirically from chl-a increase to begin with) it confirms that the characteristics of the bloom images are captured by the relatively sparse sampling of Argo floats (Figure 5.16). The long period of high light and low chl-a indicate that both areas are limited by micronutrients or grazing for a significant period of the year. In the case of the northern area this is after a very strong spring bloom but nitrate and phosphate both remain significantly above limiting concentrations (Sanders *et al.* 2007).

Figure 5.15 also shows that the area north of the plateau is light limited for approximately 130 days, from jday 130 to 260. This is longer than the residence time estimated for surface water in the bloom area (section 3.2.5) so it is possible for island influenced water to mix across this whole area during the light limited winter period. This agrees with the observation of the bloom occurring across the whole area. The gap in the data for south of the plateau between jday 130 and 200 is because the orbit of the SeaWiFS satellite is such that data are not available at these latitudes for this time period.

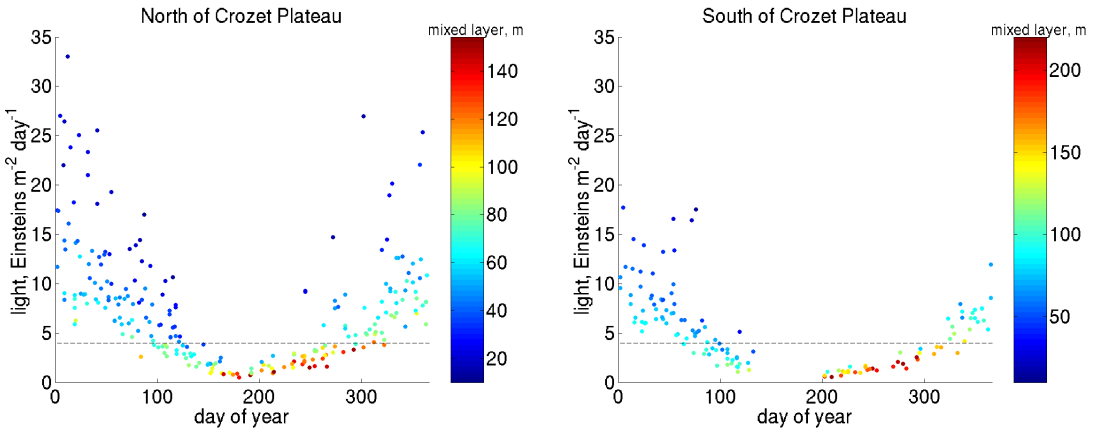

Figure 5.15 Light availability (Einsteins day^{-1} m^{-2}, calculated from mixed layer depth from Argo float profiles and SeaWiFS PAR data) against day of year north and south of the plateau.

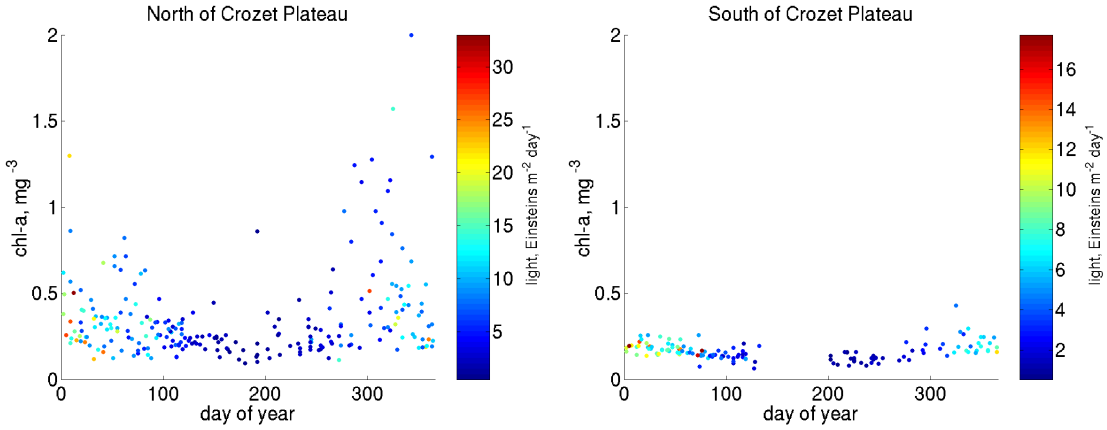

Figure 5.16 Chl-a values at the location of Argo float profiles against day of year for north and south of the plateau.

5.6.2 Other Sub-Antarctic islands

The data used for this method is global. It is therefore easy to use the method to investigate other places that have certain similarities with the Crozet Plateau area. This allows the situation around the Crozet Plateau to be put into a wider context and also highlights certain features of these other areas. In this section the method is applied around other Sub-Antarctic Islands.

Following the same procedure as section 5.6.1 the areas around South Georgia, the Kerguelen Islands, Bouvet Island, Macquarie Island and Prince Edward Islands were studied. The period between jday 120 and 220 is excluded due to the lack of satellite data.

In each case a box was drawn around the islands, offset so as to cover the downstream area. MADT and merged SeaWiFS/MODIS images for each area were studied to determine where this was, together with consultation with the literature for South Georgia (Ward *et al.* 2002; Korb *et al.* 2004; Meredith *et al.* 2005), Kerguelen (Blain *et al.* 2001; Bucciarelli *et al.* 2001) and Prince Edward Islands (Ansorge *et al.* 1999). Heard and Campbell Islands have been excluded from the analysis as there is no deep water close enough to them so Argo profiles are lacking.

Inevitably each box will include areas not directly influenced by the islands. In most cases this will be water typical of open Southern Ocean conditions, but around Bouvet ice-edge water may be included and the effects of South Georgia cannot be isolated from the wider Drake Passage/Scotia Arc situation. A control area of a similar size was also selected from the Pacific sector, away from any islands or landmasses, to help characterise the conditions expected in non-island influenced conditions, though there will always be local and regional variations. The areas selected are shown in Figure 5.17 while Figure 5.18 shows the merged SeaWiFS/MODIS image with the peak chl-a concentrations found in each area, selected from either 2004 or 2005 (the years when most float profiles are from), together with the contours of satellite absolute dynamic height (surface geostrophic streamlines). The axes for Figure 5.18 have been enlarged slightly relative to Figure 5.17, to provide context for the area chosen. It should be noted that there are problems with the absolute dynamic height data in the immediate vicinity of South Georgia, causing contours to pass through the island, an unreal eddy south-east of the island and reduced northwestwards flow along the shelf-break to the north-east.

Figure 5.17 shows the distribution of float profiles around these areas that have co-located satellite chl-a and PAR values. There are clear gaps in the data where the topography is too shallow for Argo floats (<1000m, and a reduction in floats in depths between 1000m and 2000m). This is most marked around Kerguelen and north of Prince Edward Islands. The latter causes problems for this method as a small bloom associated with the Prince Edward Islands can occur in the area not sampled (Figure 5.18).

Figure 5.19 shows that South Georgia, Kerguelen and Crozet follow a similar pattern. Figure 5.20 shows that they all have a similar light climate, Crozet receiving slightly more light due to its more northerly location. The data from Kerguelen strongly supports

the diagnosis of a critical light level of 4 Einsteins day^{-1} m^{-2} but there appears to be a response to lower light levels around South Georgia. This may be because of the greater number of high chl-a datapoints, such that the spread in light levels due to fluctuations in mixed layer depth and PAR means that some have low light levels. Removing data where the matchup between profile location and time do not exactly match a satellite chl-a value makes little difference, but variations in the 8-day period and 9km by 5km pixel could be significant. Alternatively there could be higher initial iron concentrations and this could allow phytoplankton to better utilise available light (Sunda and Huntsman 1997). South Georgia is also notable for the high chl-a values persisting through period of light availability, indicating either a stronger source of iron or a higher initial concentration.

The other islands show a much lower response to the increased light although Figure 5.20 shows that the seasonal progression of light is similar. In the case of the Prince Edward Islands this in part due to the shallow water and hence lack of profiles north of the islands where a small bloom occurs (Figure 5.18). In the case of Bouvet and Macquarie the chl-a images confirm that there is not a significant bloom associated with the islands. The chl-a against light plots and satellite chl-a images for these areas are qualitatively similar to the area selected from the Pacific sector away from the impact of nearby islands or land masses. Figure 5.20 shows that very deep mixed layers can occur around Macquarie in the winter. Re-stratification causes the light levels to increase strongly through spring but these deep mixed layers would act to dilute any iron supply from the islands through the winter, removing most of the iron below the euphotic depth and therefore out of reach of phytoplankton unless it is brought back to the surface by physical processes.

This analysis shows that there is overall similarity in the light availability around all the Sub-Antarctic islands considered. This shows that there is sufficient light for phytoplankton growth in those areas that do not support a strong bloom. The lack of blooms therefore indicates that at least one other necessary condition is not present in these areas. From the results of this study, other CROZEX results (Planquette *et al.* 2007), Keops (Blain *et al.* 2007) and the artificial iron enrichment experiments (de Baar *et al.* 2005; Boyd *et al.* 2007), this is most likely iron, as it is hard to see why grazing should vary so significantly between islands.

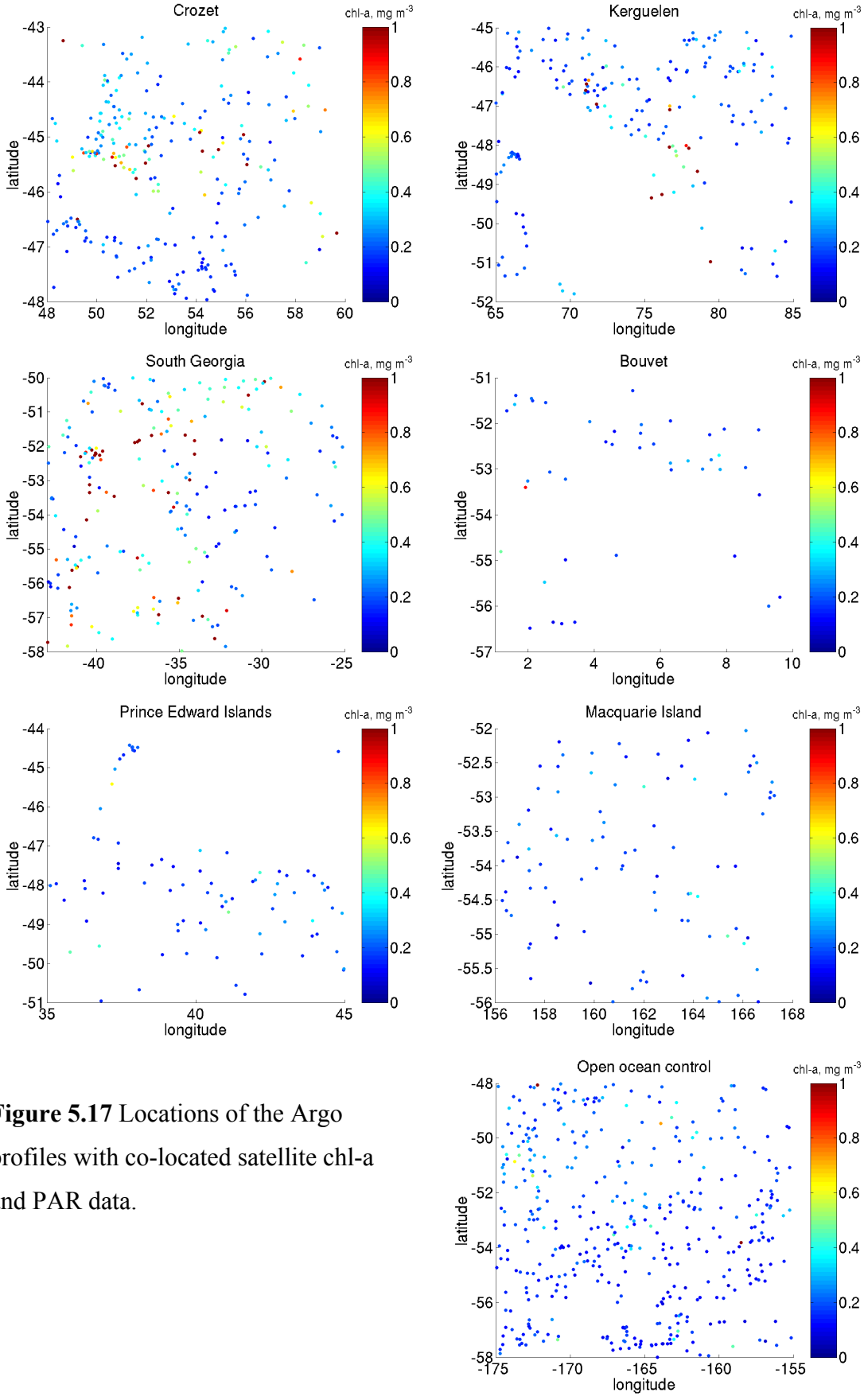

Figure 5.17 Locations of the Argo profiles with co-located satellite chl-a and PAR data.

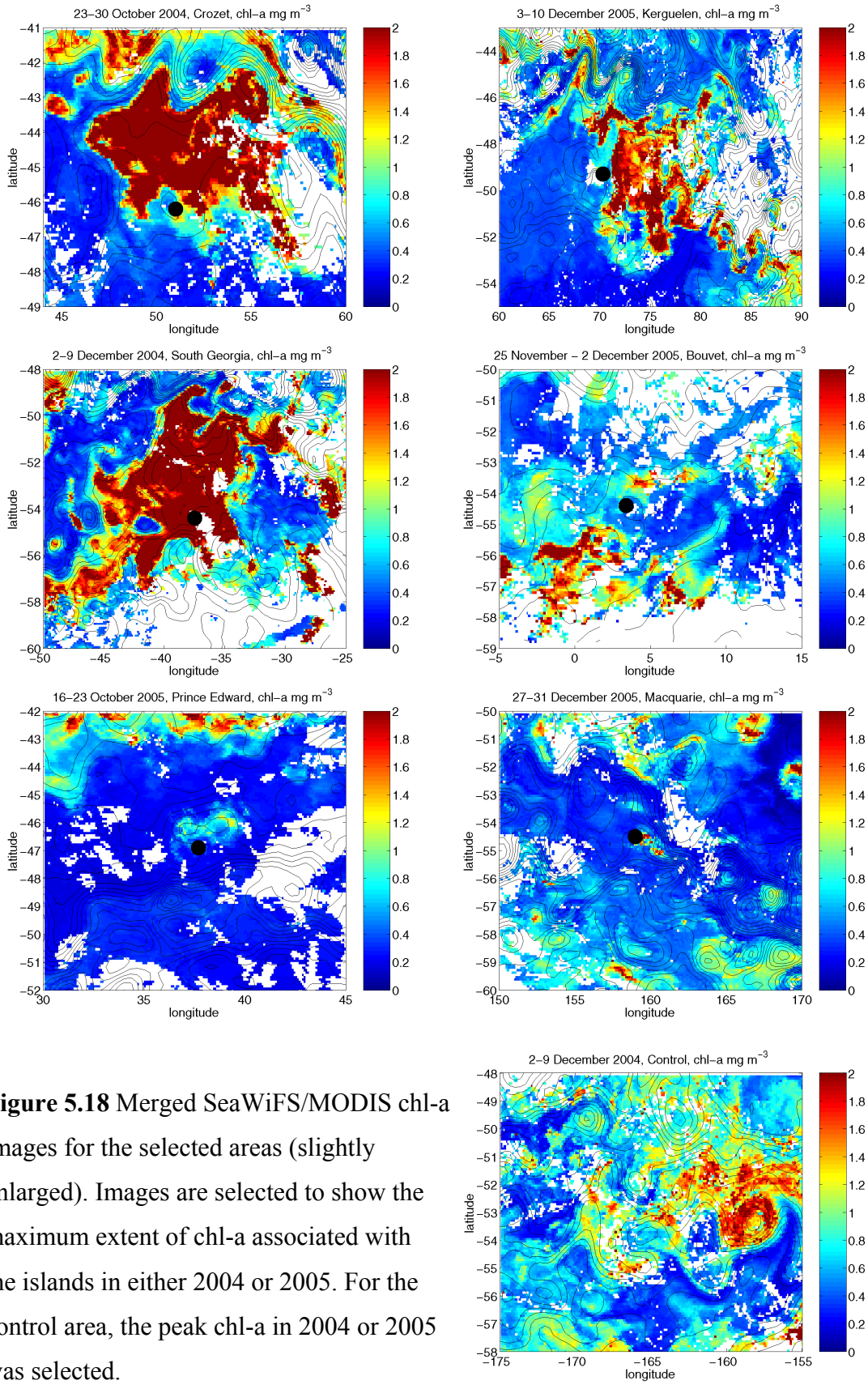

Figure 5.18 Merged SeaWiFS/MODIS chl-a images for the selected areas (slightly enlarged). Images are selected to show the maximum extent of chl-a associated with the islands in either 2004 or 2005. For the control area, the peak chl-a in 2004 or 2005 was selected.

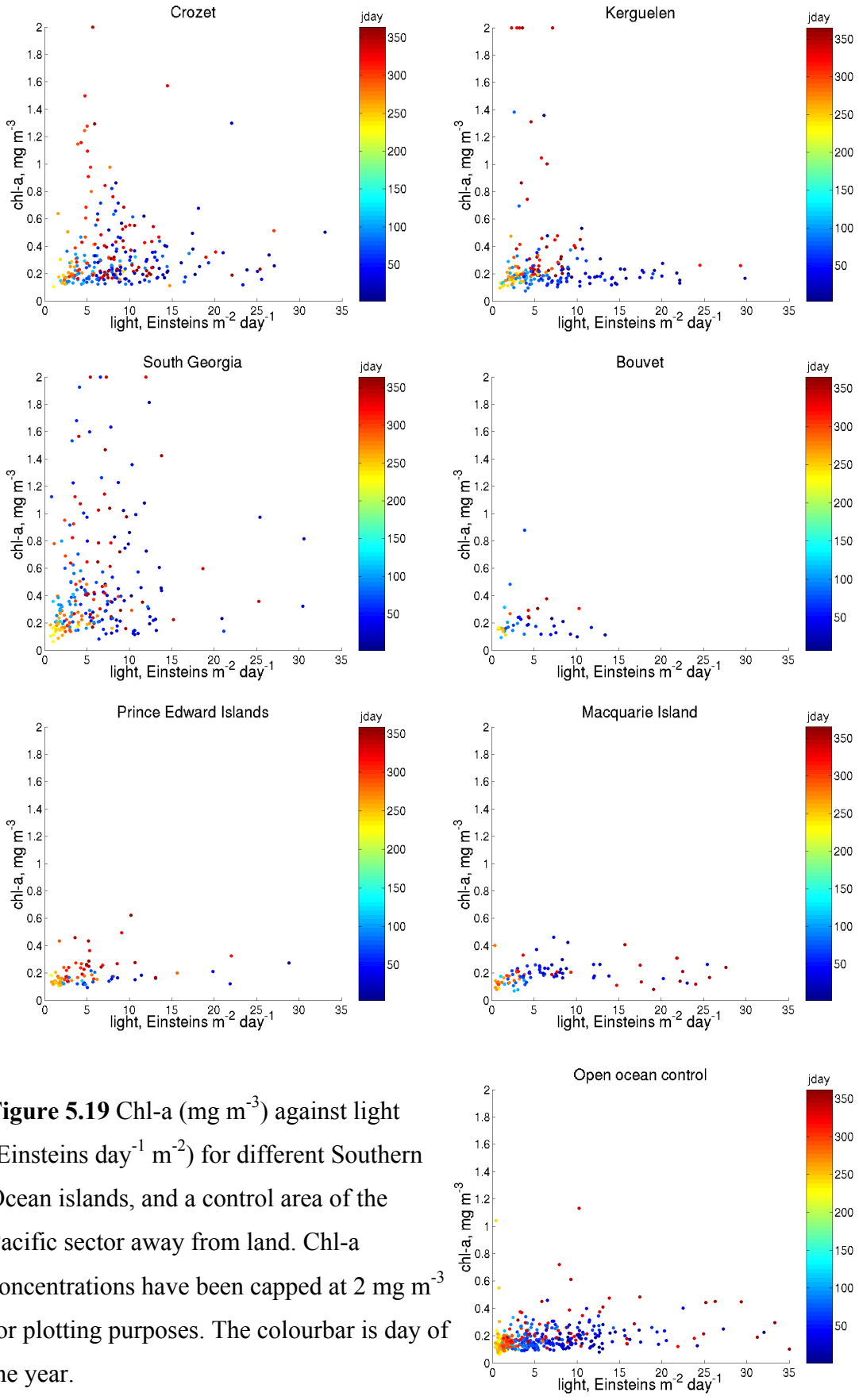

Figure 5.19 Chl-a (mg m^{-3}) against light (Einsteins day^{-1} m^{-2}) for different Southern Ocean islands, and a control area of the Pacific sector away from land. Chl-a concentrations have been capped at 2 mg m^{-3} for plotting purposes. The colourbar is day of the year.

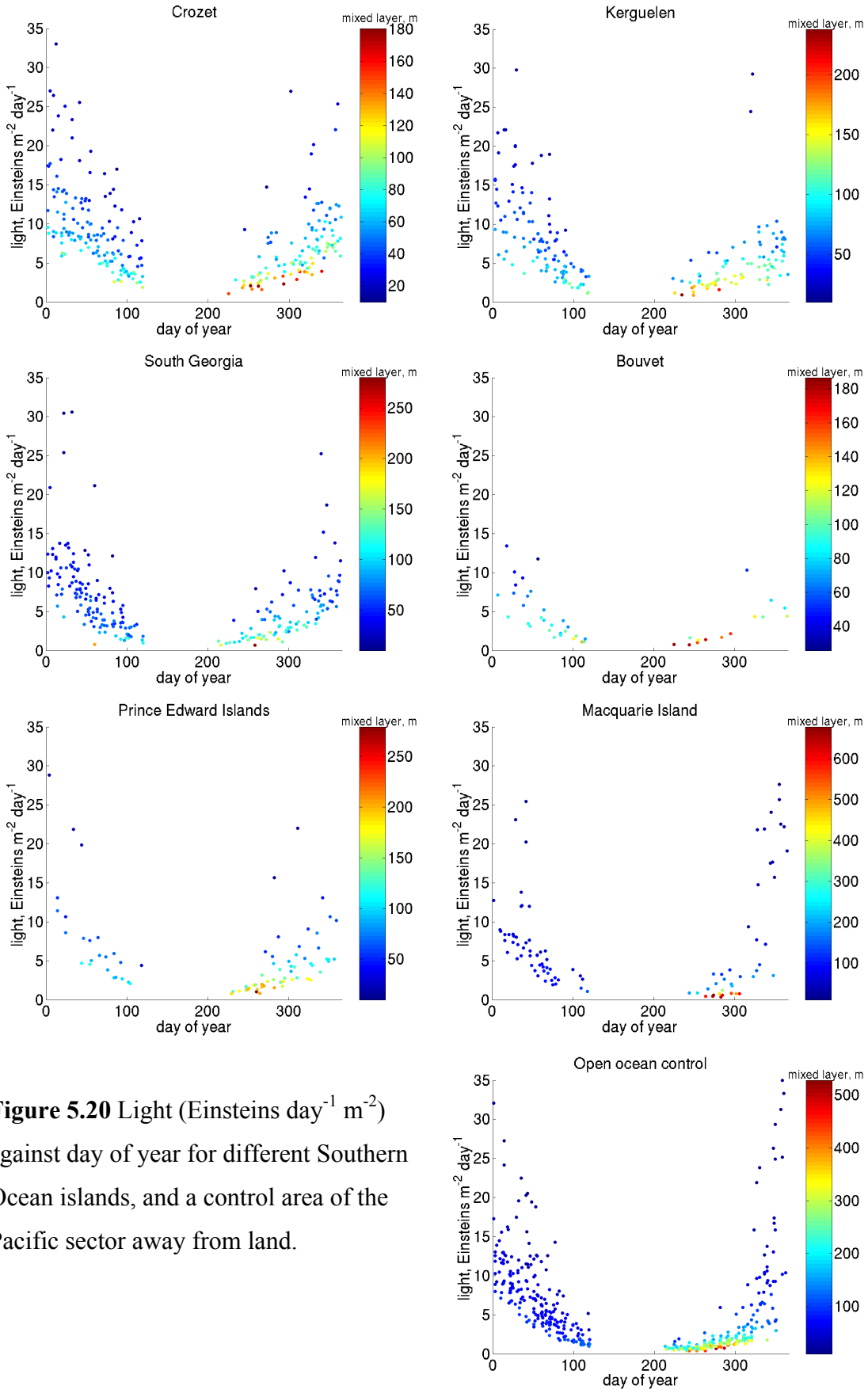

Figure 5.20 Light (Einsteins day^{-1} m^{-2}) against day of year for different Southern Ocean islands, and a control area of the Pacific sector away from land.

5.7 Artificial iron enrichment experiments

In a synthesis of the artificial iron enrichment experiments conducted in HNLC conditions de Baar (2005) showed that there was a significant link between the maximum chl-a concentrations reached in each of the experiments and the mixed layer depth during the experiment. This is reproduced below as Figure 5.21, slightly different to the original as the mixed layer depths from the time of peak chl-a have been used if available (Coale *et al.* 1996; Boyd *et al.* 2000; Rollwagen Bollens and Landry 2000; Law *et al.* 2003; Tsuda *et al.* 2003; Boyd *et al.* 2004; Coale *et al.* 2004; Bakker *et al.* 2005; Cisewski *et al.* 2005) and the peak chl-a values given in Boyd *et al.* (2007) are used, which do not all agree with those in de Baar *et al.* (2005). The data are presented in Table 5.1.

There are some problems in comparing between experiments as there is no set definition of the mixed layer depth and not all the criteria have been given, or are directly comparable to this study – the distribution of SF_6 tracer being used by Law (2003). The mixed layer depths from EisenEx are found using a density difference criterion of 0.02 kg m^{-3} (Cisewski *et al.* 2005), this comparing to the 0.05 kg m^{-3} criterion used in this work. This will produce shallower mixed layers and so higher light availability, but it is impossible to quantify by how much without studying the particular density profiles.

There are also problems using chl-a as a measure of the bloom strength as one result of the alleviation of iron stress is an increase in the chl-a:carbon ratio. For instance, during the SOIREE bloom the percentage increase in biomass was half the percentage increase in chl-a. The growth rates used here include this problem so should be treated with caution. There is likely to be some consistency in this effect between experiments, though chl-a:C may be higher in experiments with deeper mixed layers due to photoacclimation of phytoplankton to low light conditions.

As stated in de Baar *et al.* (2005) the relationship between mixed layer depth and peak chl-a is statistically significant (for original plot chl-a=523$(mld)^{-1.36}$, P=0.003, t=-5.55, R^2=0.90, n=7). Therefore, once iron limitation has been lifted, light is the factor that is likely to control phytoplankton concentrations. This gives a strong indication that there is not a secondary limiting nutrient that controls the response after iron limitation is lifted but there are few datapoints and the relationship depends strongly on the results from SEEDS.

It is however not stated in the review by de Baar (2005) whether this relationship between light and chl-a response is due to the effects of light on the growth rate of phytoplankton or through a self-shading effect whereby phytoplankton concentrations increase until light is limiting. Figure 5.22 and Figure 5.23 show that the mixed layer depth does affect the growth rate, as is expected in systems where nutrients are not limiting and in which the timescales are too short for grazing control to be effective on large (>10μm) phytoplankton.

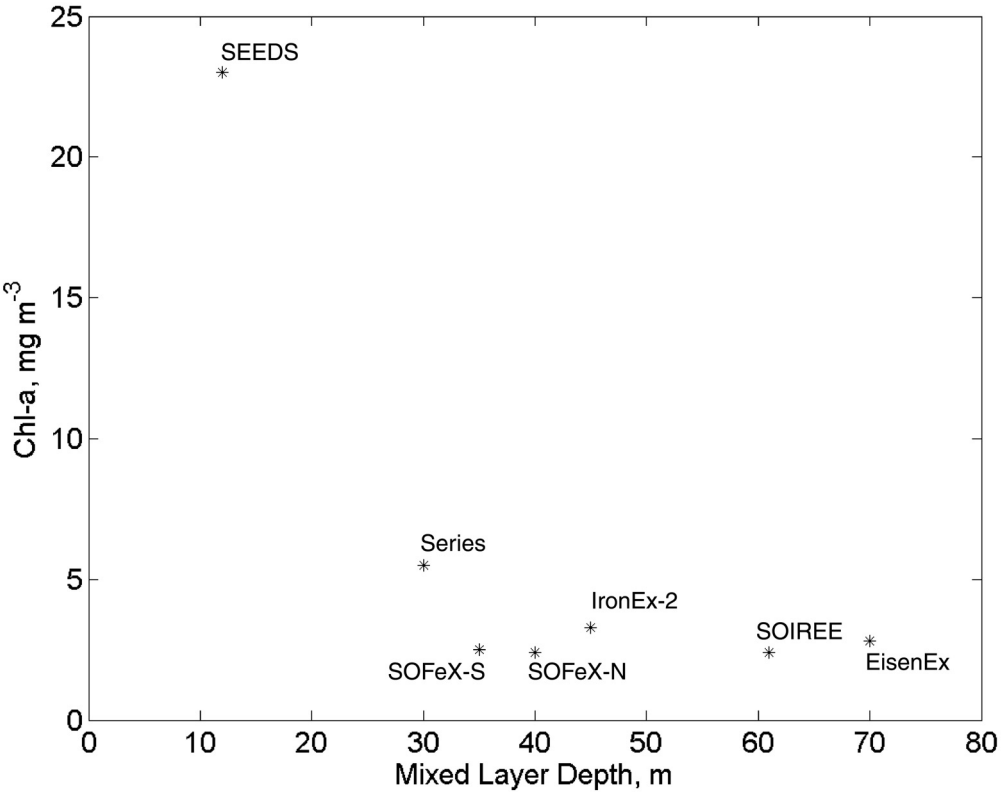

Figure 5.21 Peak chl-a against mixed layer depth for artificial iron enrichment experiments (following de Baar *et al.* 2005)

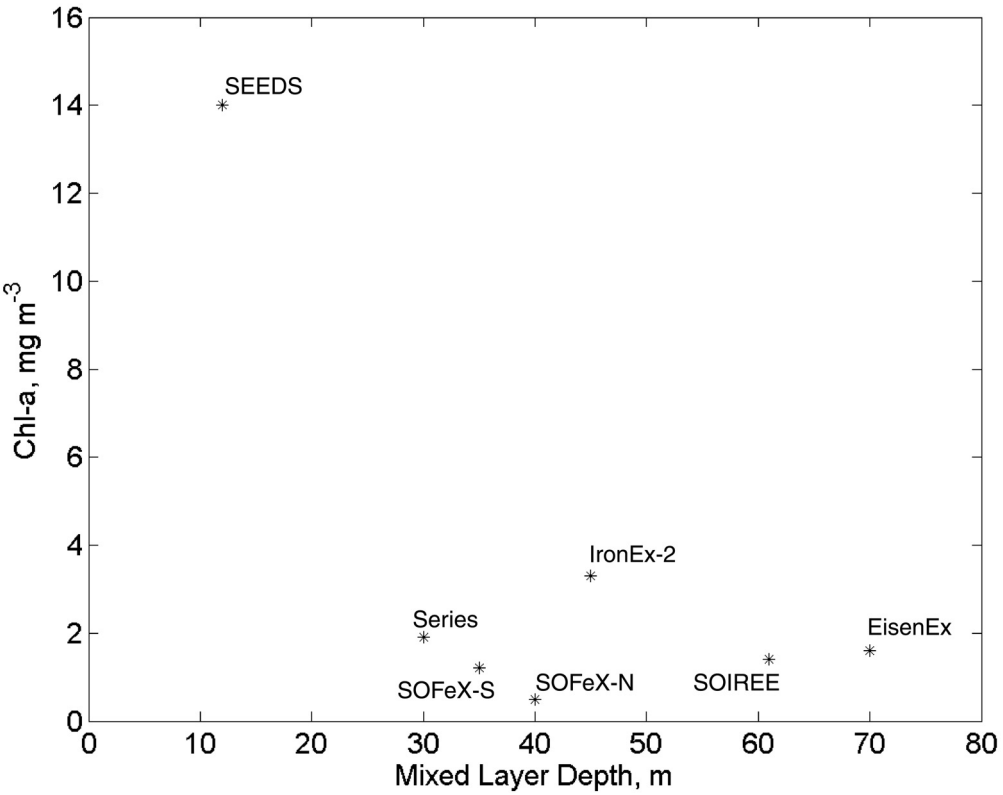

Figure 5.22 As Figure 5.21 but taking the chl-a concentration after 10 days of the experiment rather than at the peak.

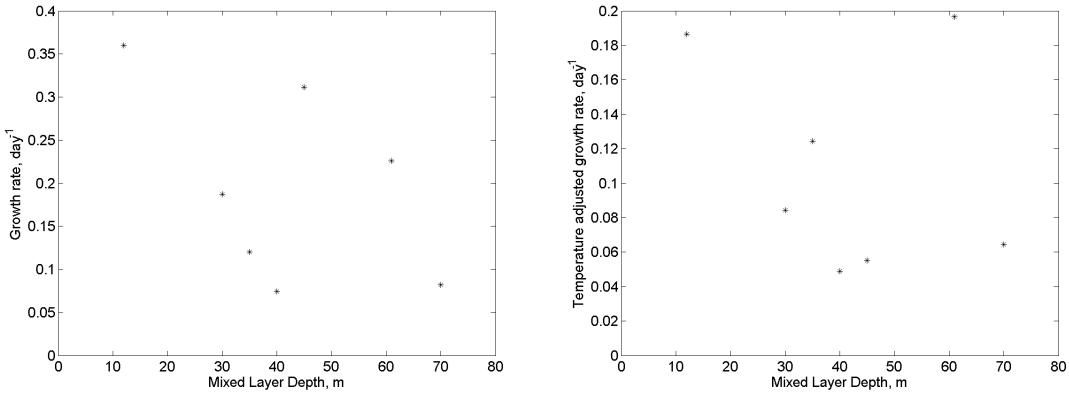

Figure 5.23 Growth rate for iron enrichment experiments, right hand plot is corrected for the effects of surface temperature (by dividing by $2^{SST/10}$) on growth rate (Eppley 1972; Goldman and Carpenter 1974).

The approach of this section of looking at a mixed layer depth averaged light intensity that is needed for bloom development gives one approach for testing which of the factors is important in setting the peak chl-a concentrations. If the increase in phytoplankton is

such that the light availability in the mixed layer depth reduces (due to increased attenuation) to close to the limiting light availability then self-shading is likely to be the dominant effect. If however the light remains significantly above limiting levels (and relatively close to initial light levels) then self-shading is unlikely to be significant. There are of course potentially significant problems in applying the critical light to areas with significantly different phytoplankton community structures, although, if this is the case, it is also unlikely to be valid to analyse the combined dataset of all enrichment experiments together when looking at the response to light availability.

The same attenuation relationship, that found around the Crozet Plateau, has been used in each case. Where a value has been given in the literature for a specific experiment it is similar to that calculated though slightly lower. This means that the light availability estimates may be biased low. It is not clear however that the relationship will be valid at very high concentrations such as those found during the SEEDS experiment. Where given, the criteria for mixed layer depth will bias the depths found to be lower than those found in this study and therefore bias the light availability high.

Name	Location	Initial chl-a	10 day chl-a	Peak chl-a	Day of peak after enrichment	MLD	Growth rate	Temp	PAR	Attenuation	Initial light	Light at peak chl-a
IronEx-2	EEP	0.2	3.3	3.3	9	45	0.31	25	50	0.14	15.5	8.1
Soiree	SO	0.2	1.4	2.3	11	61	0.23	2	25	0.13	5.6	3.2
EisenEx	SO	0.5	1.6	2.8	21	70	0.08	3.5	45	0.13	7.3	4.9
SEEDS	NWP	0.9	14	23	9	12	0.36	9.5	30	0.24	35.7	10.8
SOFeX-N	SO	0.3	0.5	2.4	28	40	0.07	6	33	0.13	10.8	6.5
SOFeX-S	SO	0.2	1.2	2.5	21	35	0.12	-0.5	23	0.13	9.6	5.2
Series	NEP	0.4	1.9	5.5	14	30	0.19	11.5	42	0.16	18.0	8.9
EiFeX	SO	0.6	N/A	3.0	N/A	100	N/A	4.5	N/A	N/A	N/A	N/A

Table 5.1 Details of artificial iron enrichment experiments. MLD and PAR values are for the time of peak chl-a where possible, otherwise they are values quoted in Boyd *et al.* (2007) or, for PAR, de Baar *et al.* (2005). EIFEX is included but not further considered due to lack of PAR data. EEP=East Equatorial Pacific, SO=Southern Ocean, NWP=North-West Pacific, NEP=North-East Pacific.

It can be seen from Table 5.1 that the light level at the peak of the bloom for the Southern Ocean experiments was close to the 4 Einsteins m^{-2} day^{-1} critical level identified in section 5.6.1. This agrees with them becoming close to or reaching a chl-a concentration at which self-shading was important. The mixed layer depth deepened considerable during the SOIREE experiment (Bakker *et al.* 2005; Cisewski *et al.* 2005), which could be the cause of the anomalously low light availability at the peak and high growth rate.

The experiments outside the Southern Ocean peak at higher light levels after a shorter period of time. This suggests that nutrient limitation, such as the removal of iron by biological and chemical processes, causes the reduction in chl-a. If self-shading were important in setting the peak chl-a, it would be expected that the chl-a concentrations would level off at a particular chl-a concentration. The fact that rapid declines are observed after the peak of most artificially enriched blooms also indicates limitation from a process other than light-limitation.

During SOIREE there were also in vitro incubation experiments carried out, with light levels set at those representing a 45m, 60m and 100m mixed layer (Boyd *et al.* 2000). The response from the experiments at 45m and 60m light levels are very similar, with strong phytoplankton growth whereas there was little phytoplankton growth in the 100m light level incubation. The light availabilities in these experiments, not accounting for self-shading, are 7.4, 5.5 and 3.5 Einsteins day^{-1} m^{-2} at 45m, 60m and 100m respectively. This gives further support to the view to the diagnosis of a critical light intensity of approximately 4 Einsteins day^{-1} m^{-2}.

Overall it is therefore clear that self-shading is not the sole cause of the strong relationship found between light and peak chl-a. It appears that the peak is driven by a combination of phytoplankton growth rate (a function of light availability and water temperature) and a timescale for the experiments, possibly set by either by biological utilisation or the chemical behaviour of the added iron reducing its bioavailability.

5.8 Spatial and temporal variations in chl-a peak around Crozet Plateau

It is interesting to compare the spatial distribution of peak chl-a concentrations found around Crozet to the results for artificial fertilisation experiments, especially as the gradient in light availability (increasing to north) is against that in iron availability (increasing to south) so the dominant control on peak chl-a can be investigated. The longer timescale allowed by a

naturally iron fertilised bloom studied through remote sensing also makes it easier to detect limitation by self shading, if it is occurring, through the chl-a time series.

5.8.1 Peak of median chl-a

Following the arguments of this section, in a purely light limited system, where all other factors are homogenous, the highest surface chl-a values would occur where the light climate is best. Table 5.2 however shows that the maximum chl-a values generally increase towards the plateau, whereas, as shown above (section 5.1.1), the mixed layer depth deepens towards the plateau.

The timing of the peak to the south is also very consistent, occurring between the last week in November and second week in December each year, according to Table 5.3. This is before the peak in light availability (Figure 5.15), agreeing with the analysis of section 5.6.1 that this area is not light limited for a significant period of the austral summer.

Year\Box	A	B	C	D	E	F
1997	1.59	3.69	5.63	4.56	1.35	0.43
1998	2.59	3.10	5.44	8.13	0.80	0.35
1999	2.69	6.71	5.63	7.45	2.33	0.59
2000	1.31	1.81	3.38	8.27	0.77	0.45
2001	1.17	1.78	4.11	3.32	0.59	0.45
2002	1.63	2.50	3.21	5.25	4.11	0.69
2003	2.25	2.33	2.33	2.88	0.77	0.36
2004	3.10	3.10	2.88	2.50	0.70	0.64
2005	3.21	2.50	4.25	4.40	0.90	0.41
Mean:	**2.17**	**3.06**	**4.10**	**5.20**	**1.37**	**0.49**

Table 5.2 Seasonal maximum of the 8-day median chl-a (mg m^{-3}) in each box from adjusted SeaWiFS chl-a data.

Year\Box	A	B	C	D	E	F
1997	11	11	11	13	11	16
1998	6	9	13	12	24	15
1999	12	13	13	17	15	16
2000	8	10	17	17	28	16
2001	12	15	15	15	25	15
2002	9	11	11	13	14	16
2003	11	11	13	15	26	14
2004	12	10	10	12	30	16
2005	13	11	15	15	21	15
Mean:	**10.4**	**11.2**	**13.1**	**14.3**	**21.6**	**15.4**

Table 5.3 8-day period that the seasonal maximum of the 8-day median chl-a occurs in each box from adjusted SeaWiFS chl-a data.

As with section 4.3 where the seasonal mean chl-a was considered, the spatial and temporal structure of the chl-a peak can also be investigated, and visualised, through seasonal composite images. The images presented in Figure 5.24 show the maximum chl-a in each pixel, out of those with data, from 4th August to 29th March. Figure 5.25 shows the Julian day (adjusted to count through the end of the year) that corresponds to the 8-day dataset in which the maximum chl-a value for that pixel is attained that season. Figure 5.26 is the mean of each of these images (pixel by pixel).

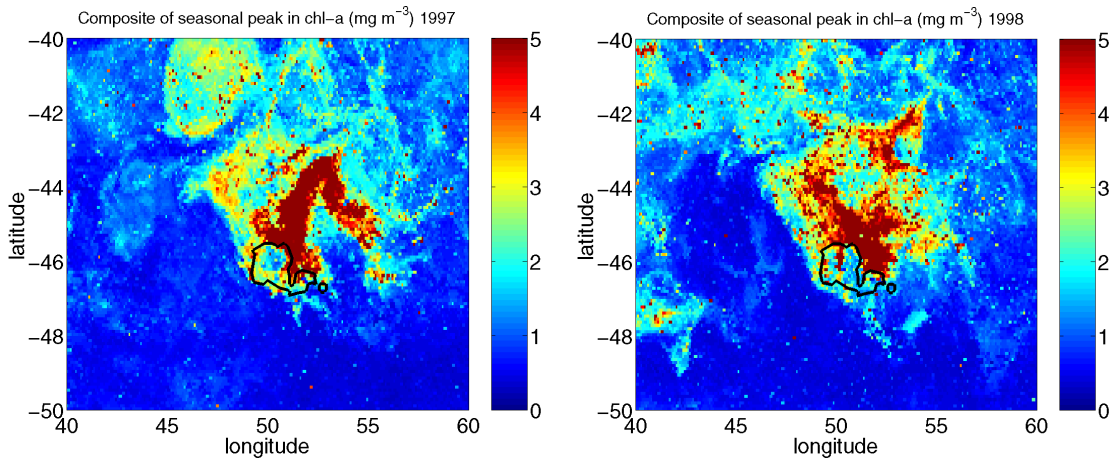

Continued on next page

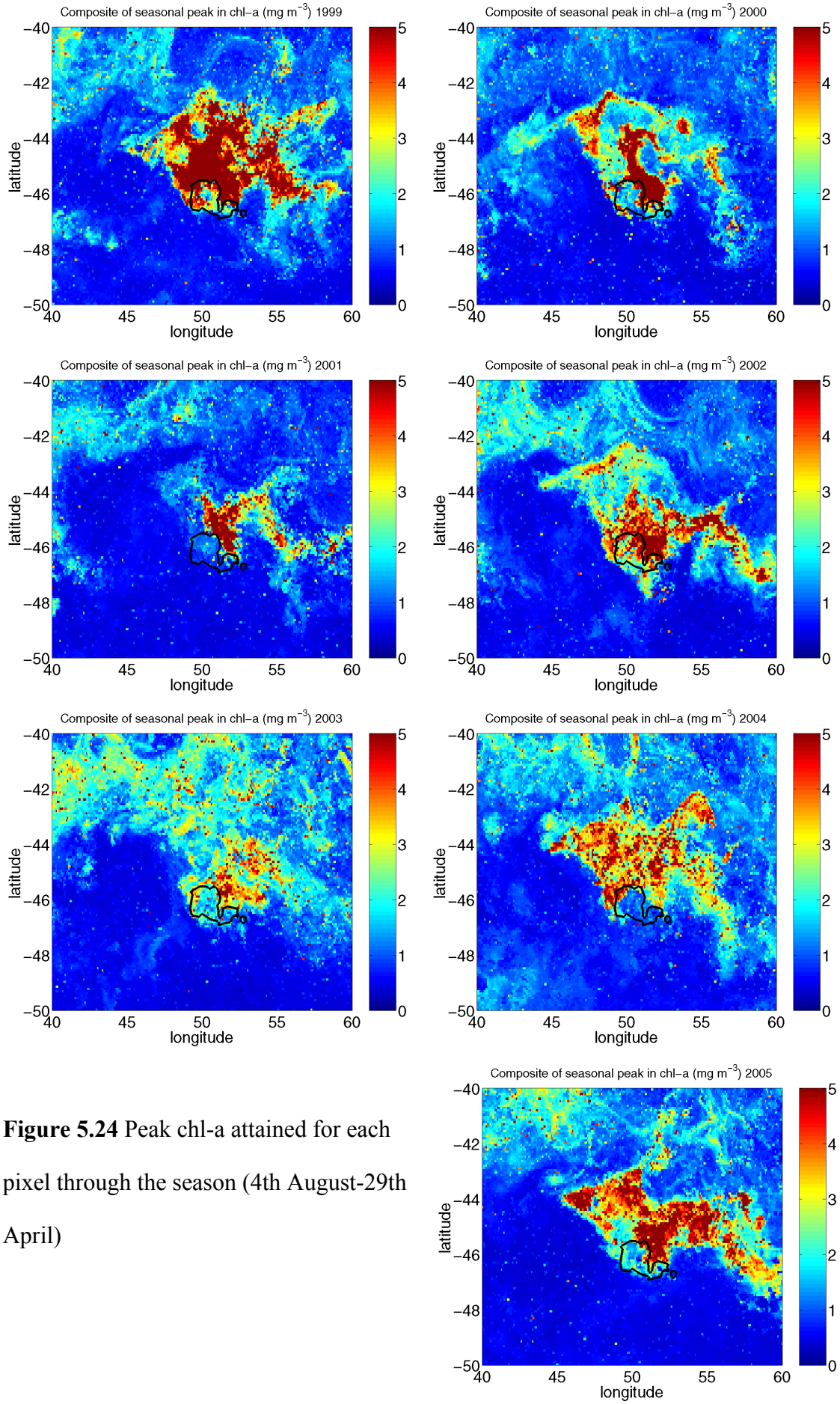

Figure 5.24 Peak chl-a attained for each pixel through the season (4th August-29th April)

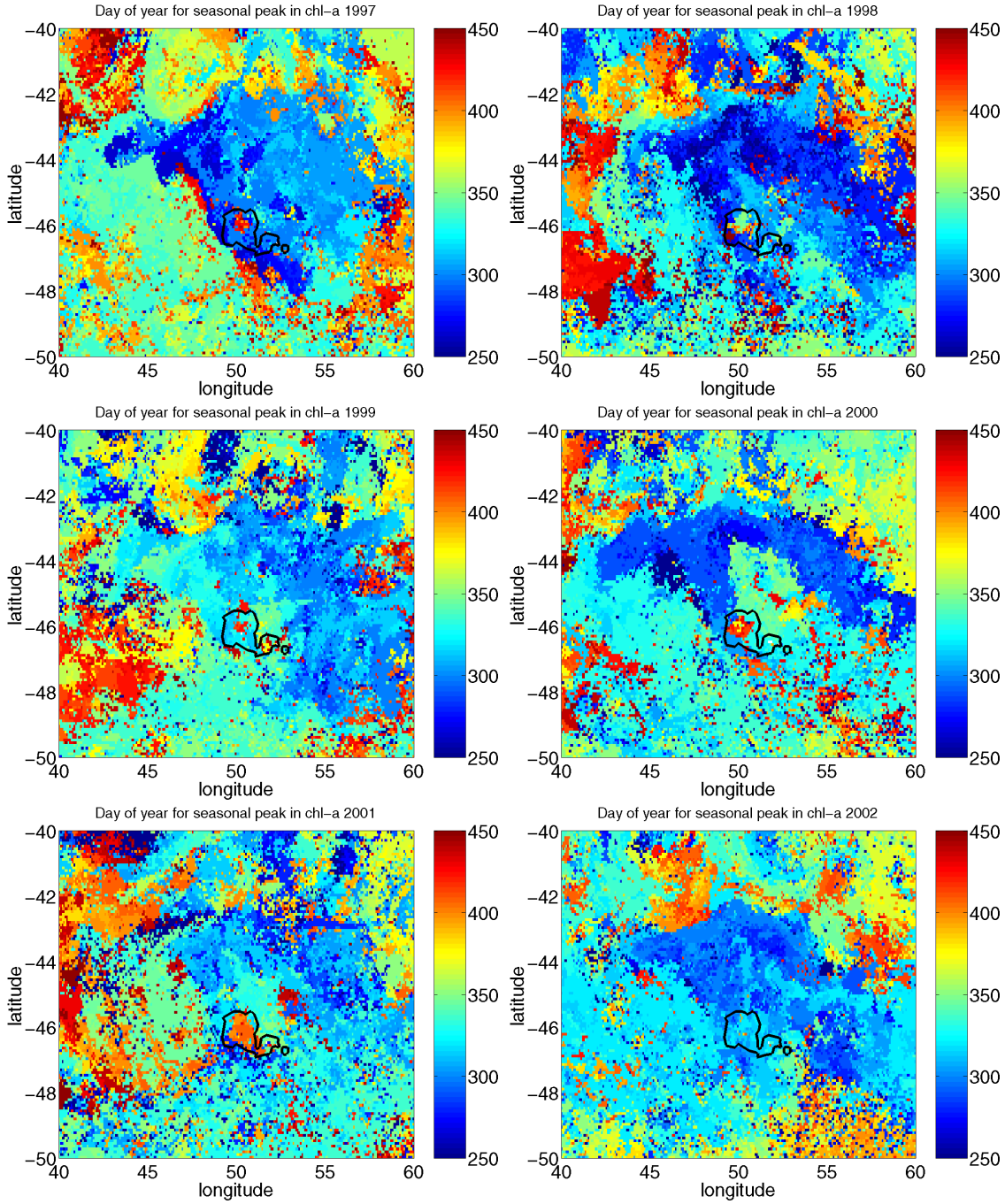

Continued on next page

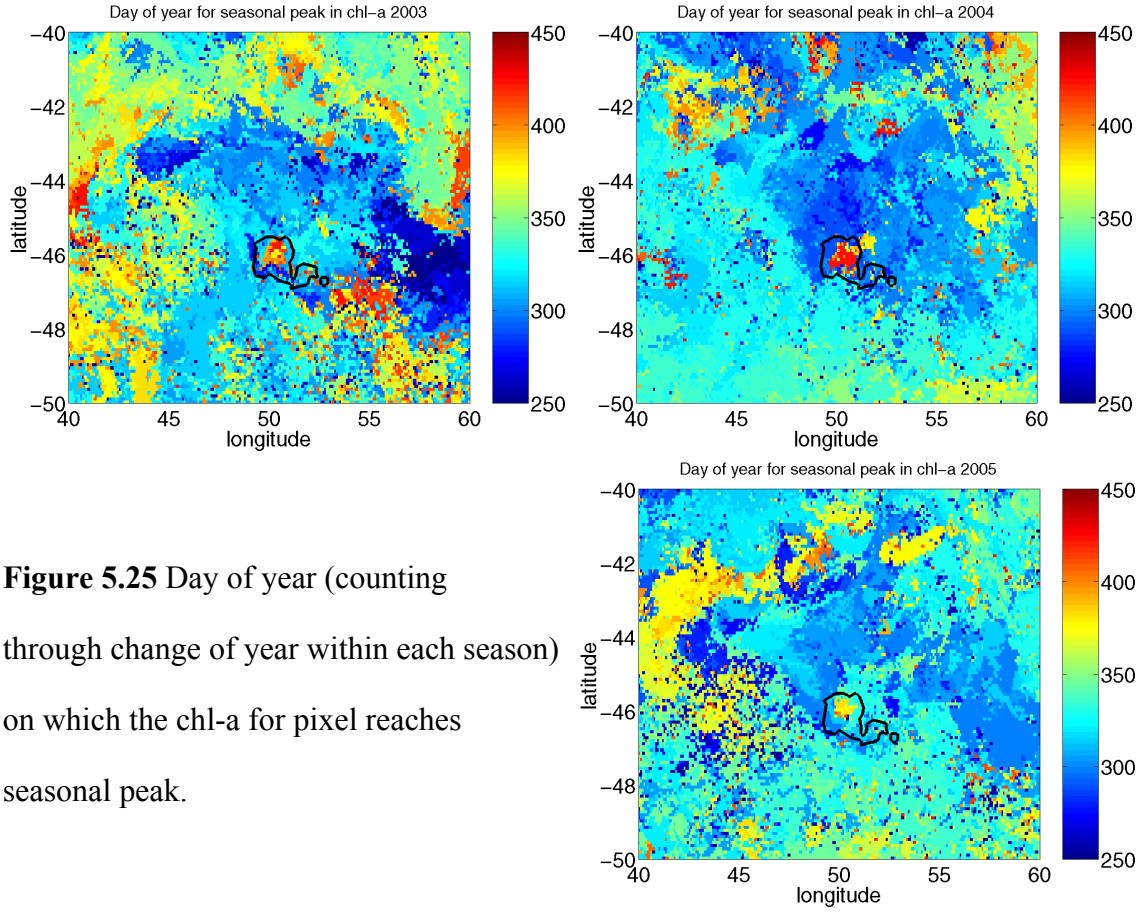

Figure 5.25 Day of year (counting through change of year within each season) on which the chl-a for pixel reaches seasonal peak.

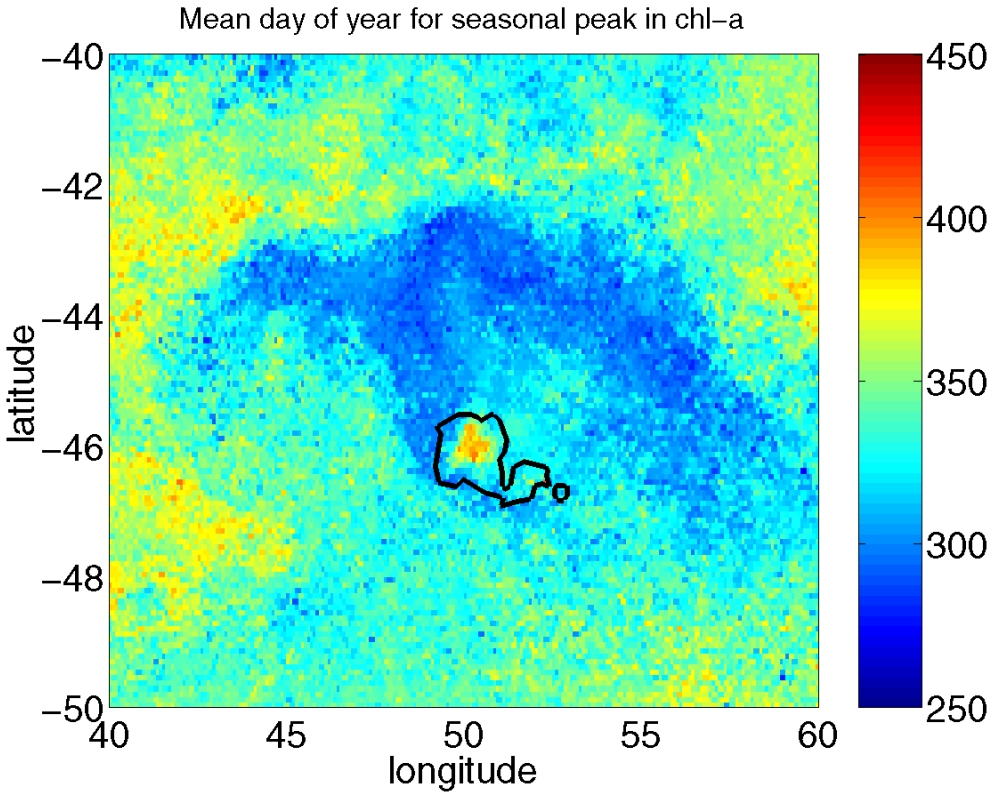

Figure 5.26 Mean of all images in Figure 5.25

Figure 5.26 shows that the peak chl-a close to the islands is attained later than the peak north of the plateau (jday 330 rather than jday 300). All the images, except that for 2002, show that the peak chl-a over the plateau occurs significantly later than elsewhere but that it is intermediate in strength between north and south of the plateau.

This spatial and temporal pattern in peak chl-a concentrations goes strongly against the results that would be expected if the peak was controlled by light availability. It has been argued above (section 4.6.1) that the chl-a decline north of the islands is due to nutrient limitation and the gradient in the magnitude of the peak is also likely to be due to the differing nutrient supply between the two main inflows into the bloom region. Water entering the area by detrainment from the NSAF, (section 3.2.6), has had little contact with the plateau so will have approximately background levels of iron (this view is supported by the very low chl-a values seen along the front) but high silicate due to its Sub-Antarctic origin. Water that has flowed around the plateau and entered the region close to the eastern islands or as Ekman flux from over the plateau will have become fertilised with iron to a greater extent. The proportion of water from detrainment from the NSAF will increase to the north and west as distance from the front decreases and distance from the plateau increases. This could create a gradient in iron, with concentrations decreasing with distance from the plateau. The numbers of a neritic zooplankton species, *Drepanopus pectinatus*, reduce with distance away from the plateau (Fielding *et al.* 2007; Pollard *et al.* 2007), supporting the concept of dilution of island influenced water away from the plateau. This gradient will be enhanced by increased biological utilisation during the longer transit period from the islands to the northern edge of the bloom, this process occurring even in winter and is discussed in section 6.3.6.

The peak chl-a being driven by iron rather than light is contrary to the findings of de Baar *et al.* (2005) where the peak of different iron enrichment experiments were driven by the light climate. The results of section 5.3 show that light availability does however control the early development of the bloom through the growth rate of phytoplankton. Table 5.3 shows that the chl-a concentrations peak earlier in the north of the bloom area, again agreeing with the concepts of iron stress causing the decline in chl-a concentrations and also that the peak chl-a is controlled by a combination of growth rate and duration of the bloom, rather than self-shading.

5.9 Summary of impact of light availability

It is clear from the analysis of section 5.3 that the gradients in light availability control the early development of the bloom north of the Crozet Plateau. There is, however, no link found between the distribution of light availability and the peak chl-a. This is contrary to the finding of de Baar et al. (2005) from synthesising the results of iron enrichment experiments. It suggests that iron is still the dominant limiting factor to productivity around the Crozet Plateau, despite the significant perturbation to prevailing Southern Ocean HNLC conditions the natural iron source causes. This is also the case around Kerguelen and South Georgia as in both areas there are periods of high light, low chl-a within the areas of the spring bloom.

Studying the results from iron enrichment experiments from this perspective, the link found between mixed layer depth and chl-a appears to be through the effect of light availability on growth rate. This interpretation is due to most experiments not being light limited at the time of peak chl-a, and the peak chl-a values not persisting, as would be expected if self-shading were the dominant cause of the limitation. This shows that enrichment experiments were also iron limited overall, as they did not reach the maximum possible chl-a concentrations. Iron availability can reduce through biological uptake, dilution and changes in iron chemistry affecting bio-availability and so become limiting shortly after a large iron release.

For over four months, the light availability to the south of the plateau is the same or greater than that found during the bloom to the north. This shows that this area is not light limited for this period and the low chl-a concentrations observed are most likely because of the circulation patterns leading to a lower iron supply. Around some Antarctic and Sub-Antarctic islands (Bouvet, Prince Edward/Marion and Macquarie) there are low chl-a concentrations but sufficient light to cause a bloom, suggesting geological (or potentially hydrological) differences between these islands and those islands that are associated, through iron supply, with large phytoplankton blooms. Over the plateau, all indications are that light availability is not significantly lower than to the south and so this area is unlikely to be light limited.

6 Variability

6.1 Time and Space – introduction

Chapters 4 and 5 describe and explain the overall location of the bloom and its time evolution. From the 9 years of SeaWiFS images, it is clear that there is significant interannual variability in the shape of the bloom, the strength of the bloom and the timing of the onset. To investigate these it is necessary to look at the key forcing factors that control each characteristic of the bloom.

The advection of iron from the islands to the east causes the bloom (this work; Planquette *et al.* 2007; Pollard *et al.* 2007). Variability in aspects of the flow are studied in section 6.2, including links to variability in the wind stress curl and the SAM index. These have important implications for the strength and shape of the bloom. Variability in the region south of the plateau is also investigated to assess how representative our sampling of the location was.

The strength of the bloom will largely be dependent on the iron concentration at the initiation of the bloom. Iron concentrations will be highest at the end of winter because light limitation reduces phytoplankton biomass and thus biological utilisation of the iron. There is, however, some enhanced chl-a during the winter and the impacts of this are investigated.

Section 5.3 has shown that the initiation of the bloom is driven by the increase of light availability brought about by reduced mixed layer depths and increased photosynthetically available radiation (PAR). The effects of the variation in wind stress and incoming irradiance on the different timings for bloom onset are covered in section 6.3.4.

6.2 Spatial variability

The factors controlling the extent of the bloom were discussed in chapter 4. The main issues are: the route of the SAF controlling the extent to the west and north, together with

water exchange between the SAF and the bloom area; the flow along the southern edge of the plateau, which follows the steep topography of the plateau around the eastern end; and the physical and biological conditions over the plateau, including how these interact with bounding circulation.

6.2.1 Conditions over and around the plateau

Figure 4.2 shows that there is interannual variability in the location of the persistent bloom that starts north of the eastern islands, Ile de la Possession and Ile de l'Est. The extremes are 1999 when it extended around the edge of the plateau to the western edge, and 2005 where it reached the north-east corner before turning strongly eastwards. In 2004 there was not a clear signal from this bloom in the seasonal composites.

Following from the argument of section 4.6.2 that the persistent bloom is caused by advection of iron away from the island, the variability in its location is most likely driven by variations in the strength of the flow around the eastern end of the islands. Variations in this flow through the winter may also affect the iron supply to the spring bloom area. A potential source of variability is strength of the closed circulation over the plateau.

It has been shown that the bottom pressure record at nearby Kerguelen (Meredith and Hughes 2004) is coherent with the Southern Annular Mode (SAM) index and the local wind stress curl. In both cases the records are in phase. Both of these are to be expected. Increased wind stress curl will cause a convergent Ekman flux over the Kerguelen Plateau because stronger, predominantly westerly, winds to the south push more water north over the plateau than the lighter winds to the north cause to flow off the plateau. This will lead to higher water levels, and hence greater bottom pressure, over the plateau until a balance is reached whereby this increased water level causes a balance between the Ekman fluxes. This increased water level will then lead to a barotropic closed circulation around the plateau.

The oceanic response, over and around the Crozet Plateau, to atmospheric forcing is therefore examined. This includes an initial assessment of the relationship between the SAM index and local wind stress and wind stress curl. The coherence between the wind stress curl and SAM index with features of the closed circulation around the plateau is

then examined. A link is expected with the dynamic height over the plateau due to the arguments of the previous paragraph. This may lead to an effect on the closed circulation around the plateau. It is also possible that the wind stress curl affects the northward flow to the east of the plateau, because the closed circulation is a component of this flow and also because the wind stress curl might have an effect on the proportion of the SSAF that turns northwards.

6.2.1.1 Atmospheric forcing

The SAM index (see section 1.2.6) measures geopotential height perturbations in the southern hemisphere south of 20°S (Figure 6.1). The structure is centred on approximately 45°S so that a positive SAM index corresponds to an increase in eastward wind stress south of 45ºS and a reduction in eastward wind stress north of 45ºS (Thompson and Wallace 2000). Therefore at or around 45ºS the effect of a positive SAM index is an increase in local wind stress curl, rather than an increase in local westerly wind stress, as it is over the majority of the Southern Ocean to the south. Figure 6.2 shows this coherence, at timescales greater than 25 days. This coherence is much stronger than that found between the SAM index and local wind stress around the Crozet Plateau (Figure 6.3). A similar coherence is therefore expected between bottom pressure and the SAM index as that found between the bottom pressure and local wind stress curl. These links between the SAM and wind stress curl explain the link between SAM index and bottom pressure around Kerguelen presented in Meredith and Hughes (2004).

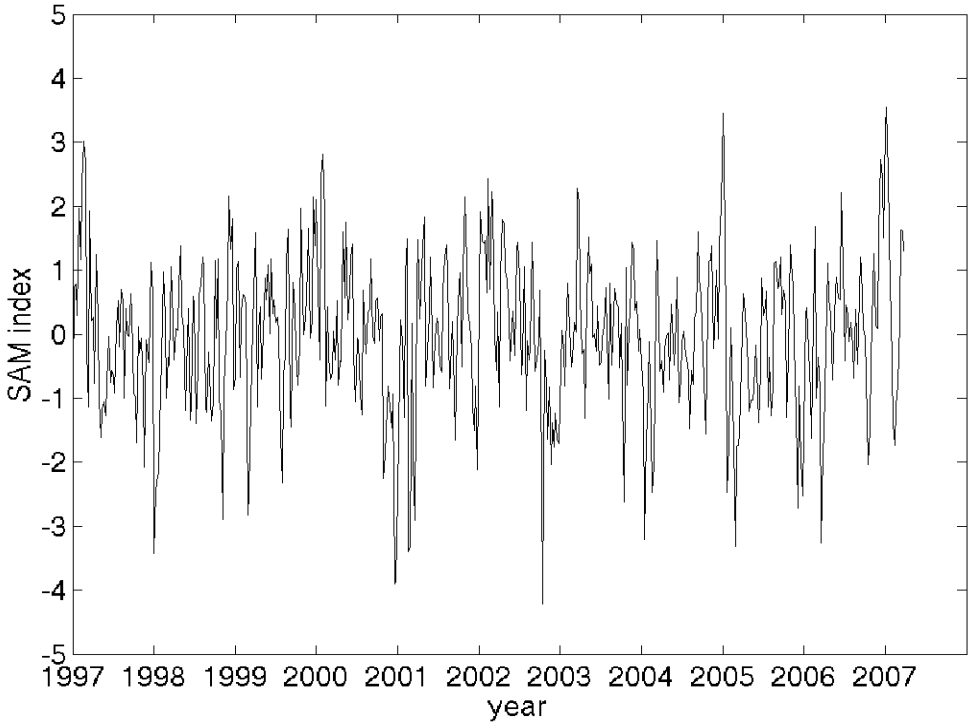

Figure 6.1 SAM index from 1997 to early 2007. The daily SAM indices were downloaded from http://www.cpc.noaa.gov/products/precip/CWlink/all_index.html.

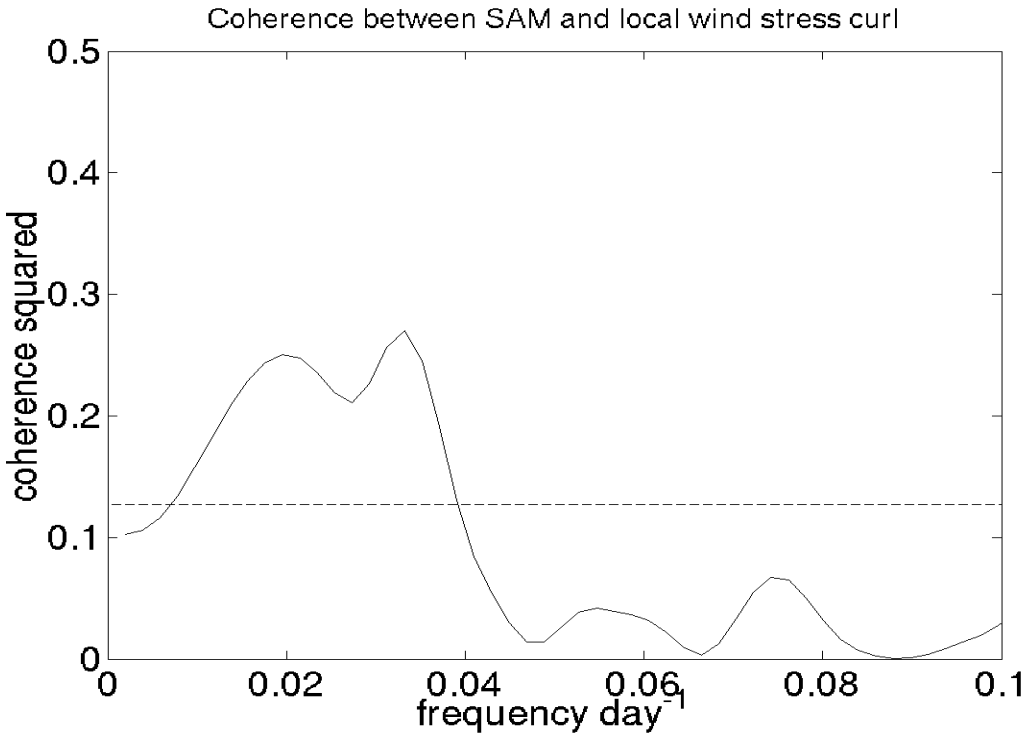

Figure 6.2 Coherence squared between the SAM index and wind stress curl around the Crozet Plateau. The 95% confidence level is shown as the dashed line.

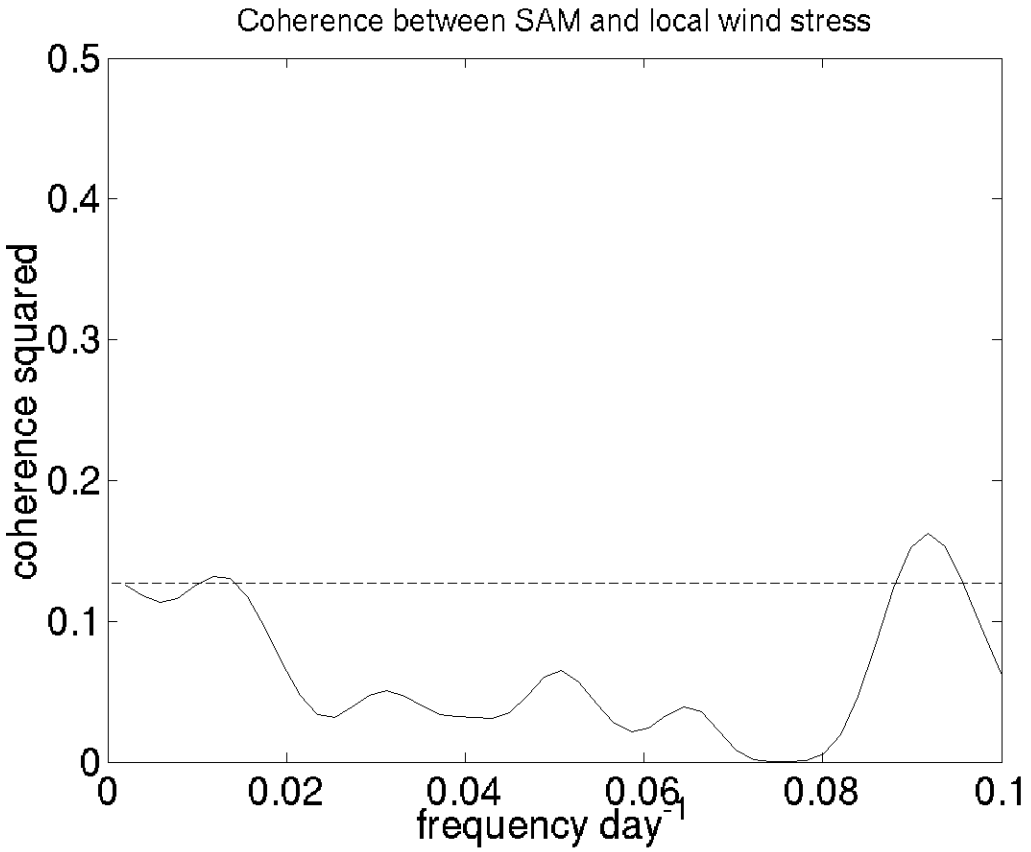

Figure 6.3 Coherence squared between wind stress north of the Crozet Plateau and the SAM index. The 95% confidence level is shown as the dashed line.

6.2.1.2 Ocean response to atmospheric forcing

Altimetry data are available every 7 days so it is possible to resolve timescales greater than 28 days. The timescales for the coherence at Kerguelen were around 100 days so this should be sufficient temporal resolution. Data are used after April 2002 because before that point there were too few altimetric satellites to properly resolve the variability of the flow around the plateau.

As was introduced in section 3.1.3, cuts were made through weekly absolute dynamic height data: an east-west cut along 45.8-46.6°S, 40-60°E and a north-south cut along 40-60°S, 50.3-51°E. The turning points were then found along these lines. For the east-west cut a maximum was found between 44.7 and 48.0ºE (this is the west side of the NSAF), a minimum between 47.0 and 50.7 ºE (this is between the northward NSAF and southward closed circulation), a maximum between 49.7 and 53.0ºE (the height over the plateau,

also east side of closed circulation and west side of flow east of plateau) and a minimum between 52.0 and 57.0ºE (the east side of the northward flow east of the plateau). The second maximum is the peak dynamic height recorded over the plateau, and the difference to the minima each side is a measure of the strength of the flow around the islands: northwards to the east, which includes a part of the southern branch of the SAF and southwards to the west, which is the closed circulation around the plateau. It is possible that there is a significant coherence between any of these time series and the local wind stress curl and the SAM index (see section 6.2.1).

The time series produced (Figures 6.4-6.6) had frequencies of 52, 26, 4 and 2 weeks removed to remove tidal and seasonal effects, although there is still a possibility of tidal aliasing due to the satellite orbit periods and deviation of spring tide periods from 14 and 28 days.

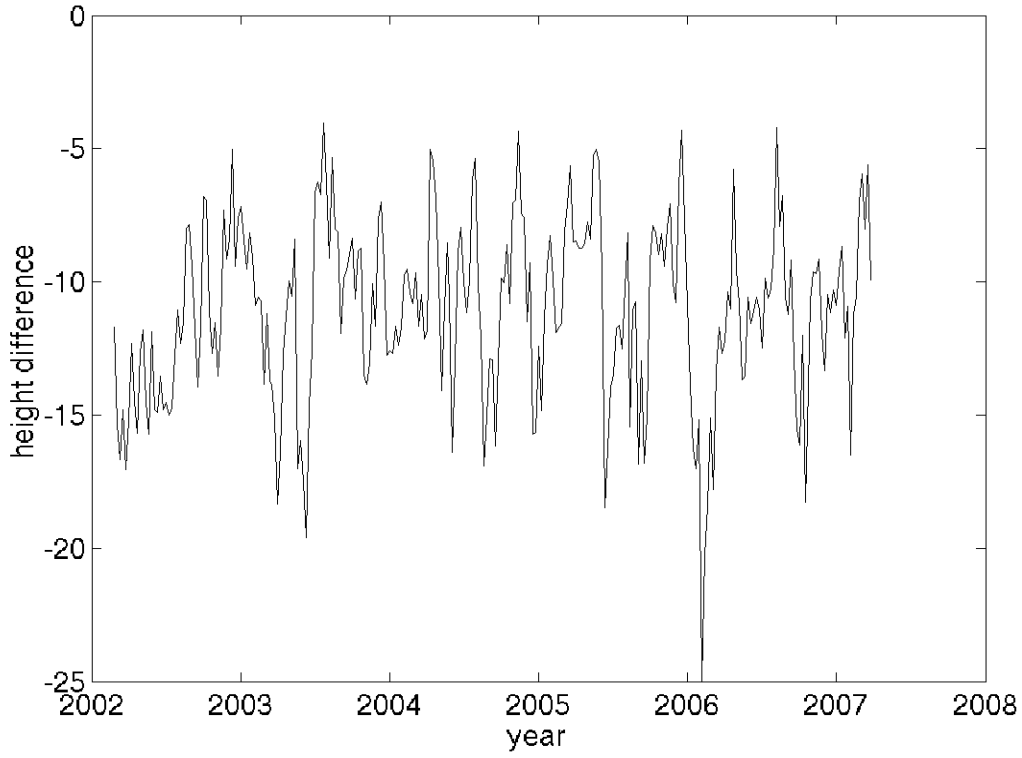

Figure 6.4 Time series of dynamic height difference west of the Crozet Plateau corresponding to the southward flow close to the plateau.

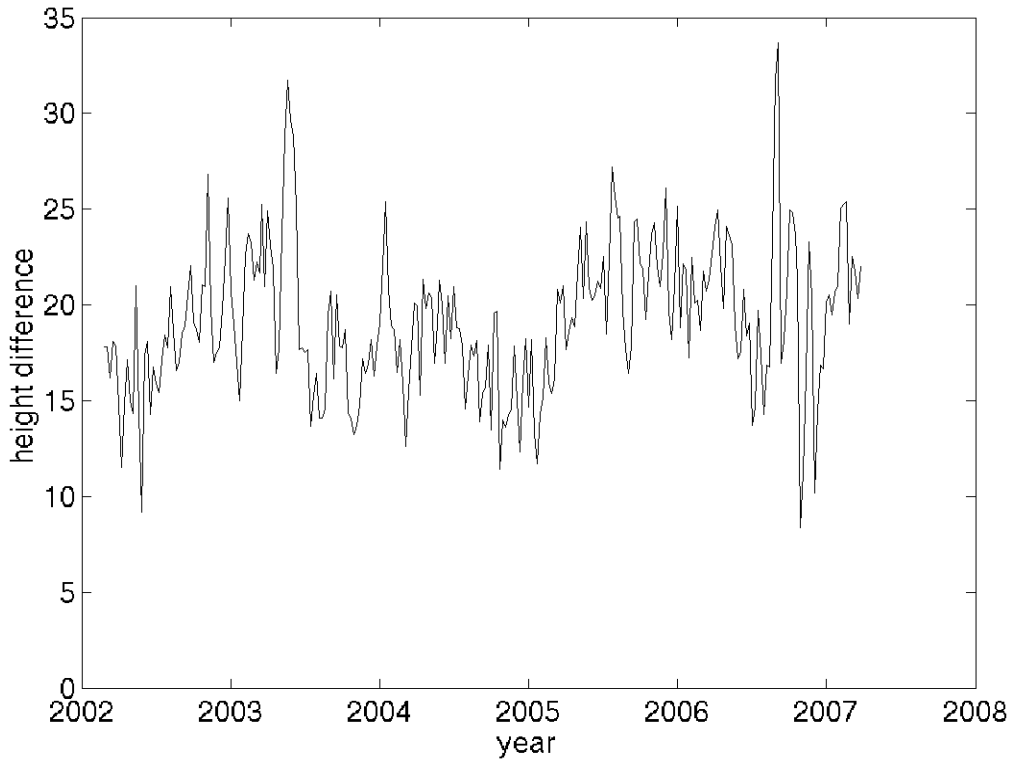

Figure 6.5 Time series of dynamic height difference east of the Crozet Plateau

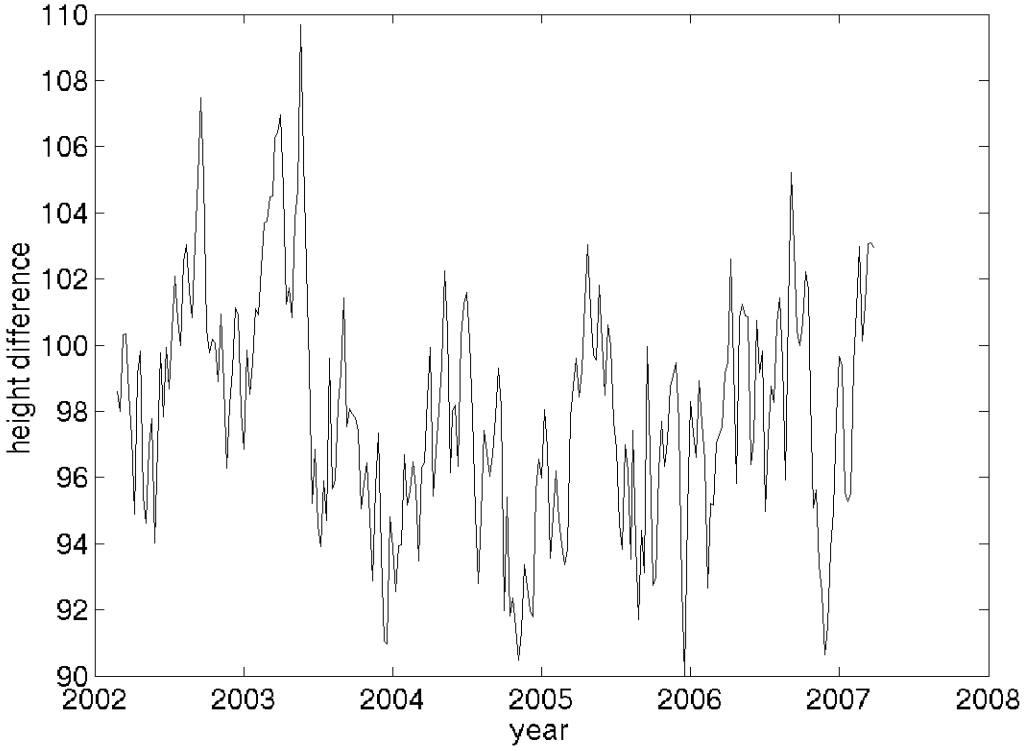

Figure 6.6 Time series of peak absolute dynamic height above the Crozet Plateau

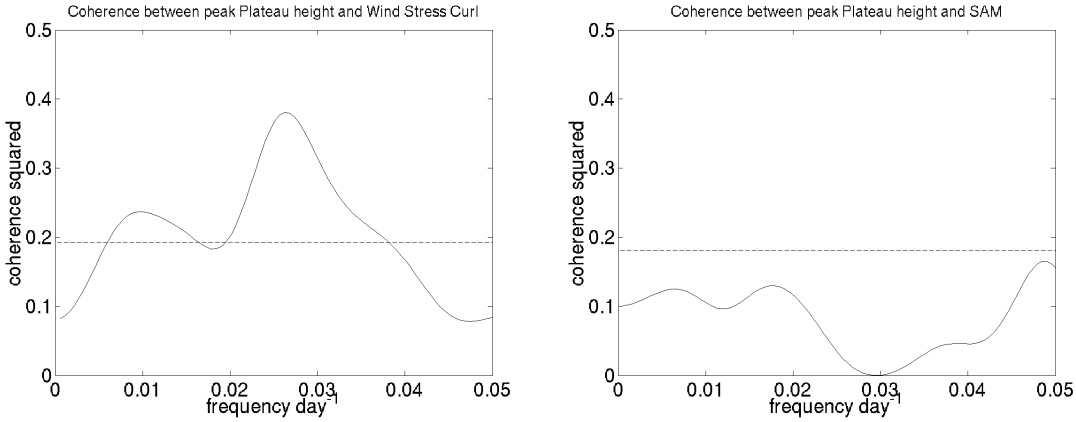

Figure 6.7 Coherence squared between the peak dynamic height over the plateau and local wind stress curl and SAM index. 95% Confidence level is shown by the dashed line.

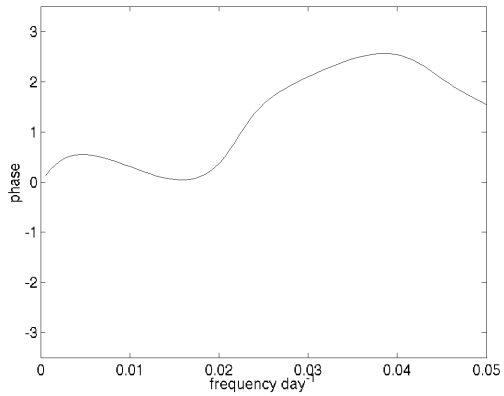

Figure 6.8 Phase (in radians) between peak plateau height and wind stress curl around the plateau.

There is a significant coherence between the local wind stress curl and the peak dynamic height over the plateau (Figure 6.7). There is however no significant coherence found between the peak dynamic height and the SAM index. There is also no link found between the dynamic height differences either side of the plateau (data not shown) and the wind stress curl or SAM index.

The coherence between the peak dynamic height and the wind stress curl is in agreement with that found over the Kerguelen Plateau (Meredith and Hughes 2004). The phase (Figure 6.8), at timescales greater than 50 days is also in agreement with that found around Kerguelen. At shorter timescales the phase changes, either reflecting a lag

between the forcing and response or because of problems close to the temporal resolution of the altimetry data. The lack of coherence with the SAM index, despite the SAM and local wind stress curl being coherent, is probably due to the sea surface height data around the Crozet Plateau being inherently noisier (data interpolated in time and space between satellite tracks) than a direct pressure record. This increased noise could result in a link with the direct forcing mechanism (local wind stress curl) being significant but the more indirect link with the SAM index, a globally averaged value, is not statistically significant. Analysis of a one-year bottom pressure record from the Crozet Plateau against NCEP zonal wind stress also shows a link to the wind stress curl (Mike Meredith, pers comm.).

There is also no link found between the wind stress curl and the closed circulation, despite the closed circulation being driven by the enhanced dynamic height over the plateau. This may be due to other aspects of the flow affecting the measure used of the closed circulation (the difference between two altimetric heights) and also the inherent increase in noise in the data due to it being derived from the difference of two datapoints.

6.2.2 Branches of SAF

As the NSAF and SSAF result from the splitting of an originally combined front, there is likely to be coherence between their relative strengths. The two fronts are clearly coherent and out of phase (Figure 6.9 and Figure 6.10), indicating that the main source of variability is from the bifurcation of the original flow, with a varying proportion of the total flow going in each direction. This variability is over timescales >200days, with Figure 6.9 indicating that this extends up to at least 4 years. It is interesting to note that the amplitude of the signal in each flow is similar (approximately 8dyn cm). It is likely that the variation is in the split of the total flow and therefore the amplitudes could be interpreted as representing this change in volume flow. The fact that the variations have similar surface amplitudes and probably similar volume anomalies suggests that the variable part of the flow has a similar depth structure in each flow, even though the mean flows appear to have different depth structures (see section 3.2.3.1).

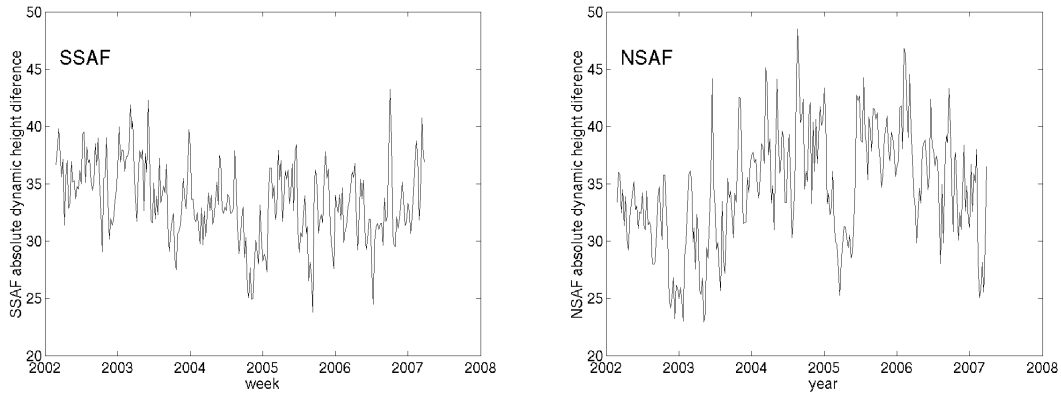

Figure 6.9 Absolute dynamic height difference across the two branches of the SAF.

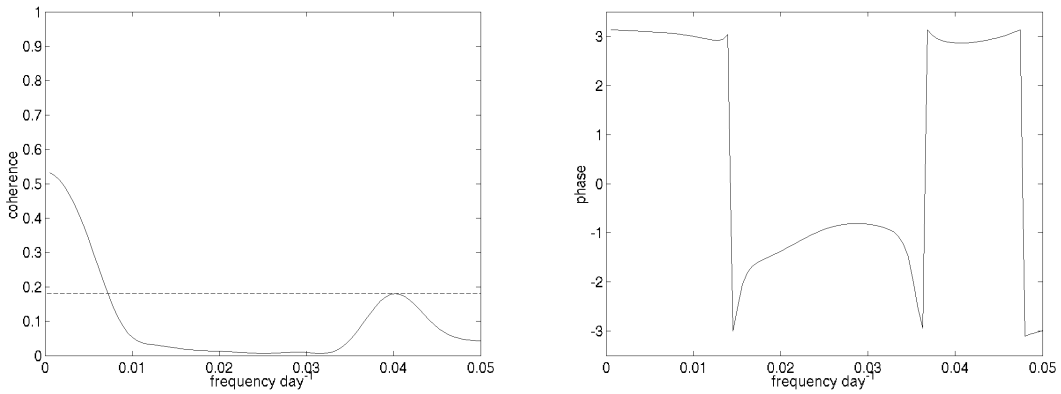

Figure 6.10 Coherence squared and phase difference between the two branches of the SAF.

The SSAF splits again at the south-eastern corner of the Crozet Plateau. Part of it turns northward, following the topography of the Crozet Plateau, with part of it continuing eastwards. This is an important flow because it is the net flow that sustains the persistent bloom through advection of iron from the eastern islands of the Crozet Plateau. Detrainment from this flow also supplies iron to the spring bloom. Figure 6.11 shows that, although there is some coherence between the strength of the northward flow and the SSAF, it is not strong. This means that the variation in the SSAF may not strongly influence inflow to the persistent bloom area. Figure 6.12 therefore presents data for the northward flow past the eastern end of the plateau.

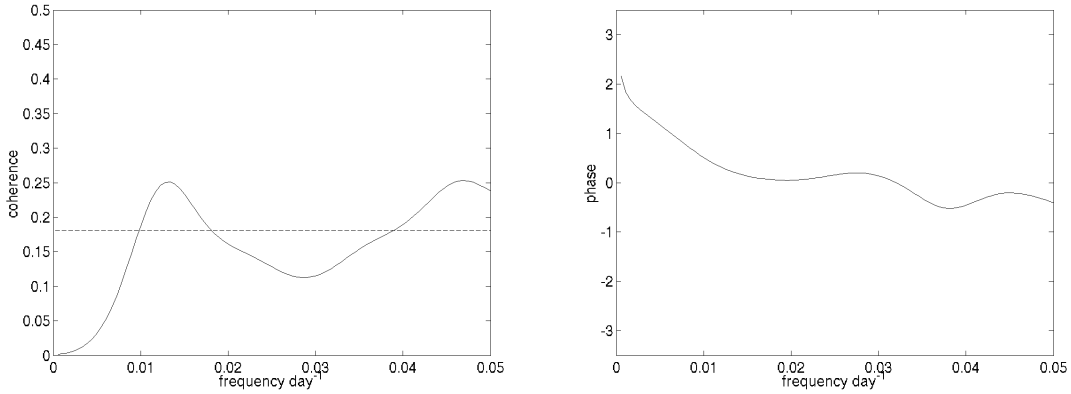

Figure 6.11 Coherence squared and phase difference between the SSAF surface geostrophic flow south of the Crozet Plateau and the northward surface geostrophic flow to the east of the Crozet Plateau.

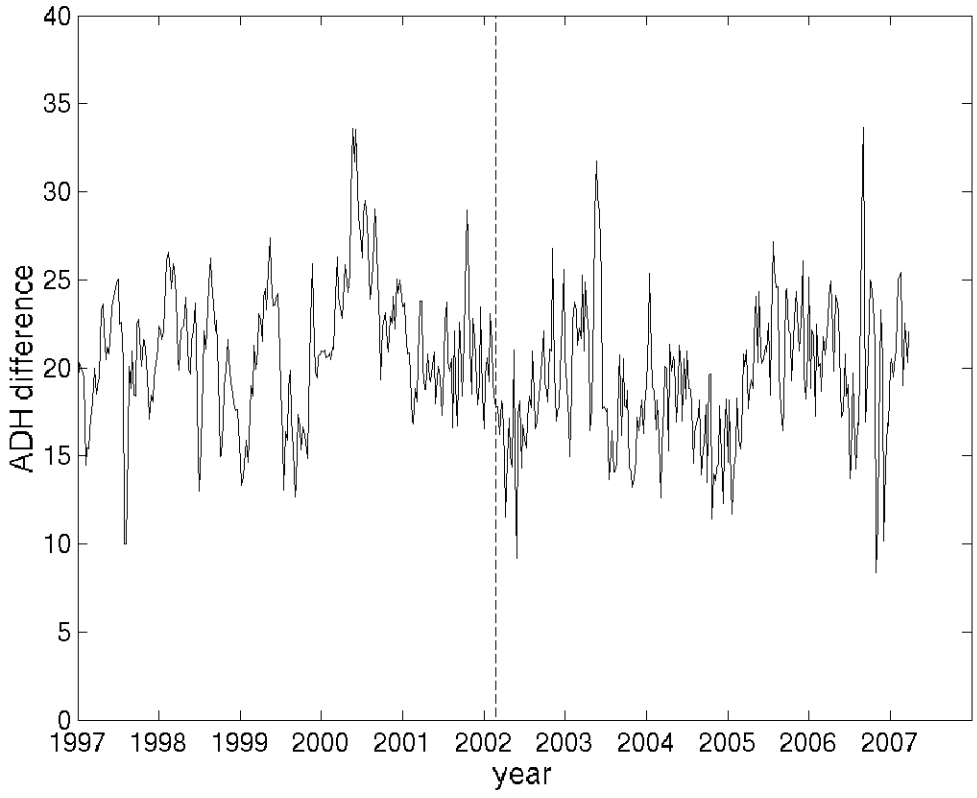

Figure 6.12 Time series of the northward surface geostrophic flow to the east of the Crozet Plateau. The vertical dashed line marks the time from when more satellite data are available so data to the left should be treated with caution.

6.2.3 Variations over the plateau

It was seen in section 4.6.3 that generally low (<1.5 mg m^{-3}) chl-a concentrations are found over the plateau, except in 2002 when levels were much higher (≈4 mg m^{-3}) and 1999 when they exceed mg m^{-3}. Good altimetry data are available from 2002, providing an opportunity to study the circumstances of the high chl-a values to try to understand the causes of the low values at other times. As discussed in section 4.6.3, the use of the word 'low' here is relative to the bloom area to the north, because *a priori* it would be expected that the area over the plateau would have a high supply of iron and therefore support a strong spring bloom.

It can be seen in Figure 6.13 that there is a break in the closed circulation, with absolute dynamic height contours crossing the northern edge of the plateau. It appears that this feature has been forced by variability to the north, because the next dynamic height contour to the north is similarly deflected south. Geostrophic flow follows dynamic height contours so this feature will act to homogenise the conditions between the plateau and the bloom area. Under normal conditions the area over the plateau is kept distinct from the bloom area to the north by the closed circulation. The area to the north-west of the plateau, the source area for water flowing on to the plateau (assuming that overall it follows the absolute dynamic topography contours), has low chl-a but to the east, where the flow is away from the plateau and islands, the chl-a concentrations are very high (4-5 mg m^{-3}). The flow could be diluting the effect of grazing on the plateau, allowing iron that is usually present to be more fully utilised. Without *in situ* data it is still not possible to draw firm conclusions on this issue.

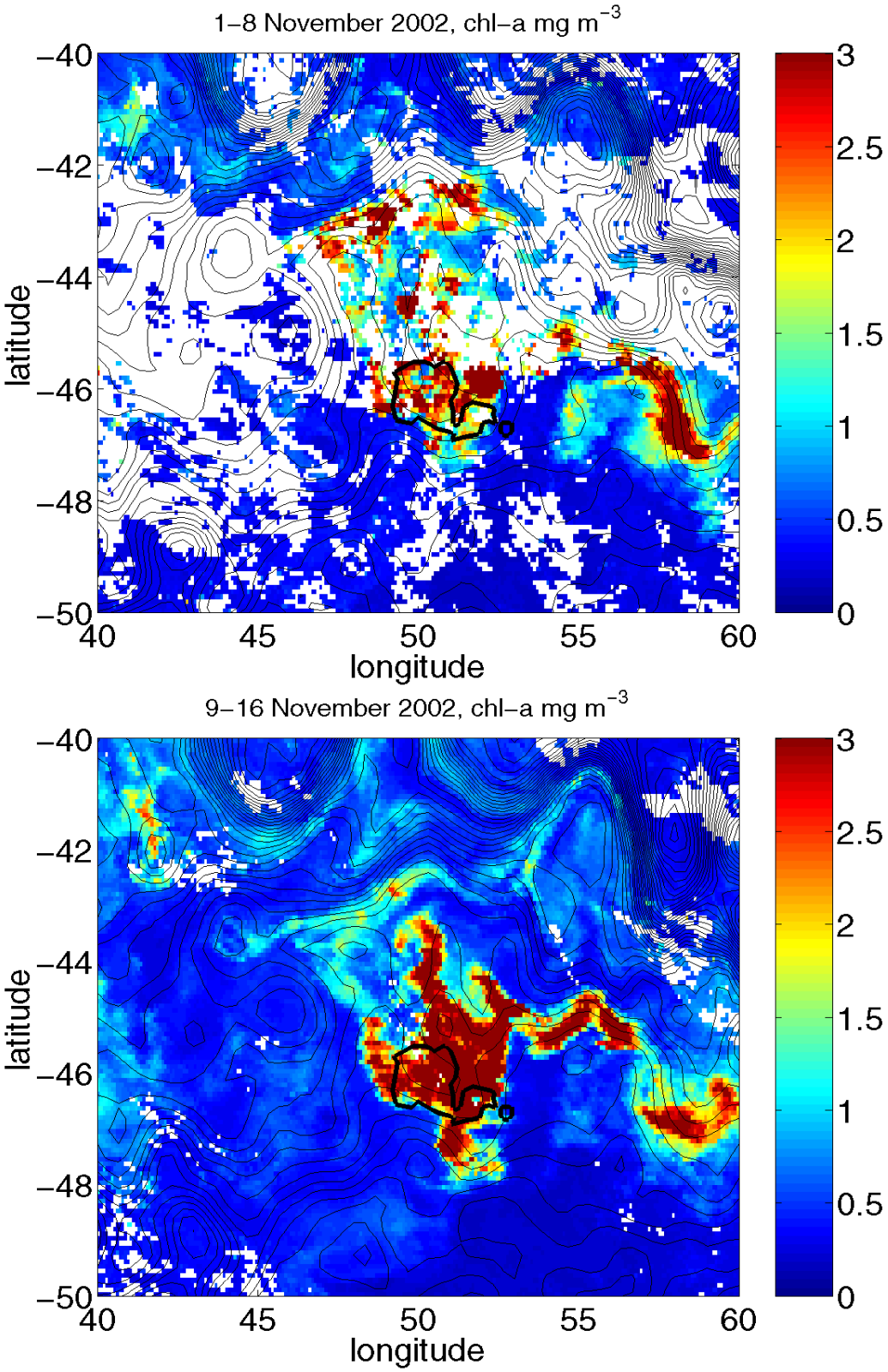

Figure 6.13 Merged SeaWiFS/MODIS images, with contours of absolute dynamic height overlain, showing the anomalously high chl-a levels over the plateau in spring 2002.

6.2.4 South of the Plateau

Figure 6.14 shows that there is some interannual variability in the chl-a levels south of the Crozet Plateau. This area is important to the CROZEX sampling strategy because it was used as a HNLC control area upstream of the influence of the Crozet Plateau. As can be seen in Figure 6.14, the sampling in 2004 (21-23/11/04 3-5/1/05) occurred during a period of unusually high chl-a concentrations.

There are two possible causes for the high values observed: either a change in the flow pattern bringing more productive waters to the area, or a change in the productivity of the water present. These two can be tested through a combination of absolute dynamic height and ocean colour data. Figure 6.14b shows that there are higher chl-a concentrations to the south of our southern sampling location in most years so a northward shift in the flow may contribute to the shift in late 1999, 2002 and 2004 to higher chl-a concentrations.

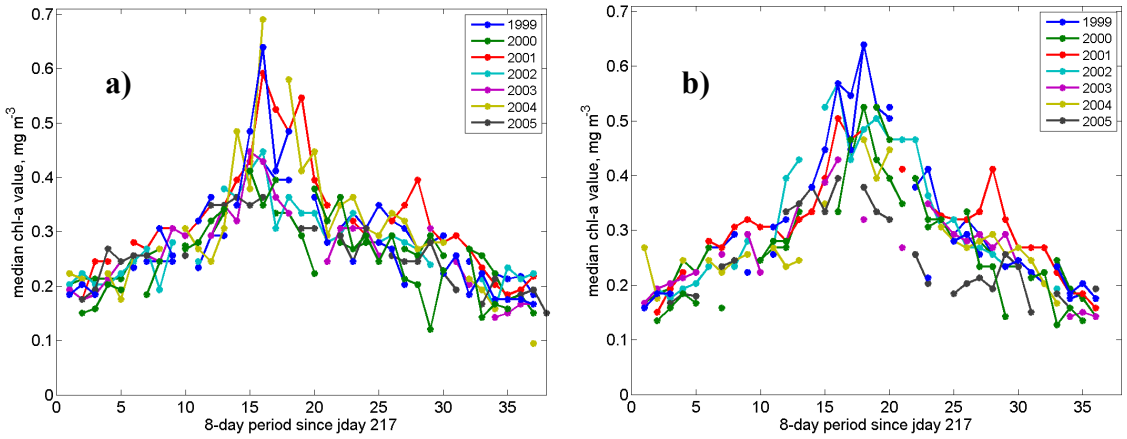

Figure 6.14 Chl-a south of the plateau, a) 48-50°S, b) 50-52°S

Figure 6.15 however shows that there are not northward shifts at these times in dynamic height contours so these changes appear to be due to changes in productivity within the water masses, although the driving force for these shifts is not known. This is supported by Figure 6.16, which shows strongly enhanced chl-a concentrations upstream of the study area in 2004 (note, though, the low colourbar limit). The cause of this change in surface chl-a is not clear. Shallower mixed layer depths may help to enhance the chl-a, although it was shown in section 5.6.1 that the area was not light limited. Increased iron supply during the preceding winter may also cause a similar change.

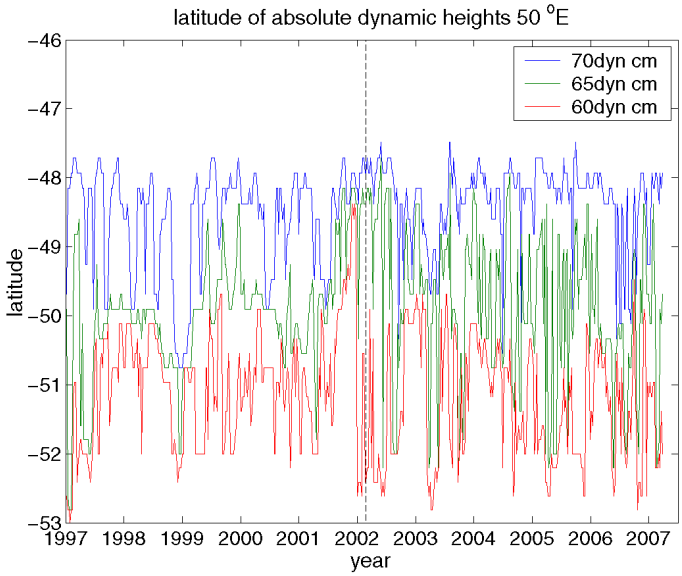

Figure 6.15 Latitudes of three dynamic heights that pass close to 49°S. Data are not necessarily reliable before the dashed line.

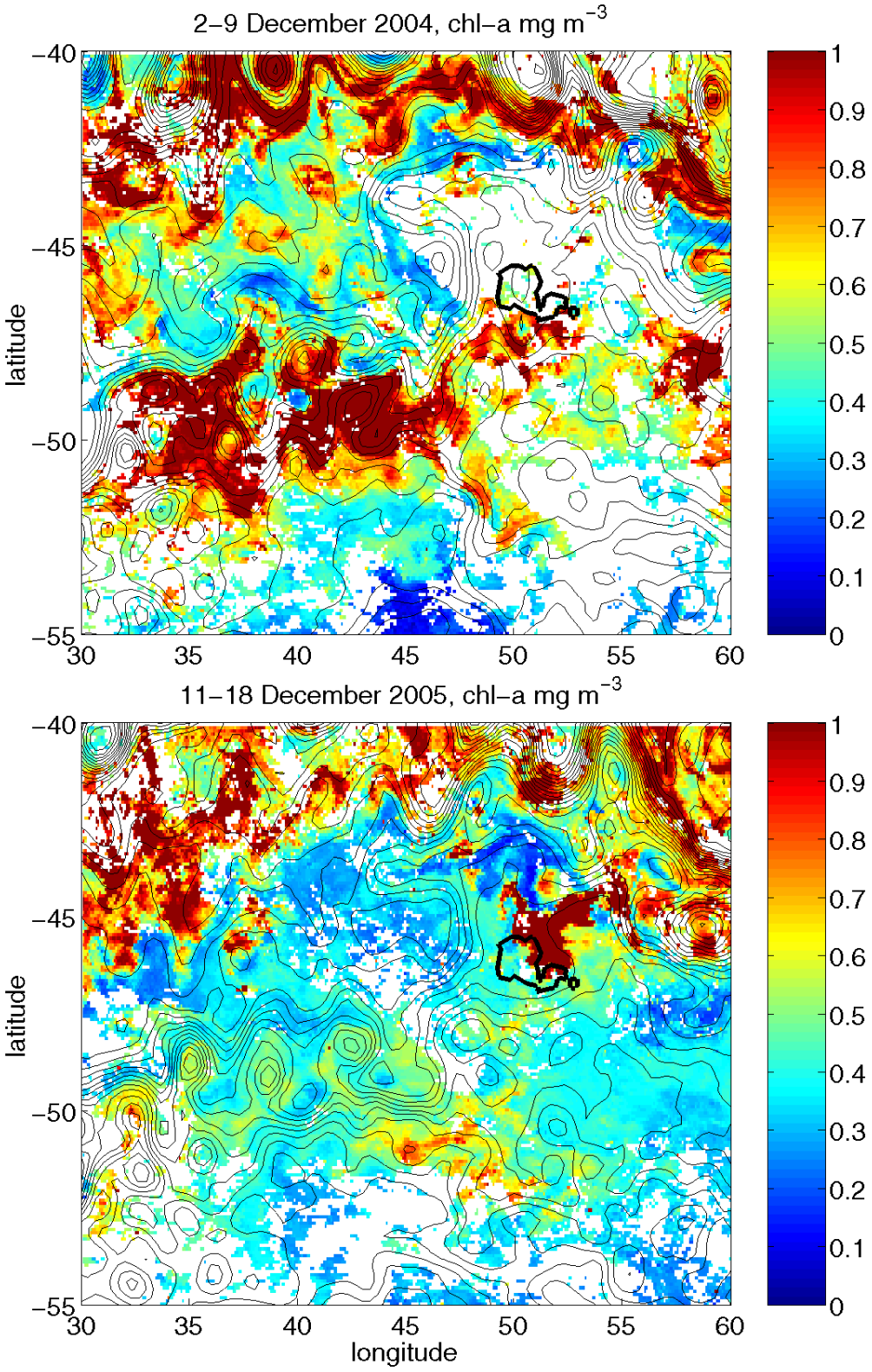

Figure 6.16 Large area (and low colourbar limit) SeaWiFS image for peak chl-a south of the plateau in 2004 and 2005 with overlain absolute dynamic height contours.

6.3 Interannual variability

The first part of this section uses the average strength of the spring bloom in 43-45.5°S, 49-52°E, 4th August - 8th January as a proxy for the initial iron concentrations. This relates to boxes A-C from section 4.5. Box D is treated separately as the persistent bloom, close to the eastern islands.

The section looks at factors that could influence the strength and timing of the spring bloom over interannual timescales. After investigating these factors, conditions during anomalous periods – early spring 2005, winter 2000 and the plateau in 2002 – are investigated in light of the overall findings.

6.3.1 Effects of winter iron utilisation

In section 5.6.1 it was shown that the bloom area was consistently light limited over the winter period. This result however comes from Argo float profiles and so the data are only from 2003-2006, with most data from 2004-2006. Figure 4.5 shows that these years showed very low chl-a during the corresponding period, agreeing with strong light limitation. Earlier years, 2000 in particular (the end of the 1999 plot), show enhanced chl-a during the winter. This shows that in these years there were periods where the area was not totally light limited. This therefore means that some of the iron being advected into the bloom area is being used during the winter and so it is likely that the standing stock at the end of winter will be reduced.

This possibility can be tested by comparing the time averaged chl-a concentrations during the spring bloom period (4th August-8th January, Boxes B-D) with the average concentrations from the same area from the preceding winter period (9th May-3rd August) and the summer periods either side (9th January-8th May). The winter period is chosen to approximately reflect the light limited period found in section 5.6.1. It is interesting to note that the Crozet area is the only area of the Southern Ocean where this comparison can be made because satellite chl-a values are not available south of 46°S for a period during the winter, due to the relationship between the orbit of the SeaWiFS satellite and the tilt of the Earth. Other areas of the Southern Ocean, specifically Kerguelen and South Georgia, are too far south for there to be winter satellite data.

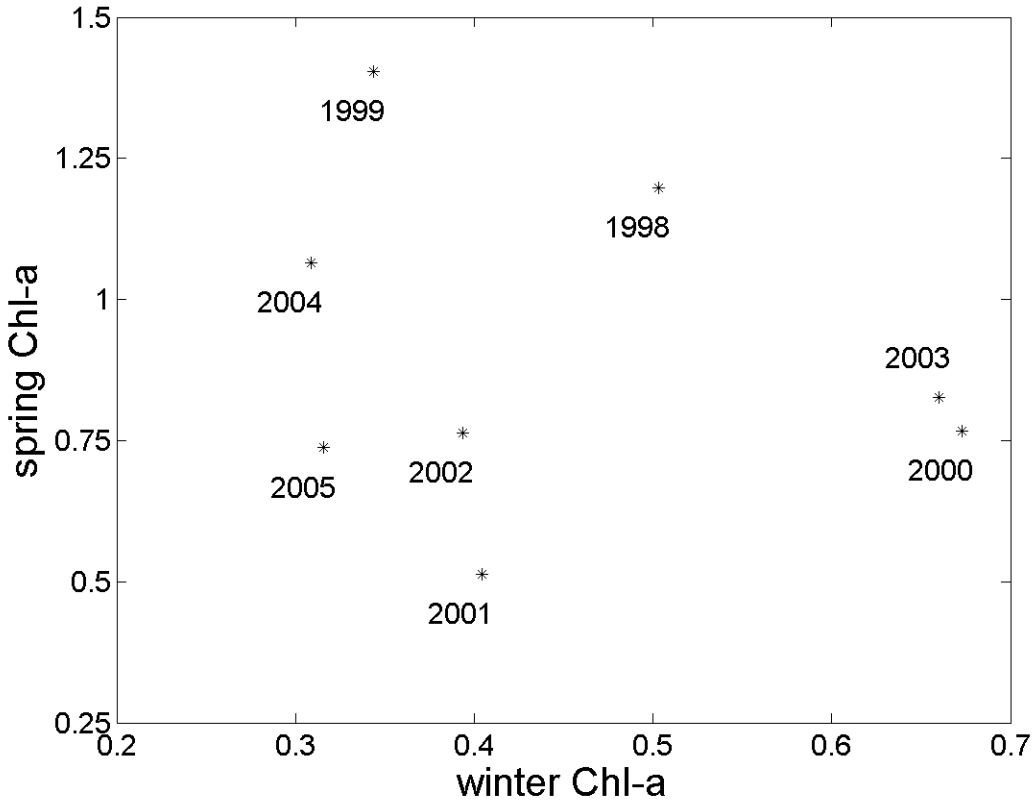

Figure 6.17 Time averaged chl-a concentrations over the spring bloom plotted against the time averaged chl-a from the preceding winter period.

Figure 6.17 suggests that there is a relationship between the spring average chl-a concentrations and those from the preceding winter, supporting the idea that one of the controls on the standing stock of iron at the beginning of the spring bloom is the amount of growth during the winter period. The r^2 value is low, 0.12, when winter chl-a is considered alone, but with winter wind stress curl there is a strong link with spring chl-a, r^2=0.88, see section 6.3.3.

Figure 6.18 shows that there is a significant link between the strength of the spring bloom and the chl-a levels in the following summer: $Chl_{summer}=0.23(\pm0.14)Chl_{Spring}+0.25(\pm0.15)$. It is likely that the link with the following summer is, at least in part, linked to the recycling of iron in the surface waters after the spring bloom and transport (by mixing and mesoscale motions) of iron from below the mixed layer – a stronger spring bloom indicating that there is more iron in the system that year. Figure 6.19 shows that there is a similar, but weaker relationship in the more dynamically active persistent bloom area,

suggesting some inter-seasonal consistency in the resupply of iron. However, the link in the spring bloom being stronger (r^2=0.69 for spring bloom, r^2=0.52 for persistent bloom) suggests that there is little inflow of iron to the spring bloom region during the summer period because variability in any such inflow would likely reduce the strength of the relationship. There is no significant relationship between the amount of chl-a in the spring-bloom area in summer and the amount in the persistent bloom area at the same time, supporting the view that there is not a strong connection between the two areas in summer.

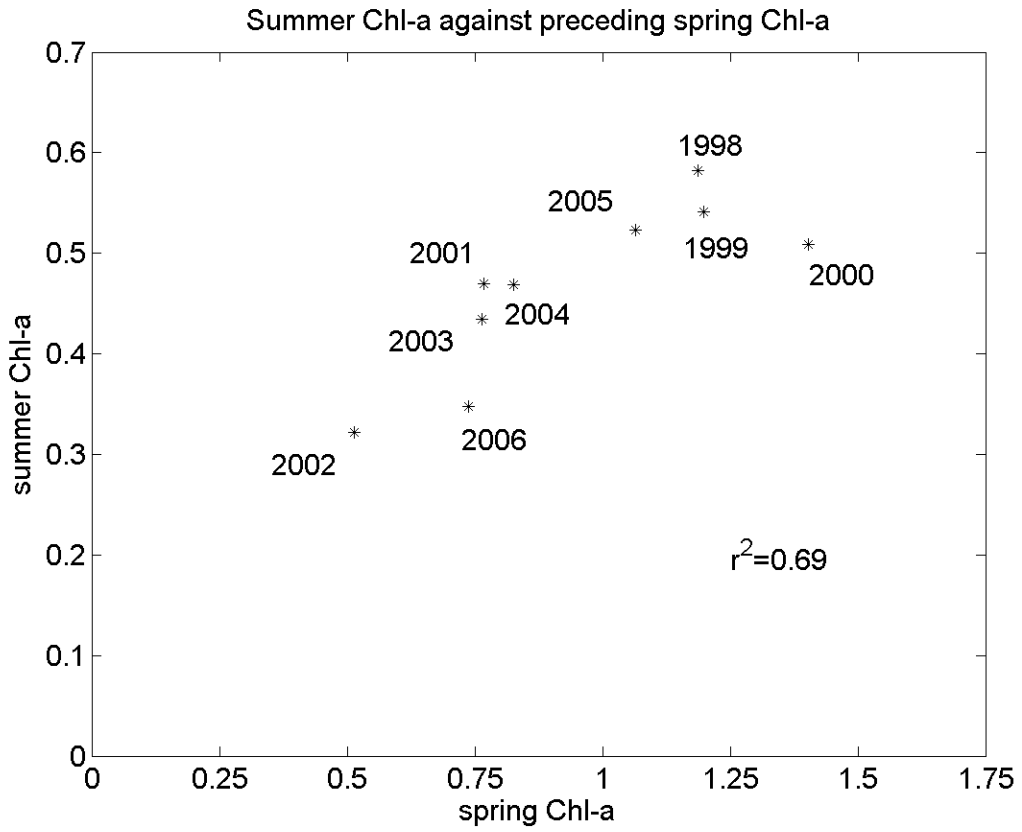

Figure 6.18 Links between the strength of the spring bloom in the 'spring bloom area' and the chl-a in the same area the following summer period (years are for summer rather than spring).

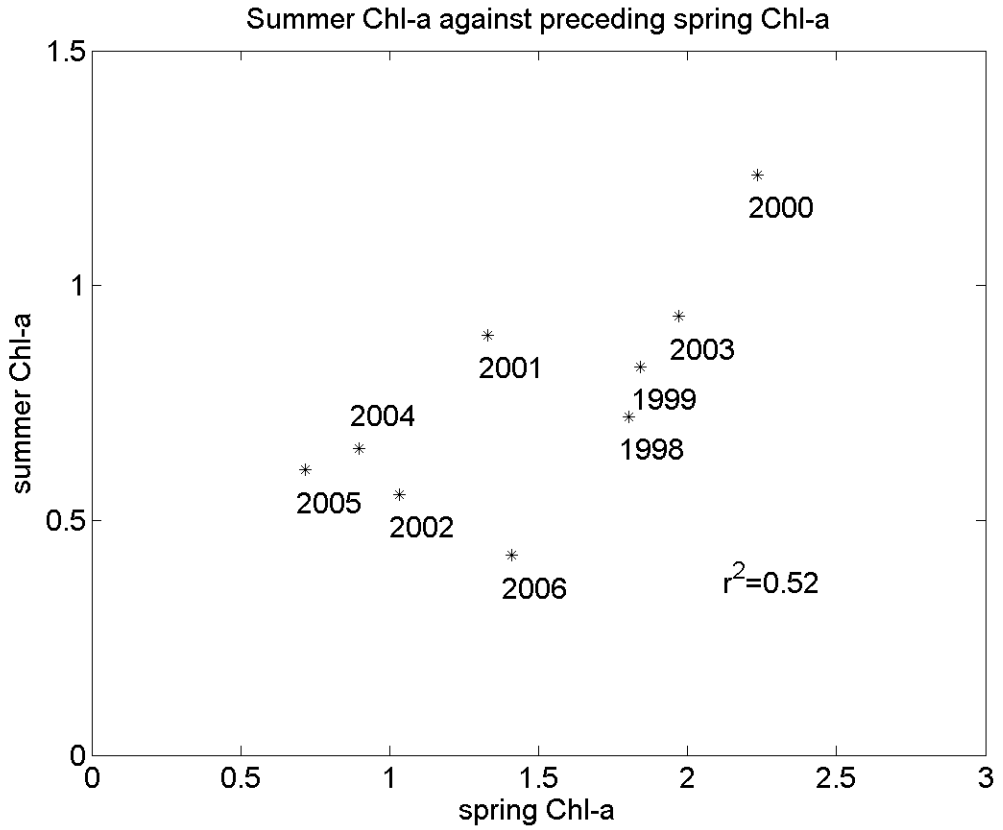

Figure 6.19 Links between the strength of the spring bloom in the 'persistent bloom area' and the chl-a in the same area the following summer period (years are for summer rather than spring).

6.3.2 Biological response to wind stress curl

It has been shown that the wind stress curl affects the dynamics around the plateau, in such a way that the wind stress curl causes the anticyclonic circulation around the plateau. This circulation advects iron from the identified source of the eastern islands to the spring bloom area to the west. A link is therefore possible between the wind stress curl during the preceding winter and the iron concentration in the spring bloom area, with higher wind stress expected to result in higher initial iron concentrations.

Figure 6.20 shows that there is considerable variability in the wind stress curl, over periods that could significantly influence the supply of iron to the bloom area. Figure 6.21 shows that there is a strong link between the winter wind stress curl and spring chl-a. This link is analysed using multiple regression, along with the effects of winter chl-a, in section 6.3.3, where it is shown to be statistically significant.

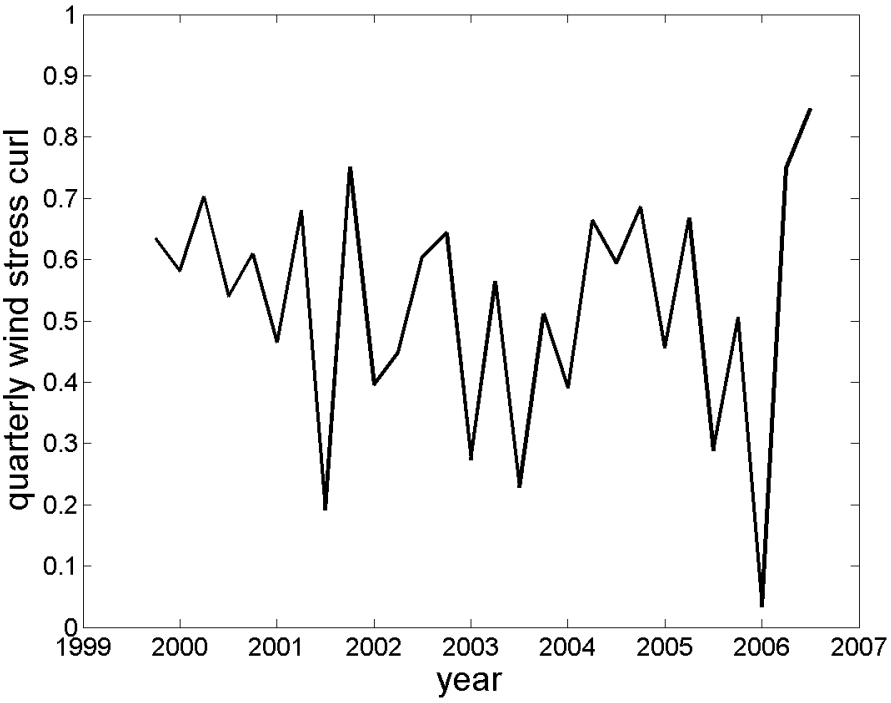

Figure 6.20 3-month averages of wind stress curl around the Crozet Plateau

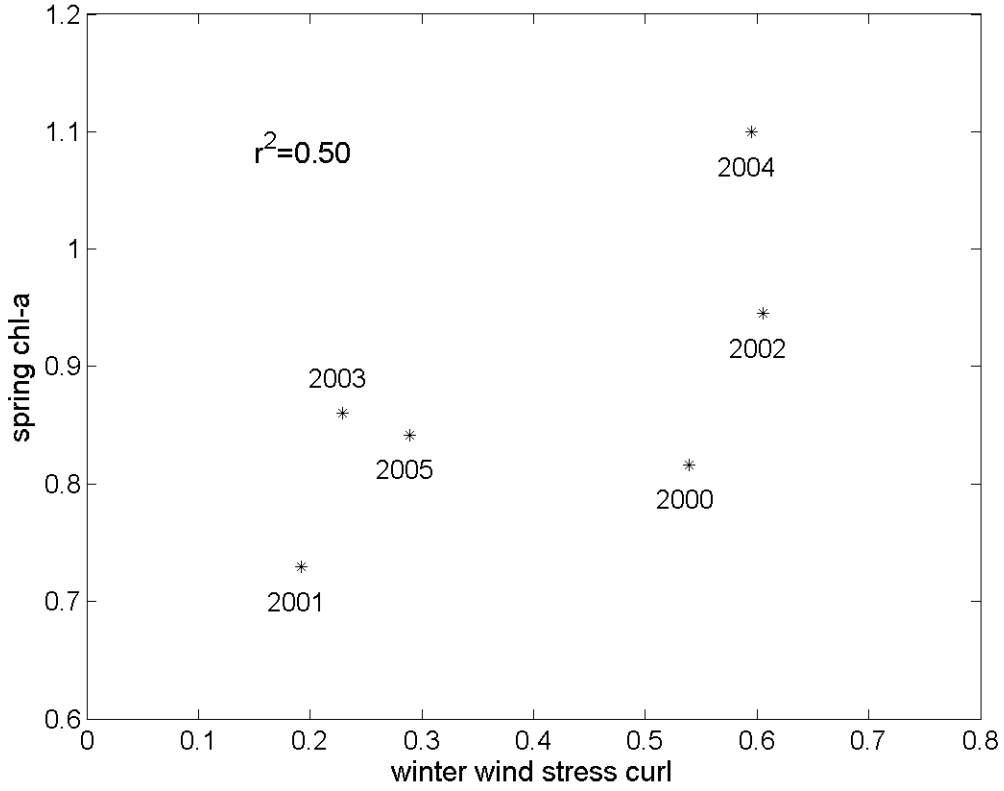

Figure 6.21 Spring chl-a in the spring bloom area against the wind stress curl the preceding winter.

6.3.3 Multiple regression of bloom strength factors

Multiple regression has been used to analyse the effects of winter wind stress curl and winter chl-a on integrated spring chl-a concentrations. There are reasons why these variables may potentially be dependent (e.g. high wind stress curl being caused by light winds north of the plateau, which in turn allows sufficient stratification for winter growth) but empirically they are independent and are treated as such. It is expected that increased winter chl-a will lead to a lower iron concentration at the end of winter and therefore lower spring chl-a whereas increased wind stress curl should lead to a stronger anticyclonic flow around the Crozet Plateau and therefore increased iron supply and higher spring chl-a.

Statistically significant (95% confidence interval for gradient not including 0) relationships are found between integrated spring bloom strength and both wind stress curl (WSC) and chl-a concentrations during the preceding winter period (Chl_W):

$$Chl_S = 0.86(\pm 0.15) + 0.59(\pm 0.43) \times WSC - 0.46(\pm 0.45) Chl_W \quad r^2 = 0.88 \qquad \textbf{6-1}$$

These significant relationships, together with signs of the relationships agreeing with the hypotheses, show that these two factors are important in explaining the interannual variability in the bloom strength. The high r^2 value also implies that between them they explain most of the observed variance in the spring bloom strength. It is interesting to note that the constant in the relationship is higher than the chl-a values observed south of the Crozet Plateau (0.25-0.35 mg m^{-3} averaged over the same period). This indicates that there are supply routes other than flow caused by the wind stress curl. These will include the net flow around the islands forced purely by the steep topography and northward Ekman flux away from the plateau. These may also contribute to the variability, but the factors considered explain the majority of the observed variability.

6.3.4 Variation in initiation of bloom

The initiation of the annual bloom has been described in section 4.7 and explained in section 5.3. The data presented there show that there are variations in the timing of the blooms between years and its spatial development. Due to the low spatial resolution of

the Argo floats and the fact that only since 2004 have there been a significant number of floats in the area, it is not possible to repeat the analysis for an individual year. It is also not possible to model the mixed layer for the period in question because data for some of the heat and freshwater fluxes are not available at the necessary spatial resolution, and possibly quality; global re-analysis products have to be interpreted with caution in areas such as around Crozet where there are few *in situ* observations and strong spatial gradients in the conditions due to the location close to the edge of the Southern Ocean. Mixed layer depth models are also semi-empirical so need a good data set to be tuned against (Chen and Rothstein 1994). There is not a high resolution data set in any location to ground truth the output and the sensitivity it shows to the input forcings.

Instead it is necessary to look at the key forcings of the mixed layer: wind stress and incoming insolation. Good data for these goes back to 1999 (QUIKSCAT wind stress) and 1997 (SeaWiFS PAR) respectively.

There is a benefit in this approach in that the phytoplankton will respond to upper layer stability before an actual mixed layer forms – if they are not mixed vertically in the mixed layer then the theories relating mixed layer to average light received by phytoplankton break down (Huisman *et al.* 1999).

6.3.4.1 Definition of initiation

As the effects of wind stress and insolation are being studied directly through the chl-a response it is necessary to define what is deemed to be the initiation of the bloom. If the mixed layer is considered purely as a step function, that goes immediately from deeper than the critical depth to shallower, then the chl-a should be at a background level before the step, and increase approximately exponentially afterwards. The increase will differ significantly from exponential at high chl-a levels when self-shading is significant, but in the early stages this is not a significant effect (see section 5.3). For the following study, the initiation is taken as the last 8-day period before a continual increase in chl-a concentration to greater than 1mg m^{-3}.

The period when the increase is most likely to have started is between the mid-point of the 8-day period identified by the above criteria to the midpoint of the following period

because earlier than this the increase is likely to be seen in the identified period (which, by construction must represent a fall in chl-a) and later than this it is unlikely to be seen in the following 8-day period (which equally by construction must represent an increase). These 8-day periods, shifted forward 4 days relative to the chl-a periods, are therefore used when studying the effects of wind stress and PAR.

6.3.4.2 Initiation dates

The initiation dates, following the definition in section 6.3.4.1 are shown in Table 6.1.

Year	Initiation	1 mg m^{-3}
1997	n/a (before data)	269
1998	n/a (cloud)	245
1999	269	285
2000	237	277
2001	269	317
2002	253	285
2003	253	285
2004	229	277
2005	229	293

Table 6.1 Day of year for the initiation of the bloom and for the chl-a to reach 1 mg m^{-3}

It is possible that higher iron concentrations at the beginning of the bloom may increase the ability of phytoplankton to acclimatise to low light, allowing them to respond earlier to increasing light availability.

It is likely that if stratification occurs early then the light level following the event will be lower than after a later stratification. This is because PAR is likely to be lower and also the mixed layer may be deeper. This means that the phytoplankton will have greater iron demands and possibly consume a significant amount of iron (Sunda and Huntsman 1997).

Figure 6.22 shows that there is no link between the date of the bloom initiation and the overall strength of the spring bloom (used as a proxy for the initial iron). It suggests a

link between the date the bloom reaches 1 mg m^{-3} and the seasonally averaged chl-a. Including this variable in the multiple regression, however, (section 6.3.3) shows no significant link: regression coefficient 0.003±0.008. There is also no link to the time difference between initiation and the chl-a concentrations reaching 1 mg m^{-3}, which may also have measured growth at low light, or low growth rates due to low iron.

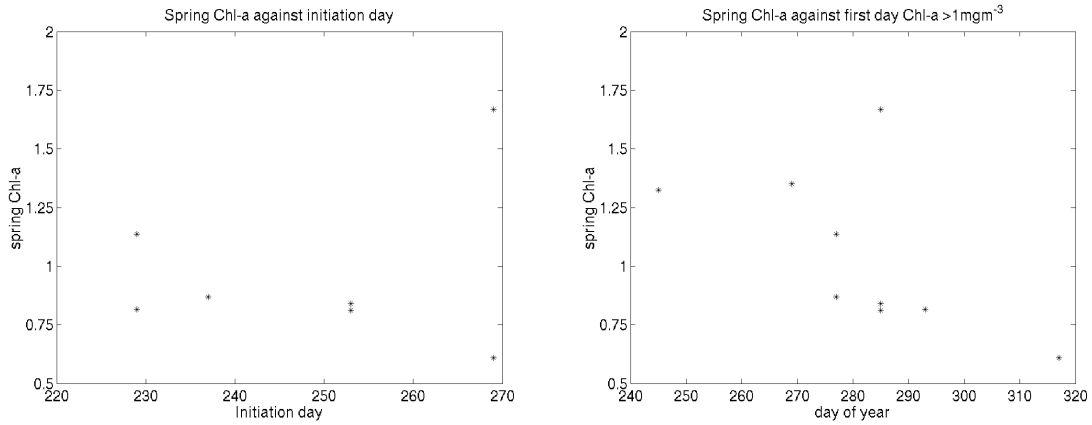

Figure 6.22 Strength of the spring bloom against measures of the start of the bloom.

6.3.4.3 PAR and wind stress

PAR and wind stress vary in different ways. There is a seasonal increase in the maximum possible PAR values (due to geometry) with variations below this due to varying weather conditions. Wind stress varies very significantly (from ≈0 to over 12 Nm^{-2}) over timescales of a day to a week but does not have a strong trend through the period. This difference means that PAR never varies significantly from the seasonal trend in the direction that would cause rapid stratification. In this situation, where the onset of stratification is being considered, PAR is being used as a measure of the total incoming irradiance. This assumes that the spectral composition of the irradiance is constant (the units of PAR are a measure of the number of photons rather than the total energy – a shift towards shorter wavelengths will increase the total energy but not PAR). PAR is also only integrated over part of the visible spectrum. Data from the cruises shows that the link is good on most days, especially days with high irradiance, which are the important ones in this section. PAR is also available at suitable temporal and spatial resolution from SeaWiFS.

PAR and wind stress have to be considered together in looking at the initiation in each year. This is due to the combined effect of buoyancy input and reduction in turbulence needed for a significant reduction in the mixed layer. Section 3.2.6.1 shows that temperature stratification is dominant and therefore a reduction in the mixed layer is likely to be due to an increase in the heat content, although freshwater fluxes may be significant in particular cases (there is no reliable way to assess this in the area, at the accuracy and spatial resolution required). For each year the chl-a, the wind stress and PAR are plotted for a period encompassing the identified initiation points and the bloom growth phase. The (wind stress, PAR) data pairs are also plotted and coloured to show their timing in relation to the initiation period identified.

This is because the necessary conditions for the mixed layer to shallow are both a reduction in the turbulence in the mixed layer and an input of heat energy to cause a warming in the upper part of the mixed layer. Before this threshold is exceeded, calm periods do occur but have little effect on the chl-a concentrations because without significant buoyancy input the original mixed layer is maintained throughout the calm period. The mixed layer will not actually be mixing, so phytoplankton near the surface will stay there, receive sufficient light and will grow. However, without an increase in the stratification these phytoplankton will get rapidly mixed downwards again throughout the original mixed layer once wind stress increases again. The growth may then be reversed if the mixed layer is deeper than critical depth. Equally, if there is significant turbulence throughout the depths of the mixed layer any heat input will be mixed over the whole depth and will not lead to a significant shallowing of the mixed layer. The increased density difference this causes at the base of the mixed layer does however reduce the deepening effects of an increase in turbulence.

The following figures (Figure 6.23 to Figure 6.36) present the chl-a, windstress and PAR data for the period of bloom initiation each year from 1999-2005 (the period for which QuikSCAT wind stress data are available). Wind stress data are every 12 hours, PAR data daily and chl-a data from 8-day images. The second panel for each year shows the distribution of (wind stress, PAR) data pairs. Both morning and afternoon wind data are used, each with the corresponding daily PAR value. When PAR values are missing the data are plotted with an open circle, using the 8-day mean PAR; this allows the wind stress data to be shown but such points should be interpreted with caution.

The figures show considerable detail, some of which is referred to in later sections, but the key result is that in all identified initiation periods there is at least one (wind stress, PAR) data pair such that wind stress<1 Nm^{-2} and PAR>20 Einsteins m^{-2} day^{-1}. This is taken as an empirical necessary condition for initiation. It is clearly not a sufficient condition for initiation because data pairs from periods preceding the initiation period also fall within this area. In some cases subsequent high wind stress or low PAR means that any effect of this calm period with high irradiance is not long lasting. In other years, such as 2001, the period preceding the initiation has similar conditions but a response is not seen in the chl-a concentrations, this could be due to effects of differing cloud cover in satellite images meaning the box average reduces slightly rather than increasing. The data are from the spring bloom area north of the main plateau ('north' on legend) and persistent bloom area near the islands ('near' on legend).

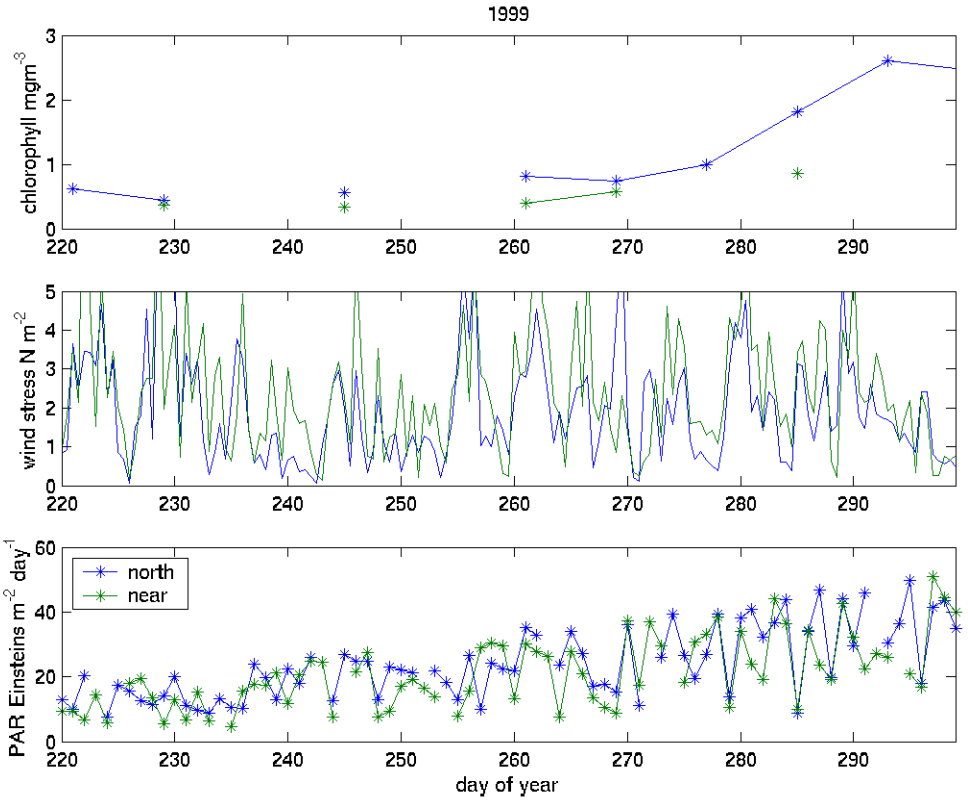

Figure 6.23 Chl-a, wind stress and PAR during the initiation of the bloom in 1999.

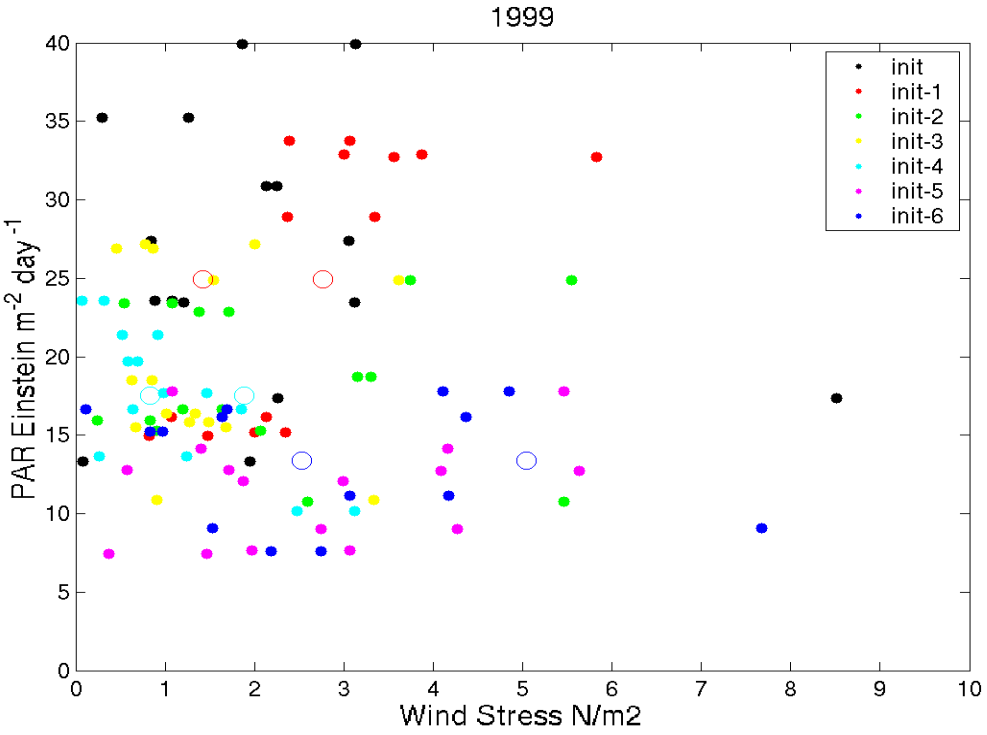

Figure 6.24 (Wind stress, PAR) data pairs from north of the plateau, 1999.

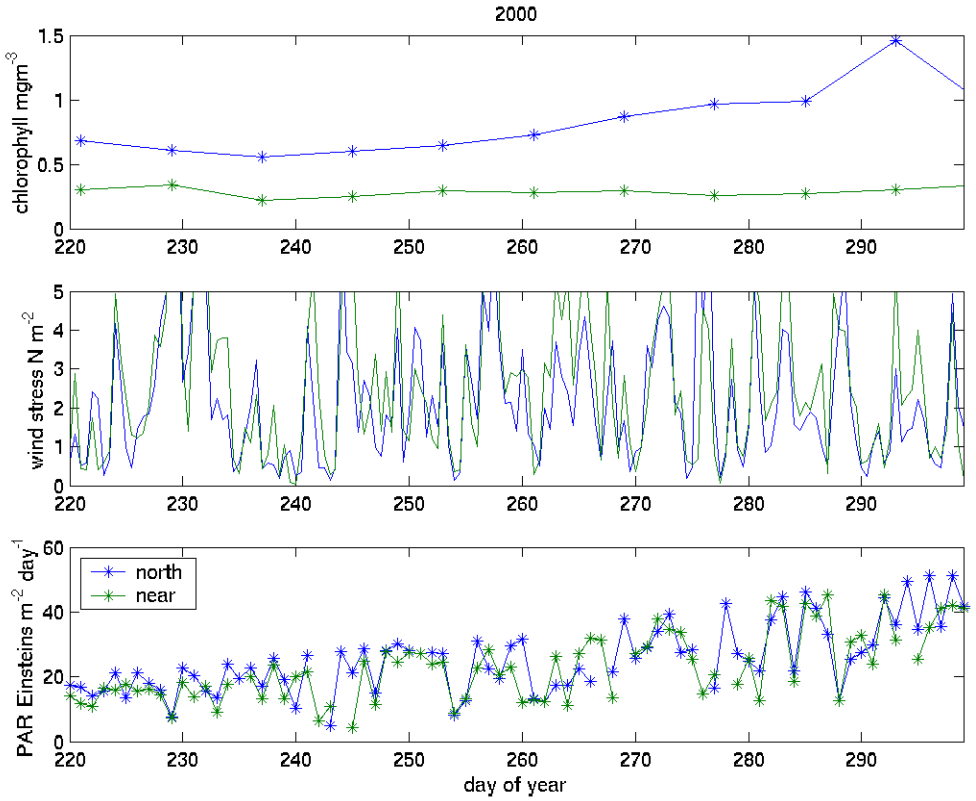

Figure 6.25 Chl-a, wind stress and PAR during the initiation of the bloom in 2000.

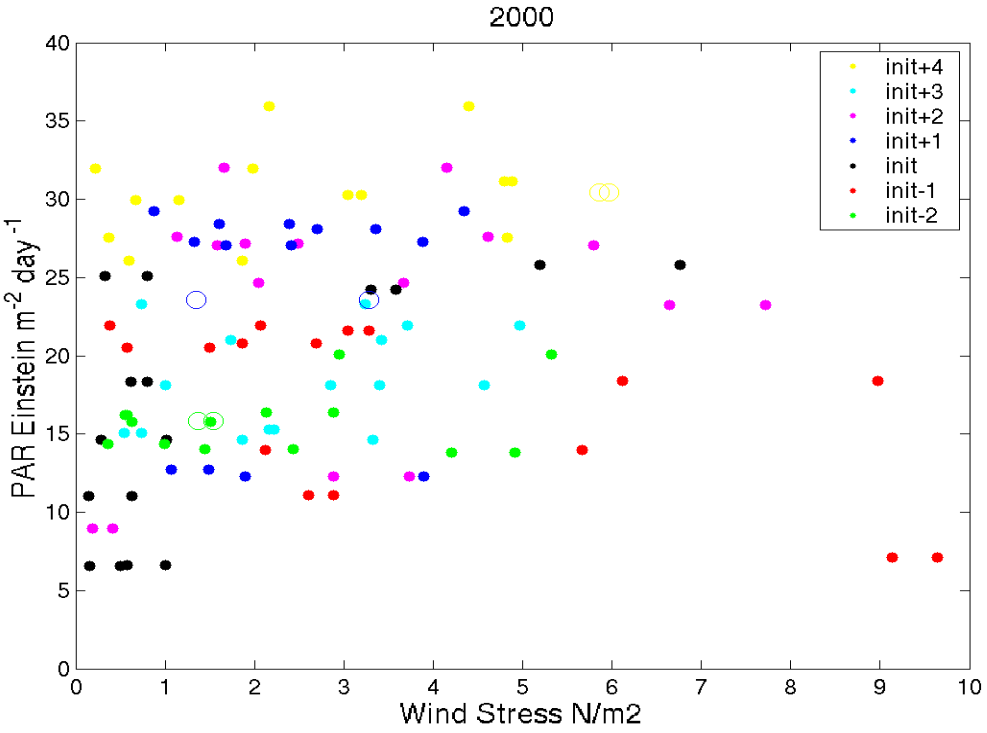

Figure 6.26 (Wind stress, PAR) data pairs from north of the plateau, 2000.

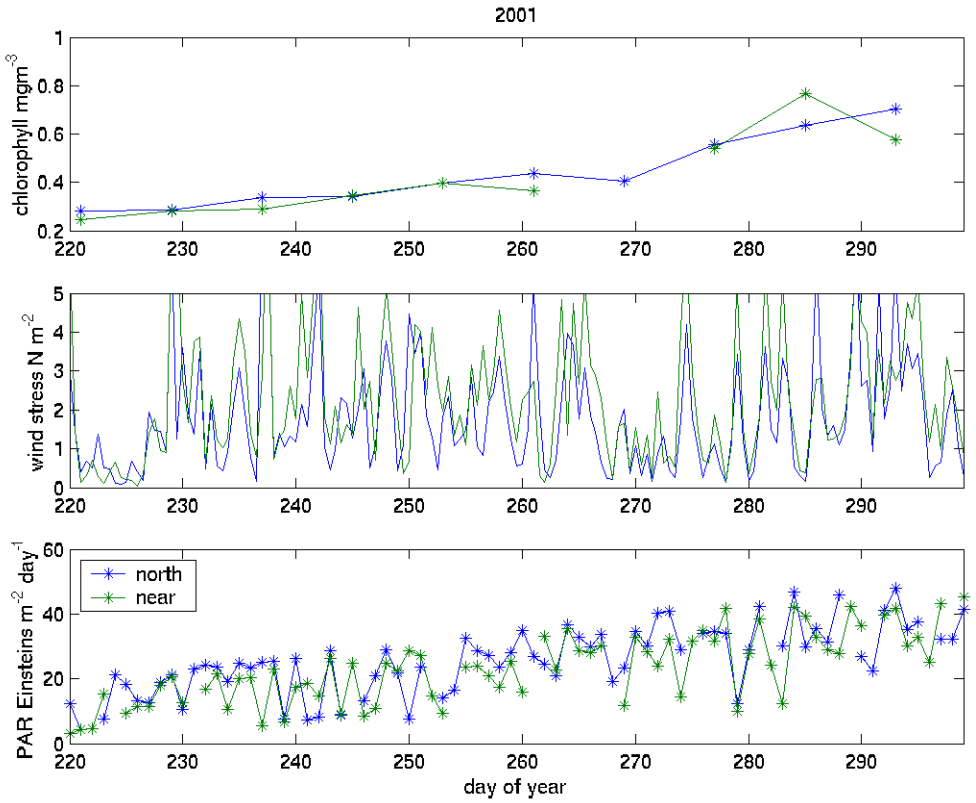

Figure 6.27 Chl-a, wind stress and PAR during the initiation of the bloom in 2001.

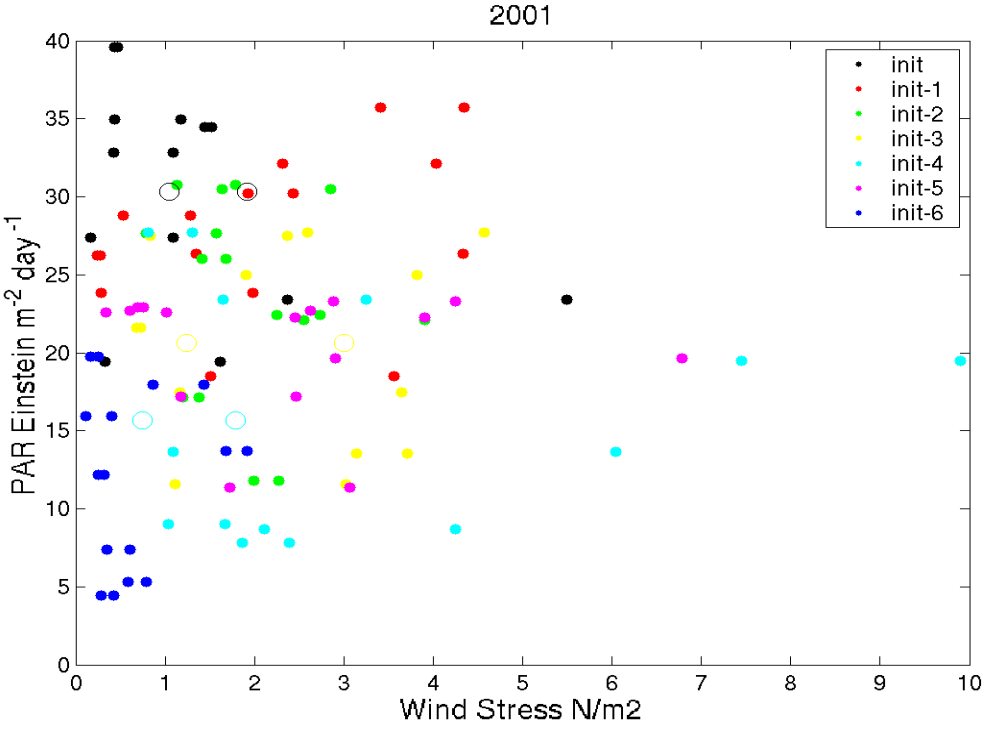

Figure 6.28 (Wind stress, PAR) data pairs from north of the plateau, 2001.

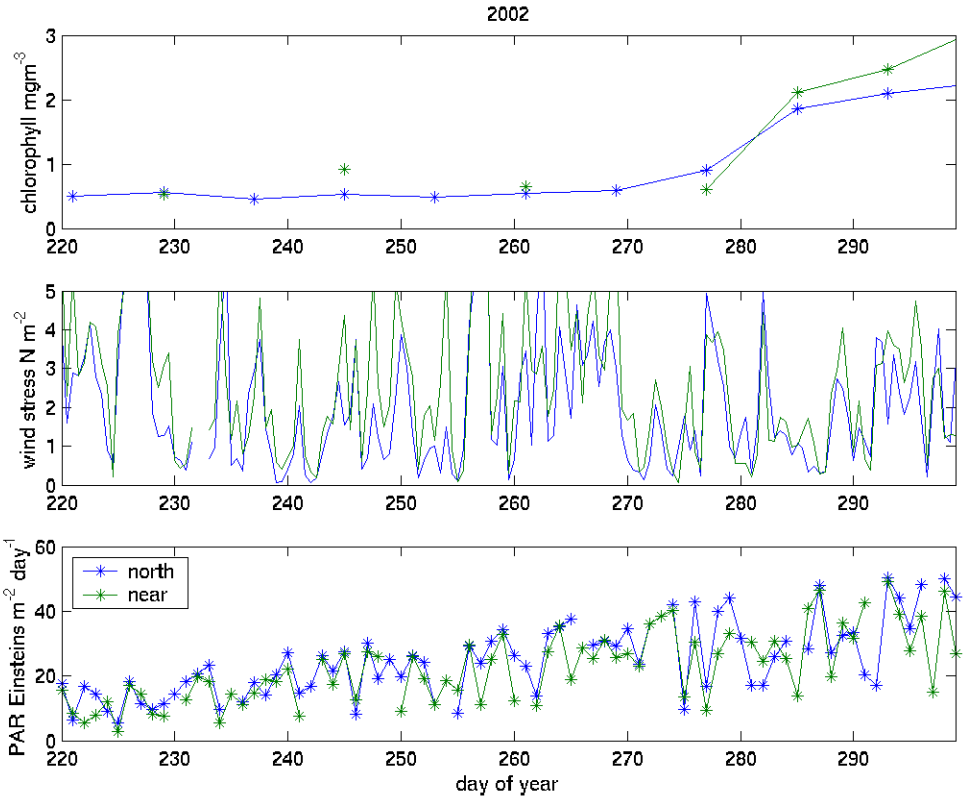

Figure 6.29 Chl-a, wind stress and PAR during the initiation of the bloom in 2002.

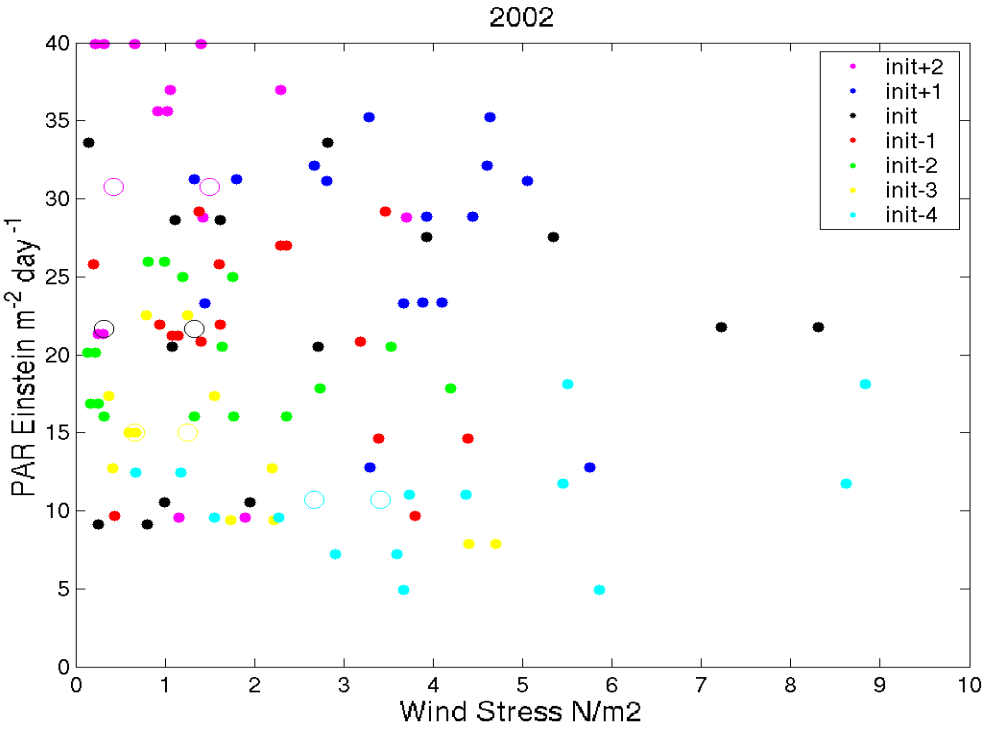

Figure 6.30 (Wind stress, PAR) data pairs from north of the plateau, 2002**.**

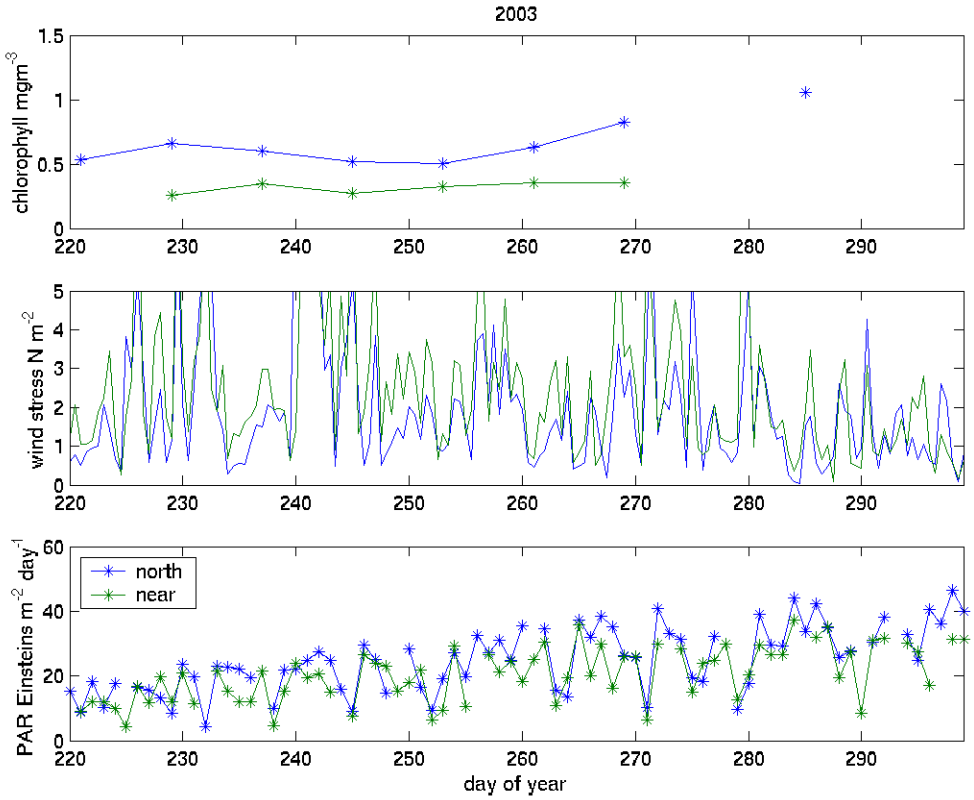

Figure 6.31 Chl-a, wind stress and PAR during the initiation of the bloom in 2003.

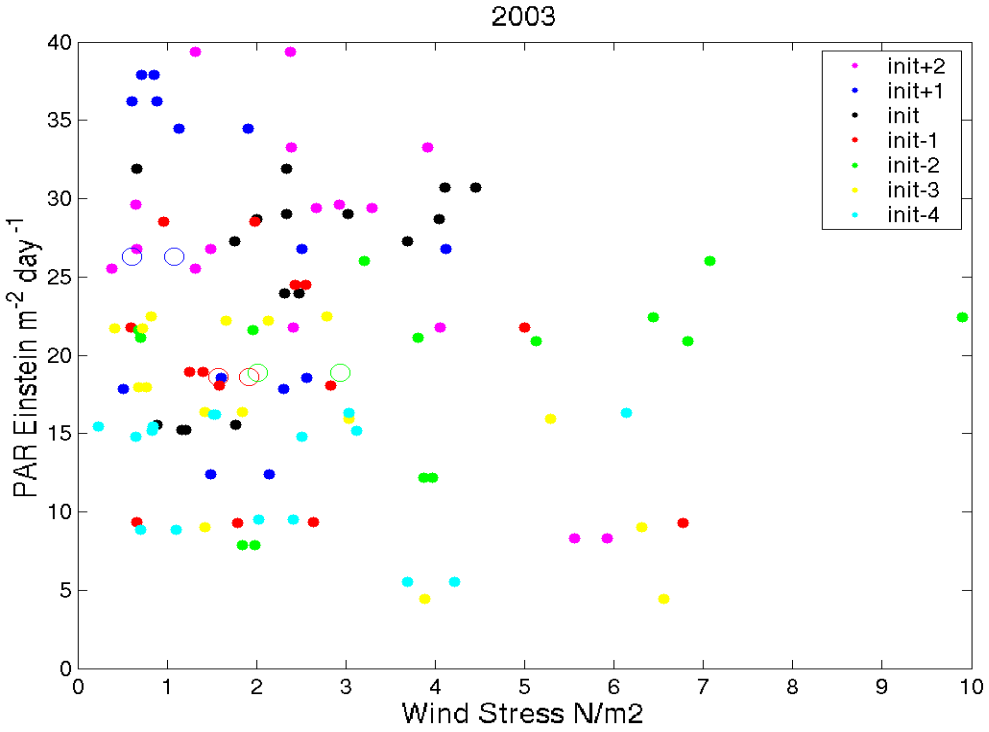

Figure 6.32 (Wind stress, PAR) data pairs from north of the plateau, 2003.

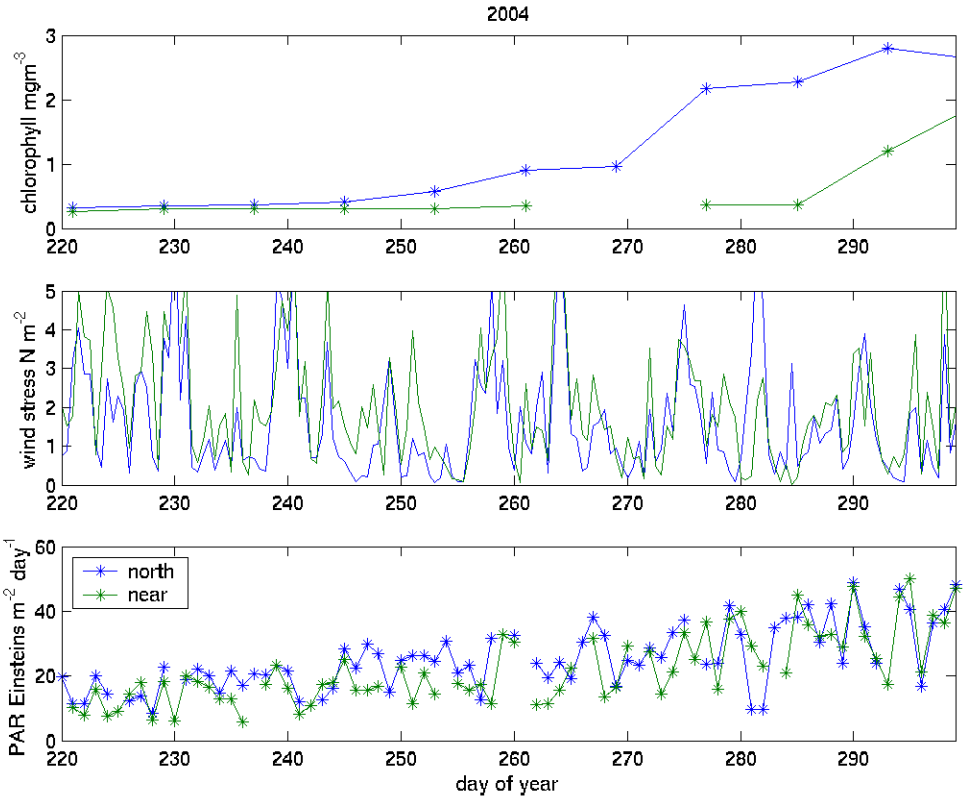

Figure 6.33 Chl-a, wind stress and PAR during the initiation of the bloom in 2004.

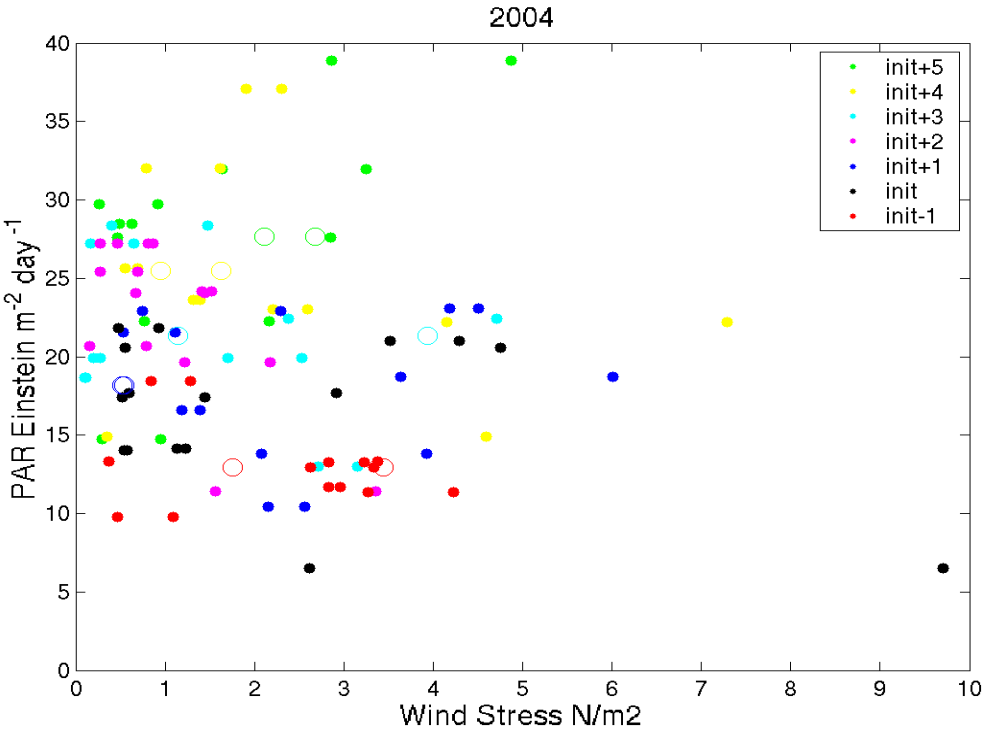

Figure 6.34 (Wind stress, PAR) data pairs from north of the plateau, 2004.

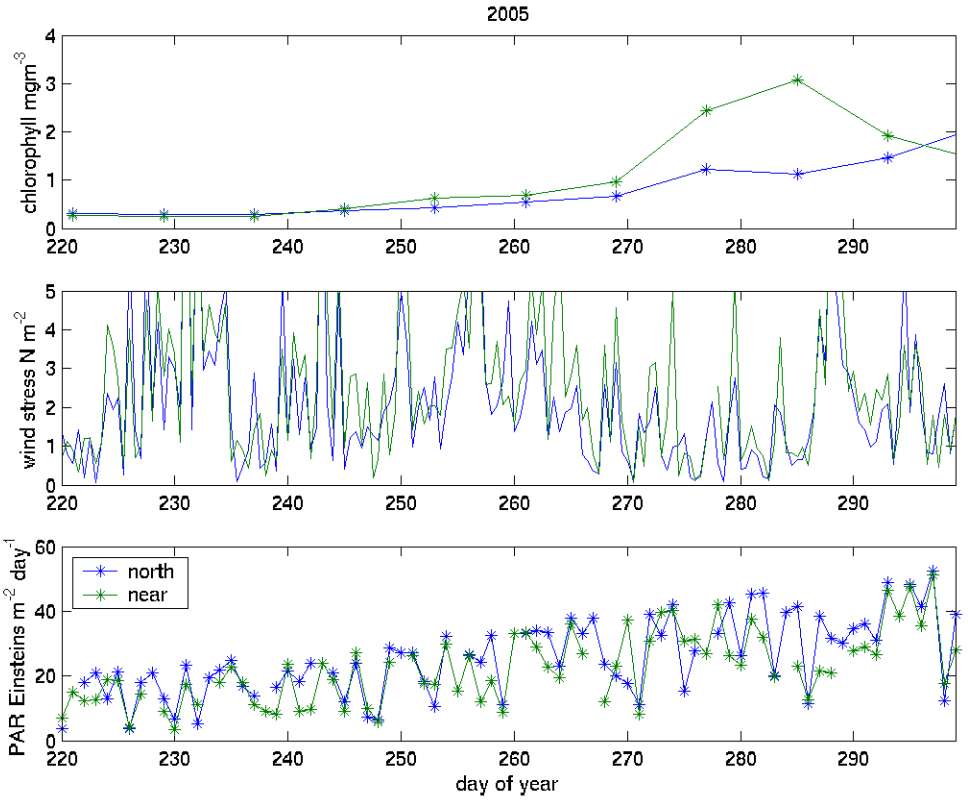

Figure 6.35 Chl-a, wind stress and PAR during the initiation of the bloom in 2005.

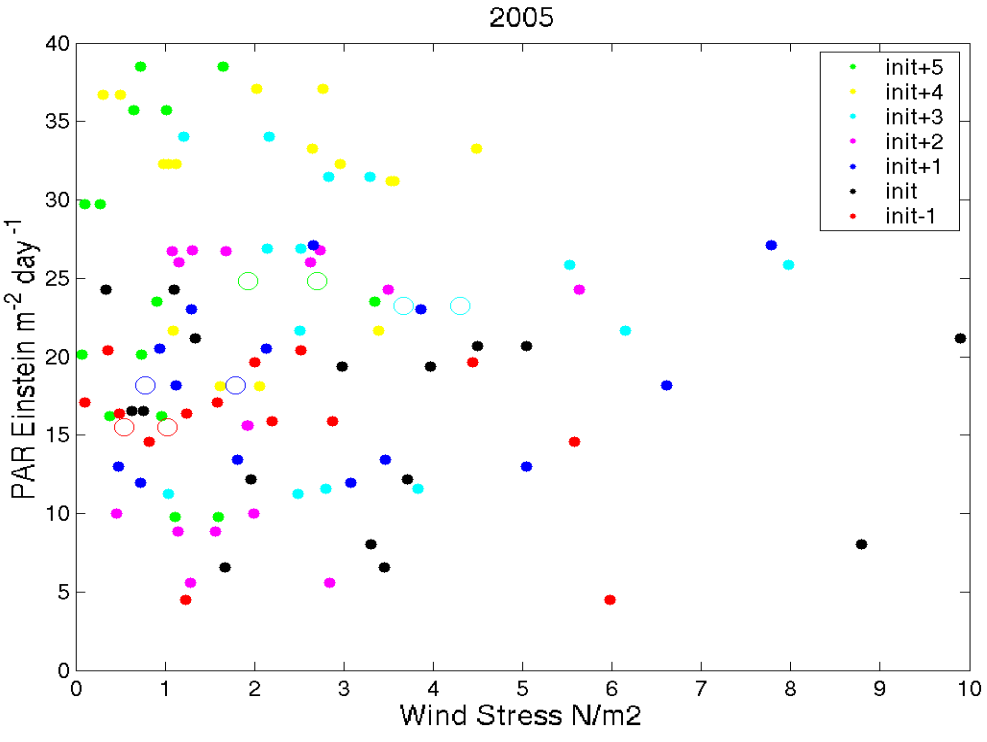

Figure 6.36 (Wind stress, PAR) data pairs from north of the plateau, 2005.

The points with very low wind stress (<0.5 Nm^{-2}) and low PAR (<10 Einsteins m^{-2} day^{-1}) are likely to be during foggy conditions. These conditions were encountered several times during the research cruises when the air temperature exceeded the water temperature. They are to be expected in an area of cold water surrounded by warm water because warm moist air will rapidly lose heat to the surface waters leading to it reaching saturation point and the water vapour beginning to condense out. Such conditions will lead to a heat and freshwater flux into the surface layers so will aid stratification. It is not clear how significant this effect will be relative to direct solar heating. It is not evident in all years and is unlikely to show significant seasonality.

It can be seen that the exact timing of bloom initiation is set by interaction between wind stress and PAR but the overall seasonal cycle is mostly controlled by the seasonality of incoming irradiance. The proposed minimum criteria for stratification to occur or a day with wind stress <1 Nm^{-2} and PAR >20 Einsteins m^{-2} day^{-1} is used in the following sections looking at particular events concerning the bloom.

6.3.5 Latitudinal progression of the bloom 2005

It is noticeable in Figure 6.35 that the chl-a increases close to the eastern islands before it does north of the plateau. This is against the pattern seen in other years. Section 4.7 also shows that chl-a normally increases in this area later than north of the plateau. This is due to deeper mixed layers and also later stratification (the increase in the mixed layer not being sufficient to explain the extra delay). The later stratification is due to the inflow from south of the plateau that advects water of more southerly origin around the eastern end of the plateau. Therefore the possible causes for an earlier development of the bloom north of the eastern islands are a reversal of the gradient in the forcing of the mixed layer and a change in the circulation around the eastern end of the islands.

Figure 6.35 shows a reversal of the PAR gradient on jday 270. The daily PAR near the islands is 37 Einsteins m^{-2} day^{-1} whereas north of the plateau it is 18 Einsteins m^{-2} day^{-1}. This coincides with a short period of low wind stress (<0.2 Nm^{-2}). There is also a calm period (<0.7 Nm^{-2}) between jday 247 and 249 near the eastern islands when the windstress north of the plateau is >1 Nm^{-2}. The first part of this coincides with very low PAR (<10 Einsteins m^{-2} day^{-1}) but PAR is higher (24 Einsteins m^{-2} day^{-1}) on jday 249.

Chl-a concentrations start to diverge from this point, suggesting that the mixed layer shallowed north of the islands during this period.

In comparison, there are periods during 2004 (jdays 237-238, 245-247 and 266) where the wind stress is <1 Nm^{-2} north of the main plateau but not north of the eastern islands. PAR is higher over the main bloom area in each case. The wind stress is lower close to the islands on jday 280 and 284, this corresponding to the beginning of the increase of chl-a there.

Figure 6.12 shows that the flow around the eastern end of the plateau was relatively high in late 2005. Figure 6.37 shows though that this flow is offset to the east of the increased chl-a and therefore was not advecting water of southerly origin to the area. Figure 6.38, an equivalent image from 2004 for comparison, shows a northwards contour closer to the eastern end of the plateau, suggesting a greater influence of water with a southerly origin, which would reduce the growth of phytoplankton close to the islands, due to the deeper mixed layer depths (section 5.3).

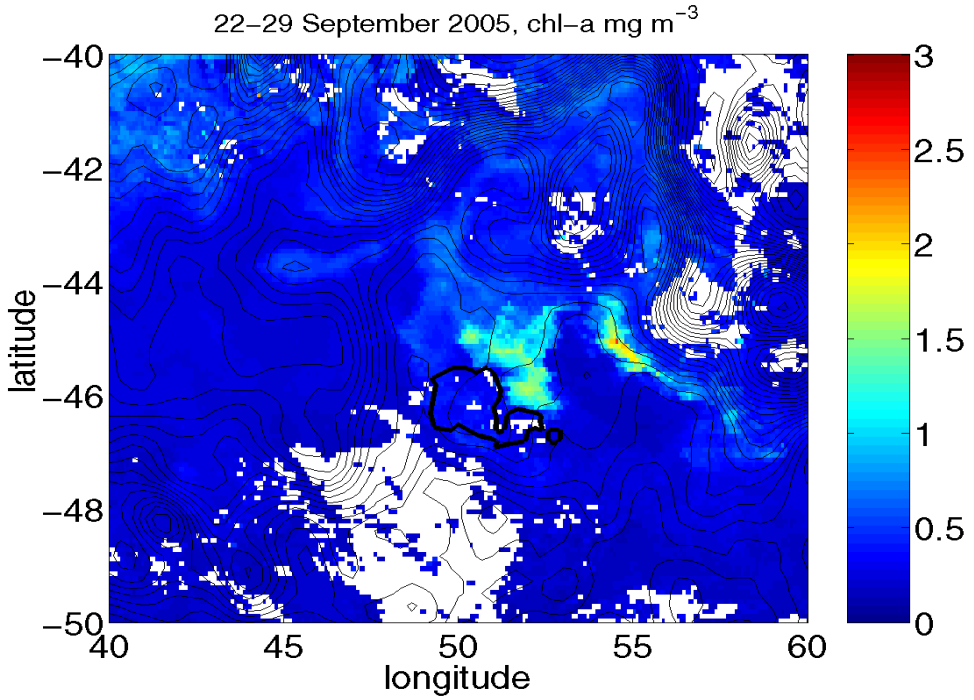

Figure 6.37 Chl-a image, with overlain dynamic height contour, showing the unusual development of the bloom in early 2005

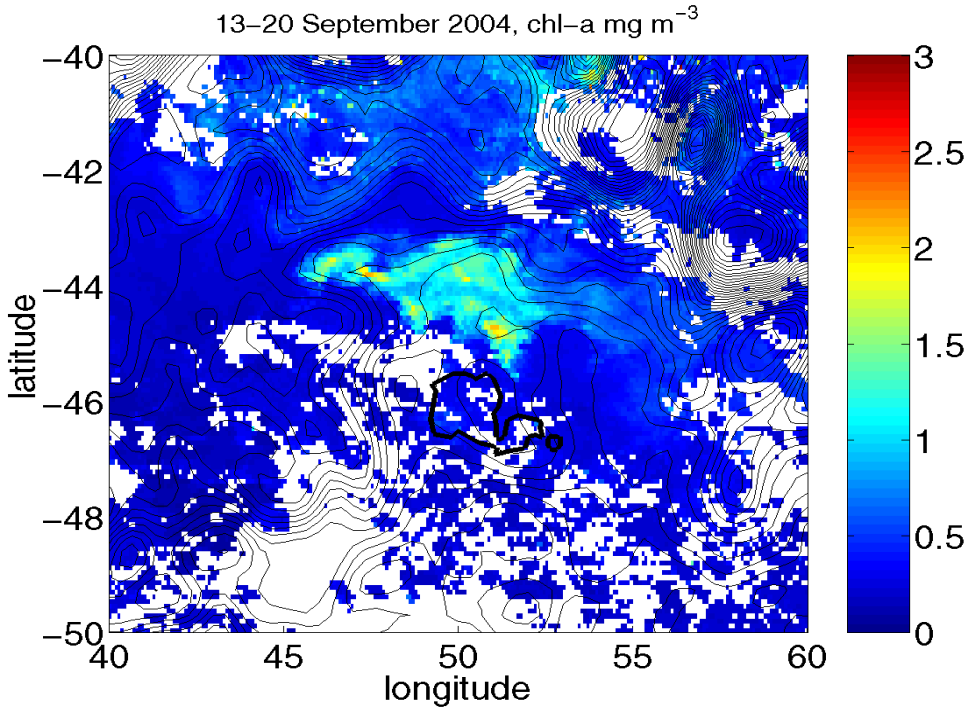

Figure 6.38 Chl-a image, with overlain dynamic height contour, showing the usual development of the bloom in early 2004

6.3.6 Winter 2000

It was seen in section 6.3.1 that chl-a values in the spring bloom were affected by the chl-a values present in the preceding winter period. The highest chl-a levels were seen in the winter of 2000 (Figure 4.5). The possible causes for this are investigated here, following the arguments of section 6.3.4.3.

It can be seen from Figure 6.39 that there were prolonged calm periods from jday 100-107 and 113-130 at the beginning of the winter period. These correspond to the latest dates for which PAR exceeds 20 Einsteins m^{-2} day^{-1}, the value identified in section 6.3.4.3 as the lowest value associated with the initiation of the bloom. It is therefore likely that there was a relatively shallow mixed layer during this period in both areas. The larger response in chl-a from the area close to the eastern islands agrees with this area being close to the iron source. After jday 130 (10^{th} May) the wind stress increases again but the standing stock of chl-a stays strongly enhanced over the normal winter values of 0.3-0.4 mg m^{-3}. These phytoplankton will most likely be existing in a light stressed environment, due to the strong winds and low incoming irradiance. The exact impact of this increased winter stock of phytoplankton could potentially be quite complicated because as well as using iron they may also take up a significant amount of silicate (Takeda 1998) and also possibly affect the zooplankton population dynamics by allowing a greater overwintering survival rate. All of these effects are likely to reduce the strength of the spring bloom.

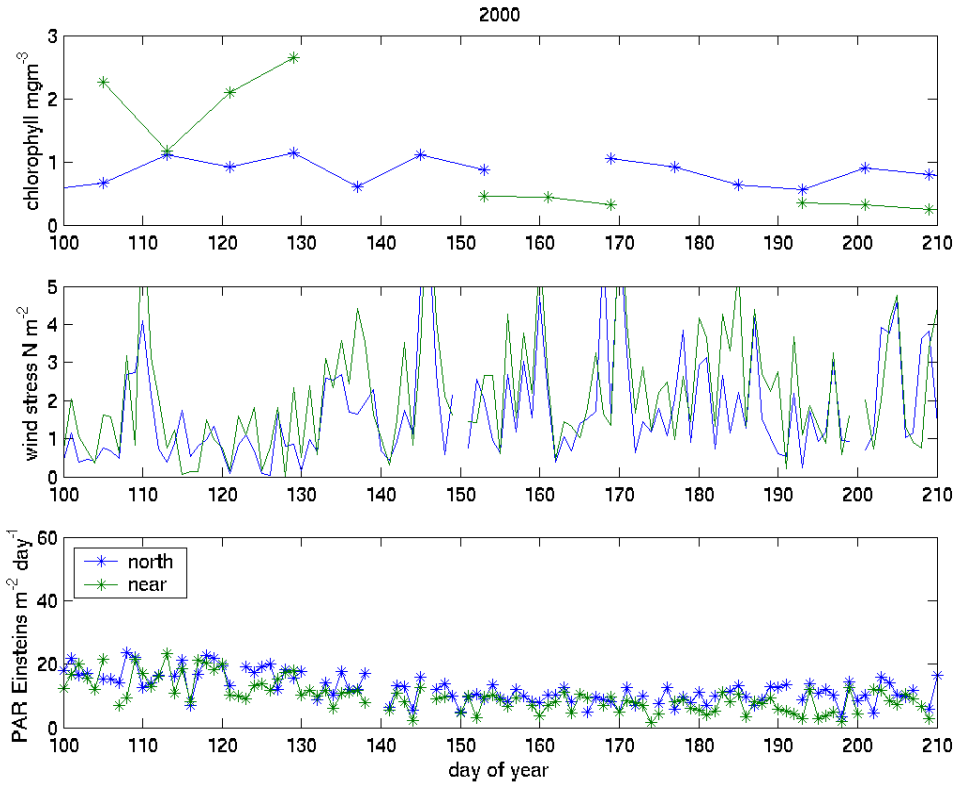

Figure 6.39 Chl-a, wind stress and PAR during the winter period in 2000.

6.3.7 Plateau conditions in Spring 2002 (revisited)

Following the discussion in section 6.2.3, together with arguments put forward in section 4.6.3, it is worth considering whether there is evidence for increased stratification over the plateau during 2002, when there were high chl-a concentrations over the plateau. Figure 6.40 shows that the increase in chl-a over the plateau in 2002 was actually preceded by an unusually prolonged period (jday 256-269) of strong winds (note change in axis limits compared to previous plots) and there is nothing to suggest strong forcing towards enhanced stratification. The equivalent plot is shown for 2005 for comparison (note different chl-a scales), which shows low wind stress, high PAR periods that are similar to the conditions following the strong wind event in 2002. There is a potential that the strong winds (which were westerlies, data not shown) somehow caused the increase in chl-a. They could possibly act through temporarily changing the surface circulation (such a change was shown in section 6.2.3 but appears to be forced by variations to the north) or increasing mixing to bring iron to the surface waters. The latter possibility requires the surface waters not to be already fertilised with iron, which, though seemingly unlikely, is possible. Countering these possibilities is the fact that it is likely that winter

storms would have a similar mixing effect most winters, leaving the area iron fertilised for a spring bloom. It is most likely that the change in circulation pattern seen in 2002 is the cause of the high chl-a, rather than *in situ* atmospheric forcing.

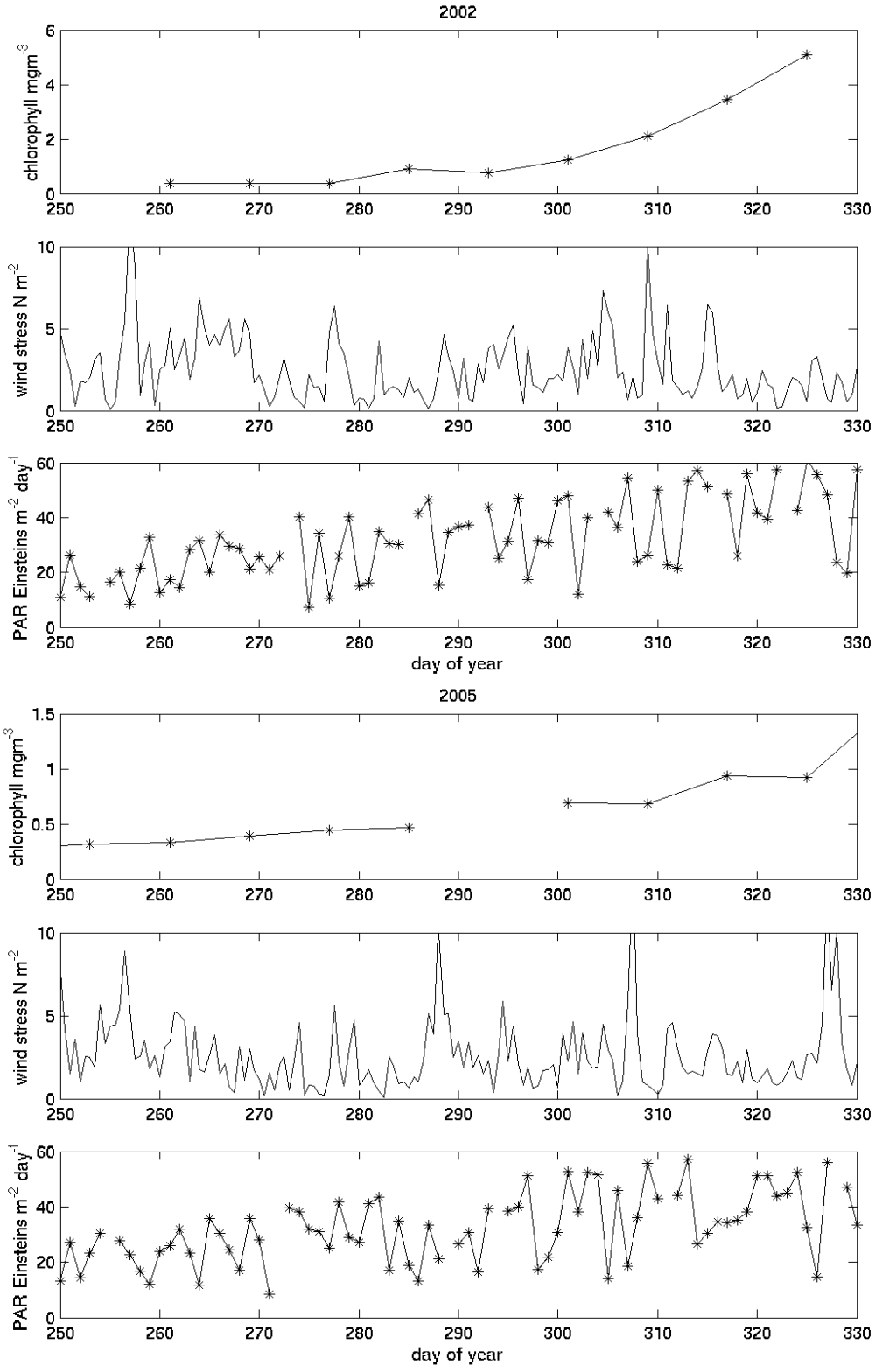

Figure 6.40 Chl-a, wind stress and PAR over the plateau in 2002 and 2005.

6.4 Potential for change and significance

Changes in either wind stress or irradiance could change the timing or strength of the bloom through changes in the iron supply and light availability, through mixed layer depth and incoming irradiance.

There is a current trend towards a higher SAM index (Marshall 2003), linked to either climate change (Fyfe *et al.* 1999) or changes in ozone concentrations (Thompson and Solomon 2002). This is leading to increased wind stress over most of the Southern Ocean and hence deeper mixed layers, which could reduce the length of the period where light is not limiting. However, around Crozet the SAM is more strongly linked to the local wind stress curl (Figure 6.2) than the wind stress (Figure 6.3). The wind stress curl influences the closed circulation around the plateau and a stronger wind stress curl is linked to a stronger spring bloom. It is therefore likely that long term changes in the SAM will have a positive effect on the phytoplankton concentrations north of the Crozet Plateau. There is unlikely to be a significant effect on the timing of the bloom, unless there is a shift in the local weather patterns.

Following the bloom there is a period when the chl-a levels vary between pre-bloom levels (≈0.3 mg m^{-3}) and a level that reduces with distance from the eastern islands (≈2 mg m^{-3} close to the islands, ≈1 mg m^{-3} in the main bloom area). This continues until light is limiting so the period of these slightly enhanced values may be reduced by increased wind stress, if there is actually a link. Many factors influence stratification however and others (e.g. incoming irradiance, air temperature and precipitation) may change linked to the changes in the climate and/or SAM and these may enhance, reduce or reverse the possible change linked to wind stress changes.

7 Conclusions

This work significantly enhances the knowledge of the different productivity regimes around the Crozet Plateau and their causes and consequences. The four main productivity regimes identified are shown in Figure 7.1: a spring bloom north of the Crozet Plateau, fertilised by iron from the Crozet Islands advected there during the light limited winter period; a persistent bloom north of the Crozet Islands, fertilised by iron advected from the Crozet Islands all year; an area over the Crozet Plateau where chl-a concentrations are enhanced over background Southern Ocean levels but are much lower than those found in the two bloom areas at their peak; and an area to the south that has chl-a concentrations similar to the open Southern Ocean, due to the lack of a flow from the Crozet Islands to the area, meaning that iron concentrations will not be enhanced over background levels.

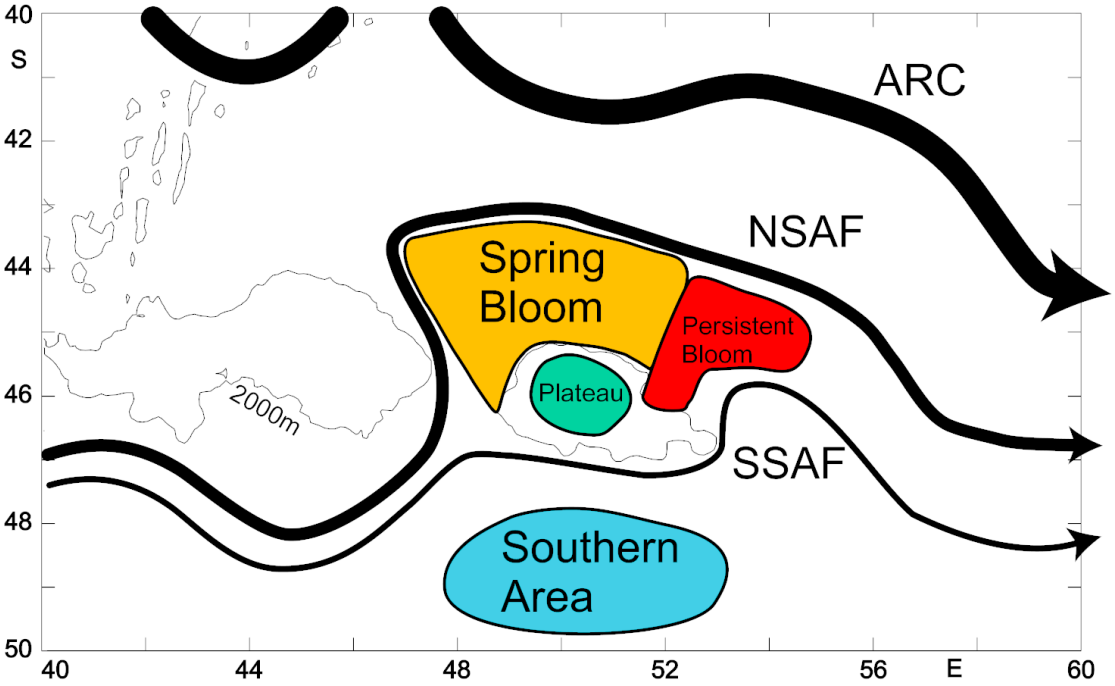

Figure 7.1 Figure 4.3 reproduced as a summary of the key circulation features and productivity areas. The Del Cano rise is the closed 2000m contour to the west, the Crozet Plateau is under the 'Plateau' area.

The main source of data for describing the spatial and temporal structure of the bloom is NASA ocean colour images (Feldman and McClain 2006). Without these, this work would not have been possible. Indeed the initial knowledge of the existence and shape of

the bloom that was a key element in forming the CROZEX project comes from this source. These data however have calibration problems in the Southern Ocean and it was therefore necessary to find a local correction function so that satellite and *in situ* estimates of production and export could be directly comparable. Such a correction function was found in section 2.5.6:

$CHL_{in\ situ} = -0.08+2.05\times CHL_{merged}$

by comparing *in situ* measurements with corresponding individual pixel values from daily satellite images.

Argo float profiles provide year-round subsurface information not available from any other source, allowing significantly increased analysis of remotely sensed data. The float trajectories are also a useful source of information about the flow patterns, together with absolute dynamic height, hydrographic data and drifter trajectories. Understanding of the circulation is vital to understanding the location and characteristics of the different productivity areas. The circulation is therefore summarised, followed by descriptions of each of the four productivity areas.

7.1 Circulation

The Del Cano Rise (DCR) causes the SAF to split into two branches. The NSAF (northern branch) follows the topography of the DCR northwards, to the west of the Crozet Plateau before turning back eastwards 200-300km north of the Crozet Plateau. The SSAF (southern branch) flows across the gap between the DCR and Crozet Plateau and follows the topography of the Crozet Plateau northwards, past the largest two of the Crozet Islands, situated at the eastern end of the plateau. The SSAF has a similar strength at the surface to the NSAF but most of the deep flow is strongly tied to the DCR so the volume flux associated with the SSAF is significantly lower than that of the NSAF. The NSAF, SSAF and Crozet Plateau enclose an area of long residence time north of the Crozet Plateau. The inflows into this area are detrainment from the SSAF (from the south and east) and NSAF (from north and west). As the NSAF and SSAF are strongly controlled in parts of their paths by topography there is little interannual variability in the overall location of the productivity areas.

There is a closed circulation around the Crozet Plateau. This is driven by the wind stress curl around the plateau causing convergent Ekman flux over the plateau, a local maximum in sea surface height (seen in absolute dynamic height data) and so a barotropic circulation seen in Argo float trajectories. The wind stress curl is coherent with the Southern Annular Mode (SAM) index, due to the location of the Crozet Plateau close to the pivot point of the mode, between increased westerly wind stress to the south and increased easterly wind stress to the north. No direct coherence between the strength of the recirculation and the SAM index was found however.

At approximately 42°E the Polar Front (PF) splits southwards from the merged Polar Front/Sub-Antarctic Front that passes between the Del Cano Rise and the Ob Lena (Conrad) Rise. The PF moves southwards with distance east from here, reaching approximately 52°S by the longitude of the Crozet Plateau. Between this flow and the Crozet Plateau is an area of weak flow.

7.2 Spring Bloom

The area referred to as the spring bloom in Figure 7.1 occupies the area with long residence time bounded to the west and north by the NSAF, to the south by the Crozet Plateau and to the east by the SSAF. The mixing between the southern, iron-fertilised inflow from the SSAF and the northern, non iron-fertilised inflow from the NSAF very likely causes a gradient in iron concentrations at the end of winter.

Due to the iron fertilisation there is a spring bloom that fills the entire area and extends into the NSAF due to water exchange between the NSAF and spring bloom area. On average, across the years of satellite ocean colour data used (1997-2005), the bloom starts in north of the area and spreads south. This southward spread can be explained by the light environment during the bloom initiation. The mixed layer deepens to the south by 10.8 ± 1.0 metres degree^{-1} latitude, this being the dominant reason for the change in light availability. This bloom reaches chl-a concentrations of up to 4.5 mg m^{-3} and collapses after 2-3 months, very likely due to the depletion of iron, a process possibly complicated by the depletion of silicate at a similar point in the bloom. After the collapse in chl-a concentrations, they very rarely increase above 1 mg m^{-3} again, indicating that there is

not a strong resupply of iron to the area during the period of light availability, presumably due to biological utilisation closer to the eastern islands.

The summer chl-a concentrations are strongly affected by the concentrations in the previous spring, indicating that they are driven by iron present during the spring becoming available through biological recycling and/or vertical movements of iron from below the mixed layer rather than continual supply of iron. Most of the interannual variability of the spring chl-a concentrations is explained by the strength of the wind stress curl the previous winter (acting through increasing the strength of the recirculation around the plateau and so westward advection of iron) and the biological utilisation during the winter (acting to reduce the initial iron concentrations at the start of spring).

7.3 Persistent Bloom

The area identified as the persistent bloom is bounded to the south by the eastern islands – Ile de la Possession and Ile de l'Est. These are not a boundary to the flow, with part of the SSAF following the topography of the Crozet Plateau northwards past them. This very strongly implies that the islands are the dominant iron source for the bloom. Ile de la Possession has been identified as a source of iron through *in situ* sampling (Planquette *et al.* 2007) (Ile de l'Est was not sampled but is geologically similar). This flux was shown to be sufficient to fertilise the persistent and spring blooms, though that was under the assumption that the flux from the shelf area was similar. The satellite data suggests that the islands are a stronger source than the plateau. However, the variability of the persistent bloom identified in section 4.6.2 also suggests that one transect away from the islands is unlikely to fully represent the iron flux through the year. It is therefore possible, indeed quite likely given the short time periods of enhancement of the persistent bloom through the summer, that the flux on the transect measured was lower than the mean flux and that the whole bloom could be fully fertilised even if the plateau was a weaker source than the islands (as the estimate from the islands is likely to be biased low).

There is a strong bloom in the spring in this area as well. This starts later than the bloom in the spring bloom area, with chl-a concentrations reaching 8 mg m^{-3} in some years. The delay, of 13 days relative to just north of the main plateau, cannot be explained by the overall latitudinal gradient in mixed layer depth and incoming irradiance. The extra delay

is most likely due to the northward flow around the eastern end of the islands, meaning that the surface water characteristics are typical of a more southerly latitude. The peak value of the chl-a attained during the bloom in spring is higher than in the spring bloom area. This, together with the gradient to higher peak chl-a to the south within the spring bloom area, very strongly suggests that iron controls the strength of the peak of the bloom. The gradient in mixed layer depth and incoming irradiance reduces light availability towards the south, the reverse of the gradient needed to explain the varying strengths of the bloom. Distance from the islands (an identified iron source) and dilution by water detraining from the NSAF lead to a predicted initial iron gradient in the appropriate direction to explain the observed gradient in peak chl-a.

The proximity of an iron source, and a net flow from it into the area, leads to chl-a concentrations regularly exceeding 2mg m^{-3} after the main bloom event. The spatial extent of the increased chl-a is very tightly tied to the islands, mostly to the north and west of these islands, consistent with the flow pattern. This shows particularly in chl-a composite images through the period of light availability. These also show higher integrated chl-a concentrations close to the islands compared to the spring bloom area.

7.4 Plateau

By far the most enigmatic area is that over the main Crozet Plateau. The area is poorly charted so the ship did not enter the area during the research cruises. It is also too shallow for Argo floats to enter under normal conditions but two floats have crossed the south-western corner due to drift at the surface while transmitting data. The majority of the plateau is shallower than 350m, many areas shallower than 200m and there are numerous small islands. It therefore seems likely that iron from the sediments or islands would enter the surface waters either directly or due to mixing, including deep winter mixing. The main plateau is geologically distinct from the eastern islands, though how this might affect iron flux is unknown.

The generally low chl-a concentrations (<1 mg m^{-3}) are therefore surprising. The possible causes for this are: there is not a strong iron source from any of the sediments or islands; the area is persistently light-limited due to surface and bottom mixed layers merging

throughout the year; and the area is grazing controlled due to high overwintering populations and high growth rates of neritic zooplankton.

It is likely that the closed circulation around the plateau reduces exchange of water on and off the plateau. This would act to enhance the isolation of the plateau area, allowing it to be under a separate regime from the surrounding deep water. Evidence that the closed circulation helps to isolate the region over the plateau comes from 2002 when the circulation appears to have 'opened', leading to flow from the spring bloom area on to the plateau. This coincides with the highest chl-a concentrations observed over the plateau.

There is evidence against the second of these hypotheses, light limitation, as the Argo float profiles that have come from the plateau area show mixed layer depths typical of the latitude and time of year and do not show significant bottom mixed layers, although it should be noted that areas where Argo floats are advected to may show characteristics more typical of open ocean conditions at that time due to advection of surface waters. A gradient in SST towards lower values over the plateau would be expected if the mixed layer was deeper but this is not observed.

The chl-a concentrations oscillate through the period of high light availability (over the whole area, this not being well known over the plateau). This implies that there is either a sporadic supply of iron or is part of the phytoplankton-zooplankton population dynamics if iron is replete. It certainly suggests that there is the potential for iron to build up in the surface waters over the plateau through winter, as chl-a is higher than the open HNLC region to the south. Data to confirm this, and, if correct, explain the lack of a strong spring bloom would be very interesting, though logistically very hard to obtain.

7.5 South of the plateau

The area to the south of the Crozet Plateau is typical of the HNLC conditions in the open (non-land affected) Southern Ocean. It is replete in macronutrients and the light availability is high enough to support strong phytoplankton growth – for at least 4 months it is consistently higher than that found in the spring bloom area during the period of high chl-a there. Despite this, chl-a concentrations are low: generally <0.5 mg m^{-3}, rarely

reaching ≈1mg m^{-3}, both low compared to the concentrations reached north of the plateau in similar light conditions.

The circulation patterns around the Crozet Plateau are consistent with the iron supplied to the surface waters close to the eastern islands not reaching significantly south of the plateau. This is due to the northward flow past the islands, the predominantly northward Ekman flow due to the prevailing westerly winds, and the SSAF flowing along the south side of the plateau that will advect water leaving the plateau southwards off to the east.

The observed phytoplankton size and grazing pressure to the south is consistent with the ecumenical iron hypothesis (Morel *et al.* 1991), adapted by Smetacek *et al.* (2004) as there is a bimodal distribution of phytoplankton (Moore *et al.* 2007; Seeyave *et al.* 2007). There are both small phytoplankton that have lower iron stress due to greater surface area:volume ratio but high grazing pressure (Fielding *et al.* 2007) and large phytoplankton that have high iron stress but maintain a net growth rate by reducing their grazing loss term.

7.6 Other areas

The response of phytoplankton to light around South Georgia and Kerguelen is very similar to that north of the Crozet Plateau. However, other islands in the Southern Ocean – Bouvet, Prince Edward and Macquarie – do not cause a similar response. High chl-a concentrations are observed in areas of long residence time (spring bloom) and net flow (persistent bloom and South Georgia) so it is likely that the difference between islands is geological, linked to the iron flux into the surface waters.

Using a similar, empirical, approach to assess the light availability in mesoscale iron enrichment experiments from ships indicates that those conducted away from the Southern Ocean did not become light limited. The link found between mixed layer depth and peak chl-a by de Baar *et al.* (2005) is therefore likely due to the effects of light availability on growth rate, rather than the limiting effect of self-shading. The experiments conducted in the Southern Ocean do reach levels of light availability that indicate self-shading may be important. However, in some of these cases, chl-a concentrations then drop rapidly, suggesting that the peak was caused by a decline in iron

availability. The peak chl-a is then determined by the residence time of iron after addition, the growth rate of phytoplankton during that time and any changes in chl-a:carbon ratios that occur due to the alleviation of iron stress.

7.7 Future work

The comparison with other areas of the Southern Ocean confirms that Crozet is a special place and one of only three areas of the Southern Ocean showing similar characteristics. There is still much to learn about the area, despite the many achievements of the CROZEX program. With time, and continued funding, the dataset of remotely sensed and Argo data will continue to grow, leading to further opportunities of analysis. Ultimately though, it will be necessary for further research cruises to return to the area to further our knowledge in many areas. The following are a few brief ideas relating to the possibilities for further study around the Crozet Plateau.

It would be very interesting to be present at the initiation of the bloom, to get actual measurements of the initial iron concentrations (needed to confirm the hypothesised north/south gradient and to further assess the carbon export:iron ratio). In addition it would allow study of the processes of stratification and the biological response. Such a cruise would very likely lose a large proportion of time to bad weather.

Being present for the peak of the bloom would help to assess the relationships between silicate concentrations, species composition and iron concentration and allow associated export events to be studied. It might also be possible to assess whether physical or biogeochemical processes (or both) at the edge of the NSAF cause continued high chl-a concentrations observed in some years.

In situ measurements from over the plateau (at any time) would help to answer many questions about controls on phytoplankton in this area. Samples from the western islands would be very difficult to obtain (logistically and politically/environmentally) but they would allow consideration of the importance of the geological differences between the main plateau and eastern islands. Further iron measurements from around the islands and plateau would allow further and more accurate calculation of the iron flux to the bloom areas, especially if together with more accurate lateral and vertical mixing estimates.

More work could also be done studying the effects of the phytoplankton bloom on higher trophic levels – the Crozet Islands hold millions of breeding pairs of seabirds and also large populations of pinnipeds, but the limited evidence available suggests that they move to frontal areas to the north and south but do not strongly utilise the bloom area. Hopefully these and other questions can be answered by future work, which will be strongly guided and enhanced by the results of this work and the rest of the CROZEX program.

References

Abraham, E. R., C. S. Law, P. W. Boyd, S. J. Lavender, M. T. Maldonado and A. R. Bowie (2000). "Importance of stirring in the development of an iron-fertilized phytoplankton bloom." Nature **407**: 727-730.

Allen, J. T., L. Brown, R. Sanders, C. M. Moore, A. Mustard, S. Fielding, M. I. Lucas, M. Rixen, G. Savidge, S. Henson and D. Mayor (2005). "Diatom carbon export enhanced by silicate upwelling in the northeast Atlantic." Nature **437**: doi:10.1038/nature03948.

Allen, J. T. and D. A. Smeed (1996). "Potential Vorticity and Vertical Velocity at the Iceland-Faeroes Front." Journal of Physical Oceanography **26**: 2611-2634.

Ansorge, I. J., P. W. Froneman, E. A. Pakhomov, J. R. E. Lutjeharms, R. Perissinotto and R. C. van Ballegooyen (1999). "Physical-biological coupling in the waters surrounding the Prince Edward Islands (Southern Ocean)." Polar Biology **21**: 135-145.

Aoki, S. (2002). "Coherent sea level response to the Antarctic Oscillation." Geophysical Research letters **29**(20): 11-1 - 11-4.

Arrigo, K. R. and G. L. van Dijken (2004). "Annual changes in sea-ice, chlorophyll a, and primary production in the Ross Sea, Antarctica." Deep-Sea Research II **51**: 117-138.

Atkinson, A., M. J. Whitehouse, J. Priddle, G. C. Cripps, P. Ward and M. A. Brandon (2001). "South Georgia, Antarctica: a productive, cold water, pelagic ecosystem." Marine Ecology Progress Series **216**: 279-308.

Aumont, O. and L. Bopp (2006). "Globalizing from ocean in situ iron fertilization studies." Global Biogeochemical Cycles **20**(GB2017): doi:10.1029/2005GB002591.

Bakker, D. C. E., Y. Bozec, P. D. Nightingale, L. Goldson, M.-J. Messias, H. J. W. de Baar, M. Liddicoat, I. Skjelvan, V. Strass and A. J. Watson (2005). "Iron and mixing affect biological uptake in SOIREE and EisenEx, two Southern Ocean iron fertilisation experiments." Deep-Sea Research II **52**: 1001-1019.

Banse, K. (1996). "Low seasonality of low concentrations of surface chlorophyll in the Subantarctic water ring: underwater irradiance, iron or grazing?" Progress in Oceanography **37**: 241-291.

Barth, J. A., T. J. Cowles and S. D. Pierce (2001). "Mesoscale physical and bio-optical structure of the Antarctic Polar Front near 170W during austral spring." Journal of Geophysical Research **106**(7): 13879-13902.

Belkin, I. M. and A. L. Gordon (1996). "Southern Ocean fronts from the Greenwich meridian to Tasmania." Journal of Geophysical Research **101**(2): 3675-3696.

Bhaskar, T. V. S. U., D. Swain and M. Ravichandran (2006). "Inferring mixed-layer depth variability from Argo observations in the western Indian Ocean." Journal of Marine Research **64**: 393-406.

Blain, S., B. Queguiner, L. Armand, S. Belviso, B. Bombled, L. Bopp, A. Bowie, C. Brunet, C. Brussard, F. Carlotti, U. Christaki, A. Corbiere, I. Durand, F. Ebersbach, J.-L. Fuda, N. Garcia, L. Gerringa, B. Griffiths, C. Guigue, C. Guillerm, S. Jacquet, C. Jeandel, P. Laan, D. Lefevre, C. Lo Monaco, A. Malits, J. Mosseri, I. Obernosterer, Y.-H. Park, M. Picheral, P. Pondaven, T. Remenyi, V. Sandroni, G. Sarthou, N. Savoye, L. Scouarnec, M. Souhaut, D. Thuiller, K. Timmermans, T. Trull, J. Uitz, P. van Beek, M. Veldhuis, D. Vincent, E. Viollier, L. Vong and T. Wagener (2007). "Effects of natural iron fertilization on carbon sequestration in the Southern Ocean." Nature **446**(doi:10.1038/nature05700): 1070-1074.

Blain, S., P. Treguer and S. Belviso (2001). "A biogeochemical study of the island mass effect in the context of the iron hypothesis: Kerguelen Islands, Southern Ocean." Deep Sea Research I **48**: 163-187.

Boebel, O., T. Rossby, J. R. E. Lutjeharms, W. Zenk and C. Barron (2003). "Path and Variability of the Agulhas Return Current." Deep Sea Research II **50**: 35-56.

Bopp, L., K. E. Kohfield and C. Le Quere (2003). "Dust impact on marine biota and atmospheric CO2 during glacial periods." Paleoceanography **18**(2): doi:10.1029/2002PA000810.

Borowski, D., R. Gerdes and D. Olbers (2002). "Thermohaline and Wind Forcing of a Circumpolar Current with blocked Geostrophic Contours." Journal of Physical Oceanography **32**: 2520-2540.

Boyd, P. W., A. C. Crossley, G. R. DiTullio, F. B. Griffiths, D. A. Hutchins, B. Queguiner, P. N. Sedwick and T. Trull (2001). "Control of phytoplankton growth by iron supply and irradiance in the subantarctic Southern Ocean: Experimental results from the SAZ Project." Journal of Geophysical Research **106**(C12): 31573-31583.

Boyd, P. W., T. Jickells, C. S. Law, S. Blain, E. A. Boyle, K. O. Buesseler, K. H. Coale, J. J. Cullen, H. J. W. de Baar, M. Follows, M. Harvey, C. Lancelot, M. Levasseur, N. P. J. Owens, R. T. Pollard, R. Rivkin, J. Sarmiento, V. Schoemann, V. Smetacek, S. Takeda, A. Tsuda, S. Turner and A. J. Watson (2007). "Mesoscale Iron Enrichment Experiments 1993-2005: Synthesis and Future Directions." Science **315**: 612-617.

Boyd, P. W., J. LaRoche, M. Gall, R. Frew and R. M. L. McKay (1999). "Role of iron, light and silicate in controlling algal biomass in subantarctic waters SE of New Zealand." Journal of Geophysical Research **104**(C6): 13395-13408.

Boyd, P. W., C. S. Law, C. S. Wong, Y. Nojiri, A. Tsuda, M. Levasseur, S. Takeda, R. Rivkin, P. J. Harrison, R. Strzepek, J. Gower, R. M. L. McKay, E. R. Abraham, M. Arychuk, J. Barwell-Clarke, W. Crawford, D. Crawford, M. Hale, K. Harada, K. Johnson, H. Kiyosawa, I. Kudo, A. Marchetti, W. Miller, J. Needoba, J. Nishioka, H. Ogawa, J. Page, M. Robert, H. Salto, A. Sastri, N. Sherry, T. Soutar, N. Sutherland, Y. Taira, F. Whitney, S.-K. E. Wong and T. Yoshimura (2004). "The decline and fate of an iron-induced subarctic phytoplankton bloom." Nature **428**: 549-553.

Boyd, P. W., A. J. Watson, C. S. Law, E. R. Abraham, T. Trull, R. Murdoch, D. C. E. Bakker, A. Bowie, M. Charette, P. Croot, K. Downing, R. Frew, M. Gall, M. Hadfield, J. Hall, M. Harvey, J. G., J. La Roche, M. R. L. Liddicoat, M. T. Maldonato, R. M. L. McKay, S. Nodder, S. Pickmere, R. Pridmore, S. R. Rintoul, K. Safi, A. Waite and J. Zeldis (2000). "A mesoscale phytoplankton bloom in the polar Southern Ocean stimulated by iron fertilization." Nature **407**: 695-702.

Bryden, H. L. and S. A. Cunningham (2003). "How wind-forcing and air-sea heat exchange determine the meridional temperature gradient and stratification for the Antarctic Circumpolar Current." Journal of Geophysical Research **108**(C8): doi:10.1029/2001JC001296.

Bucciarelli, E., S. Blain and P. Treguer (2001). "Iron and manganese in the wake of the Kerguelen Islands (Southern Ocean)." Marine Chemistry **73**: 21-36.

Campbell, J. W. (1995). "The lognormal distribution as a model for bio-optical variability in the sea." Journal of Geophysical Research **100**(C7): 13,237-13,254.

Chen, D., A. J. Busalacchi and L. M. Rothstein (1994). "The roles of vertical mixing, solar radiation, and wind stress in a model simulation of the sea surface temperature seasonal cycle in the tropical Pacific Ocean." Journal of Geophysical Research **99**(C10): 20345-20359.

Chen, D. and L. M. Rothstein (1994). "Hybrid vertical mixing scheme and its application to tropical ocean models." Journal of Physical Oceanography **24**: 2156-2179.

Cisewski, B., V. H. Strass and H. Prandke (2005). "Upper-ocean vertical mixing in the Antarctic Polar Front Zone." Deep-Sea Research II **52**: 1087-1108.

Coale, K. H., K. S. Johnson, F. P. Chavez, K. O. Buesseler, R. T. Barber, M. A. Brzezinski, W. P. Cochlan, F. J. Millero, P. G. Falkowski, J. E. Bauer, R. H. Wanninkhof, R. M. Kudela, M. A. Altabet, B. E. Hales, T. Takahashi, M. R. Landry, R. R. Bidigare, X. Wang, Z. Chase, P. G. Strutton, G. E. Friedrich, M. Y. Gorbunov, V. P. Lance, A. K. Hilting, M. R. Hiscock, M. Demarest, W. T. Hiscock, K. F. Sullivan, S. J. Tanner, R. M. Gordon, C. N. Hunter, V. A. Elrod, S. E. Fitzwater, J. L. Jones, S. Tozzi, M. Koblizek, A. E. Roberts, J. Herndon, J. Brewster, N. Ladizinsky, G. Smith, D. Cooper, D. Timothy, S. L. Brown, K. E. Selph, C. C. Sheridan, B. S. Twining and Z. I. Johnson (2004). "Southern Ocean Iron Enrichment Experiment: Carbon Cycling in High and Low-Si Waters." Science **304**: 408-414.

Coale, K. H., K. S. Johnson, S. E. Fitzwater, R. M. Gordon, S. J. Tanner, F. P. Chavez, L. Ferioli, C. Sakamoto, P. Rogers, F. J. Millero, P. Steinberg, P. Nightingale, D. Cooper, W. P. Cochlan, M. R. Landry, J. Constantinou, G. Rollwagen, A. Trasvina and R. M. Kudela (1996). "A massive phytoplankton bloom induced by an ecosystem-scale iron fertilisation experiment in the equatorial Pacific Ocean." Nature **383**: 495-501.

Craneguy, P. and Y. H. Park (1999). "Topographic control of the Antarctic Circumpolar Current in the south Indian Ocean." C. R. Acad. Sci. Paris, Sciences de la terre et des planetes **328**: 583-584.

Curry, R., B. Dickson and I. Yashayaev (2003). "A change in the freshwater balance of the Atlantic Ocean over the past four decades." Nature **426**: 826-829.

de Baar, H. J. W., P. W. Boyd, K. H. Coale, M. R. Landry, A. Tsuda, P. Assmy, D. C. E. Bakker, Y. Bozec, R. T. Barber, M. A. Brzezinski, K. O. Buesseler, M. Boye, P. L. Croot, F. Gervais, M. Y. Gorbunov, P. J. Harrison, W. T. Hiscock, P. Laan, C. Lancelot, C. S. Law, M. Levasseur, A. Marchetti, F. J. Millero, J. Nishioka, Y. Nojiri, T. van Oijen, U. Riebesell, M. J. A. Rijkenberg, H. Saito, S. Takeda, K. Timmermans, M. Veldhuis, A. M. Waite and C. S. Wong (2005). "Synthesis of iron fertilization experiments: From the Iron Age in the Age of Enlightenment." Journal of Geophysical Research **110**(C09S16): doi:10.1029/2004JC002601.

de Baar, H. J. W., J. T. M. de Jong, D. C. E. Bakker, B. M. Loscher, C. Veth, U. V. Bathmann and V. Smetacek (1995). "Importance of iron for plankton blooms and carbon dioxide drawdown in the Southern Ocean." Nature **373**: 412-415.

Dierssen, H. M. and R. C. Smith (2000). "Bio-optical properties and remote sensing ocean color algorithms for Antarctic Peninsula waters." Journal of Geophysical Research **105**(C11): 26,301-26,312.

Donlon, C. J. and I. S. Robinson (1997). "Observations of the oceanic thermal skin in the Atlantic Ocean." Journal of Geophysical Research **102**(C8): 18585-18606.

Duce, R. A. and N. W. Tindale (1991). "Atmospheric transport of Iron and its deposition in the Ocean." Limnology and Oceanography **36**(8): 1715-1726.

Eppley, R. W. (1972). "Temperature and phytoplankton growth in the sea." Fishery Bulletin **70**: 1063-1085.

Feldman, G. C. and C. R. McClain (2006). Ocean Color Web, MODIS Reprocessing 1.1, NASA Goddard Space Flight Center. N. Kuring and S. W. Bailey.

Feldman, G. C. and C. R. McClain (2006). Ocean Color Web, SeaWiFS Reprocessing 5.1, NASA Goddard Space Flight Center. N. Kuring and S. W. Bailey.

Fennel, K., M. R. Abbott, Y. H. Spitz, J. G. Richman and D. M. Nelson (2003). "Modelling Controls of phytoplankton production in the southwest Pacific Sector of the Southern Ocean." Deep Sea Research II **50**: 769-798.

Fielding, S., P. Ward, R. T. Pollard, S. Seeyave, J. F. Read, J. A. Hughes and T. Smith (2007). "Community structure and grazing impact of mesozooplankton during late spring/early summer 2004/2005 in the vicinity of the Crozet Islands (Southern Ocean)." Deep-Sea Research II **54**(18-20): 2106-2125.

Franck, V. M., M. A. Brzezinski, K. H. Coale and D. M. Nelson (2000). "Iron and silicic acid concentrations regulate Si uptake north of the Polar Frontal Zone in the Pacific sector of the Southern Ocean." Deep Sea Research II **47**: 3315-3338.

Frouin, R., B. Franz and M. Wang (2001). Algorithm to estimate PAR from SeaWiFS data Version 1.2 - Documentation.

Fyfe, J. C., G. J. Boer and G. M. Flato (1999). "The Arctic and Antarctic Oscillations and their projected changes under global warming." Geophysical Research Letters **26**(11): 1601-1604.

Gervais, F. and U. Riebesell (2002). "Changes in Primary productivity and chlorophyll-a in response to iron fertilization in the Southern Polar Frontal Zone." Limnology and Oceanography **47**(5): 1324-1335.

Gill, A. E. (1982). Atmosphere-Ocean Dynamics, Academic Press.

Gille, S. T. (1997). "The Southern Ocean Momentum Balance: Evidence for Topographic Effects from Numerical Model Output and Altimeter Data." Journal of Physical Oceanography **27**: 2219-2232.

Gille, S. T. (2002). "Warming of the Southern Ocean since the 1950s." Science **295**: 1275-1277.

Gille, S. T. (2003). "Float Observations of the Southern Ocean Part I: Estimating mean fields, bottom velocities and topographic steering." Journal of Physical Oceanography **33**: 1167-1181.

Gille, S. T., D. P. Stevens, R. T. Tokmakian and K. J. Heywood (2001). "Antarctic Circumpolar Current response to zonally averaged winds." Journal of Geophysical Research **106**(2): 2743-2759.

Giret, A., S. Tourpin, S. Marc, O. Verdier and J.-Y. Cottin (2002). "Volcanisme de l'île aux Pingouins, archipel Crozet, témoin de l'hétérogénéité du manteau fertile au sud de l'océan Indien; Penguins Island, Crozet archipelago, volcanic evidence for a heterogeneous mantle in the southern Indian Ocean." Comptes Rendus Geosciences **334**: 481-488.

Goldman, J. C. and E. J. Carpenter (1974). "A kinetic approach to the effect of temperature on algal growth." Limnology and Oceanography **19**: 756-766.

Gregg, W. W. and N. W. Casey (2004). "Global and regional evaluation of the SeaWiFS chlorophyll data set." Remote Sensing of Environment **93**: 463-479.

Gunn, B. M., E. C. Abranson, N. D. Watkins and J. Nugier (1972). Petrology and Geochemistry of Iles Crozet: a Summary. Antarctic Geology and Geophysics. R. J. Adie.

Hall, A. and M. Visbeck (2002). "Synchronous Variability in the Southern Hemisphere Atmosphere, Sea Ice, and Ocean Resulting from the Annular Mode." Journal of Climate **15**: 3043-3057.

Hense, I., R. Timmerman, A. Beckmann and U. V. Bathmann (2003). "Regional ecosystem dynamics in the ACC: simulations with a three-dimensional ocean-plankton model." Journal of Marine Systems **42**: 31-51.

Hoffman, L. J., I. Peeken, K. Lochte, P. Assmy and M. J. W. Veldhuis (2006). "Different reactions of Southern Ocean phytoplankton size classes to iron fertilization." Limnology and Oceanography **51**(3): 1217-1229.

Holeton, C. L., F. Nedelec, R. Sanders, L. Brown, C. M. Moore, D. P. Stevens, K. J. Heywood, P. J. Statham and C. H. Lucas (2005). "Physiological state of phytoplankton communities in the Southwest Atlantic sector of the Southern Ocean, as measured by fast repetition rate fluorometry." Polar Biology **DOI 10.10.1007/s00300-005-0028-y**.

Holliday, N. P. and J. F. Read (1998). "Surface Oceanic Fronts between Africa and Antarctica." Deep Sea Research I **45**(2): 217-238.

Holm-Hansen, O., M. Kahru, C. D. Hewes, S. Kawaguchi, T. Kameda, V. A. Sushin, I. Krasovski, J. Priddle, R. E. Korb, R. P. Hewitt and B. G. Mitchell (2004). "Temporal and spatial distribution of chlorophyll-a in surface waters of the Scotia Sea as determined by both shipboard measurements and satellite data." Deep Sea Research II **51**: 1323-1331.

Huang, R. X. and S. Russell (1994). "Ventilation of the subtropical North Pacific." Journal of Physical Oceanography **24**: 2589-2605.

Hughes, C. W. and P. D. Killworth (1995). "Effects of Bottom Topography in the large scale Circulation of the Southern Ocean." Journal of Physical Oceanography **25**(11): 2485-2497.

Hughes, C. W., M. P. Meredith and K. J. Heywood (1999). "Wind-Driven Transport Fluctuations through Drake Passage: a Southern Mode." Journal of Physical Oceanography **29**: 1971-1992.

Hughes, C. W., P. L. Woodworth, M. P. Meredith, V. Stepanov, T. Whitworth and A. R. Pyne (2003). "Coherence of Antarctic sea levels, Southern Hemisphere Annular Mode and flow through the Drake Passage." Geophysical Research Letters **30**(9): 17-1 - 17-4.

Huisman, J., P. van Oostven and F. J. Weissing (1999). "Critical Depth and Critical Turbulence: Two different mechanisms for the development of phytoplankton blooms." Limnology and Oceanography **44**(7): 1781-1787.

Jickells, T. D., Z. S. An, K. K. Andersen, A. R. Baker, G. Bergametti, N. Brooks, J. J. Cao, P. W. Boyd, R. A. Duce, K. A. Hunter, H. Kawahata, N. Kubilay, J. laRoche, P. S. Liss, N. Mahowald, J. M. Prospero, A. J. Ridgwell, I. Tegen and R. Torres (2005). "Global Iron Connections Between Desert Dust, Ocean Biogeochemistry, and Climate." Science **308**: 67-71.

Johnson, K. S., F. P. Chavez and G. E. Friederich (1999). "Continental-shelf sediment as a primary source of iron for coastal phytoplankton." Nature **398**: 697-700.

Johnson, K. S., R. Gordon, M. and K. H. Coale (1997). "What controls iron concentrations in the world ocean?" Marine Chemistry **57**: 137-161.

Kara, A. B., P. A. Rochford and H. E. Hurlburt (2000). "An optimal definition for ocean mixed layer depth." Journal of Geophysical Research **105**(C7): 16803-16821.

Kara, B., P. A. Rochford and H. E. Hurlburt (2003). "Mixed layer depth variability over the global ocean." Journal of Geophysical Research **108**(3): doi:10.1029/2000JC000736.

Killworth, P. D. (1992). "An Equivalent-Barotropic Mode in the Fine Resolution Antarctic Model." Journal of Physical Oceanography **22**: 1379-1387.

Korb, R. E. and M. J. Whitehouse (2004). "Contrasting primary production regimes around South Georgia, Southern Ocean: large blooms versus high nutrient low chlorophyll waters." Deep Sea Research I **51**: 721-738.

Korb, R. E., M. J. Whitehouse and P. Ward (2004). "SeaWiFS in the Southern Ocean: spatial and temporal variability in phytoplankton biomass around South Georgia." Deep Sea Research II **51**: 99-116.

Kwok, R. and J. C. Comiso (2002). "Spatial patterns of variability in Antarctic surface temperature: Connections to the Southern Hemisphere Annular Mode and the Southern Oscillation." Geophysical Research Letters **29**(14): 10.1029/2002GL015415.

Lalli, C. M. and T. R. Parsons (1997). Biological Oceanography An Introduction, Butterworth Heinemann.

Landry, M. R., M. E. Ondrusek, S. J. Tanner, S. L. Brown, J. Constantinou, R. R. Bidigare, K. H. Coale and S. E. Fitzwater (2000). "Biological response to iron fertilization in the eastern equatorial Pacific (IronEx II). I. Microplankton community abundances and biomass." Marine Ecology Progress Series **201**: 27-42.

Law, C. S., E. R. Abraham, A. J. Watson and M. I. Liddicoat (2003). "Vertical eddy diffusion and nutrient supply to the surface mixed layer of the Antarctic Circumpolar Current." Journal of Geophysical Research **108**(8): 3272-3286.

Levitus, S., J. Antonov and T. Boyer (2005). "Warming of the world ocean, 1955-2003." Geophysical Research Letters **32**(L02604): doi:10.1029/2004GL021592.

Li, M. and C. Garrett (1997). "Mixed layer deepening due to Langmuir circulation." Journal of Physical Oceanography **27**: 121-132.

Lutjeharms, J. R. E. and I. J. Ansorge (2001). "The Agulhas Return Current." Journal of Marine Systems **30**: 115-138.

Maldonato, M. T., P. W. Boyd, P. J. Harrison and N. M. Price (1999). "Co-limitation of phytoplankton growth by light and Fe during winter in the NE subarctic Pacific Ocean." Deep Sea Research II **46**: 2475-2485.

Marshall, G. J. (2003). "Trends in the Southern Annular Mode from Observations and Reanalyses." Journal of Climate **16**: 4134-4143.

Martin, J. H. (1990). "Glacial-interglacial CO_2 change: The Iron hypothesis." Paleoceanography **5**(1): 1-13.

Martin, J. H., R. M. Gordon and S. E. Fitzwater (1990). "Iron in Antarctic waters." Nature **345**: 156-158.

Meredith, M. P., M. A. Brandon, E. J. Murphy, P. N. Trathan, S. E. Thorpe, D. G. Bone, P. P. Chernyshkov and V. A. Sushin (2005). "Variability in hydrographic conditions to the east and northwest of South Georgia, 1996-2001." Journal of Marine Systems **53**: 143-167.

Meredith, M. P. and C. W. Hughes (2004). "On the wind Forcing of the bottom pressure variability at Amsterdam and Kerguelen Islands, southern Indian Ocean." Journal of Geophysical Research **109**(C03012): doi:10.1029/2003JC002060.

Meredith, M. P., J. L. Watkins, E. J. Murphy, P. Ward, D. G. Bone, S. E. Thorpe, S. A. Grant and R. S. Ladkin (2003). "Southern ACC Front to north east of South Georgia: Pathways, Characteristics and Fluxes." Journal of Geophysical Research **108**(C5): 3162-3178.

Mitchell, B. G., E. A. Brody, O. Holm-Hansen, C. McClain and J. Bishop (1991). "Light Limitation of Phytoplankton Biomass and Macronutrient Utilization in the Southern Ocean." Limnology and Oceanography **36**(8): 1662-1677.

Moore, C. M., A. E. Hickman, A. J. Poulton, S. Seeyave and M. Lucas (2007). "Iron-light interactions during the CROZet natural iron bloom and EXport experiment (CROZEX) II: taxonomic responses and elemental stoichiometry." Deep-Sea Research II **54**(18-20): 2066-2084.

Moore, C. M., S. Seeyave, A. E. Hickman, J. T. Allen, M. Lucas, H. Planquette, R. T. Pollard and A. J. Poulton (2007). "Iron-light interactions during the CROZet natural iron bloom and EXport experiment (CROZEX) I: phytoplankton growth and photophysiology." Deep-Sea Research II **54**(18-20): 2045-2065.

Moore, J. K., M. R. Abbott and J. G. Richman (1999). "Location and Dynamics of the Antarctic Polar Front from Satellite Sea Surface Temperature data." Journal of Geophysical Research **104**(C2): 3059-3074.

Moore, J. K., M. R. Abbott, J. G. Richman, W. O. Smith, T. J. Cowles, K. H. Coale, W. D. Gardner and R. T. Barber (1999). "SeaWiFS satellite ocean colour data from the Southern Ocean." Geophysical Research Letters **26**(10): 1465-1468.

Morel, F. M. M., J. G. Rueter and N. M. Price (1991). "Iron nutrition of phytoplankton and its possible importance in the ecology of ocean regions with high nutrient and low biomass." Oceanography **4**(2): 56-61.

Munk, W. and E. Palmen (1951). "Note on the dynamics of the Antarctic Circumpolar Current." Tellus **3**: 53-55.

Naveiro Garabato, A. C., J. T. Allen, H. Leach, V. H. Strass and R. T. Pollard (2001). "Mesoscale Subduction at the Antarctic Polar Front driven by Baroclinic instability." Journal of Physical Oceanography **31**(8): 2087-2107.

Naveiro Garabato, A. C., K. L. Polzin, B. A. King, K. J. Heywood and M. Visbeck (2004). "Widespread Intense Turbulent Mixing in the Southern Ocean." Science **303**: 210-213.

O'Reilly, J. E., S. Maritorena, B. G. Mitchell, D. A. Siegel, K. L. Carder, S. A. Garver, M. Kahru and C. McClain (1998). "Ocean color chlorophyll algorithms for SeaWiFS." Journal of Geophysical Research **103**(C11): 24,937-24,953.

Orsi, A. H., T. Whitworth and W. D. Nowlin (1995). "On the meridional extent and fronts of the Antarctic Circumpolar Current." Deep Sea Research I **42**(5): 641-673.

Panetta, R. L. (1993). "Zonal jets in wide baroclinically unstable regions: Persistence and scale selection." Journal of Atmospheric Science **50**: 2073-2106.

Park, Y. H., E. Charriaud and P. Craneguy (2001). "Fronts, transport and Weddell Gyre between Africa and Antarctica." Journal of Geophysical Research **106**(2): 2857-2879.

Park, Y. H. and L. Gamberoni (1995). "Large scale circulation and its variability in the south Indian Ocean." Journal of Geophysical Research **100**(C12): 24911-24930.

Park, Y. H., L. Gamberoni and E. Charriaud (1993). "Frontal Structure, Water Masses, and Circulation in the Crozet Basin." Journal of Geophysical Research **98**(7): 12361-12385.

Perry, K. L. (2001). SeaWinds on QuikSCAT Level 3 Daily, Gridded Ocean Wind Vectors (JPL SeaWinds Project).

Phillips, H. E. and S. R. Rintoul (2000). "Eddy Variability and Energetics from Direct Current Measurements in the Antarctic Circumpolar Current South of Australia." Journal of Physical Oceanography **30**: 3050-3076.

Planquette, H., P. Statham, G. Fones, M. A. Charette, C. M. Moore, I. Salter, F. H. Nedelec, S. Taylor, M. French, A. R. Baker, N. Mahowald and T. Jickells (2007). "Dissolved iron in the vicinity of the Crozet Islands, Southern Ocean." Deep-Sea Research II **54**(18-20): 1999-2019.

Platt, T., S. Sathyendranath, A. M. Edwards, D. S. Broomhead and O. Ulloa (2003). "Nitrate supply and demand in the mixed layer of the ocean." Marine Ecology Progress Series **254**: 3-9.

Pollard, R. T., M. I. Lucas and J. F. Read (2002). "Physical controls on biogeochemical zonation in the Southern Ocean." Deep Sea Research II **49**: 3289-3305.

Pollard, R. T. and J. F. Read (2001). "Circulation pathways and transports of the Southern ocean in the vicinity of the Southwest Indian Ridge." Journal of Geophysical Research **106**(2): 2881-2898.

Pollard, R. T. and L. A. Regier (1992). "Vorticity and Vertical Circulation at an Ocean Front." Journal of Physical Oceanography **22**: 609-622.

Pollard, R. T. and R. I. C. Sanders (2006). RRS Discovery cruises 285/286, 3 Nov - 10 Dec 2004, 13 Dec 2004 - 21 Jan 2005; CROZet circulation, iron fertilization and EXport production experiment, Southampton Oceanography Centre, Cruise Report No. 60**:** 260 pp.

Pollard, R. T., R. I. C. Sanders, M. Lucas and P. Statham (2007). "The Crozet Natural Iron Bloom and Export Experiment (CROZEX)." Deep-Sea Research II **54**(18-20): 1905-1914.

Pollard, R. T., P. Treguer and J. Read (2006). "Quantifying nutrient supply to the Southern Ocean." Journal of Geophysical Research **111**(C05011): doi:10.1029/2005JC003076.

Pollard, R. T., H. J. Venables, J. F. Read and J. T. Allen (2007). "Large scale circulation around the Crozet Plateau controls an annual phytoplankton bloom in the Crozet Basin." Deep-Sea Research II **54**(18-20): 1915-1929.

Popova, E. E., R. T. Pollard, M. Lucas, H. J. Venables and T. R. Anderson (2007). "Real time forecasting of the ecosystem dynamics during the CROZEX experiment and the roles of the light, iron, silicate and circulation." Deep-Sea Research II **54**(18-20): 1966-1988.

Poulton, A. J., C. M. Moore, S. Seeyave, M. Lucas, S. Fielding and P. Ward (2007). "Phytoplankton community composition around the Crozet Plateau, with emphasis on diatoms and Phaeocystis." Deep-Sea Research II **54**(18-20): 2085-2105.

Raven, J. A. (1990). "Predictions of MN and Fe use Efficiencies of Phototrophic Growth as a Function of Light Availability for Growth and of C Assimilation Pathway." New Phytologist **116**(1): 1-18.

Razouls, S., G. Du Reau, P. Guillot, J. Maison and C. Jeandel (1998). "Seasonal abundance of copepod assemblages and grazing pressure in the Kerguelen Island area (Southern Ocean)." Journal of Plankton Research **20**(8): 1599-1614.

Razouls, S., P. Koubbi and P. Mayzaud (1996). "Spatio-temporal distribution of mesozooplankton in a sub-Antarctic coastal basin of the Kerguelen Archipelago (southern Indian Ocean)." Polar Biology **16**: 581-587.

Read, J. F., M. I. Lucas, S. E. Holley and R. T. Pollard (2000). "Phytoplankton, nutrients and hydrography in the frontal zone between the Southwest Indian Subtropical Gyre and the Southern Ocean." Deep Sea Research I **47**: 2341-2368.

Read, J. F. and R. T. Pollard (1993). "Structure and Transport of the Antarctic Circumpolar Current and Agulhas Return Current at 40^{o}E." Journal of Geophysical Research **98**(7): 12281-12295.

Read, J. F., R. T. Pollard and J. T. Allen (2007). "Sub-mesoscale structure and the development of an eddy in the Subantarctic Front north of the Crozet Islands." Deep-Sea Research II **54**(18-20): 1930-1948.

Reay, D. S., J. Priddle, D. B. Nedwell, M. J. Whitehouse, J. C. Ellis-Evans, C. Dueubert and D. P. Connelly (2001). "Regulation by low temperature of phytoplankton growth and nutrient uptake in the Southern Ocean." Marine Ecology Progress Series **219**: 51-64.

Reddy, T. E. and K. R. Arrigo (2006). "Constraints on the extent of the Ross Sea phytoplankton bloom." Journal of Geophysical Research **111**(C07005): doi:10.1029/2005JC003339.

Rhines, P. (1975). "Waves and turbulence on a β-plane." Journal of Fluid Mechanics **69**: 417-443.

Rintoul, S. R. and M. H. England (2002). "Ekman transport Dominates Local Air-sea Fluxes in Driving Variability of Subantarctic Mode Waters." Journal of Physical Oceanography **32**(5): 1308-1321.

Rintoul, S. R., C. W. Hughes and D. Olbers (2001). The Antarctic Circumpolar Current System. Ocean Circulation and Climate. G. Siegler, J. Church and W. J. Gould**:** 271-302.

Rintoul, S. R. and S. Sokolov (2001). "Baroclinic transport variability of the Antarctic Circumpolar Current south of Australia." Journal of Geophysical Research **106**(C2): 2795-2814.

Rio, M.-H. and F. Hernandez (2004). "A mean dynamic topography computed over the world ocean from altimetry, in situ measurements, and a geoid model." Journal of Geophysical Research **109**(C12032): doi:10.1029/2003JC002226.

Rollwagen Bollens, G. C. and M. R. Landry (2000). "Biological response to iron fertilization in the eastern equatorial Pacific (IronEx II). II. Mesozooplankton abundance, biomass, depth distribution and grazing." Marine Ecology Progress Series **201**: 43-56.

Ryabchenko, V. A., M. J. R. Fasham, B. A. Kagan and E. E. Popova (1997). "What causes short-term oscillations in ecosystem models of the ocean mixed layer." Journal of Marine Systems **13**: 33-50.

Sabine, C. L., R. A. Feely, N. Gruber, R. M. Key, K. Lee, J. L. Bullister, R. Wanninkhof, C. S. Wong, D. W. R. Wallace, B. Tilbrook, F. J. Millero, T.-H. Peng, A. Kozyr, T. Ono and A. F. Rios (2004). "The Oceanic Sink for Anthropogenic CO2." Science **305**: 367-371.

Salter, I., R. S. Lampitt, R. I. C. Sanders, A. J. Poulton, A. E. S. Kemp, B. Boorman, K. Saw and R. Pearce (2007). "Estimating Carbon, Silica and Diatom Export from a Naturally Fertilised Phytoplankton Bloom in the Southern Ocean using PELAGRA: a novel drifting sediment trap." Deep-Sea Research II **54**(18-20): 2233-2259.

Sanders, R. I. C., P. Morris, M. Stinchcombe, S. Seeyave, H. J. Venables, M. Lucas and C. M. Moore (2007). "New production and the f-ratio around the Crozet Plateau in austral summer 2004-5 diagnosed from seasonal changes in inorganic nutrient levels." Deep-Sea Research II **54**(18-20): 2191-2207.

Sandwell, D. T. and W. H. F. Smith (1997). "Marine gravity anomaly from Geosat and ERS1 satellite altimetry." Journal of Geophysical Research **102**(5): 10039-10054.

Sarmiento, J. L., N. Gruber, M. A. Brzezinski and J. P. Dunne (2004). "High-latitude controls of thermocline nutrients and low latitude biological productivity." Nature **427** (6969): 56-60.

Schmitz, W. J. (1996). On the World Ocean Circulation, Vol., II: The Pacific and Indian Oceans/A Global Update. Woods Hole Oceanographic Institution, Technical Report**:** WHOI-96-08, 237 pp.

Sedwick, P. N., S. Blain, B. Queguiner, F. B. Griffiths, M. Fiala, E. Bucciarelli and M. Denis (2002). "Resource limitation of phytoplankton growth in the Crozet Basin, Subantarctic Southern Ocean." Deep Sea Research II **49**: 3327-3349.

Seeyave, S., M. Lucas, C. M. Moore and A. J. Poulton (2007). "Phytoplankton productivity and community structure across the Crozet Plateau." Deep-Sea Research II **54**(18-20): 2020-2044.

Skyllingstad, E. D. and W. D. Smyth (2000). "Resonant Wind-Driven Mixing in the Ocean Boundary Layer." Journal of Physical Oceanography **30**: 1866-1890.

Smetacek, V., P. Assmy and J. Henjes (2004). "The role of grazing in structuring Southern Ocean pelagic ecosystems and biogeochemical cycles." Antarctic Science **16**(4): 541-558.

Sokolov, S. and S. R. Rintoul (2007). "Multiple jets of the Antarctic Circumpolar Current South of Australia." Journal of Physical Oceanography **37**: 1394-1412.

Spall, M. A. (1991). "A diagnostic study of the wind- and buoyancy- driven North Atlantic circulation." Journal of Geophysical Research **96**: 18509-18518.

Speer, K., S. R. Rintoul and B. Sloyan (2000). "The Diabatic Deacon Cell." Journal of Physical Oceanography **30**: 3212-3222.

Strass, V. H., A. C. Naveiro Garabato, R. T. Pollard, H. I. Fischer, I. Hense, J. T. Allen, J. F. Read, H. Leach and V. Smetacek (2002). "Mesoscale frontal dynamics: shaping the environment of primary production in the Antarctic Circumpolar Current." Deep Sea Research II **49**(18): 3735-3769.

Strzepek, R. F. and P. J. Harrison (2004). "Photosynthetic architecture differs in coastal and oceanic diatoms." Nature **431**(7009): 689-692.

Sunda, W. G. and S. A. Huntsman (1997). "Interrelated influence of iron, light and cell size on marine phytoplankton growth." Nature **390**: 389-392.

Sverdrup, H. U. (1953). "On conditions for the vernal blooming of phytoplankton." Jounal du Conseil Permanent International l'Exploration de la Mer **18**: 287-295.

Takeda, S. (1998). "Influence of Iron availability on nutrient consumption ratios of diatoms in oceanic waters." Nature **393**: 774-777.

Tang, W. and W. T. Liu (1996). Equivalent Neutral Wind, JPL Publication 96-17.

Tansley, C. E. and D. P. Marshall (2001). "On the dynamics of Wind-Driven Circumpolar Currents." Journal of Physical Oceanography **31**: 3258-3273.

Thompson, D. W. J. and S. Solomon (2002). "Interpretation of recent Southern Hemisphere climate change." Science **296**: 895-899.

Thompson, D. W. J. and J. M. Wallace (2000). "Annular Modes in the Extratropical Circulation Part I: Month-Month Variability." Journal of Climate **13**: 1000-1016.

Thorpe, S. E., K. J. Heywood, M. A. Brandon and D. P. Stevens (2002). "Variability of the southern ACC front north of South Georgia." Journal of Marine Systems **37**: 87-105.

Timmermans, K. R., L. J. A. Gerringa, H. J. W. de Baar, B. van der Wagt, M. J. W. Veldhuis, J. T. M. de Jong and P. Croot (2001). "Growth rates of large and small Southern Ocean diatoms in relation to availability of iron in natural seawater." Limnology and Oceanography **46**(2): 260-266.

Timmermans, K. R., B. van der Wagt and H. J. W. de Baar (2004). "Growth rates, half-saturation constants, and silicate, nitrate, and phosphate depletion in relation to iron availability of four large, open-ocean diatoms from the Southern Ocean." Limnology and Oceanography **49**(6): 2141-2151.

Trathan, P. N. and E. J. Murphy (2003). "Sea surface temperature anomalies near South Georgia: Relationships with the Pacific El Nin˜o regions." Journal of Geophysical Research **108**(C4): doi:10.1029/2000JC000299.

Treguier, A. M. and R. L. Panetta (1994). "Multiple Zonal Jets in a Quasigeostrophic Model of the Antarctic Circumpolar Current." Journal of Physical Oceanography **24**: 2263-2277.

Tsuda, A., S. Takeda, H. Saito, J. Nishioka, Y. Nojiri, I. Kudo, H. Kiyosawa, A. Shiomoto, D. Tsumune, T. Yoshimura, T. Aono, A. Hinuma, M. Kinugasa, K. Suzuki, Y. Sohrin, Y. Noiri, H. Tani, Y. Deguchi, N. Tsurushima, H. Ogawa, K. Fukami, K. Kuma and T. Saino (2003). "A mesoscale iron enrichment in the western Subarctic Pacific induces a large centric diatom bloom." Science **300**: 958-961.

Ward, P., M. J. Whitehouse, M. P. Meredith, E. J. Murphy, R. Shreeve, R. E. Korb, J. L. Watkins, S. E. Thorpe, R. Woodd-Walker, A. Brierley, N. J. Cunningham, S. A. Grant and D. G. Bone (2002). "The Southern Antarctic Circumpolar Current Front: physical and biological coupling at South Georgia." Deep Sea Research I **49**(12): 2183-2202.

Welschmeyer, N. A. (1994). "Fluoremetric analysis of Chlorophyll a in the presence of chlorophyll b and Pheopigments." Limnology and Oceanography **39**(8): 1985-1992.

Wollf, G. (2006). Initial Cruise Report, D300 Benthic CROZET, 1st December 2005 - 14th January 2006, http://www.bodc.ac.uk/data/information_and_inventories/cruise_inventory/report/d300.pdf

Wong, A. P. S., N. L. Bindoff and J. A. Church (1999). "Large-scale freshening of intermediate waters in the Pacific and Indian oceans." Nature **400**(440-443).